(NASA-TM-86083) SPACEBORNE SENSORS (1983-2000 AD): A FORECAST OF TECHNOLOGY (NASA) 230 p HC A11/MF A01 CSCL 22B

N84-26743

Unclas G3/19 19603

NASA

Technical Memorandum 86083

SPACEBORNE SENSORS (1983-2000 AD): A FORECAST OF TECHNOLOGY

Theodor Kostiuk and Bill Clark

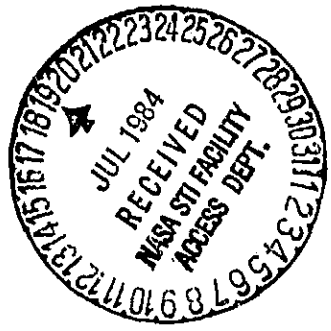

APRIL 1984

National Aeronautics and Space Administration

Goddard Space Flight Center
Greenbelt, Maryland 20771

SPACEBORNE SENSORS (1983-2000 AD):

A FORECAST OF TECHNOLOGY

by

THEODOR KOSTIUK

Infrared and Radio Astronomy Branch
NASA/Goddard Space Flight Center
Greenbelt, MD 20771

and

BILL P. CLARK

Computer Sciences Corporation
System Sciences Division
Silver Spring, MD 20910

PREFACE

This work provides a technical review and forecast of space technology as it applies to spaceborne sensors for future NASA missions. The goal was to develop a format for categorization of sensor systems covering the entire electromagnetic spectrum, including particles and fields. An attempt has been made to relate major generic sensor systems to their subsystems, their components, and to basic research and development. In addition, more general supporting technologies such as cryogenics, optical design, and data processing electronics have been addressed where appropriate. The dependence of many classes of instruments on common components, basic R&D and support technologies is also illustrated.

A forecast of important system designs and instrument and component performance parameters is provided for the 1983-2000 AD time frame. Some insight into the scientific and applications capabilities and goals of the sensor systems is also given.

This document is a reprint of Chapter 12 "Payloads" in Volume IIB of the publication "NASA Space Systems Technology Model: Space Technology Trends and Forecasts" (NASA/OAST, Washington, DC, Jan. 1984). The goal of this volume is to provide a document that a mission or advanced planner would be able to use to determine what technologies and capabilities will be available for future missions. It attempts to provide insight into system trade-offs and allows an informed zeroth order design. The material and forecasts presented here are based in part on data presented in the 1981 edition of this publication, other publications listed in the References and inputs provided by various individuals active in their field. These individuals, along with other experts are listed at the end of each section as sources for more detailed information.

ACKNOWLEDGEMENTS

The authors wish to especially thank and acknowledge Peter Gentieu for his major contribution to the Passive Ultraviolet Sensors Section. We are also grateful to Kumar Krishen for his careful review of and suggestions on the Active Microwave Sensors Section; James Cutts, David Hinkley, and Frank Allario for coordinating their respective center inputs; Michael Anuto and Alfred Cron for technical assistance; and Lee Holcomb for providing the initial impetus for this effort. A special appreciation is also extended to all the contributors who responded to our call to share their expertise.

CONTENTS

CONTENTS (CONT.)

1 INTRODUCTION

1.1 Overview. The practical expectations of a limited number of future deep space missions and the routine availability of space transportation systems (Shuttle) and large orbiting space platforms (e.g., LDR, space station) have greatly influenced current research and development of remote sensing technology. Stand-alone single purpose instruments are being replaced by multifunctional systems capable of some degree of autonomous operation and on-board decision making (smart sensors). Some of the proposed new space systems are also larger, heavier, and more power consumptive than those that could be supported by past free flying spacecraft.

Multifunctional operation will enable the same system to make observations at different spectral and spatial resolving powers in various spectral regions, image the source, measure low level and intense signals, and allow for changing the observing mode automatically, while providing on-board data storage and compaction.

This trend requires multiple receiver or detector systems to obtain large spatial coverage in the minimum amount of time. Linear arrays of receivers or detectors in the staring and "push broom" mode can obtain surface coverage or vertical atmospheric coverage in earth sensing applications. Two-dimensional detector array cameras can obtain images of planets, the Sun, and astrophysical objects in the infrared, visible, ultraviolet, and x-ray wavelengths. By filtering or dispersing (e.g., using a grating) received radiation onto detector or receiver arrays, simultaneous spectral information can be obtained on the same source. As a result of these potential advantages, single and mosaic detector array technology and on-chip data readout and processing electronics have become principal areas for future development.

Sensors are being developed to obtain higher spatial and spectral resolutions. Spatial resolution is often determined by the size of the

radiation collecting aperture (as in coherent detection systems). With the availability of the Shuttle, large single mirror or deployable spaceborne antennas and telescopes are now feasible. These can allow arbitrarily high useful spatial resolution with radar (SAR), microwave and millimeter wave systems (e.g., LDR) as well as at infrared, visible and ultraviolet wavelengths, where the Earth's atmospheric effects limit the resolution attainable from the ground on astrophysical objects. Other technology which can enhance spatial resolution such as synthetic apertures in radar, laser pulse rates/widths and fast electronics in LIDAR, and relative pixel size in multielement arrays in the ultraviolet and x-ray regions are also being considered.

New technology is being developed to enhance the spectral resolution capabilities of sensors and to permit the detection, measurement, and study of narrow spectral features such as molecular and atomic lines formed in low density regions and extreme phenomena such as naturally occurring lasers and masers. Ground-based heterodyne spectrometers capable of the required resolving powers and sensitivities in the millimeter and infrared regions exist and must be developed into spaceborne systems. Heterodyne systems in the submillimeter and long infrared wavelength regions are yet to be fully developed even for ground-based use.

Extending the spectral regions of operation of existing sensor types or developing new instruments operating at new wavelengths is the thrust for the future. Several spectral regions such as the long infrared (λ>13 μm) the submillimeter (λ<1 mm), and the extreme far ultraviolet (10-200 nm) are prime targets for the future. These wavelength regions are highly absorbed by the Earth's atmosphere and technology in them is not yet well developed. From space platforms, atmospheric attenuation is of no concern. Not only are improvements in optics and detectors important in these regions, but the development of radiation sources, such as solid state devices, electron tubes, and CW lasers for use as local oscillators in submillimeter or IR heterodyne spectrometers and high power pulsed lasers in the infrared through the ultraviolet for use in LIDAR and laser ranging systems, is needed.

The trend towards multifunctional, multidetector, high speed systems which will collect and generate an ever increasing amount of information, requires the development of associated electronics to handle these data. High speed electronics, high data rate processing, on-board data compaction, as well as communication systems and on-ground processing, are all areas needing parallel development in order to take advantage of the increasing capabilities of sensor systems. Of these, only those areas integral to sensor instruments will be forecast.

One of the most important parameters describing a sensor is its ability to detect a desired signal or source, i.e., its sensitivity. Since in most systems some form of thermal noise limits the sensor performance, cooling the detectors, amplifiers or optics can greatly enhance the sensitivity. Virtually all instruments in the infrared are dependent on cryogenic cooling. Therefore, improvements in cryogenic technology are essential for future space systems.

Size, weight, and power requirements are perhaps the most important practical parameters for the spaceborne sensor. Cryogenic requirements often determine the size, weight, and required power of a given instrument. Large optics can also determine the size and weight. Electronics (e.g., R.F.) and electron tubes and lasers are generally the principal consumers of power. These components (as in the case of high power laser systems) also contribute significantly to the total size, weight, and power dissipation requirements. With the availability of the Shuttle and the promise of large orbiting space platforms many systems (e.g., LIDAR) which have extreme requirements become feasible space instruments. The trend, however, is definitely in the direction of improved efficiency, higher temperature operation, and miniaturization of components and systems for future space missions.

1.2 Work Breakdown Structure

Figure 1.1 illustrates the structure of this technology forecast. When applicable, generic sensor systems are separated into active and passive categories within their operational wavelength or energy

regions. Each sensor system (listed in the boxes) consists of components and subsystems which, in many cases, can be used in more than one instrument type. For example, CCD detector arrays can be used in UV and visible cameras as well as in LIDAR applications; and CO_2 lasers can be used in infrared and submillimeter heterodyne systems as well as in LIDAR systems. Certain basic R&D efforts, such as development of new detector and optical materials, and high speed integrated solid state electronics, are important to a broad range of applications in sensor technology. In addition, all resultant spaceborne systems will require data processing, computer, and communications support. These areas as well as other supporting technologies are treated more fully elsewhere. This interrelationship between generic sensor types, components, basic research and development, and supporting technologies is the focus of the present sensor work breakdown structure illustrated in Fig. 1.

This work attempts to highlight important generic sensors in all spectral and energy regions and to forecast not only the system performance parameters through 2000 AD but to forecast and show their relationship to system components and basic R&D. The forecasts are given in tabulated and plotted form. Many of the figures forecasting parameters show as many as three curves. Those labeled A are projections assuming present day funding levels for that development. Curves marked B are forecasts based on increased funding or on major technological breakthroughs. The most probable development is labeled P. Caution must be exercised in determining technology readiness levels of the sensors discussed in this chapter since many areas are in the earliest stages of development. Some data, however, are presented in terms of technology readiness levels discussed in Appendix I.

The application and research areas associated with particular sensors and sensor types are also briefly discussed. A summary of the spectral regions covered and examples of the sources and problems that can be studied in each region with various instruments is given in Fig. 2. Broken bars indicate regions where adequate technology does not yet exist.

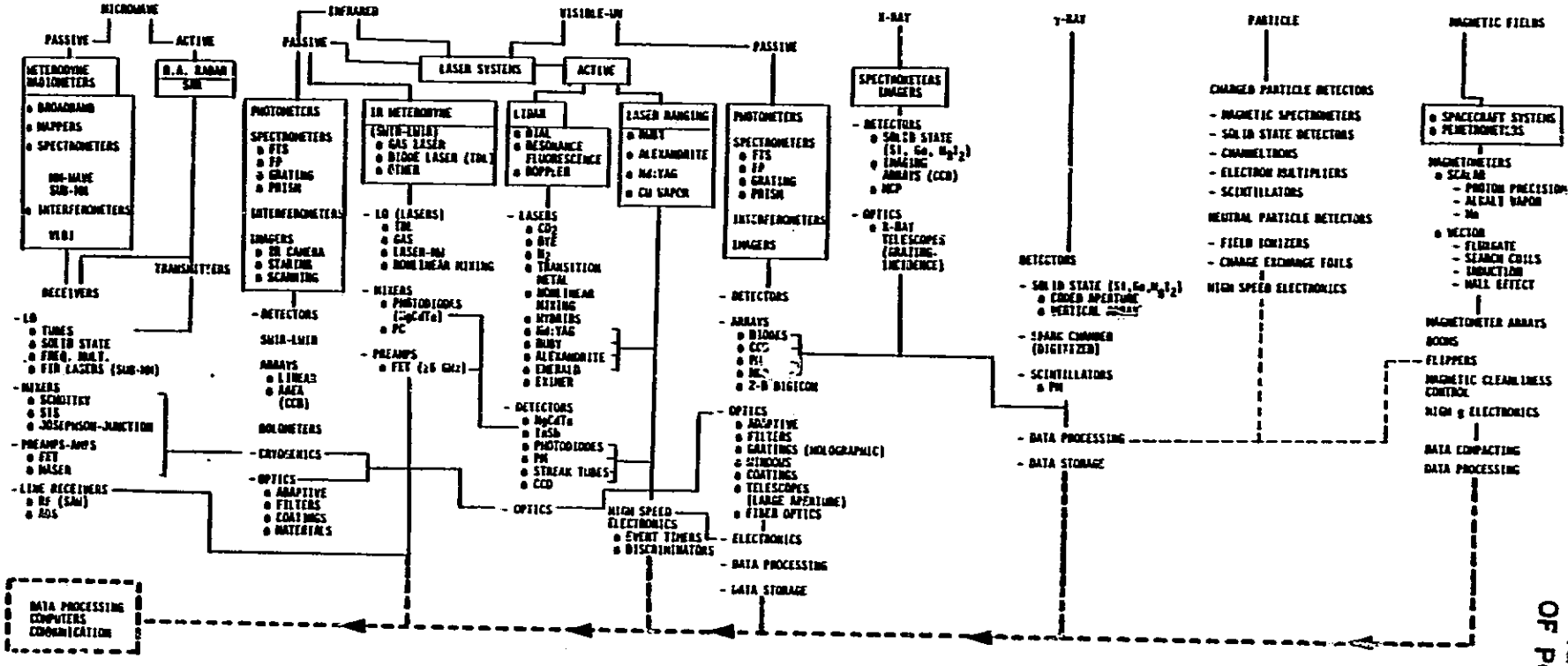

Figure 1. Work Breakdown Structure

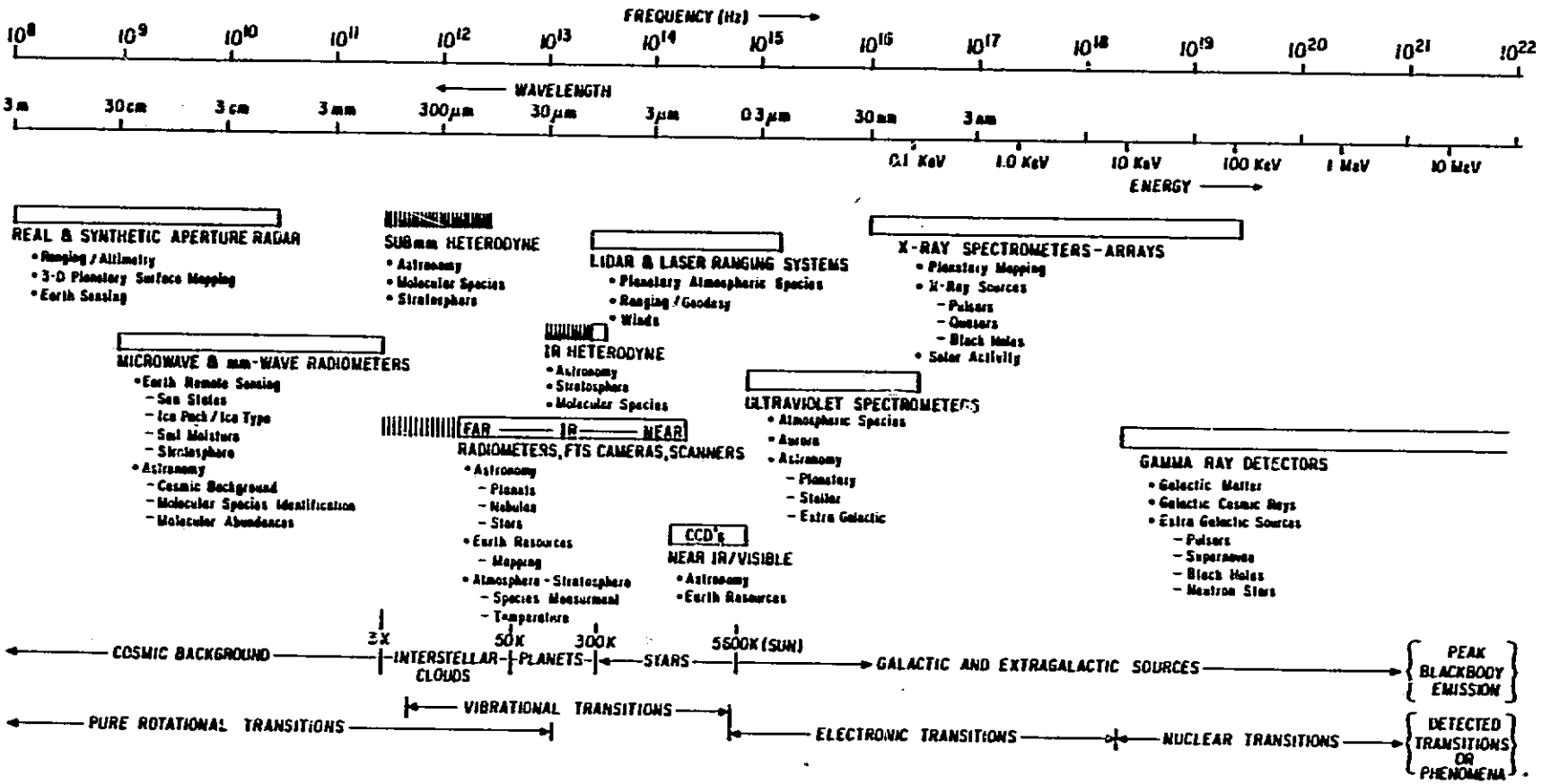

Figure 2. Sensor Summary

Finally, lists of prominent institutions and individuals engaged in work in the various fields described (many of whom contributed inputs to this forecast) are given, so that further information on a particular area can be obtained if desired. Neither the sensor complement nor institutions and individuals lists are meant to be complete and are only based on information available to the authors at the present time.

1.3 Summary of Projections

Instruments developed for remote sensing applications follow the Work Breakdown Structure (WBS) presented above. These include active microwave (radar) systems, passive microwave systems (radiometers), passive infrared systems (photometers, spectrometers, and imagers), passive laser systems (IR heterodyne), active laser systems (LIDAR), passive visible systems, passive ultraviolet systems, x-ray systems, gamma ray systems, magnetic field sensors, particle sensors, and supporting subsystems including cryogenics and optics. In the following subsections, instruments representing the state of the art for Earth remote sensing and astronomy applications will be contrasted with future systems and their capabilities. Where possible a working baseline system has been selected for comparison with future capabilities. Significant sensor parameters presented in the main document are summarized in Table I.

TABLE I.

PARAMETER FORECAST FOR MAJOR SYSTEMS

PARAMETER	SOA VALUE	2000 VALUE
ACTIVE MICROWAVE		
Synthetic Aperture Radar (600 cm - 3 cm)		
Resolution		
Planetary	100 m	50 m
Earth Orbit	25 m	10 m
Swath Width	220 km	400 km
Multipolarization	N/A	HH, HV, VH, VV
Multifrequency	Dual (L,X)	Multiple (L,S,C,X,Ku)
Signal Amplitude Precision	3 dB	2 dB
Frequency Range	0.05-10 GHz	0.01-60 GHz

TABLE I. (CONT.)

PARAMETER FORECAST FOR MAJOR SYSTEMS

PARAMETER	SOA VALUE	2000 VALUE
Conventional Radar		
Antenna (Weight for 100 m Diameter System)		
Phased Array		4000 lb
Parabolic Reflector		8000 lb
PASSIVE MICROWAVE (21 cm - 0.1 mm)		
Broadband Radiometers for Earth Sensing (21 - 0.15 cm)		
Receiver Power	10 W	<5 W
Receiver Weight	8 kg	<1.0 kg
Sensitivity	0.6 K	0.4 K
Beam Efficiency	95%	98%
Footprint	2-100 km	50 m
Broadband Radiometers for Astronomy		
Representative Instruments (10 mm - 3.3 mm)		
Differential Microwave Radiometer		
Noise Equivalent Temperature ($mK-sec^{1/2}$)	20	1
Far IR Spectrophotometer (10 mm - 0.1 mm)		
Bolometer NEP ($WHz^{-1/2}$)	10^{-14}	10^{-17}
Operating Temp. (K)	1.5	0.1
Millimeter and Submillimeter Heterodyne Radiometers		
5 mm Radiometer		
Noise Temp. (K)	1000	50
1 mm Radiometer		
Noise Temp. (K)	500	100
0.5 mm Radiometer		
Noise Temp. (K)		
Narrowband	1000	200
Broadband	50,000	500

TABLE I- (CONT.)

PARAMETER FORECAST FOR MAJOR SYSTEMS

PARAMETER	SOA VALUE	2000 VALUE
0.1 mm Radiometer		
Noise Temp. (K)		
Narrowband	5000	1000
Broadband	100,000	5000
Representative Systems		
Millimeter Wave Radiometer		
Noise Temp. (K)		
30 GHz	50	10
100 GHZ	200	20
300 GHz	2000	100
Submillimeter Spectrometer		
Noise Temp. (K)		
300 GHz	2000	100
1000 GHz	100,000	8000
Submillimeter Laser Heterodyne Spectrometer		
Noise Temp. (K) at 690 GHz	6000	500
Laser Power (mW)	10	100
Laser Operating Frequency (GHz)	3000	10,000
PASSIVE INFRARED SENSORS		
Representative Instruments for Astronomy		
Fourier Transform Spectrometer		
Spectral Coverage (μm)	2-500	2-1000
NEP ($WHz^{-1/2}$)	10^{-16}	10^{-18}
Minimum Detectable Flux (Wm^{-2} Hz^{-1})	10^{-22}	10^{-26}
Resolution (cm^{-1})	0.1	0.01
IR Mapping Spectrometers (0.1-20 μm)		
Detectivity (cm $Hz^{1/2}$ W^{-1})	2×10^{13}	10^{14}
Detector Array Size	17 elements	128 x 128 elements
Data Rate (bps)	1.1×10^{4}	10^{6}

TABLE I- (CONT.)

PARAMETER FORECAST FOR MAJOR SYSTEMS

PARAMETER	SOA VALUE	2000 VALUE
Earth Sensors		
Multispectral Linear Arrays (0.4-12.5 μm)		
IFOV (m)	30	10
Pixels per Scene	3×10^{8}	2×10^{9}
Acquisition Data Rate	85 Mbs	500 Mbs
IR Camera Systems for Astronomy (2-30 μm)		
NEP at 15 μm ($WHz^{-1/2}$)	7×10^{-16}	5×10^{-19}
Array Size	64 x 64	500 x 500
IR Cameras for Astronomy (>30 μm)		
Integrated Array NEP ($WHz^{-1/2}$) at 100 μm	N/A	4×10^{-19}
Integrated Array Size	N/A	64 x 64
Infrared Detector Technology (1-1000 μm)		
Discrete Detector NEP ($W-Hz^{-1/2}$)		
InSb 5 μm	1×10^{-16}	1×10^{-17}
Si:X 15 μm	3×10^{-16}	5×10^{-19}
Ge:Ga 100 μm	3×10^{-17}	1×10^{-19}
Bolometers 100-1000 μm	5×10^{-16}	1×10^{-17}
Monolithic Arrays (1-12 μm)		
8-12 μm Detectivity (HgCdTe) ($cm\ Hz^{1/2}W^{-1}$)	5×10^{11}	2×10^{12}
5 μm Detectivity (InSb) ($cm\ Hz^{1/2}W^{-1}$)	5×10^{12}	10^{13}
Elements per Focal Plane		
LWIR	500	2000
SWIR	5000	10,000
PASSIVE LASER SYSTEMS		
IR Heterodyne Spectrometer (3-30 μm)		
10 μm Laser LO Power per Mode	400 μW	10 mW
28 μm Laser LO Power per Mode	80 μW	500 μW

TABLE 4. (CONT.)

PARAMETER FORECAST FOR MAJOR SYSTEMS

PARAMETER	SOA VALUE	2000 VALUE
Temperature of Operation (K)		
10 μm	10-70	70-100
28 μm	N/A	40-70
Photomixer Bandwidth (GHz)		
10 μm	1.5	5
28 μm	0.5	1
Photomixer Efficiency (%)		
10 μm	40	60
28 μm	N/A	50
ACTIVE LASER SYSTEMS (0.2-12 μm)		
CO_2 Laser DIAL (9-12 μm)		
NEP ($WHz^{-1/2}$)	10^{-12}	10^{-16}
Laser Pulse Energy	100 mJ	1 J
Transition Metal DIAL (1.5-2.3 μm)		
Pulse Energy	100 mJ	500 mJ
Dye Laser DIAL (0.28-1.06 μm)		
Pulse Energy	300 mJ	1 J
PRF	10 pps	40 pps
Solid-State Laser DIAL (0.7-0.8 μm)		
Peak Power (W)	3×10^6	10^{10}
Eximer Laser LIDAR (0.2-0.4 μm)		
Pulse Energy	3 J	25 J
Coverage of 200-400 nm	10%	100%
Efficiency	2%	4%
Shots per Laser Lifetime	10^7	10^8
Doppler LIDAR (9-11 μm)		
PRF (Hz)	1	100
LIDAR Ranging System-Alexandrite (0.4-0.8 μm)		
Timing Precision (sec)	5×10^{-11}	2×10^{-13}
Ranging Error	10 mm	0.5 mm

TABLE I-2 (CONT.)

PARAMETER FORECAST FOR MAJOR SYSTEMS

PARAMETER	SOA VALUE	2000 VALUE
LIDAR Ranging System-Cu Vapor (0.5-0.6 μm)		
Laser Efficiency (%)	0.1	1.0
Laser Lifetime	100 h	10^8 h
PASSIVE VISIBLE SYSTEMS (0.4-1.1 μm)		
CCD Detector Arrays		
Mosaic	10^6 elements	10^7 elements
Single Chip	5×10^5 elements	10^6 elements
Quantum Efficiency	10% @ 0.6 μm	60% @ 0.4 μm
Noise (electrons)	15	2
Readout Rate (pixels/sec)	10^6	10^9
PASSIVE ULTRAVIOLET SYSTEMS (10-300 nm)		
Telescopes		
Normal Incidence Reflectivity (%)		
> 115 nm	85	90
< 115 nm	25	50
Grazing Incidence Reflectivity (%)	70	90
Throughput (%)	50	80
Grating Efficiency in First Order		
Ruled Gratings	65%	70%
Holographic Gratings	30%	60%
Ruling Frequency		
Standard Gratings (lines/mm)	5000	7000
Holographic Gratings (lines/mm)	6000	18,000
Grating Size		
Ruled (m^2)	0.25 x 0.25	0.25 x 0.25
Holographic (m^2)	1 x 1	3 x 3
UV Detector Components		
Photocathode Q.E. (%)	50	90

TABLE L. (CONT.)

PARAMETER FORECAST FOR MAJOR SYSTEMS

PARAMETER	SOA VALUE	2000 VALUE
2-D Digicon		
CCD Element Size $(\mu m)^2$	15 x 15	7 x 7
Single Array Size	800 x 800	1600 x 1600
MCP		
Pore Size/Diameter (μm/mm)	7/25	7/150
Gain Property	$(10^6 \pm 6\%)$/25 mm	$(10^7 \pm 3\%)$/150 mm
MAMA		
Resolution/Length (μm/mm)	50/25	25/50
Anode Array Size	500 x 500	2000 x 2000
MOSAIC		
Resolution/Diameter (μm/mm)	15/35	7/35
Array Size	2300 x 2300	4800 x 4800
CCD Readout Rate	50 kHz	≥50 MHz
X-RAY SYSTEMS (40 eV - 150 keV)		
X-Ray Imaging Spectrometer (41-410 eV)		
Spatial Resolution (arc sec)	5	0.5
Spectral Resolution	0.0165 nm	0.0030 nm
Si CCD Array Detectors (0.1-8.0 keV)		
Spectral Resolution (eV)	210	100
Quantum Efficiency (%)	1	2
Imaging X-Ray Spectrometer (1-30 keV)		
Thermomigrated Al in Si		
Array Noise (FW HM)	280 eV	180 eV
Detector Noise	200 eV	130 eV
Electronics Noise	170 eV	120 eV
Pixels per Array	9	>1000
HgI_2 Energy Dispersive Spectrometer (0.5-150 keV)		
Resolution for 5.9 keV X-Rays (FWHM)	300 eV	100 eV

TABLE I. . (CONT.)

PARAMETER FORECAST FOR MAJOR SYSTEMS

PARAMETER	SOA VALUE	2000 VALUE
GAMMA RAY DETECTORS		
Germanium Detectors (0.01-10 MeV)		
Resolution (FWHM)	1.8 keV	1.5 keV
Detector Volume	200 cm^3	>400 cm^3
HgI_2 Detectors (20 keV - 5 MeV)		
Accuracy Limits	66 keV	3.3 keV
PARTICLE SENSORS		
Charged Particles		
High Energy (>100 MeV)		
Field Integral Value	10 kG m	100 kG m
Mid Energy (>50 keV)		
Detector Area		
10 μm Thickness	5 cm^2	5 cm^2
2 mm Thickness	20 cm^2	400 cm^2
Low Energy (<50 keV)		
Counting Rate (MHz)	1	100
Positional Accuracy (mm)	1	0.1
Neutral Particles		
Detector Efficiency (%)	1	100
FIELD SENSORS (0.005 nT - 10^7 nT)		
Magnetometer		
Noise (nT)	0.006	0.001
Acceleration Survival (g)	17,000	25,000

TABLE I. . (CONT.)

PARAMETER FORECAST FOR MAJOR SYSTEMS

PARAMETER	SOA VALUE	2000 VALUE
CRYOGENICS AND THERMAL CONTROL		
Joule-Thomson Adsorption Cooler		
Heat Load at 20 K	0.25 W	1.75 W
Stirling Cycle Coolers		
Lifetime in Space		
65 K Systems	1 yr	7 yr
11 K Systems	4 mo	5 yr
Heat Dissipation Systems		
Heat Transport Capacity (Wm)	10^4	5×10^5
Power Density (W/cm^2)	2	10
OPTICS		
Large Deployable Reflector (30-1000 μm)		
Diameter (m)	10	20
Areal Density (kg/m^2)	50	20
Reflector Surface Control	50 μm	2 μm

2 ACTIVE MICROWAVE SENSORS

Radar or active microwave sensors are used in a number of configurations to acquire information about the Earth and planetary surfaces. These include imaging, altimetry, sounding and scatterometry.

For surface imaging, a synthetic aperture configuration is usually required to be able to achieve high resolution (15 to 25 meters) from space. The Seasat Synthetic Aperture Radar, SAR (78), Shuttle Imaging Radar, SIR-A (81), SIR-B (84) and Venus Radar Mapper (88) are all synthetic aperture systems. The same is the case for all the imaging systems planned for the future SIR Series and System Z.

For altimetry, usually a real aperture, pulse limited system is used as was the case with the Seasat and Topex altimeter. This works well for ocean topography mapping. For global land mapping, a JPL planned Shuttle scanning radar altimeter will use a combination of synthetic aperture and real aperture system at 37 GHz to map the Earth's surface in three dimensions. In the case of future planetary missions to Mars and Titan, high frequency real aperture systems will be most likely used.

Subsurface sounding can be achieved to depths in excess of a few hundred meters through the Earth's ice sheets. A Shuttle sounder in the 60 to 100 MHz region is under study for global mapping of the Antarctic continent.

Scatterometers are usually used to determine surface backscatter over the ocean, and from it derive surface winds. Scatterometers usually use low resolution doppler filtering in conjunction with real aperture techniques. This was the case with the Seasat scatterometer (78) and will be the case with the proposed NOSS scatterometer.

2.1 Synthetic Aperture Radar

Synthetic Aperture Radar (SAR) was developed during the 1950s and 1960s as a result of the limited spatial resolution provided by conventional real aperture radar. The development of the focused synthetic

aperture technique, in which the synthetic antenna length is made equal to the linear width of the radiated beam at any range, produced much finer resolution. SAR technology made radar a feasible system for use as a terrestrial and extraterrestrial remote sensing tool.

The potential for SAR in Earth observations has been demonstrated by studies using Seasat SAR data. In addition, data obtained from the Shuttle Imaging Radar (SIR-A) has produced excellent results. Geologic analysis of Seasat data indicates that it is extremely useful for mapping large scale structural features, delineating flooded areas obscured from view by vegetation canopies and providing information on ocean waves, wind patterns, ocean currents and ice pack location. Initial analysis of SIR-A imagery indicates that it is a useful tool for delineating subsurface geologic features in extremely dry areas such as the Sahara Desert. Major applications of radar have also been identified in agriculture remote sensing of soil moisture and vegetation monitoring. However, SAR systems for this application have yet to be flown in space.

SAR is a very useful tool with regard to extraterrestrial exploration. Because it is an active sensor, it can image the dark sides of planets or peer through dense clouds at underlying geologic features at the surface. However, SAR technology must continue to develop to enhance its usefulness in both planetary and Earth remote sensing.

2.1.1 Performance Parameters

The following parameters have been identified as areas where development is needed:

- Resolution - provide better detail along and across track.
- Swath Width - wider swaths for shorter revisit times.
- Operation at multiple polarization, multiple frequencies, and multi-incidence angles to help understand signal-surface interactions and enable multiparameter retrieval.
- End to end calibration for quantitative measurements - signal amplitude accuracy and pixel location accuracy.

- Operating frequency range - growth of frequencies to broaden the use of radar.
- SAR instrument weight - reduction in weight important to planetary missions.
- Transmit/receive modules - long life, reliable, light weight, efficient monolithic chips.
- High data rate handling - first look capability via real time on-board optical processing.

Discussion and projections for important system parameters are given below and a summary is provided in Table 3.1.

TABLE 3.1

SIGNIFICANT SAR PARAMETERS

Parameter	SOA Value	2000 Value
Resolution		
Planetary	100 m	50 m
Earth Orbit	25 m	10 m
Swath Width	220 km	400 km
Multi-Incidence Angle	15°-75° in 5° Increments	
Multipolarization	Not Applicable	HH, HV, VH, VV
Multifrequency	Dual L,X	Multiple (L,S,C,X,Ku)
Signal Amplitude Precision Accuracy	3 dB	2 dB
Operating Frequency Range Upper/Lower Limit	10/0.05 GHz	60/0.01 GHz ATM Window
Instrument		
Weight	55 kg	20 kg
Size	TBD	TBD
Power Required	TBD	TBD

Resolution. Projected SAR planetary and Earth orbit spatial resolutions are shown in Fig. 3.

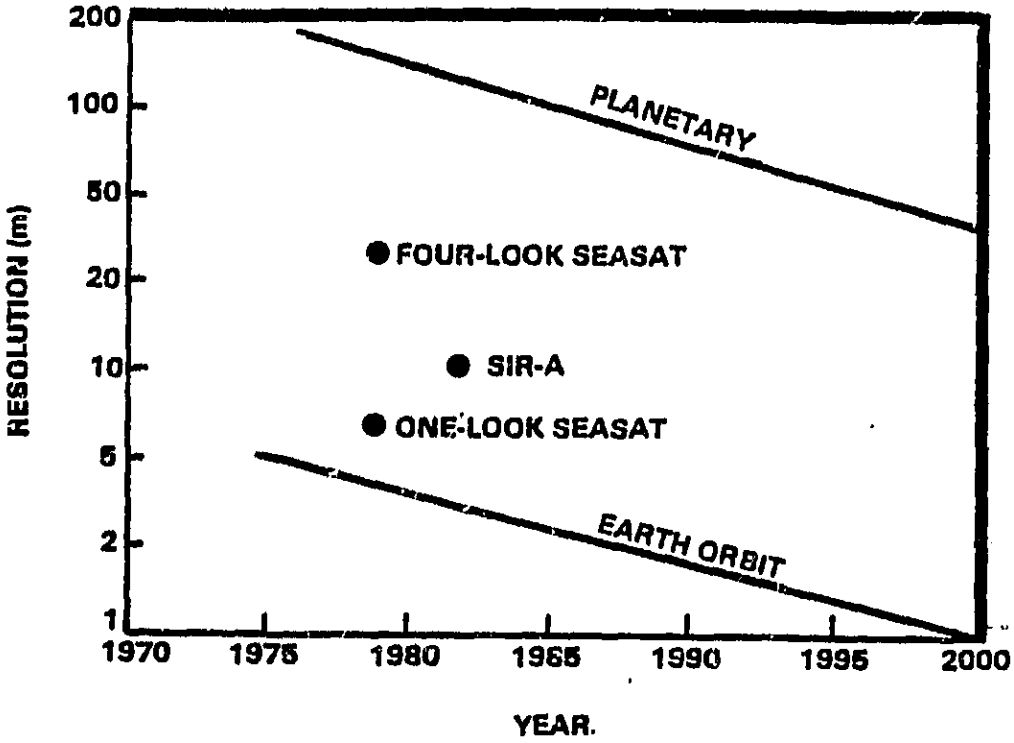

Figure 3. Space SAR Imaging/Sounding

SAR Swath Width (Fig. 4). There are three concepts for achieving a wide swath SAR system.

- Fixed Single Beam: In this concept, the wide swath is illuminated by a single narrow fan beam. No switching or phase shifting is required, but the realization of this beam requires a physically very long antenna—not an easy achievement with the tight flatness tolerances. The incidence angle will, of course, vary over the beam.
- Stepped Single Beam: In this concept sometimes called scansar, a single side-looking antenna is mechanically stepped or phase shifted to achieve a time series of beams with different centroid elevation angles. Over the wide total swath, the incidence angle varies in a manner similar to the fixed single beam.
- Multibeam or Squint Mode SAR: For this concept, the beam is switched in squint or segmented by multiple antennas to achieve a series of azimuthal beams. The incidence angle change is only that within a single beam, but the aspect angle from the flight direction varies over the total beam.

As a baseline, the antenna design for Seasat was successful in achieving a 100 km swath at a central incidence angle of 20°. The Shuttle Imaging Radar A (SIR-A) system design used a swath of 50 km at 50° incidence angle.

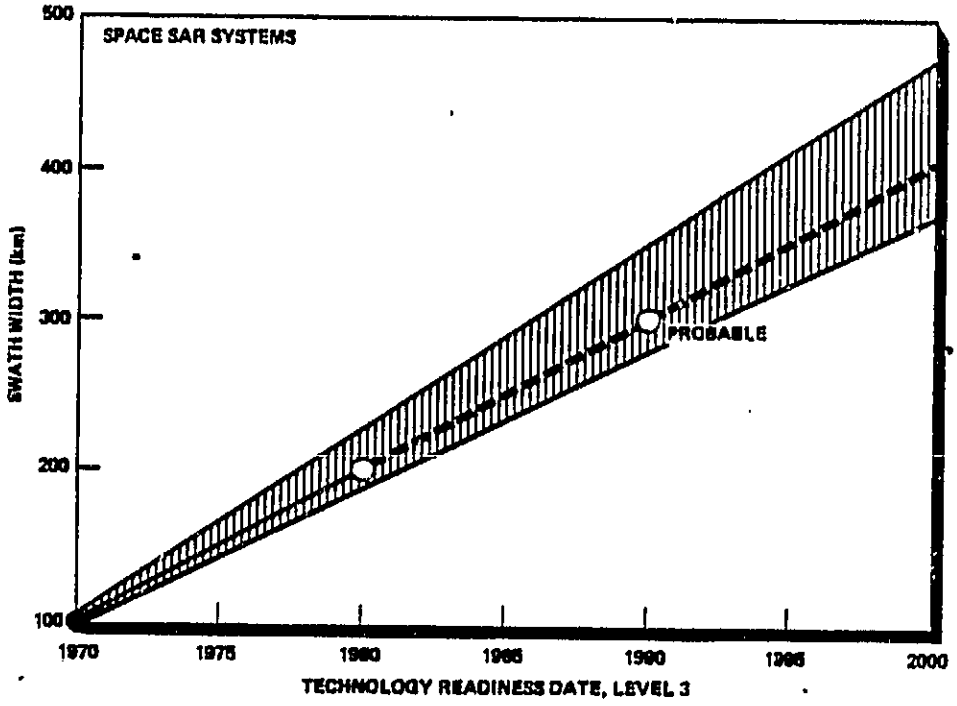

Figure _ 4. Wide Swath Radar Technology

Multipolarization and Multi-Incidence Angle. To date, no multi-polarization, multi-incidence angle SAR systems have been developed for spacecraft. The L-band system on Seasat and the Shuttle Imaging Radar (SIR-A) operated at one polarization combination (HH). However, the angle of incidence for SIR-A was 50°, whereas Seasat SAR was operated at an angle of 20°. Thus some multi-incidence angle data has already been obtained. The proposed C-band on the SIR-B instrument would be able to operate at all different linear polarizations, and multi-incidence angles would be provided by mechanically rotating the SIR-B antenna in the Shuttle bay. Incidence angles of 15° to 75° in 5° increments would be available. Additional proposed conceptual SAR design approaches include multibeam squint modes and distributed array SAR.

Multifrequency (Fig. 5). For multifrequency operation, reliable, space-qualified power sources are needed. Solid state sources provide better stability and long-operation possibilities. In addition, multifrequency SAR requires calibrated modulators and antennae which will enable establishment of accurate image intensity levels for various frequencies. Efficient design approaches for multifrequency SARs call for modular construction, and multi-mode operation. Seasat and SIR-A SARs both operate at L-band. The proposed SIR-B would be capable of operating at two frequencies: 1275 MHz (L-band) and 5330 MHz (C-band). SIR-B hardware could be modified at a future date to accommodate X-band or higher frequency radar.

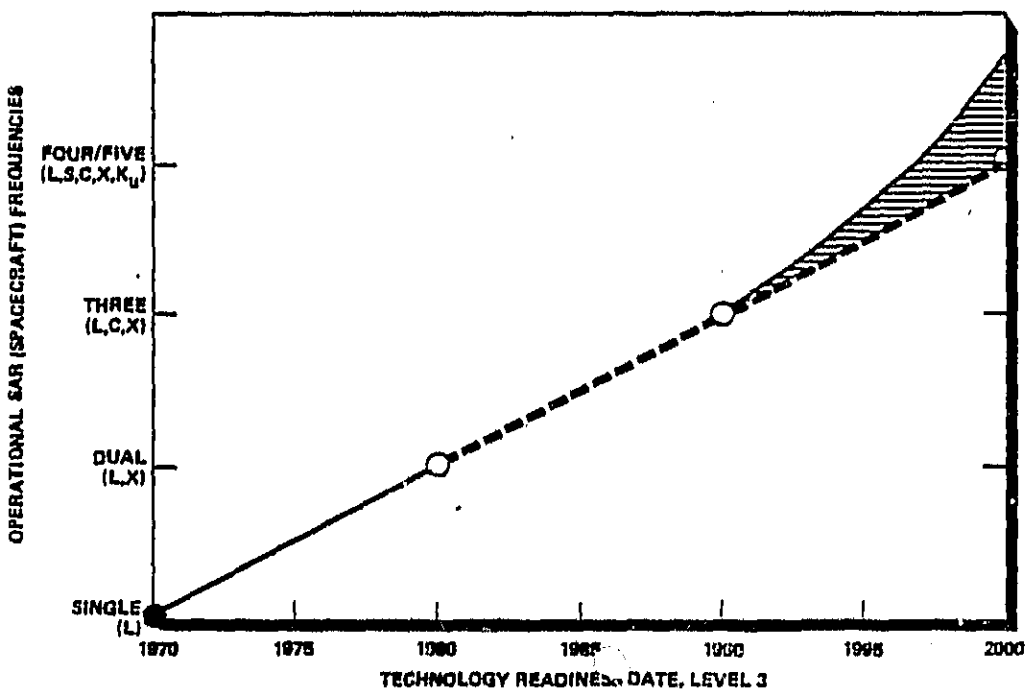

Figure 5. Multifrequency SAR Operation

Signal Amplitude Precision Accuracy (Fig. 6). Quantitative measurements of ground scatter requires knowledge of the absolute calibration of the radar system, including the antenna. The returned signal should be corrected for all system variations and any uncertainty in the antenna gain. Techniques for calibrating SAR system (minus antenna) variations are based on sending samples of the transmitted signal at various power levels through the receiver and the signal

processors. Another useful method is to image known cross-section targets. This technique has been used for spheres, corner reflectors, and other deterministic reflectors on aircraft systems. Calibration standards and techniques for extended scene imaging at multifrequencies, multipolarizations, and multi-incidence have to be established for spacecraft SARs. Figure 6 is presented on the basis of the aircraft and Seasat SAR experience.

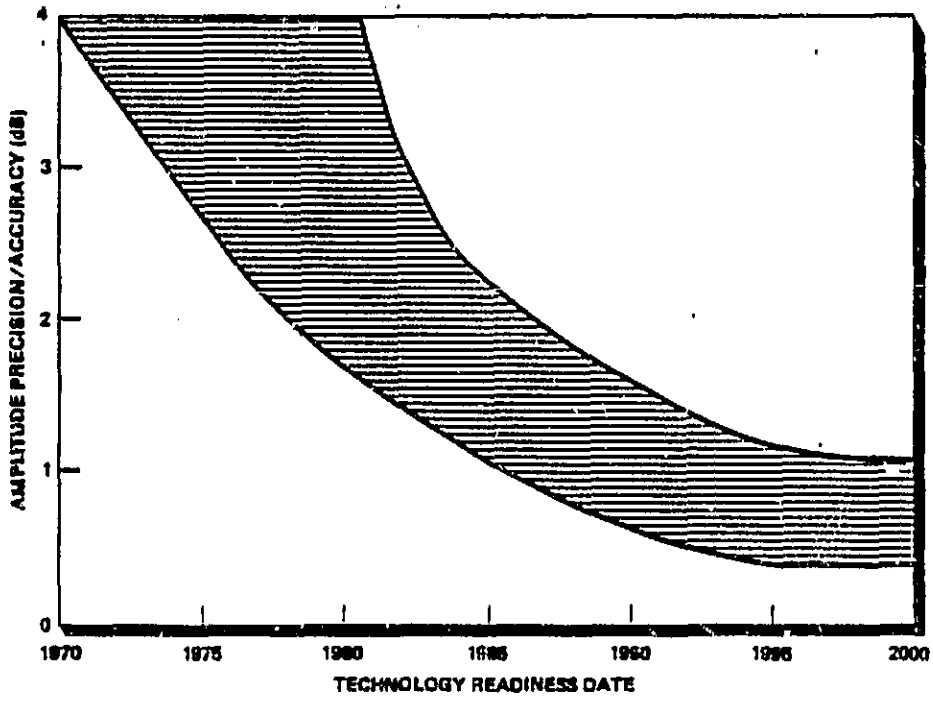

Figure 6. SAR Amplitude Precision/Accuracy

SAR Operating Frequency Range (Fig. 7). A projection of capability to higher and lower frequencies is shown. Growth in lower frequencies improves subsurface penetration. Growth to higher frequencies, based on radiometer experiences, opens up the possibility of tapping atmospheric windows and pressure-sensitive bands. In addition, the microwave regime has a similar pattern of absorption bands like those used in the visible and infrared portion of the spectrum. These provide potential for compositional differentiations in both the atmosphere and the surface. The need to obtain international agreement on the allocation of frequencies for this type of application may seriously hamper growth in the area.

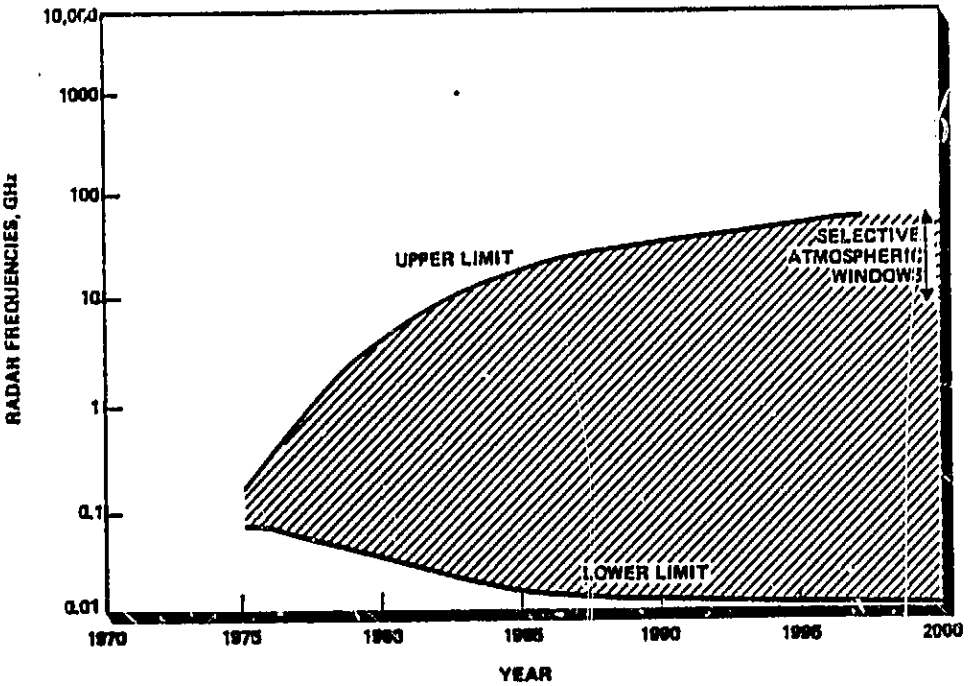

Figure 7. Spacecraft Imaging SAR Operating Frequency Range

SAR Instrument Weight. A projection for SAR instrument mass, exclusive of antenna, is presented in Fig. 8.

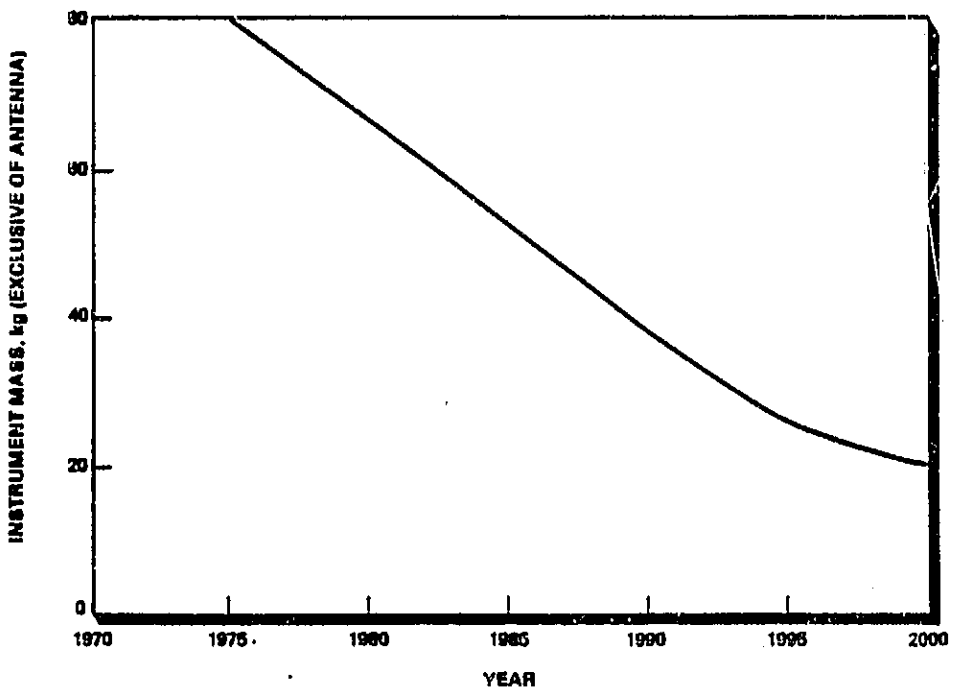

Figure 8. Space SAR Imaging/Sounding

2.1.2 Critical System Components

Critical subsystems are Transmitter/Receiver modules including solid state power devices and a signal processor. Projections for these subsystems are presented below and a summary is given in Table 2.

TABLE 2

SAR CRITICAL COMPONENT PARAMETERS

Parameter	SOA Value	2000 Value
o Transmitter/Receiver Module		
Solid State Power (CW)		
FET	12 W	15 W
IMPATT	3.5 W	8 W
Bipolar	100 W	130 W
o Signal Processor		
Data Processors	1.3 MOPS	12.0 MOPS
Radar Signal Processors	94 MOPS	1150 MOPS

Transmit/Receive Modules. Transmit/Receive Modules contain a power amplifier, low noise receiver, phase shifter, R.F. switches and control logic. A typical transceiver module is presented in Fig. 9.

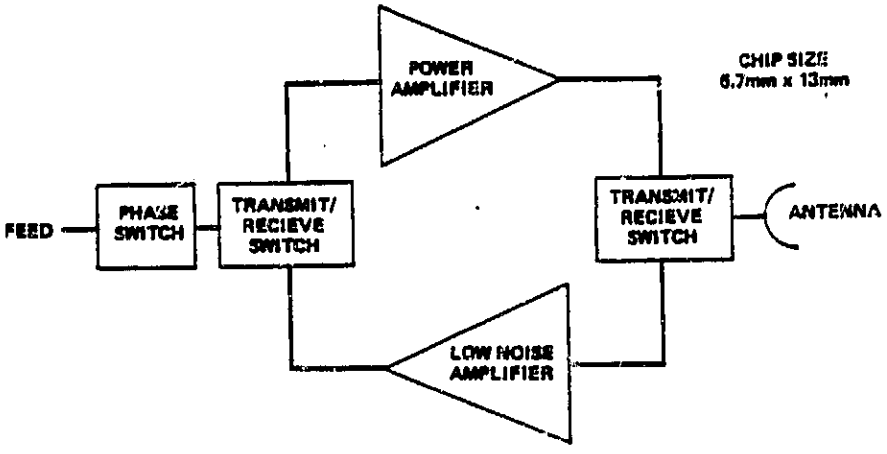

Figure 9. Typical GaAs Transceiver Module

Current solid state device power is shown in Fig. 10. The bipolar transistor appears to have a clear advantage in power yield over the FET and IMPATT diodes at frequencies below 4 GHz. At the upper frequencies, the IMPATTs offer superior performance. Power performance of both transistors falls off rapidly above 10 GHz. It would appear that no difficulty would be met in achieving the power requirements at S-band. New techniques in power combining would be required to satisfy power levels needed at the 60 GHz frequency. Such techniques will have to be compatible with both system weight and transmitter stability. IMPATT diodes currently being used in certain types of cavity combiners are able to achieve the 60 GHz power requirements, but these techniques do not lend themselves well to space antenna and array feed uses because of their weight and bulkiness. More technology development in other combining techniques is required for achieving the 60 GHz power performance.

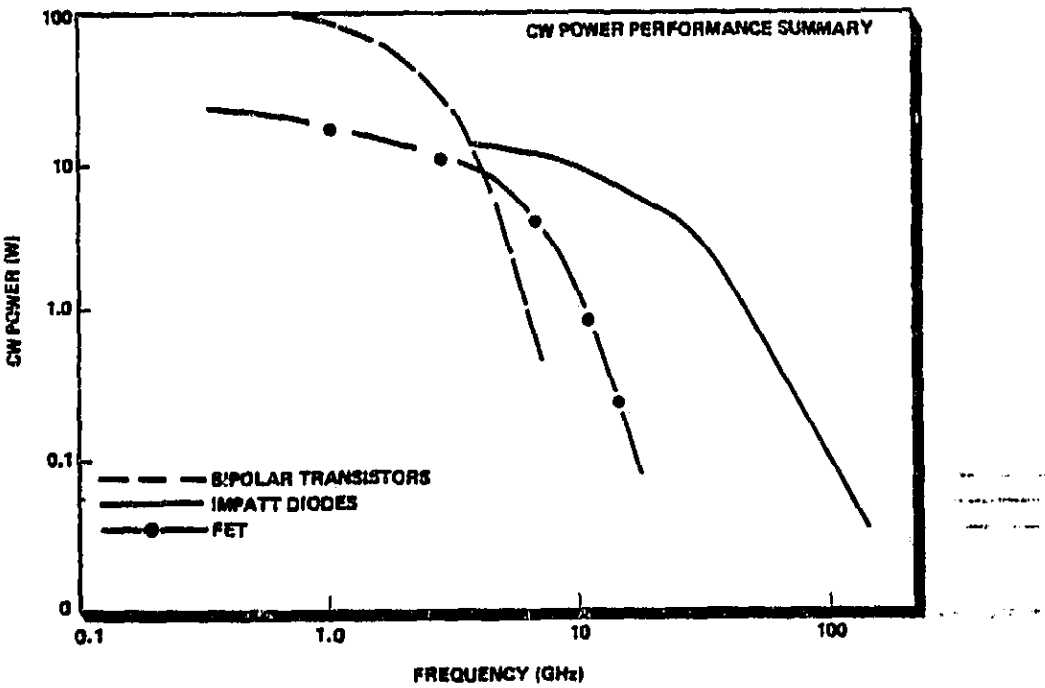

Figure 10. Solid-State Device Technology (Aerospace Corporation February 1981)

Figure 11 shows a forecast of the power performance of the three solid-state devices discussed above. The prediction is nonlinear and is based on incremental increases in single device performances achieved in the time period between 1965 and 1980. Any one of these device performance predictions can change, based on the concentration of development emphasis over a period of time. This may definitely be true for IMPATT devices in the near future, as a result of increasing interest in millimeter wave activities.

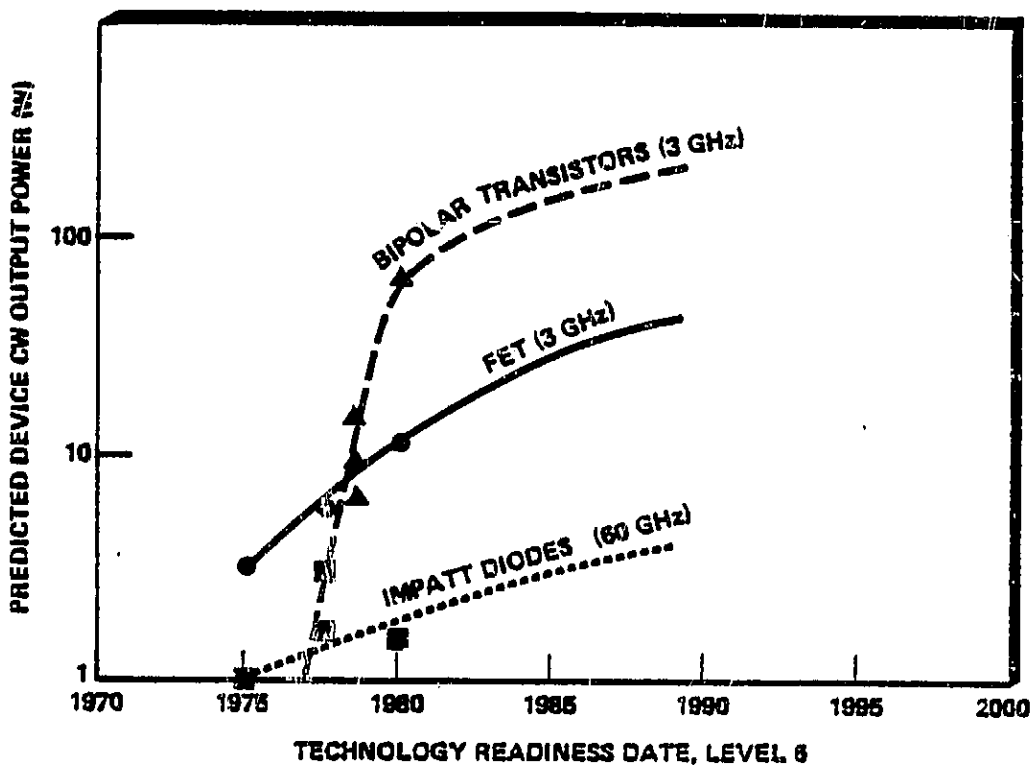

Figure 11. Solid-State Device Power Performance (Aerospace Corporation February 1981)

Signal Processor Technology. Signal processing requirements for most of the proposed microwave systems encompass a wide spectrum of processing applications. In certain cases, technology requirements are being pushed beyond the current state of the art. Desired performance in high clutter background dictates demands for high speed clutter cancellation algorithms. Multiple target detection and tracking functions accompanied by long time integration and pulse compression

schemes are also required. Filtering and surface imagery are all proposed functions to be implemented into at least one or all of the microwave systems.

Current processor capabilities, along with future projections, are shown in Fig. 12. Performance capability is shown in terms of millions of complex operations per second (MOPS) for both signal and data processor systems. Superimposed in the figure for relative comparison between performance available or projected, and performance needed, are the requirements of the signal and data processing units for performing certain indicated system functions. RF technology, using surface acoustic waves (SAW), and acousto optic technology is currently being developed for analysis and processing of signals. Acousto optic techniques in particular offer the potential of extremely small integrated devices.

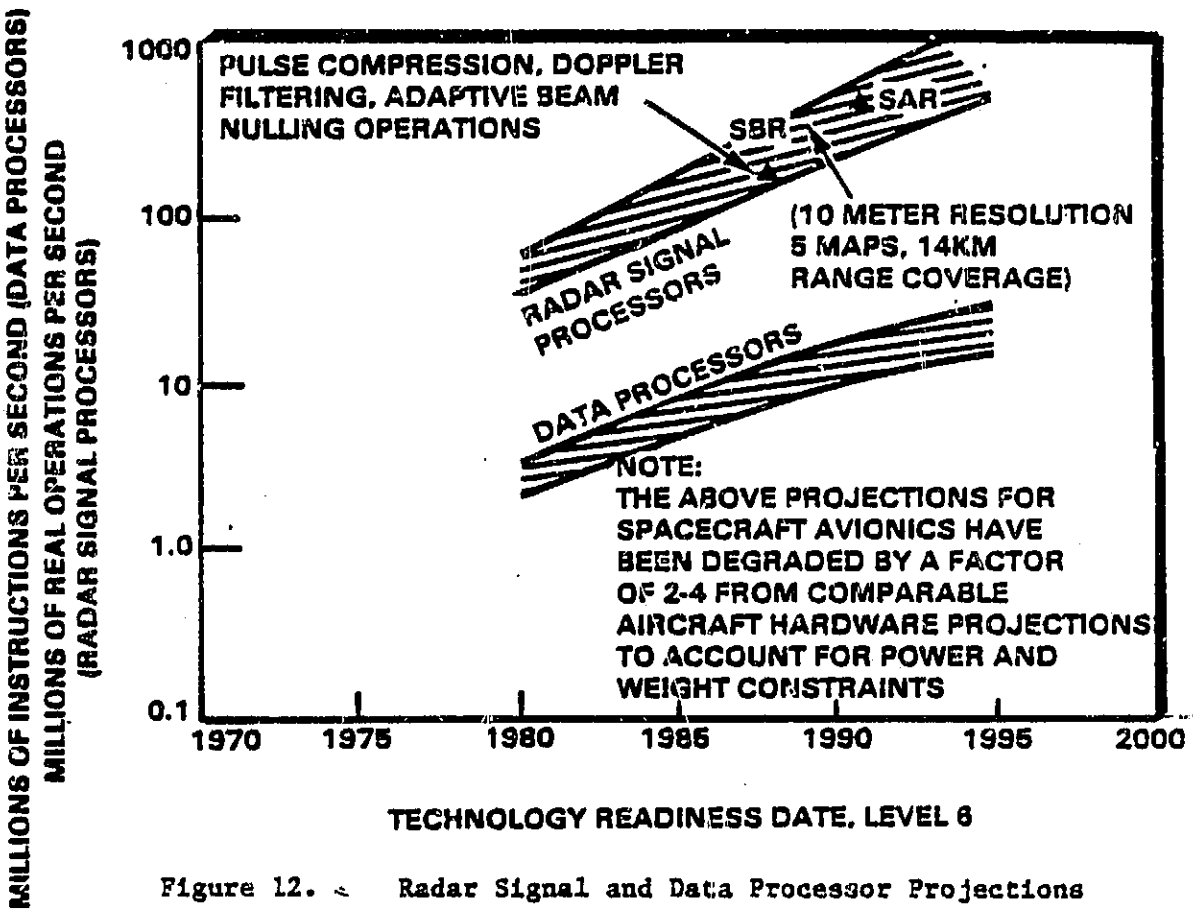

Figure 12. Radar Signal and Data Processor Projections

2.2 Real Aperture Radar (0.1 to 35 GHz)

While airborne coherent and noncoherent radars are relatively advanced, spacecraft radars have not yet been developed to their full potential. Airborne imaging radars were developed in the late 1950s for their reconnaissance capabilities by the military. Generally classified as Side Looking Airborne Radars (SLARs), these radar systems record data in an analog form on film strips, or the data are digitized and stored on magnetic tape. SLAR systems normally are designed to operate within the 0.1 to 35 GHz range. Development of sounding radars has taken place in the low frequency range (0.1-0.6 GHz). Sounding radars have been used to map areas under continental ice fields and subsurface geological features in dry desert areas. Present and future use of real aperture radar from space includes altimetry, scatterometry, ocean wave spectrometry, geological analysis and sounding. In these applications, high resolution is not required.

Technological developments are needed in high frequency, high power solid state transmitters/receivers as is discussed in the section on SAR. In addition, improvements in large space antennae, digital electronics, and signal processors, along with new methods of handling the radar echo data are needed. The basic technology description and forecast is provided in the SAR and antenna sections.

Radar component capabilities and available power sources are such that progress in achievable spatial resolution is paced mainly by available data handling rates with the ultimate spatial resolution determined by the size of practical antennas.

2.3 Antennas

Antenna technology is important, not only for real aperture and SAR radar but for all passive microwave through submillimeter wave instruments for remote sensing, such as radiometers and spectrometers. The spatial resolution is determined by the antenna dimensions and increases with antenna size. It is limited by practical considerations in construction and deployment of large antennas for use at specific frequencies. When coherence of the signal must be preserved, surface

quality and figure must also be considered. These requirements become more severe at high frequencies.

Figure 13 and Table 3 show the current level of development in terms of large satellite antenna technology. Additional technological solutions to problems in large satellite antenna development depends on the appropriate selection of antenna design. In selecting the best antenna design for any one microwave or radar system, careful consideration must be made with respect to:

- Packaging and remote deployment of very large structures
- Weight and size
- Surface and feed tolerance
- Differential thermal effects
- Precise attitude sensing and pointing control
- Sidelobe levels
- On-orbit verification and calibration testing
- Effect of spacecraft structure on antenna performance.

Any one of these foregoing factors could have severe impact on design technology or overall antenna system performance.

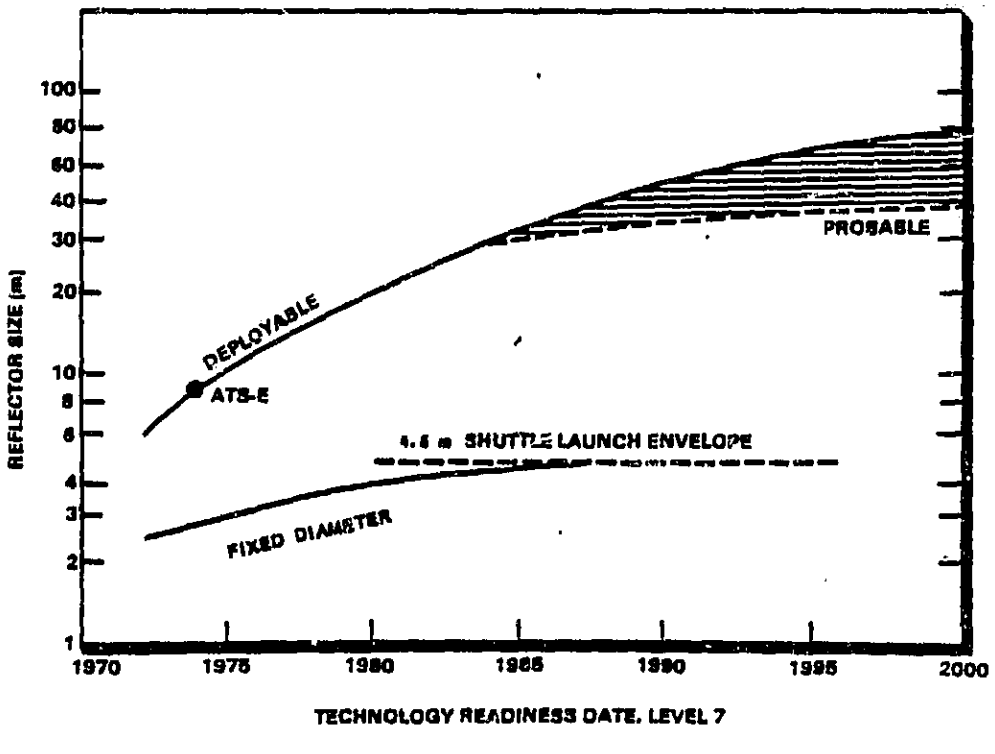

Figure 13. Antennas - Maximum Reflector Size

TABLE - 3

SUMMARY OF LARGE ANTENNA CONCEPTS

Concepts	Developers	Current or Potential Applications
Wrap - Rib	Lockheed Missile and Space Company	ATS-6 Satellite Recommended for NASA LSST
Wire Wheel/Tension Truss	Grumman Aerospace Corp.	Recommended for NASA OFT Experiment
Truss - Dish	Grumman Aerospace Corp.	Space
Radial Rib	Grumman Aerospace Corp.	Space
Hoop - Column	Harris Corporation	TDRSS Recommended for NASA LSST Alternate for NASA OFT Experiment
Truss - Hoop	Harris Corporation	Recommended for NASA OFT Experiment
Truss Radial - Rib Antenna Configuration (TRAC)	Harris Corporation	Recommended Alternate for NASA OFT Experiment
Geodesic	Harris Corporation	Space

The proposed antenna systems for space application are of two generic types: reflectors and phased array active lens. Reflectors can be of fixed dimensions or deployable. It may be necessary that large structures have surface configuration control in order to maintain specified beam quality. This requirement should be maintained at all times after deployment in space. This will impose strict requirements on packaging mechanisms and structure materials because of the desire for a lightweight system. Thermal and mechanical disturbances may require that structural deflection be sensed and controlled actively if passive methods are not adequate. In recent years several programs have been active in antenna concept investigation and concept applications. Most noted among these programs are the NASA LSST, the Applications

Technology Satellite (ATS-6), the advanced Application Flight Experiment, and the NASA Shuttle Orbiting Flight Test (OFT) program. Among these programs, no less than eight different antenna concepts have been investigated. A summary of these is presented in Table . 3, along with their developers and most recent usages. Of principle concern for use on space platforms is the size and weight of the antenna structure.

Antenna reflector size is forecast in Fig. . 13. To date, the largest reflector antenna in orbit is a 30-foot dish on ATS-6 (1974 launch). The upper curve shows the trend anticipated for deployable antennas using the ATS antenna as a base. Various approaches for deployable antennas are being investigated including flex-rib or ridged-rib/mesh, expandable truss/mesh, and segmented, folded rigid surface. Because of surface roughness considerations, the largest are expected to be most useful at frequencies below approximately 6-8 GHz. The trend for fixed antennas is illustrated in the lower curve. In this case, the Space Shuttle launch envelope is used as a upper size limit. Fixed reflector technology is directed toward the development of techniques for producing precise surfaces which can be used in a space environment at frequencies to 100 GHz.

Antenna weight as a function of fixed reflector diameter based on current technology is given in Fig. 14. In Fig. 15 a comparison is made between the weight for a fixed reflector system and that for a phased array system having the same aperture dimension. The reflector system which needs considerably more structure to achieve proper surface curvature and tolerances will be a heavier system.

Antenna gain which impacts the sensor system sensitivity is illustrated in Fig. . 16. Gain is plotted versus frequency for various antenna diameters. The foldover effect in the gain performance (Fig. 16) is due mainly to deterioration in the beam structure caused by a reduction in surface tolerance as the frequency is increased.

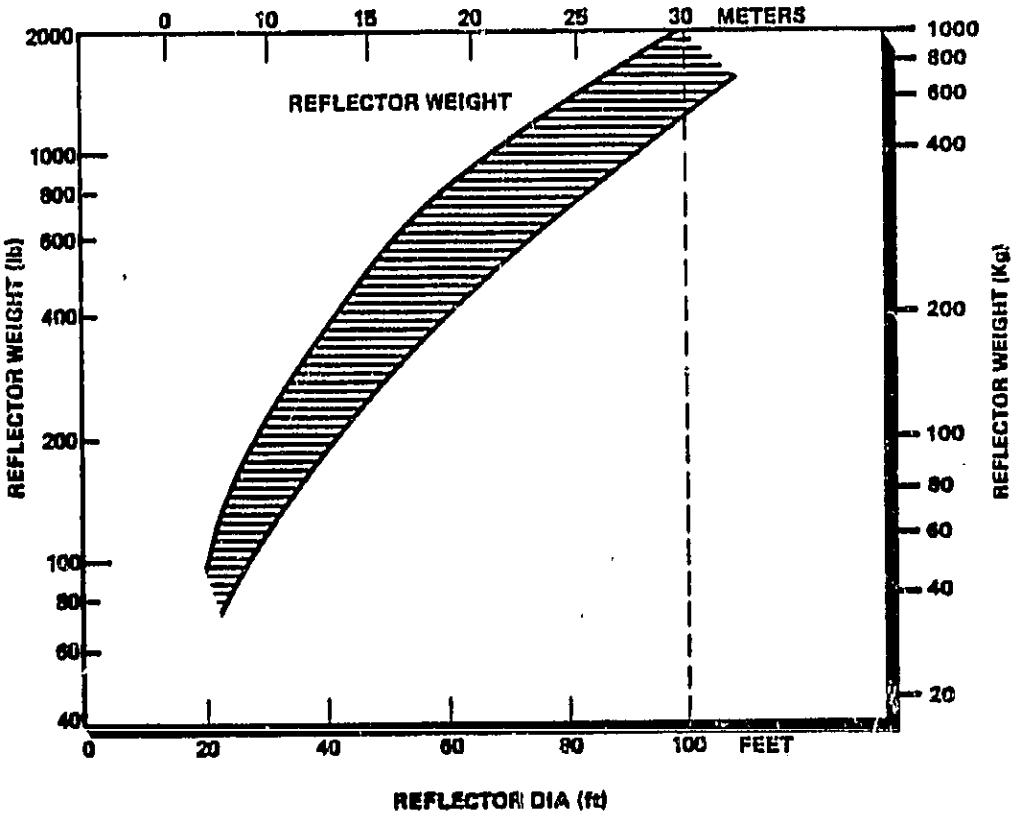

Figure 14. Reflector Mass vs. Diameter

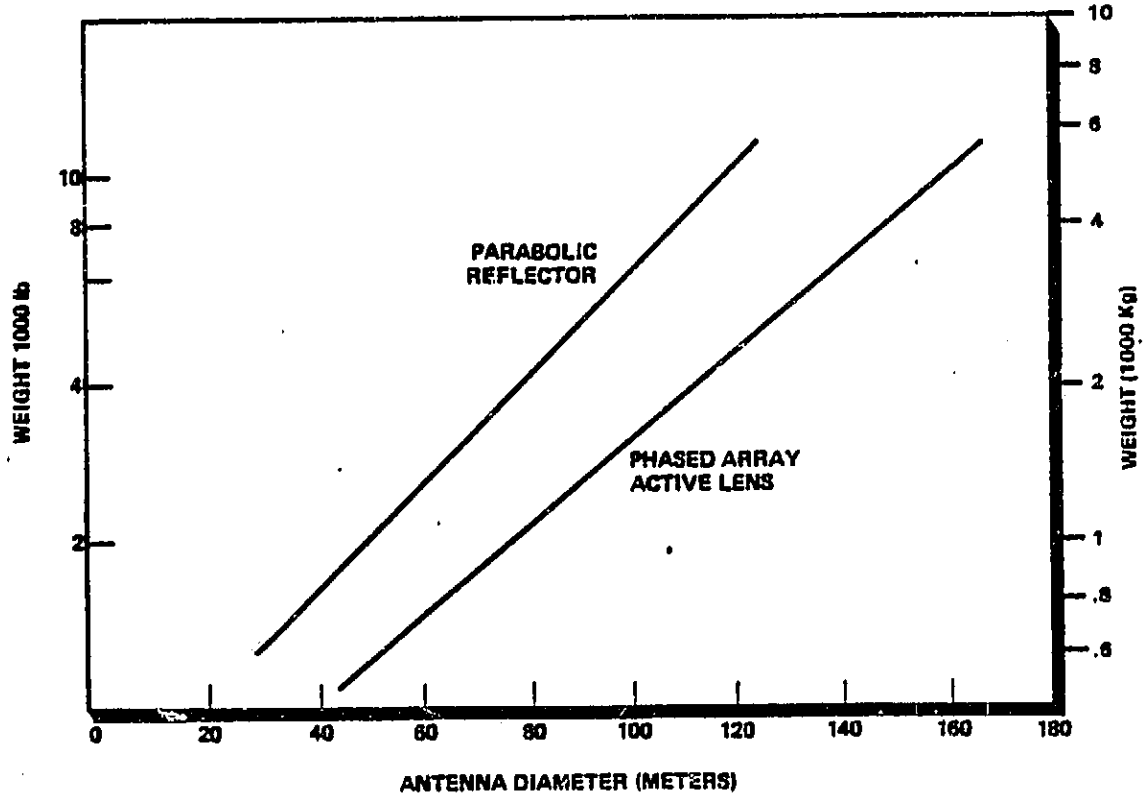

Figure 15. Weight Comparison of Single Reflector vs. Phased Array Antenna

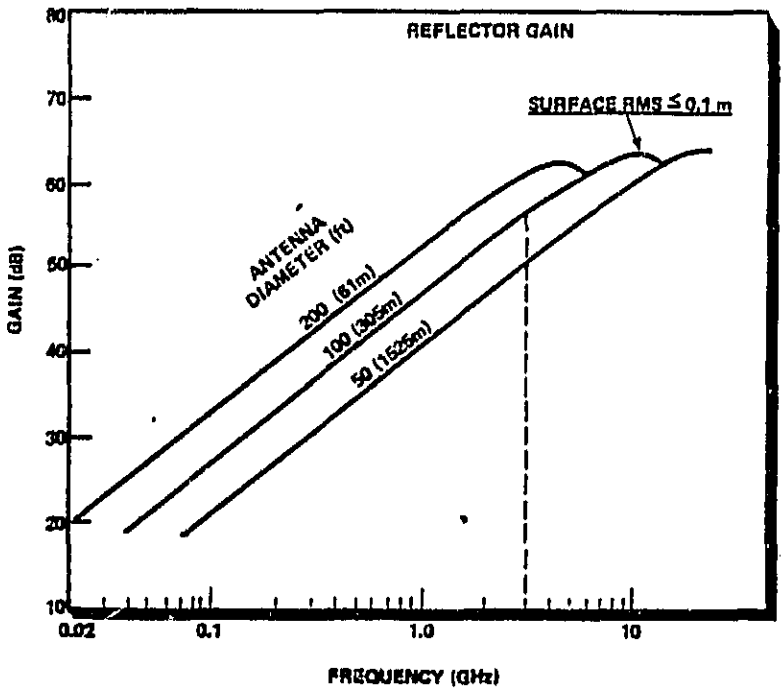

Figure 16. Antenna Gain vs. Frequency

2.4 Prominent Institutions and Individuals

Radar

NASA/Johnson Space Center
K. Krishen
J. Erickson

Jet Propulsion Laboratory
C. Elachi
W. Brown

Environmental Research Institute
of Michigan
R. Shuchman
J. Walker
R. Larson

3 PASSIVE MICROWAVE SENSORS

Passive microwave sensors consist of two generic types - broadband radiometers, used to determine basic environmental parameters such as temperature, ocean windspeed, ice pack concentrations, polar ice types, water vapor, precipitation and gross atmospheric temperature profile; and multi-channel-spectral radiometers with spectral line receivers (spectrometers) capable of measuring molecular line profiles from which molecular abundances, temperatures, pressures, winds, and other physical parameters of the region observed can be determined.

Broadband radiometers can be used to map the source (e.g., Earth surface) using various scanning techniques or multiple receiver arrays. Sensors that sound hot regions, such as the Earth's surface, have lower sensitivity requirements (higher system noise temperature) than sensors used for planetary upper atmospheric or astrophysical observations where relatively cool sources are studied against a cold background.

Passive radiometric systems have been used in experimental satellites such as Skylab, Nimbus, Tiros, and Seasat to demonstrate the feasibility of sensing atmospheric, ocean, ice, and land environments. Astronomical observation of galactic and planetary radio emissions were made by IMP, ISEE, RAE, and Mariner satellites. Millimeter wave heterodyne spectrometers using large ground based radio telescopes have provided data on molecular constituents of interstellar space, stars and planets. Spaceborne radio receivers have measured terrestrial molecular lines (O_2, H_2O) on Nimbus satellites. Very Long Baseline Interferometry (VLBI) in the microwave has been used to obtain nanoradian spatial information on astrophysical sources and measure distances on Earth to a few centimeters. A spaceborne VLBI network can further enhance these capabilities.

The principal subsystems of most microwave sensors are a collecting antenna, a heterodyne receiver and associated R.F. and digital electronics for data analysis. The heterodyne receiver is composed of a local oscillator, a mixer, preamplifiers and related electronics. For spectrometer applications a spectral line receiver must also be used to provide the power spectrum of the mixer output (the IF frequency).

3.3.1 Broadband Radiometers - Planetary Surface Sensors

Spatial information from remote measurements of planets can be best achieved through mapping of the observed region by scanning radiometers or staring arrays. The spatial resolution is determined by the antenna diameter and the wavelength of operation, and is approximated by:

$$\text{Footprint} \sim \text{Altitude} \times 1.2 \frac{\lambda}{D}$$

Antenna size versus spatial resolution for frequencies 1.4-94 GHz is given in Fig. 17.

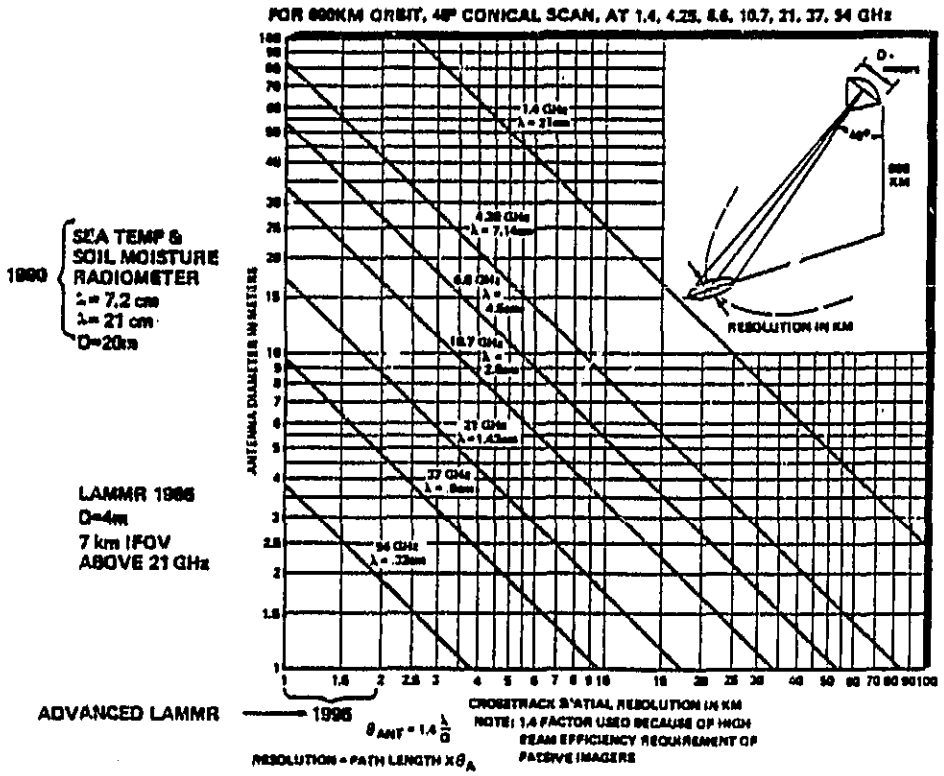

Figure 17. Antenna Size Versus Spatial Resolution

With the Space Shuttle, NASA has the capability of frequently launching several tens of thousands of pounds into the low-Earth orbit. With regard to remote sensing, there is no doubt that antennas of the order of 100 m in diameter operating in the 10-20 cm microwave band will achieve spatial resolutions approaching 1 km from low-Earth orbit. Conventional radiometry utilizing only one receiver in a cross-track scanning mode will, in general, not generate the imagery and coverage that the users of such data require. The difficulties are: (1) it is

prohibitive to move such a large antenna at the required scan rate; and (2) there is insufficient integration time available to collect accurate contiguous measurements while scanning. Arrays of microwave radiometers in the focal plane of the antenna can overcome these limitations. A plot illustrating the resolvable target size versus antenna diameter at 3 mm (100 GHz) wavelengths has been provided as Fig. . . 18. This figure is presented to illustrate what can be accomplished in terms of smallest target size resolved as a function of antenna diameter given a variable number of detectors operating at a nominal 300 km orbit.

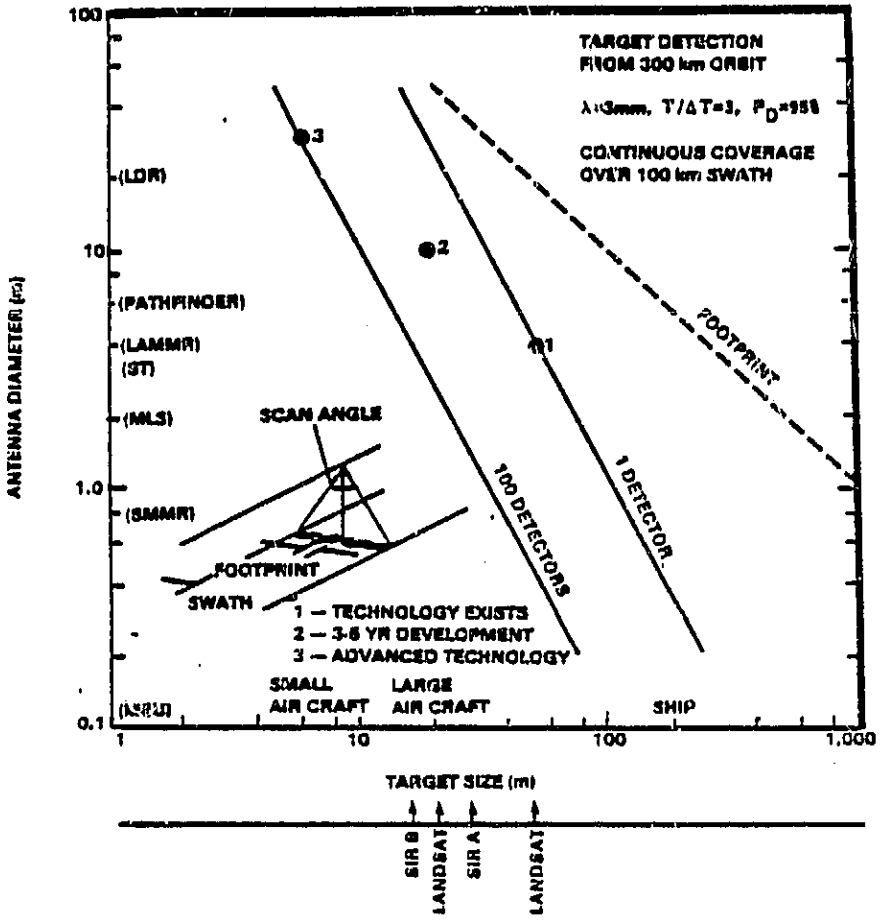

Figure . 18. Millimeter Wave Radiometric Antenna Size Requirement for Detection of Various Targets

One multidetector concept consists of using a linear radiometer array perpendicular to the orbital path of the spacecraft. Neighboring radiometers will then view adjacent contiguous pixels, generating a cross-track image swath. The image is then filled by the forward motion of the spacecraft. The advantages of this pushbroom concept are that no mechanical scanning of the antenna is required and the fixed, but squinted, receiver beams provide both swath width and sufficient integration time for accurate measurements of geophysical parameters.

3.1.1 Performance Parameters

Clearly technology challenges exist in both the design and deployment of large antennas and the development of multiple receivers with the performance parameters, weight and power consumption compatible with space applications. Projection of antenna development is given here and in Sec. 2.3 on antennas. Forecasts of L-band receiver input power requirements and weight are given as examples of these areas of development. A forecast of the development of multifrequency systems is also given.

Antenna Beamwidth (Fig. 19). This figure shows the expected decrease in antenna beamwidth that will be expected for L-band radiometers. Although it would be highly desirable to plot improved spatial resolution versus time, this is not possible because the relevant platform examples cited in the figure require various orbital altitudes, which impact the resultant resolution. The figure does, however, generally reflect improved spatial resolution versus time. For example, the 300 km orbit of Skylab resulted in a footprint of approximately 0.8 km, which is within the design target of 1 km.

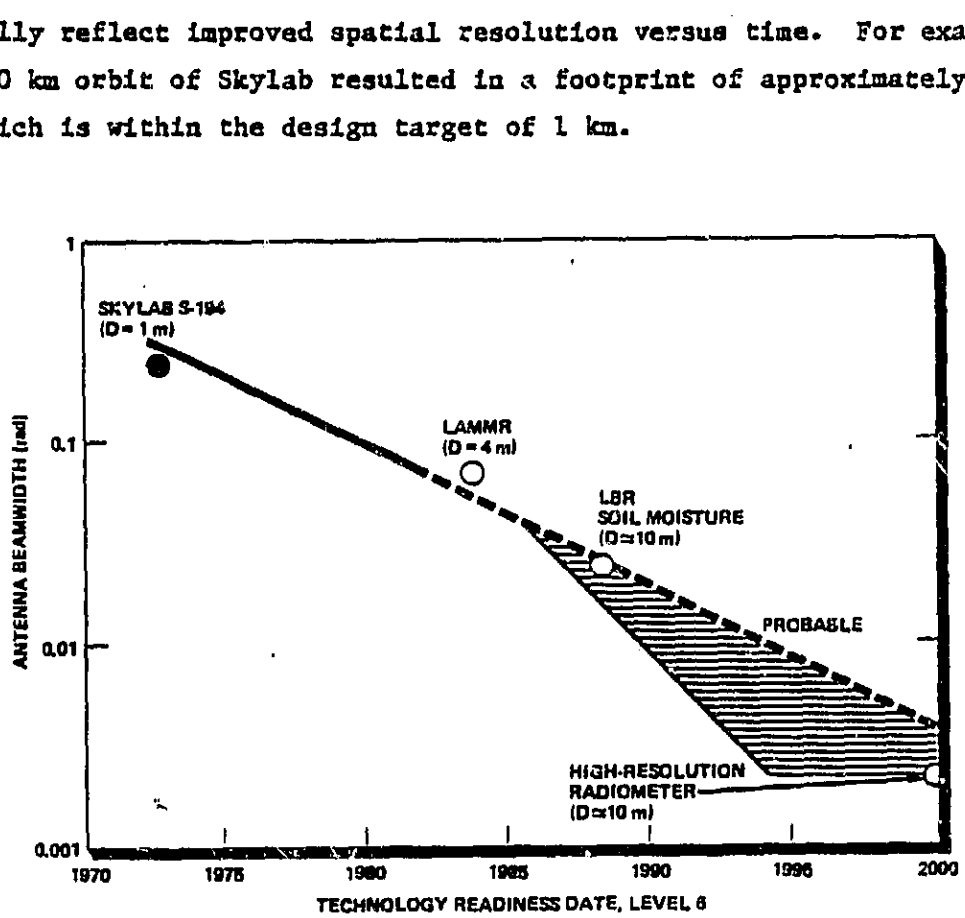

Figure 19. Antenna Beamwidth Projection

Radiometer Receiver Mass (Fig. 20). This figure shows the mass of a single radiometer ($f \leq 6.6$ GHz) versus time. The three points on the curves are actual masses for the case of the Seasat C-band SMMR, Nimbus 7 S-band (launched in 1978), and tight estimates for VOIR (Venus Orbiting Imaging Radar) L-band radiometers. We note from the figure that some modest mass reduction was achieved in the transition from Nimbus to Seasat due to a natural evolution of technology. It is expected that a reduction in size by a factor >5 will occur for units built in the 1985 time frame. When this technology is applied to the high-resolution microwave system, a mass reduction to 1.6 kg will have been realized. This reduced loading will also propagate a significant mass saving throughout the entire structural system.

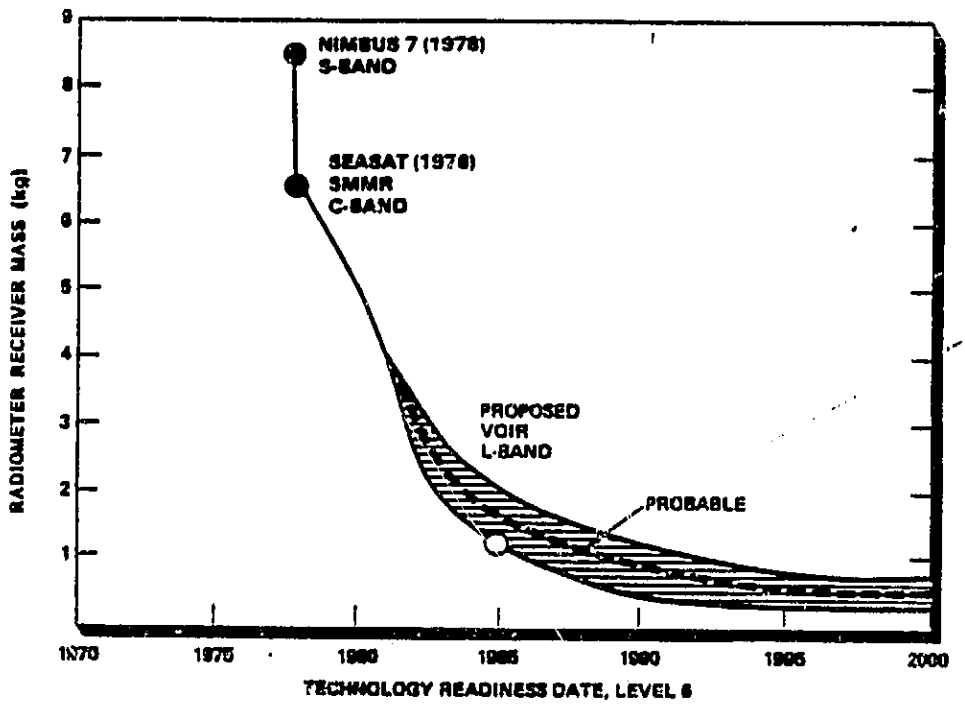

Figure 20. Radiometer Receiver Weight

Receiver Input Power (Fig. 21). This figure shows reduction in the required radiometer receiver input power versus time. As before, the points on the curve represent actual consumption of power, or that

based on hard estimates. A rather substantial drop in input power was realized as a result of improved efficiency in solid-state devices. A further reduction by a factor of 2 is expected by 1985. Future reduction will require developing means to improve internal thermal stability with less required raw input power.

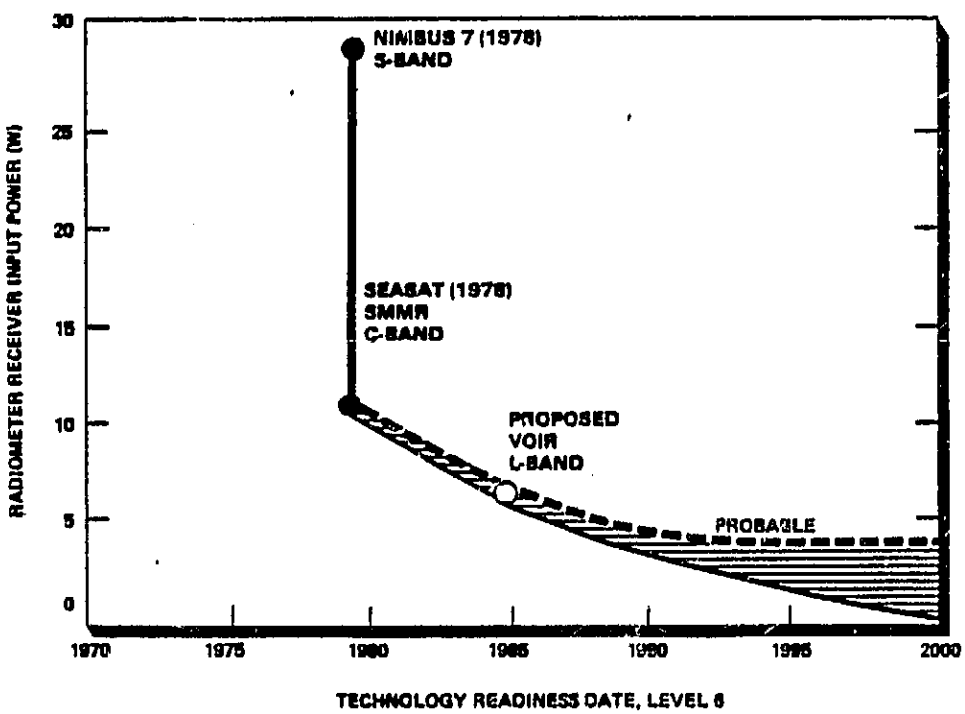

Figure 21. Receiver Input Power

Multi-frequency Operation. In addition to spatial data, multi-frequency information is important in the study of planetary surfaces and atmospheres. Large Antenna Multi-frequency Microwave Radiometer (LAMMR) concepts and system designs have recently been developed. The applications of this microwave imager technology in the various spectral bands with spatial resolution trends are shown in Fig. 22. The most significant changes in LAMMR concepts for the late 1980s and 1990s will require adding 15 GHz and 30 GHz radar channels for quantitative precipitation measurements over land with profile range gating capability.

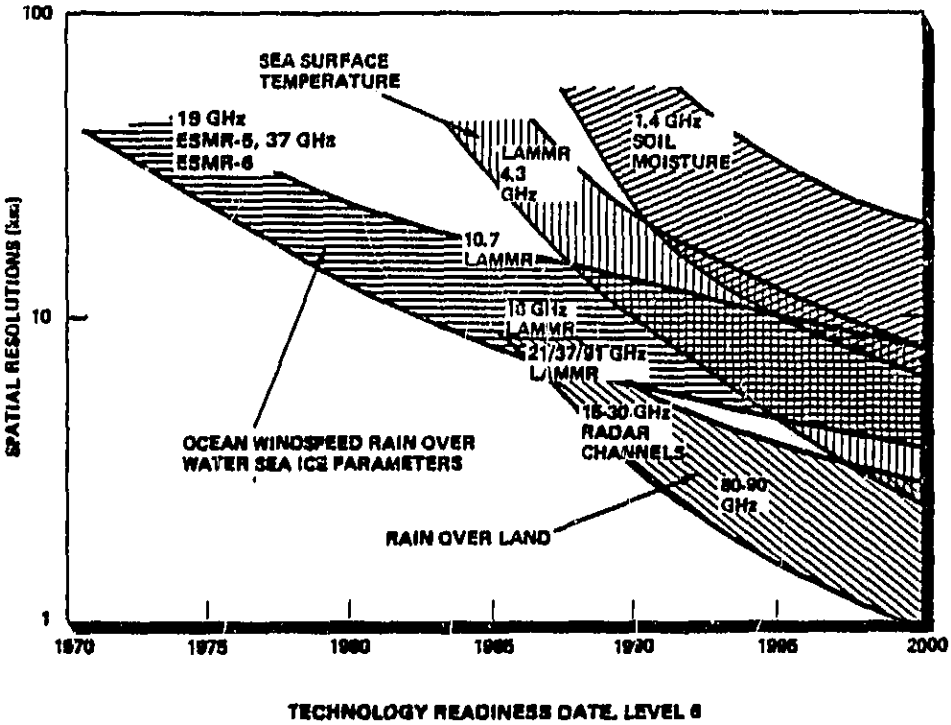

Figure 22. Spaceborne Passive Multifunction Microwave Imager Resolution Trends

3.1.2 Representative Instruments

Examples of representative broadband radiometers under development mainly for Earth and planetary remote sensing and forecasts of their performance parameters are given below.

Step Frequency Microwave Radiometer (SFMR) (41.7 to 66.7 mm). The SFMR is an instrument developed for the remote sensing of sea surface temperature, wind, wind speed, rain rate, and ice. It operates in a tunable mode utilizing either circular or linear polarization depending upon application. The system has a 20° beamwidth and a potential minimum detectable temperature difference on the order of 0.1 K to 1.0 K, depending upon the bandwidth and integration time used. Its dynamic range varies from 0 K to 310 K and front-end circuit losses are the predominant noise source. The SFMR has been tested by LaRC and found to be useful in the detection of hurricanes and ice packs. Projections for system sensitivity at bandwidths B=12 MHz and 0.5-second integration time, beam efficiency, and frequency coverage are given in Table 4.

TABLE 4

SYSTEM PARAMETER FORECAST FOR SFMR

Parameter	SOA Value	2000 Value	Theoretical Limit
Sensitivity B = 12 MHz τ = 0.5 sec	0.6K	0.4K	0.25K
Beam Efficiency (9 dB Level)	95%	98%	100%
Frequency Coverage	1.6 f_c f_c = center frequency	2.0 f_c	None

Critical subsystems include low-noise microwave amplifiers, low-loss PIN diode switches, stable microwave noise sources, and radiometer antennas. Two of these, low-noise microwave amplifiers and low-loss PIN diodes, are most important. Projections for these subsystems are presented in Table 5.

TABLE 5

PROJECTIONS FOR CRITICAL SUBSYSTEMS FOR SFMR

Critical Component and Characteristic	SOA Value	2000 Value
Low Noise Microwave Amplifiers (Noise Figure)	1.0 dB	0.5 dB
Low Loss PIN Diode Switch (Insertion Loss)	0.5 dB	0.2 dB

Pushbroom Microwave Radiometer (PBMR) (21 cm). The current prototype Pushbroom Microwave Radiometer (PBMR) was developed using the Step Frequency Microwave Radiometer (SFMR) as its baseline. This instrument was originally developed to serve as both a useful aircraft-borne remote sensing tool and an engineering model for investigation of the "push-broom" or nonscanning radiometer concept. The system operating at a center frequency f_c=1.43 GHz consists of a 3 or 4 beam antenna, four independent front-ends and a microprocesor based signal processing section which services all four radiometer channels and communicators to a data recording system over a single serial bus. The use of four radiometer front-ends allows each beam to be continually integrated providing improved sensitivity. This sensor is being used for salinity and soil moisture mapping. It has a dynamic range from 0 K to 310 K and a sensitivity of 0.6 K given that data are acquired and integrated over 0.5-second periods.

The PBMR has had a recent technology demonstration using aircraft. Space-borne systems utilizing this concept will require parabolic antennas with diameters on the order of 200 meters to achieve a footprint of one kilometer from low Earth orbit (LEO). The research goal is to achieve current and projected performance for this newer system that matches that of the SFMR (see Table ... 4).

High Spatial Resolution Millimeter Wave Radiometer (HSRMWR) (1.5-6.0 mm). This new system, under development especially for Earth remote sensing, is tunable to within 10 percent of its center frequency, will have a 10-meter picture element (resolution element) from low Earth orbit and represents a unique application of passive coherent radiometry. Its heritage is NEMS, SCAMS, MSO, SMMIR, and studies such as AMSO and LDR. Its application is high resolution thermal mapping of the Earth's surface. The resolution is comparable to that of Landsat. The HSRMWR's main advantage is the ability to penetrate clouds and acquire unique signatures of water, rain, ice, and metallic objects.

Critical parameters include spatial resolution (see Figs. 18 and 23) and temperature sensitivity. These are presented in Table 6.

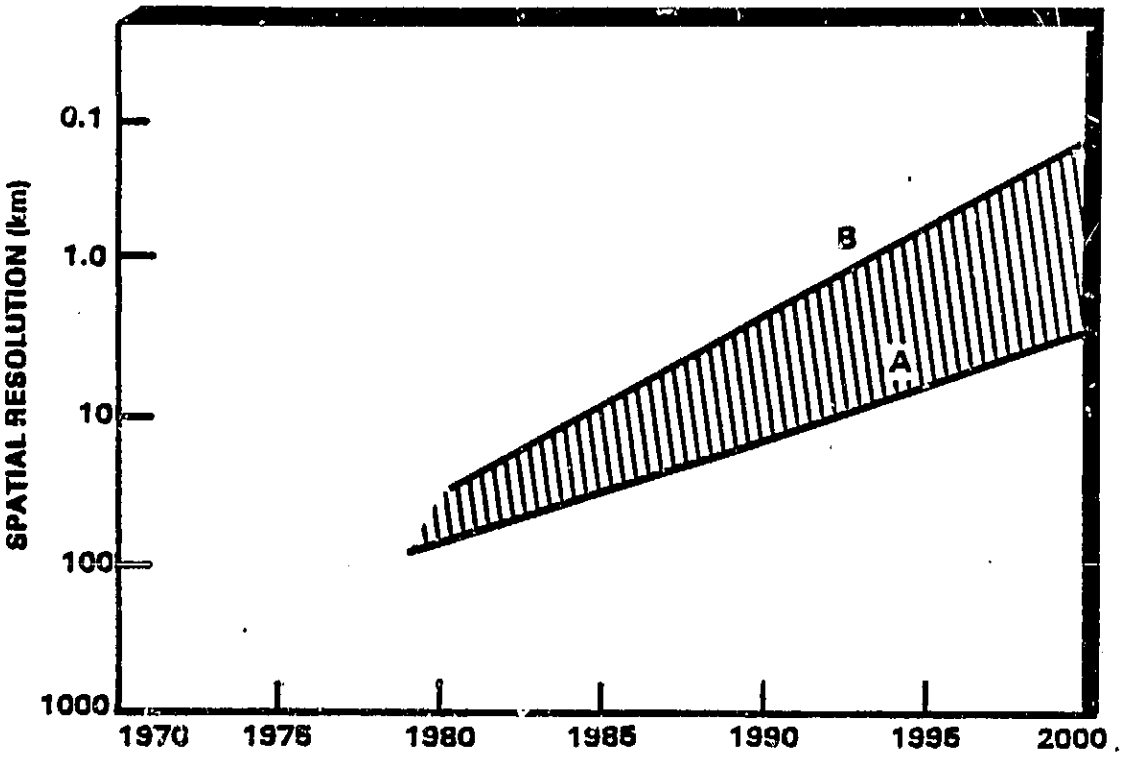

Figure 23. Projected Spatial Resolution Capability

TABLE 6

CRITICAL PARAMETERS FOR HSRMWR

Parameter	SOA Value	2000 Value	Theoretical Limit
Spatial Resolution	2-100 km	<50m	<5m may be practical limit
ΔT	1K	0.2K	~ 0.001K

Critical subsystems include the deployable reflector (20-meter diameter) and multiple feed arrays. The system is diffraction limited. A plot of the development of reflectors with diffraction limited resolution at λ = 3 mm is presented in Fig. 24.

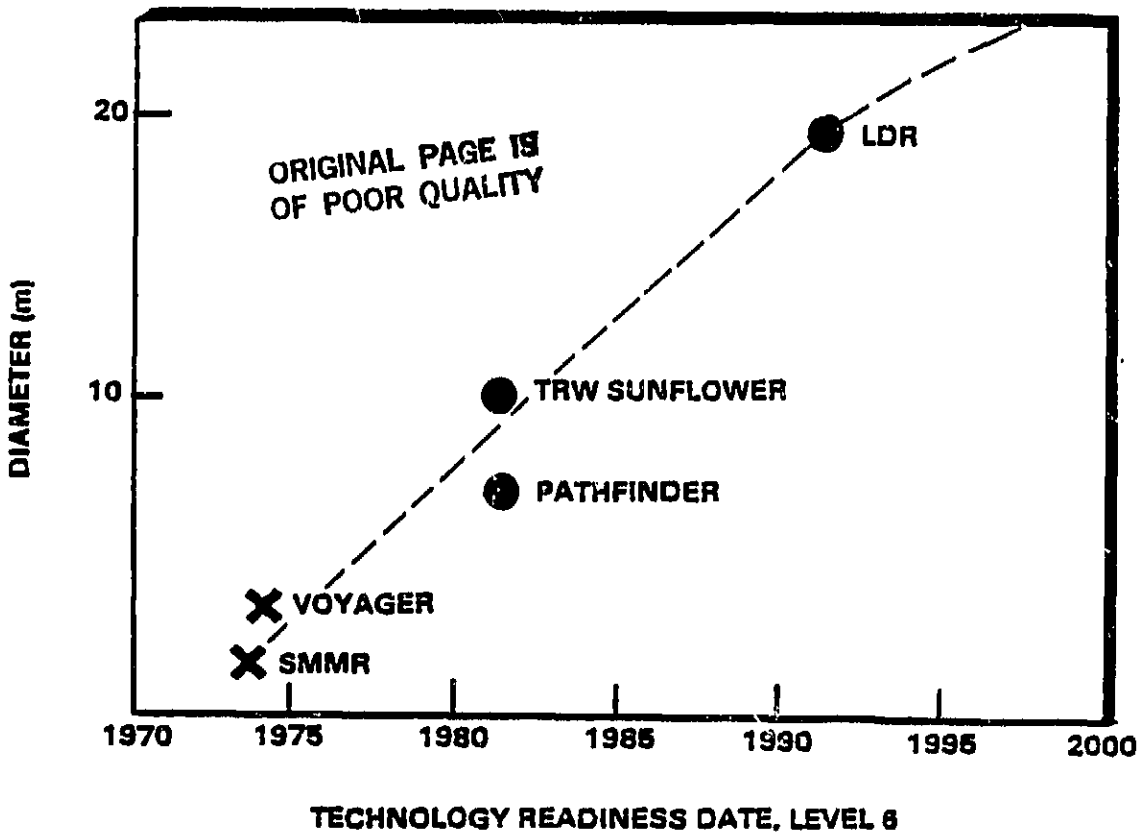

Figure 24. Reflector Capability Projection

It is projected that antennas using large segmented precision reflectors and arrays of detectors will be required for optimum operation. Linear arrays of up to 100 elements will be supplemented by rectangular arrays of up to 10^4 detectors for the best response. The driving program for the development of this instrument involves high-resolution mapping.

The forecast of parameters of components of importance are presented in Table . , 7.

Previous instruments such as SMMR had footprints or spatial resolution in the tens of kilometers. Gross features such as sea surface temperature could be determined but use over land was limited due to lack of spatial resolution. Increased resolution in the tens of meters would allow measurements of ice structure in bays, pollutants such as oil slicks near coastal zones, vehicle positions and velocities, ship positions and waves, crop identification, and snow fields.

TABLE . 7

PROJECTED VALUES FOR CRITICAL COMPONENTS

Critical Component and Characteristic	SOA Value	2000 Value
Graphite expoxy Sunflower antennas (Diameter)	4 m	30 m
Diameter/Wavelenth	40,000	400,000
Millimeter region feed arrays	1	200
Mixer Noise Temperature	T_R~1000 K	T_R~200 K
Local oscillators	Gunn diode	

3.2 Broadband Radiometers - Astronomy

Microwave systems applicable to astronomy and the measurement of cold sources include those relating to the study of cosmic background radiation. Two of these systems, the Differential Microwave Radiometer and the Far Infrared Spectrophotometer developed for flight on the Cosmic Background Explorer (COBE) satellite, are illustrative of instruments in this category and will be discussed further in the sections that follow. Both system and component performance parameters will be forecast. Since these are highly sensitive instruments system noise is limited by use of cryogenic cooling. A discussion and forecast based on improved cryogenic cooling capability is also given.

3.2.1 Passive Heterodyne Microwave Radiometer: Differential Microwave Radiometer (DMR) for COBE Satellite (3.33-9.55 mm)

This instrument has been specifically designed for the COBE satellite. Its purpose is to measure the anisotropy of the 3 K cosmic background radiation. The sensor operates discretely at 31.4, 53, and 90 GHz. It has a fixed but selectable operating frequency and the

bandwidth can be either 500 MHz or 1000 MHz. The dominant noise sources are noise due to mixer electronics and antenna sidelobes. The figure of merit for the system is the Noise Equivalent Temperature T* given in mK $sec^{1/2}$. T* ~ 20 mK $sec^{1/2}$ with sidelobes at 80^{o} off-axis reduced by 80dB from the main lobe.

The sensor is of standard Dicke design; i.e., it uses a switched microwave radiometer comparing two antennas pointed 60^{o} apart (the spacecraft rotates at 1 RPM to scan the sky rapidly). Antennas are of ultra-low-sidelobe design using corrugated hybrid mode horns, developed at JPL and UC, Berkeley. The receiver is of the standard heterodyne type with Schottky mixer diodes and Gunn diode local oscillators, with transistor or GaAs FET IF amplifiers. Mixer and preamp are radiatively cooled to 140 K for 53 and 90 GHz systems to reduce noise. All channels use ferrite Dicke switches, and all have active temperature stabilization. The design of this system is a follow-on to the original UC, Berkeley version flown on U2 aircraft. JPL and Princeton have also developed models. It is projected that the system will be in continuous operation for 1 year during which time a thermal differential sky map can be generated.

The receiver noise equivalent temperature is projected in Fig. 25 and the radiometer sensitivity and antenna sidelobe reduction parameters are projected in Table 8.

Critical subsystems include mixers, IF amplifiers, local oscillators, antennas, and latching ferrite circulators. Projections for these subsystem elements are presented in Table 9.

No additional research is necessary to fly a 20mK $sec^{1/2}$ system in 1987 on COBE. Substantial funds would be needed to make cryogenic receivers flightworthy, both on the receivers themselves and on cryogenic systems that could support the power dissipation. The cryogenic superconducting/mixer receivers themselves are still mostly laboratory phenomena and not thoroughly proven.

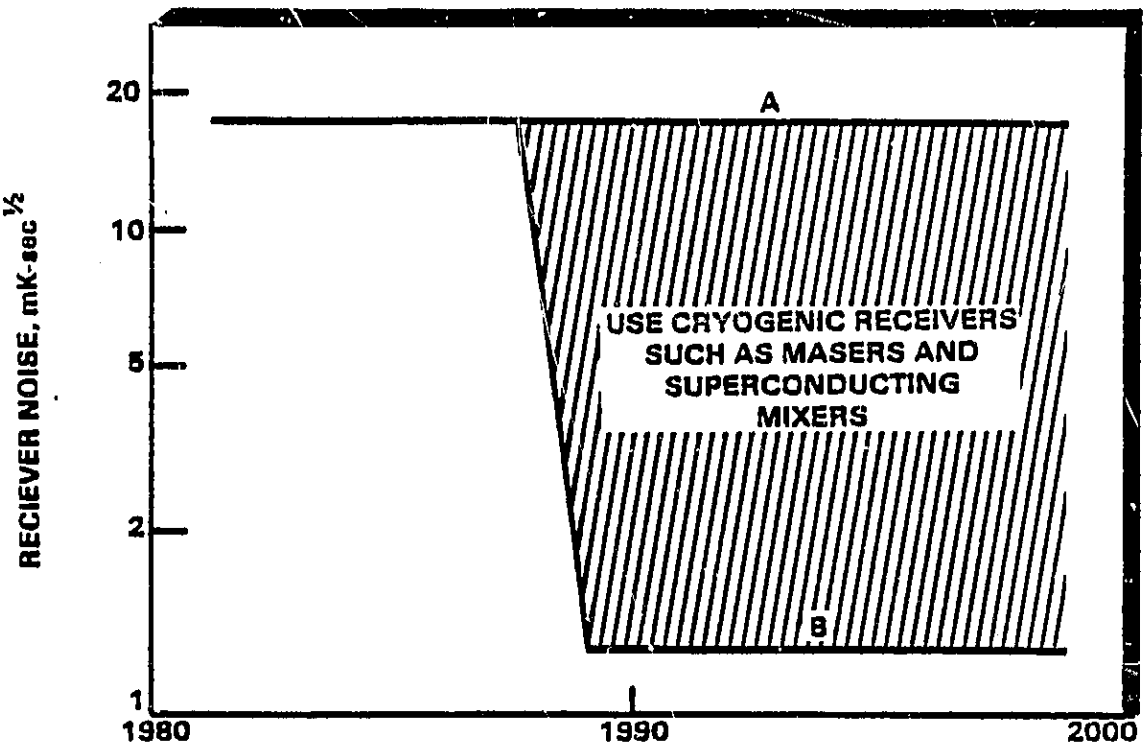

Figure 25. Projection of DMR Receiver Noise

TABLE 8

CRITICAL PARAMETERS FOR COBE RADIOMETER

Parameter	SOA Value	2000 Value	Theoretical Limit
Radiometer[a] Sensitivity for space systems	20mK $sec^{1/2}$	1mK $sec^{1/2}$	~0.2mK $sec^{1/2}$ at 100 GHz, BW=1 GHz
Antenna[b]	-80dB	-120dB	None

(a) Radiometer sensitivity could be improved with cryogenic maser amplifiers or SIS (superconducting) mixers. The 2000 value is nearly achievable in the laboratory now, and might be spaceworthy (given major funding) by 2000. It is not known how to achieve the theoretical limit set by quantum noise.

(b) The antenna sidelobes can be improved by careful design of attenuating flares, but it is hard to test well enough to prove performance.

TABLE 9

MIXER, ANTENNA, AND CIRCULATOR PROJECTIONS

Critical Component and Characteristic	SOA Value	2000 Value
Mixer DSB Noise Temp @ 90 GHz	200 K @ 20 K	50 K @ 20 K
Antenna Sidelobes	-80 dBm	-20 dBm
Latching Ferrite Circulators Loss per Junction @ 90 GHz	0.4 dB	0.2 dB

It is presently believed that the COBE sensitivity will reach the limits imposed by our astrophysical environment, which has galactic sources of diffuse microwave radiation. However, the results of the COBE mission might point out some particular frequencies or lines of sight that should be better studied, where local interference might be less and better receivers will be of additional benefit.

3.2.2 Far IR Spectrophotometer (0.1-10.0 mm)

The COBE project will use a Far IR Absolute Spectrophotometer (FIRAS) to measure diffuse background radiation in the 1 to 100 cm^{-1} spectral region. Unlike millimeter wave systems discussed previously, this instrument does not use heterodyne detection and provides some spectral resolution. It extends visible and infrared techniques into the submillimeter and millimeter region. The system consists of a Fourier transform far IR spectrometer, based on the Martin-Puplett polarizing Michelson interferometer. It is operated in a rapid scan mode and has a mean spectral resolution of 0.2 cm^{-1}. Its balanced symmetric design allows differential operation comparing sky input to a reference blackbody. It uses a separate external blackbody calibrator and is cooled to liquid helium temperature (1.5 K) to reduce instrument thermal emission and to get good detector sensitivity. It uses compos-

ite (large area) bolometer detectors and has a large etendue (throughput) to handle long wavelengths efficiently. Active temperature control of the blackbody reference, the blackbody calibrator, and the antenna is maintained. It employs a non-imaging flux concentrator (Winston cone) antenna with flared mouth to reduce diffracted sidelobes.

The spatial resolution of the system is 7^{o} and its dominant noise source is detector noise and charged particle impacts. Its performance is limited by accuracy of calibration for input flux (νI_{ν}) and by antenna sidelobes from diffraction. Its response is strongly frequency-dependent. The system sensitivity is described by the Noise Equivalent Radiance (NER) which is $\sim 10^{-13}$ W cm^{-2} sr^{-1} for each spectral element for $2 < \nu < 20$ cm^{-1}.

The blackbody calibrator accuracy which determines the system sensitivity has been plotted in Fig. 26.

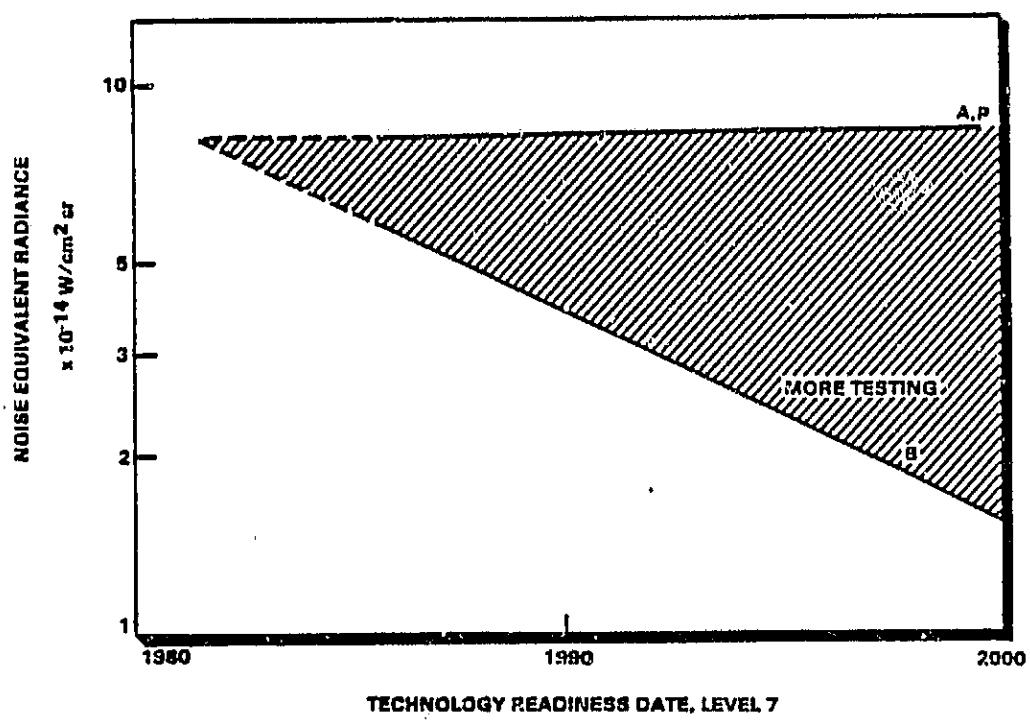

Figure 26. Blackbody Calibrator Accuracy in Units of $\nu I_{\nu} = 10^{-14}$ W cm^{-2}sr^{-1} at T = 3 K

The spectral resolution is determined by the instrument size (retroreflector travel) and is forecast in Fig. .-27 for operation at 10 cm^{-1}. System physical parameters are given in Table .-10.

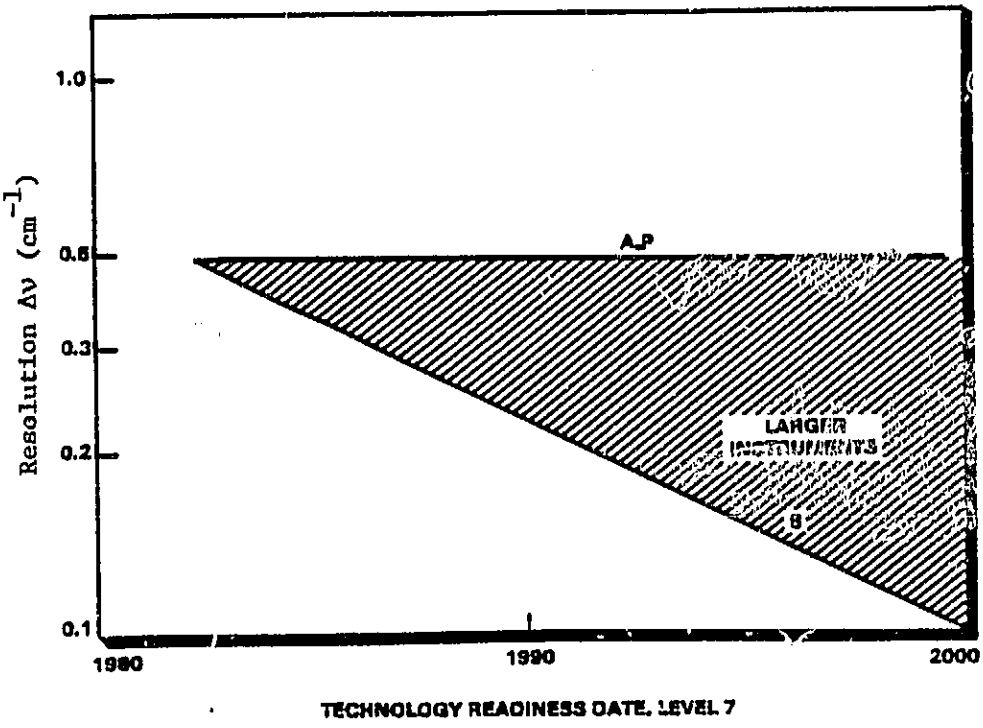

Figure .-27. Spectral Resolution at ν = 10 cm^{-1}

TABLE .-.10

FIRAS PHYSICAL PARAMETERS

Parameter	1990 Value
Weight	60 kg cooled optics 50 kg warm electronics
Size	70 cm diam. x 2 m long (optics)
Power Requirement	85 W
Cooling	1.5 K (optics)
Data Rate	1400 bps

The critical system components include detectors, calibrators, antennas, and cryogenic cooling systems. A forecast of detector bolometer noise equivalent power (NEP=input signal power which yields a signal to noise ratio of unity) is given in Fig. 28, and along with the calibrator emissivity in Table 11.

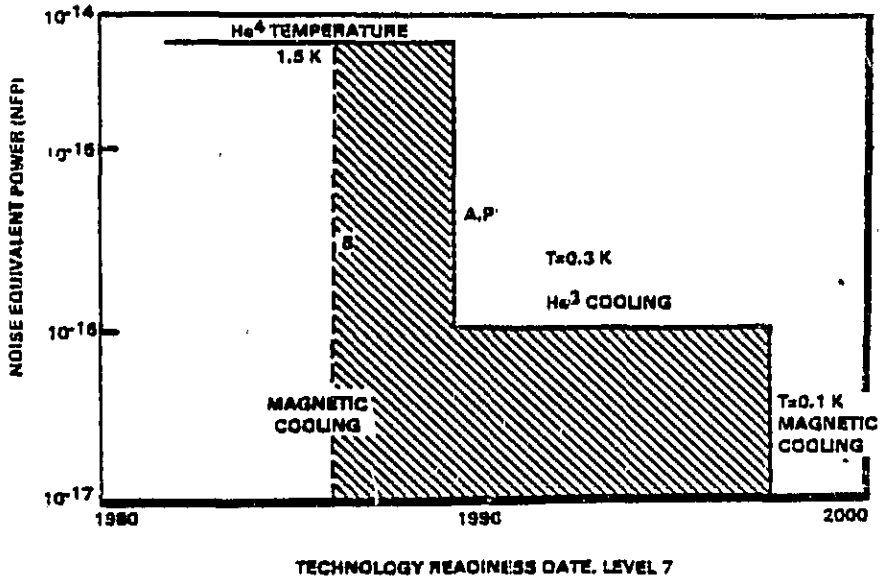

Figure 28. Detector Sensitivity for Large Far IR Bolometers (>0.25 cm^2) for Space Use

TABLE 11

BOLOMETER NEP AND CALIBRATOR EMISSIVITY PROJECTIONS

Parameter	SOA Value	2000 Value	Theoretical Limit
Noise Equivalent Power (NEP) for large (0.25 cm^2) bolometer[1]	10^{-14} W/$Hz^{1/2}$	10^{-17} W/$Hz^{1/2}$	Set by available ambient temperature
Calibrator Emissivity[2]	99.99%	99.9999%	1.0

[1]NEP limit: not required for COBE since long life allows repeated observations. For higher spectral or angular resolutions, achievable with a larger instrument, a better detector would be needed.

[2]Calibrator blackness (emissivity): designs exist but have not been tested.

The beam width for a cryogenic low sidelobe antenna is determined by the antenna size. To achieve ultimate system sensitivities substantial cooling will be needed. A forecast is given in Fig. 29. To achieve the optimum detector and system performance shown by the figures, increased support is needed to build flight coolers based on laboratory instrumentation for very low temperature far IR detectors. The other improvement required would be a much larger instrument volume in the cryostat. Detectors are cooled now by boiling liquid helium at 1.5 K. The rare isotope ^{3}He can reach 0.3 K. Adiabatic demagnetization coolers have reached 10^{-3} K in the laboratory, but achieving this temperature is not possible in space due to heating by energetic charged particles.

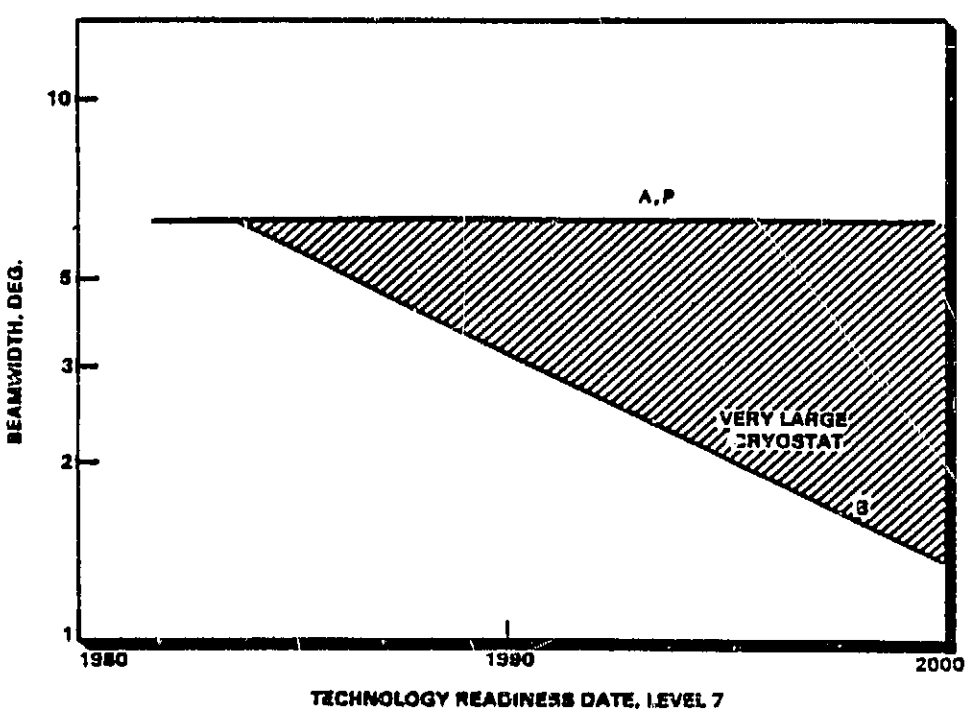

Figure 29. Beamwidth for Cryogenic Low Side Lobe Antenna (Governed by Physical Size) at 10 cm^{-1}.

Projected cryostat capabilities are illustrated in Table 12.

TABLE . 12

CRYOGENIC COOLER TEMPERATURE PROJECTION

Critical Component and Characteristics	SOA Value	2000 Value
Cryogenic Detector Cooler Temperature	1.5 K	0.1 K

3.3 Millimeter and Submillimeter Heterodyne Radiometers for Spectroscopy

The importance of millimeter and submillimeter heterodyne radiometers with multichannel spectral line receivers for atmospheric measurements from space is now well established. The first such radiometers in space operating near 5 mm wavelengths were flown on the experimental Nimbus 5 and 6 satellites to determine whether the techniques could provide useful data on atmospheric temperature profiles in cloudy regions. Following the success of the Nimbus experiments, a 5 mm heterodyne radiometer is being used for operational meteorological purposes on the TIROS-N satellites. Extending the operating range of the heterodyne radiometers to the shorter millimeter and submillimeter wavelengths will allow important measurements to be made of upper atmospheric species and physical parameters (e.g., temperature and winds). Because these radiometers can measure atmospheric thermal emission, they can provide data at any time of day or night--an important feature for understanding upper atmospheric processes.

Such instruments are also powerful tools for the study of astrophysical sources as has been shown from ground based millimeter wave observations. Measurement of molecular emission lines and astrophysics masers at spectral resolving powers $\lambda/\Delta\lambda \sim 10^6$ has become routine. There have been over 55 molecular species detected in interstellar space. Submillimeter frequencies are greatly absorbed by the Earth's atmosphere and future development of spectral line receivers for space lie in these spectral regions. Large orbiting telescope facilities such as the Large Deployable Reflector (LDR) can be used to make observations in the millimeter and submillimeter regions from space.

Since the goal is to measure weak emission from relatively cold regions the emphasis is placed on optimization of system sensitivity. Sensitivity is related to the system noise temperature at the input to the mixer and with present technology generally improves at cm wave frequencies. The noise temperature is the equivalent temperature of a blackbody thermally radiating the same power per unit spectral interval as the radiometer noise power. From the radiometer noise temperature, T_N, the sensitivity T can be calculated from the expression

$$\Delta T = \alpha T_N/(\tau\Delta f)^{1/2}$$

where α is a constant which describes losses in front of the mixer and any effects due to chopping the input signal, τ is the integration time, and Δf is spectral resolution. The spectral resolution of heterodyne radiometers is determined by intermediate-frequency (IF) electronics, and can be made arbitrarily fine up to a limit of $\sim\tau^{-1}$.

3.3.1 General Forecast

General forecasts of the noise temperature of radiometers from 5 mm to 0.1 mm are given below. Descriptions and performance parameter forecasts of several critical system components follow. Specific examples of systems under development are then used to illustrate the technology trends.

Noise Temperature for 5 mm Wavelength Radiometers (Fig. 30). Radiometers at this wavelength have been flown on Nimbus and TIROS satellites. These radiometers used Shottky-barrier diodes and transistor first stage amplifiers. Reduction in noise temperature can be achieved by cooling the mixer, using new devices such as Josephson junctions, Superconductor-Insulator-Superconductor (SIS) or quasi-particle mixers, or low-noise (maser) amplification at the signal wavelengths. Local oscillators for these radiometers can be Gunn or IMPATT solid-state devices for which current technology is adequate.

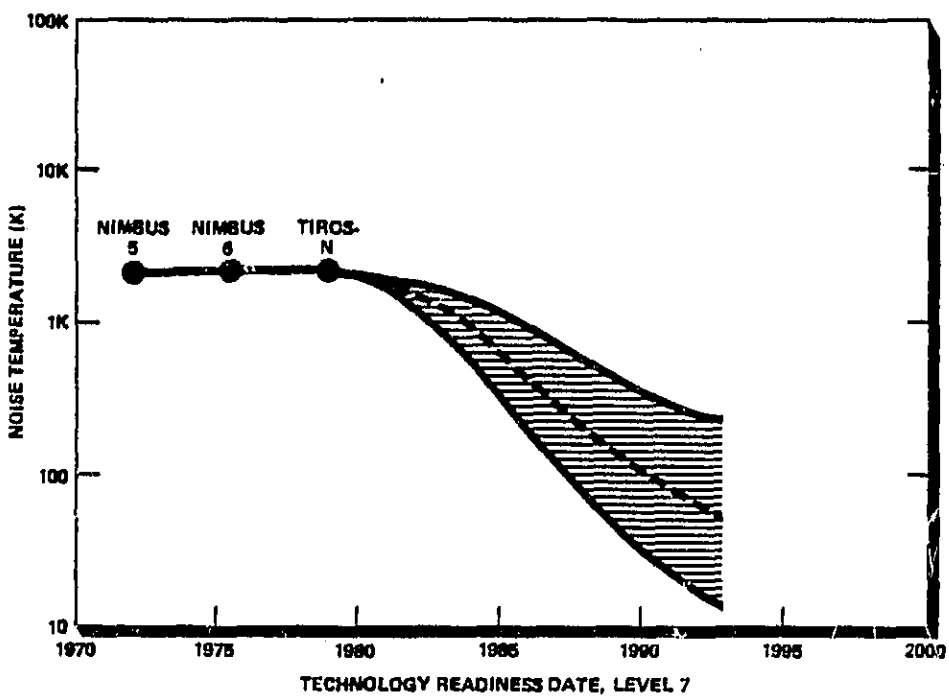

Figure 30. 5 mm Wavelength Heterodyne Radiometer Noise Temperature

Noise Temperature for 1 mm Wavelength Radiometers (Fig. 31). Present technology for 1 mm wavelength radiometers falls into two major categories. Uncooled broad bandwidth mixers using Schottky diodes can achieve noise temperatures of a few thousand Kelvins, and narrow-bandwidth mixers using "hot electron" InSb mixing at liquid helium temperatures can achieve noise temperatures of a few hundred Kelvins. Both devices could be made ready for a space test in the mid-1990s. The local oscillator is a more serious problem for the Schottky mixer (which

requires ~10^{-2} W) than for the InSb mixer (which requires ~10^{-5} W), whereas the cooling requirements are more severe for the InSb. For the Schottky mixer, either electron tubes (reflex klystrons or backward-wave oscillators) requiring ~0.5 kW power supply or less well developed solid-state systems could be used for the local oscillators. Improvements in noise temperature can be achieved by cooling and improving the coupling and diodes for Schottky mixers and by using Josephson or quasi-particle mixers which are now under development.

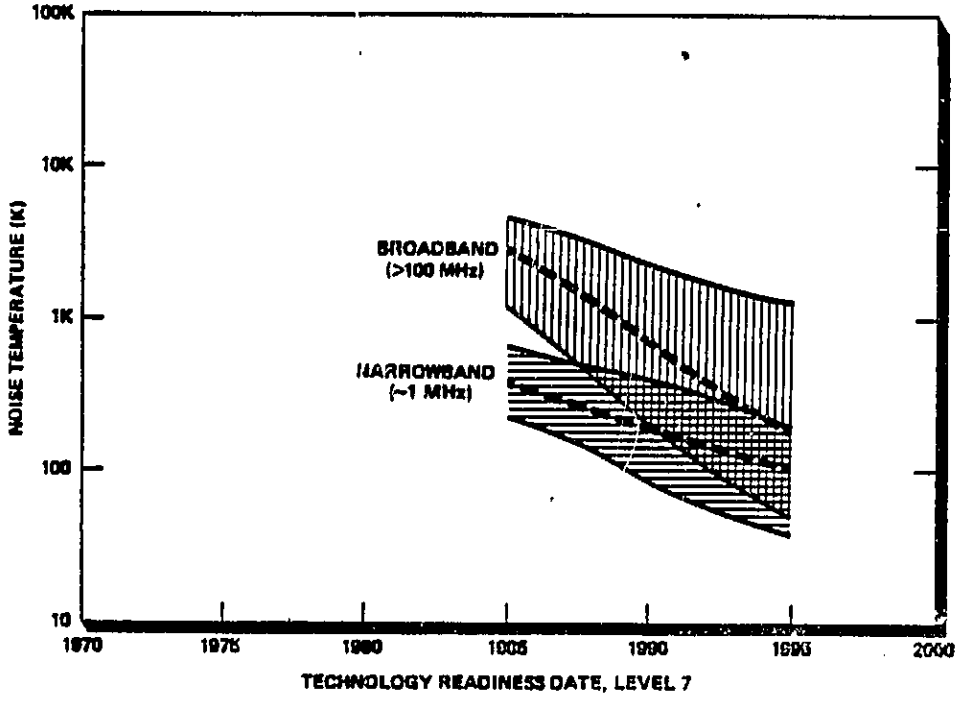

Figure 31. 1 mm Wavelength Heterodyne Radiometer Noise Temperature

Noise Temperature for 0.5 mm Wavelength Radiometer (Fig. 32). Laboratory tests have indicated that uncooled Schottky diode heterodyne radiometers with noise temperatures of a few ten thousands of Kelvins and Cryogenic InSb hot electron radiometers with noise temperatures of several hundred Kelvins are feasible. Such radiometers could be tested in space by the middle 1990s. Local oscillators for the Schottky

radiometer and cryogenic coolers for the InSb radiometers which are suitable for space must be developed. Improvements in performance can be achieved by cooling the Schottky diodes and improving the coupling of the radiation to the diodes and the diode performance. The development of quasi-particle and, perhaps, Josephson junction and SIS mixers should also improve the performance.

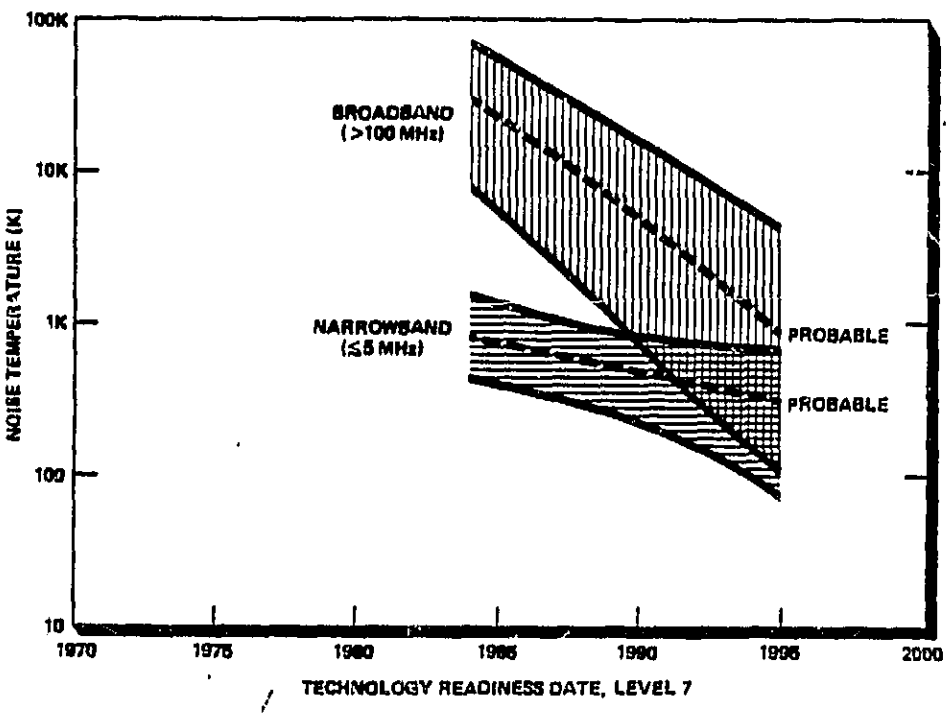

Figure 32. 0.5 mm Wavelength Heterodyne Radiometer Noise Temperature

Noise Temperatures for 0.1 mm Wavelength Radiometers (Fig. 33). It seems likely that broadband Schottky diode radiometers, with present technology, could achieve noise temperatures of the order of 100,000 K and narrowband photoconductor mixers could achieve noise temperatures of a few thousand Kelvins. However, this is very speculative as mixers at these wavelengths are only in the pioneering development stages. The only local oscillators available at these wavelengths are optically pumped gas lasers which require development for space use. With adequate research and development, however, it should be possible by the mid 1990s to have heterodyne radiometers at 0.1 mm wavelength with the

same quantum efficiency (~0.3) as has been achieved in the middle infrared. This corresponds to a few hundred Kelvins of noise temperature.

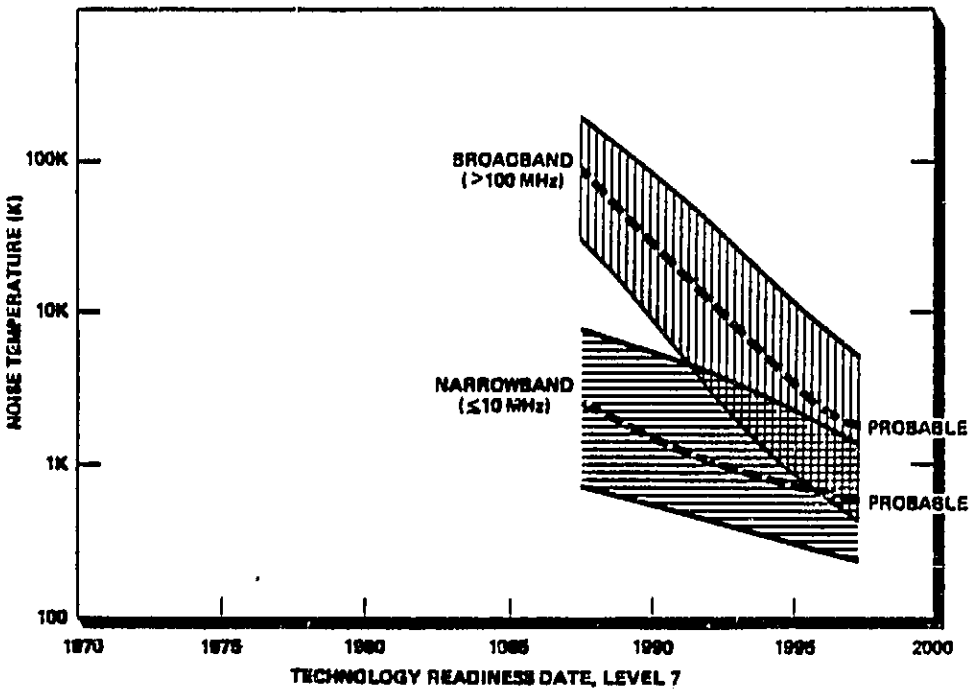

Figure 33. 0.1 mm Wavelength Heterodyne Radiometer Noise Temperature

3.3.2 Critical System Components

Critical components for millimeter and submillimeter heterodyne radiometers for spectroscopy are:

- Mixers - uncooled and cooled
- IF amplifiers - uncooled and cooled
- Local oscillators - solid state, tubes, lasers (for submillimeter)
- Quasi-optical components (couplers)
- Cryogenic refigerators
- Spectral line receivers (RF filter banks, Acoustic-Optic Spectrometers)
- Diffraction limited antennas

System noise is primarily determined by the mixer noise temperature. Schottky diode and superconducting devices such as SIS and Josephson junction mixers are applicable in these spectral regions.

Mixers - GaAs Schottky Diode. Schottky diode mixers are well established in the microwave and millimeter wavebands and have been successfully used in the submillimeter region. These mixers will be used in the majority of millimeter and submillimeter heterodyne receivers for the foreseeable future. Receivers using GaAs Schottky mixers cover the 300 μm to 1 cm spectral region. The instantaneous bandwidth can be up to 5% of the operating frequency. They are limited in performance by current diode technology, circuit design, and IF amplifier sensitivity. Receiver noise temperature T_R is the best single system descriptor. Noise comes in the form of shot noise, thermal noise, and electron scattering. Figure 34 presents the state of the art for Schottky diode mixer receiver sensitivity and a projection for the year 2000.

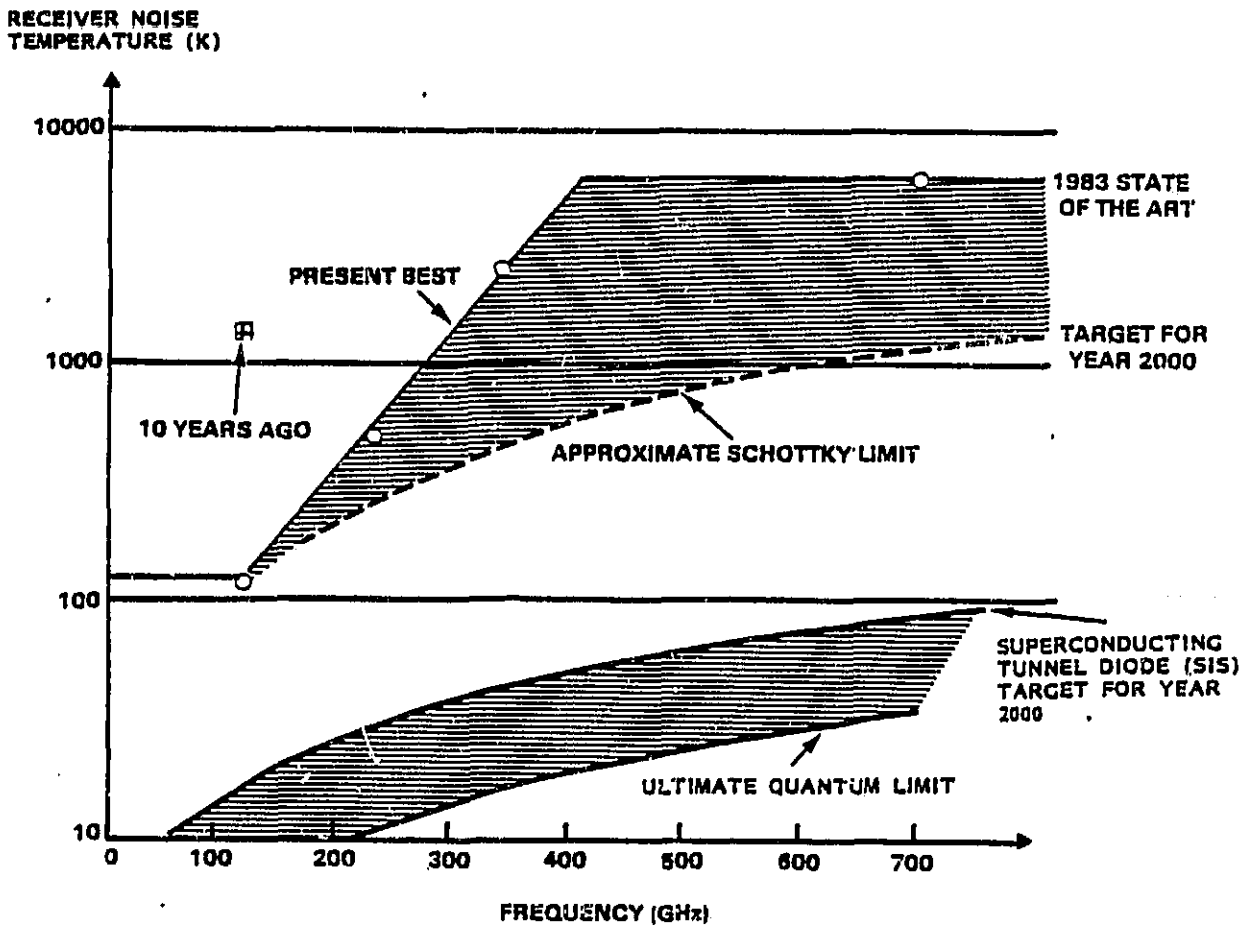

Figure 34. Receiver Sensitivity: State of the Art

Mixers - Superconductor-Insulator-Superconductor (SIS). The SIS mixers are superconducting tunnel diodes invented in 1979. These devices are presently under study and development. They cover the 300 μm (0.3 mm) to 1 cm region of the spectrum. The instantaneous bandwidth is >500 MHz with projected improvement to ∿10 GHz. Cooling to 4 K is required and this provides some limitations for use in space.

The mixer performance can be measured by the receiver noise temperature T_R. An SIS mixer receiver with solid-state local oscillator and cryogenic GaAs-FET IF amplifier can be tuned over 20% of the operating frequency and is currently shot noise limited. It is projected that as these devices mature overall receiver sensitivity will approach the fundamental quantum limit. Thus, SIS mixers would provide the ultimate in sensitive coherent detectors for NASA's future space applications in the millimeter and submillimeter bands.

The receiver sensitivity is plotted in Fig. -34. No attempt has been made to present here anything except state of the art as of 1983 and the target performance using SIS devices for the year 2000. At present, there are no coherent detectors for mm and sub-mm bands with sufficient sensitivity to take full advantage of remote sensing above the Earth's atmosphere. Such programs as the Space Platform, the Large Deployable Reflector, and selected Space Shuttle experiments can be used with SIS detectors to remedy this situation.

IF Amplifiers. These are critical components that are integral parts of the mixer. Noise in IF amplifiers contributes to the system noise temperature. The instantaneous system bandwidth is determined by the IF frequency response. GaAs FET IF amplifiers cooled to cryogenic temperatures can meet most performance requirements in the future. Work on extending their bandwidth (to ∿10 GHz), impedance matching to the mixer, and overcoming limitations imposed by the cryogenic cooling yet remains.

Local Oscillators. Adequate local oscillator sources are available below 200 GHz. These consist of solid state sources such as Impatt and Gunn diodes. Although solid state oscillators operating above 200 GHz have been reported, major development of such devices is required. Electron tube oscillators operating at these frequencies exist. Tubes such as Carcinotrons can be made to oscillate at 600-1000 GHz. They are driven nonlinearly and higher order harmonics are extracted. These sources are notoriously inefficient and inadequate for space-borne operation. Experimental backward wave oscillators, slow wave structures, need to have micro-mechanical circuit components. These are difficult to fabricate but, techniques of micro-machining in diamond may rectify this problem. Discrete line sources are available from optically pumped submillimeter lasers (e.g., CO_2 pumped submillimeter lasers). These are difficult to tune, inefficient, and relatively large in size. However, they can operate to ∿3000 GHz.

Quasi-Optical Components. These apply mainly to the submillimeter region and are needed to combine the source and local oscillator radiation with high efficiency and to couple the combined radiation onto the mixer. Interferometric methods for combining the radiation (e.g., diplexers) are presently ~75% efficient with projected improvements to ≥90% by the year 2000.

Spectral Line Receiver. Conventional IF spectrometers employ discrete channelized microwave components. For the large bandwidth and high resolution required by high frequency heterodyne receivers, these RF systems are large, heavy, and require high input power. These parameters grow with increasing number of channels. They are not practical for use in space. A new type of spectrometer using acousto-optic techniques is being developed for IF spectroscopy. An acousto-optic spectrometer (AOS) offers the potential for compact, wide bandwidth, and reliable performance. An AOS consists of a collimated coherent light source (i.e., a GaAs diode laser), a Bragg cell (e.g. lithium niobate crystal) which converts RF signals to ultrasonic waves, and a linear detector array. The RF signal sets up sound waves which diffracts a portion of the laser beam at an angle proportional to the frequency of the RF input. The diffracted laser beam is then focused and detected by an array of photodetectors. The beam intensity and position on the detector array yields the IF power spectrum.

Bulk AOS spectrometers have been used with ground based radio receivers for astronomy and have been successfully tested in the laboratory. Miniature discrete component systems and integrated systems are presently being developed. They can be made small and light and require relatively low power input. They can provide high spectral resolution and wide bandwidths by stacking several units (see Fig. 35 and Table 13). AOS spectrometers are useful for microwave, millimeter and submillimeter and infrared heterodyne systems. To further develop and optimize these components, research in integrated optics, optical waveguides and integrated lens design is needed. Understanding optimization of existing optics and development of new electro-active optical materials is also needed.

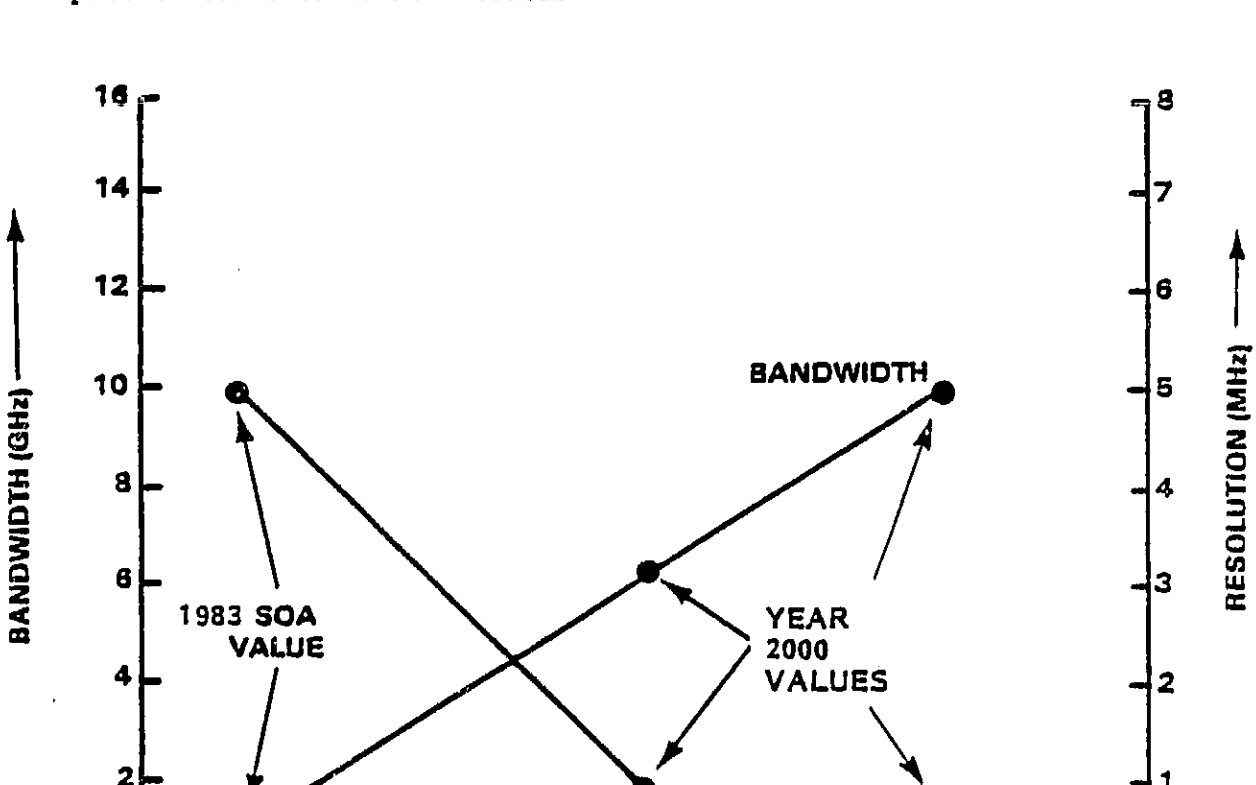

Figure 35. Acousto-Optic Spectrometer Bandwidth and Resolution Projections

TABLE 13

SIGNIFICANT PARAMETERS FOR AOS

Parameter	SOA Value	2000 Value
Bandwidth	1 GHz	>5 GHz
Resolution	5 MHz	<0.5 MHz
Size (volume)	15 x 15 x 15 cm^3	15 x 15 x 7.5 cm^3
Weight (optics)	0.5 kg	0.5 kg
Weight (with electronics)	2 kg	2 kg
Power	5 W	1 W

3.3.2 Representative Instruments

Examples of representative heterodyne radiometers for spectroscopy in the microwave through submillimeter region along with forecasts, of specific system and component parameters are given below.

Millimeter Wave Radiometer for Spectroscopy (1.0-10.0 mm). Millimeter-wave radiometers measure the spectra (power vs. frequency) using low-noise RF receivers and components. Earth sensing applications include measurements of emission spectra of ozone, water vapor, chlorine monoxide and other neutral species in the upper atmosphere (>20km). Such studies have already been done from balloons on the Balloon Microwave Limb Sounder (BMLS). Future studies of the Earth's atmosphere will be done with the Microwave Limb Sounder (MLS) on the Upper Atmospheric Research Satellite (UARS). A similar system could also be used for the study of atmospheres of other planets and for the study of astrophysical sources from space platforms.

The millimeter wave receivers forecast here cover the 30, 100, and 300 GHz region. Receiver noise forecasts are given in Fig. 36 and other relevant system and component parameters are forecast in Table 14.

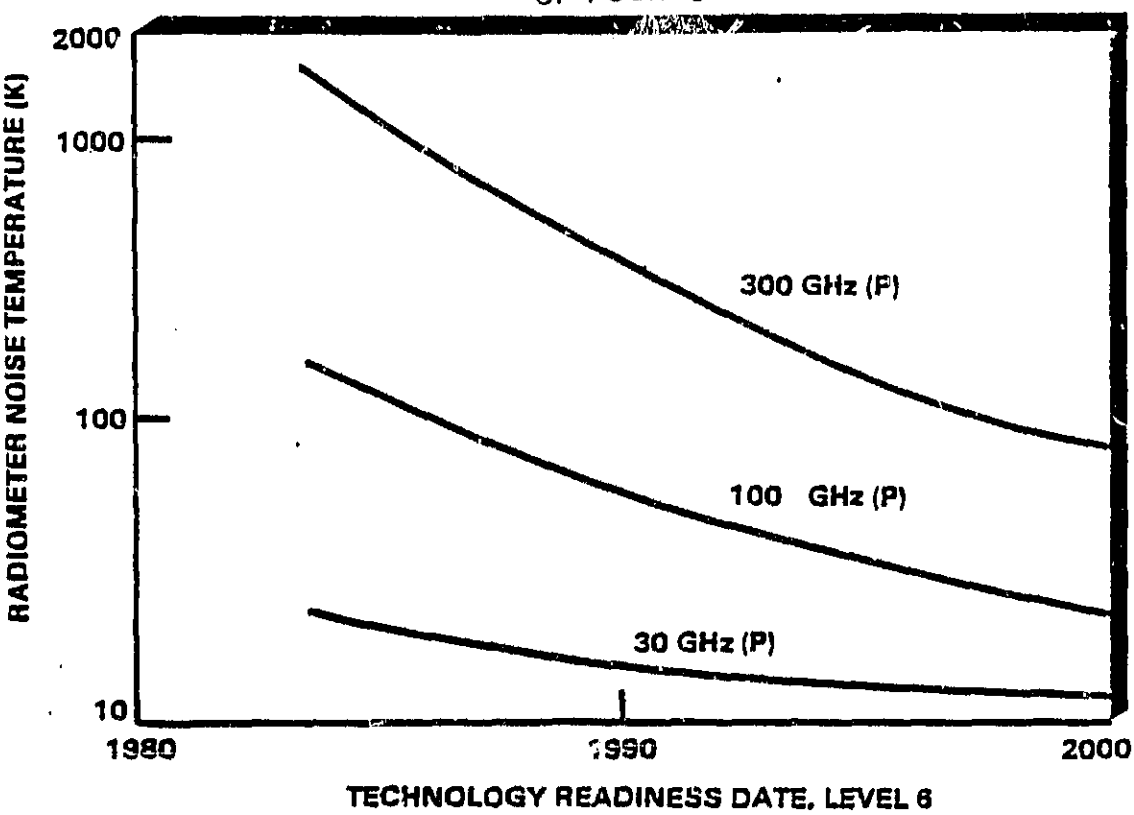

Figure 3.36. System Noise Temperature Projection for Millimeter Wave Radiometer

TABLE 3.14

MILLIMETER WAVE RADIOMETER PARAMETER PROJECTIONS

Parameter	SOA Value	2000 Value	Theoretical Limit
System Noise Temperature (K)			
30 GHz	50	10	4
100 GHz	200	20	5
300 GHz	2000	100	20
Antenna Size	2 m	100 m	
Solid-State Local Osc.			
100 GHz	20 mW	1 W	
300 GHz	1 mW	100 mW	

Physical parameters based on the proposed UARS instrument are given in Table _ 15.

TABLE _ 15
PHYSICAL PARAMETERS OF THE MLS

Weight	10 kg
Size	.05 m^3 (uncooled)
Power Requirement	40 W
Cooling Requirement	Uncooled or cooled to 20 K
Data rate	50 bytes/sec

Research in the future that can be used to upgrade the performance of this type of system includes activities involved with Large Deployable Reflectors and the development of telescopes that incorporate the LDR technology. In addition space qualified cryogenic systems are needed to assure performance as desired throughout the sensor lifetime. Driving programs for this effort involve upper atmospheric research and expanded astrophysics efforts. The latter case is of extreme importance given that the submillimeter region of the spectrum remains unexplored astrophysically.

Submillimeter Heterodyne Spectrometers (0.1-1.0 mm). Heterodyne radiometer-spectrometer systems operating in this spectral region (300-3000 GHz) are in a very early stage of development. Lack of available local oscillators and efficient (low noise) mixers, as well as their large size, weight, and high power requirement make these systems unlikely for space application in the near future. However, large orbiting facilities such as the LDR or Space Station would make submillimeter heterodyne spectroscopy for limb sounding the Earth's atmosphere and for the study of astrophysical sources possible.

Two system concepts are under development: (1) The use of electron tube oscillators (carcinotrons and backward wave oscillators) and tube oscillators with solid state frequency multipliers to obtain local oscillator frequencies to about 1000 GHz; and (2) the use of submillimeter lasers as local oscillators which can operate at discrete frequencies to about 3000 GHz.

Both concepts require quasi-optical mixers, beam combiners (diplexers), cooled IF amplifiers and spectral line receivers as described previously.

An example of the first concept is the Microwave Limb Sounder (0.3-1.0 mm). This instrument will use solid state local oscillators. Projections of receiver noise temperature and solid state local oscillator power for 300 and 1000 GHz are given in Figs. 37 and 38.

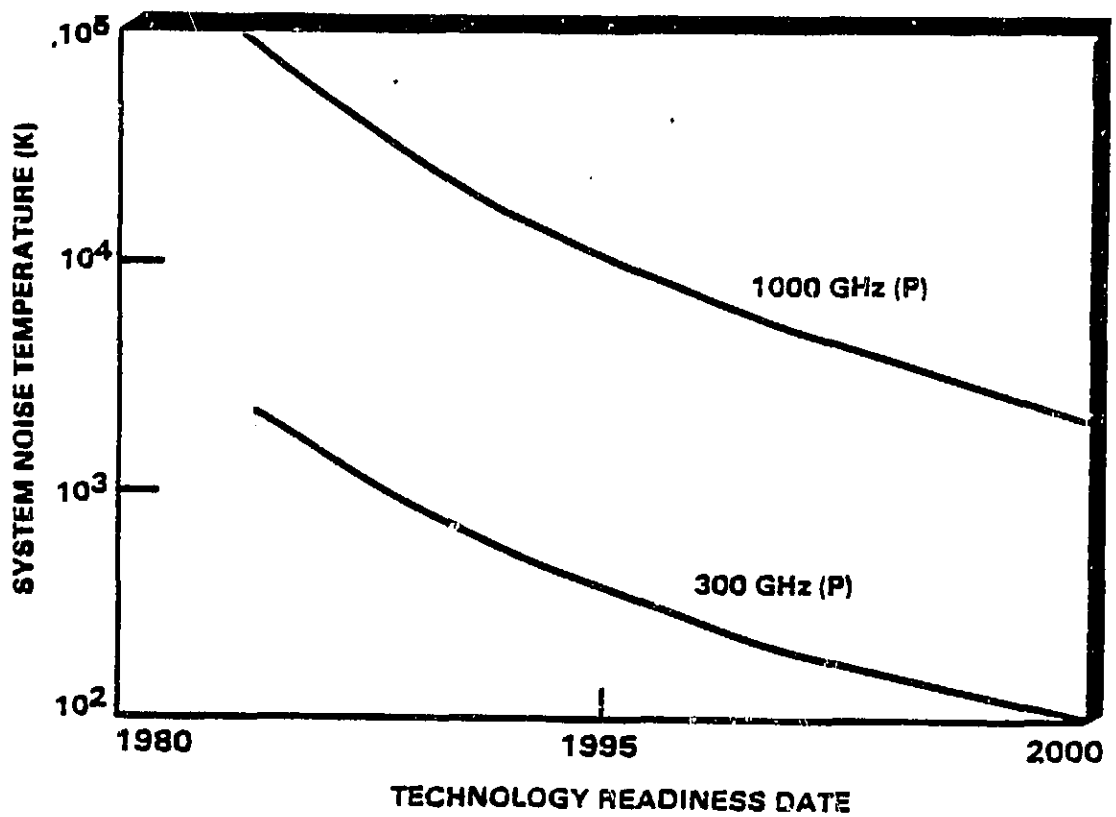

Figure 37. Submillimeter Receiver System Noise Temperature (1.0-0.3 mm)

ORIGINAL PAGE IS
OF POOR QUALITY

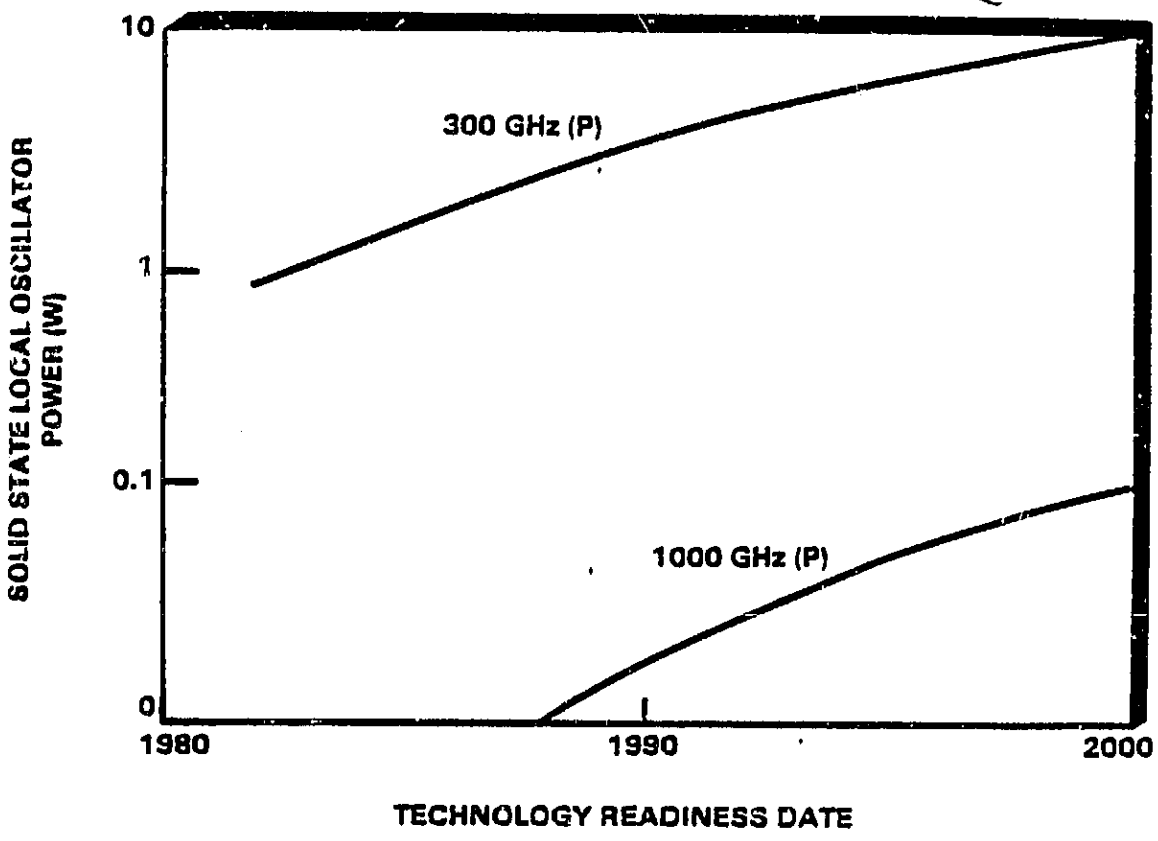

Figure 38. Submillimeter Solid State Local Oscillator Power Forecast

A system and component parameter summary is provided in Table 16. Note that the system noise temperature is determined by that of the mixer.

An example of the second concept is a system using a submillimeter gas laser optically pumped by a 10 μm CO_2 laser; a local oscillator source discretely tunable from 300 to 3000 GHz. At the present time such lasers produce a few milliwatts per line. This local oscillator along with a quasi-optical Schottky mixer provide the major components for a heterodyne system. Successful laboratory spectroscopy tests as well as ground-based astronomical observations have been performed using this local oscillator source.

TABLE . 16

SUBMILLIMETER MLS PARAMETER FORECAST

Parameter	SOA Value	2000 Value	Theoretical Limit
System Noise Temperature			
300 GHz	2,000 K	100 K	20 K
1000 GHz	100,000 K	8,000 K	50 K
Mixer Noise Temperature			
300 GHz	2,000 K	100 K	20 K
1000 GHz	100,000 K	8,000 K	50 K
Local Oscillator Power			
300 GHz	1 mW	10 mW	
1000 GHz	<10 µW	1 mW	
Lightweight Antenna Size and Figure Accuracy	1 m 12 µm	6-10 m 5 µm	
Quasi-Optics Coupler (Diplexer) Loss	1 dB	.25 dB	0 dB

System sensitivity is defined by noise temperature. Current receiver sensitivity is 6000 K at 690 GHz. A plot of projected system noise temperature is provided as Fig. -.39. System weight is an important parameter for space instruments. Radiometer weight is forecast in Fig. 40.

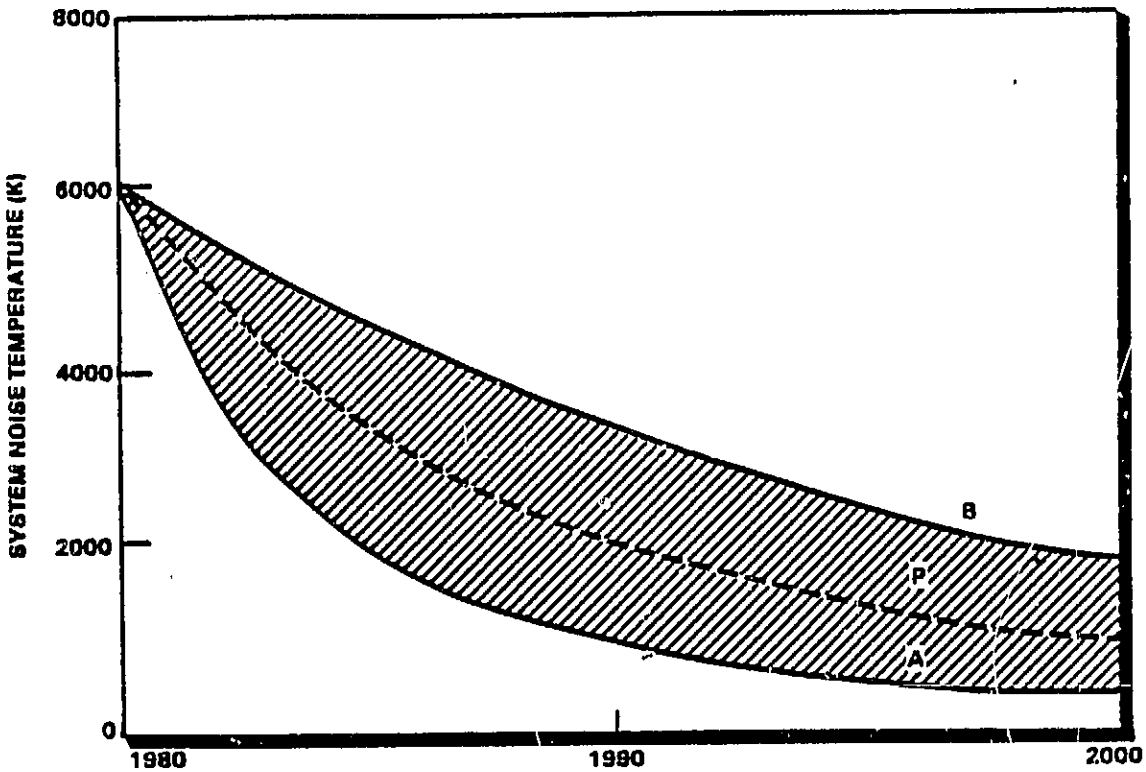

Figure 39. System Temperature of a Submillimeter Laser Heterodyne Receiver

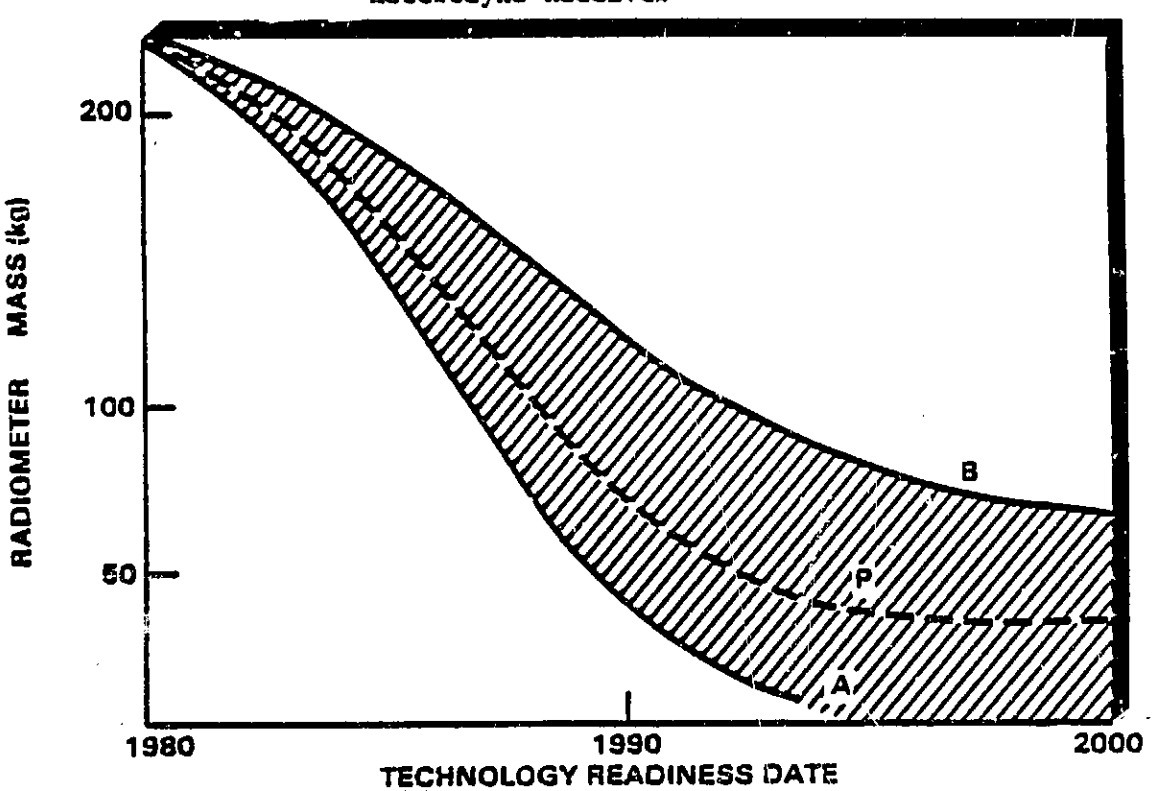

Figure 40. Submillimeter Laser Hetrodyne Radiometer Mass Projection

Adequate local oscillator (LO) power on the mixer is important for optimum heterodyne performance. Projections of local oscillator power required for the mixer and IF amplifier noise figure are provided in Fig. 41. The submillimeter laser power incident on the mixer depends on the laser local oscillator power and is related to CO_2 pump laser power. The efficiency of converting 10 μm power to the submillimeter is of significant importance for small low power consumption systems. Improvement in laser local oscillator efficiency is forecast in Fig. 42.

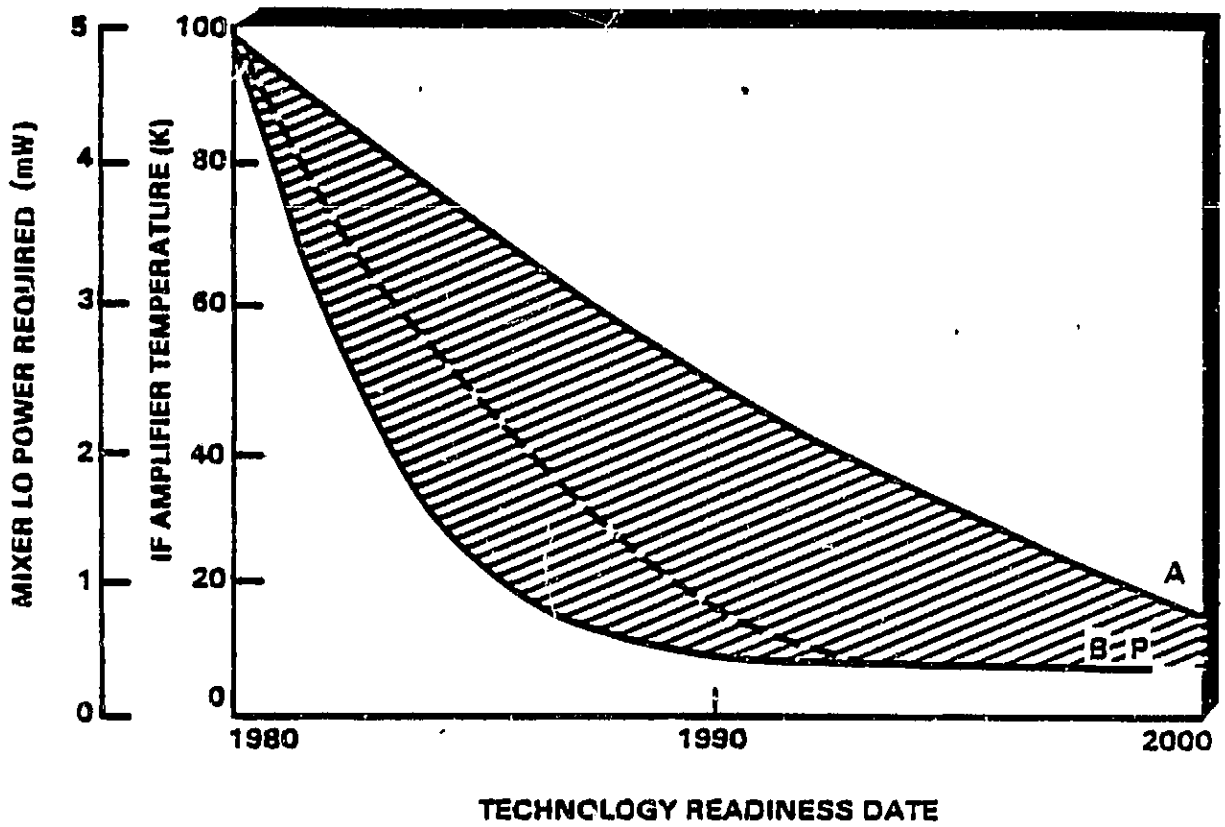

Figure 41. Projections for Receiver Components

A summary of system and component projections is given in Table 17.

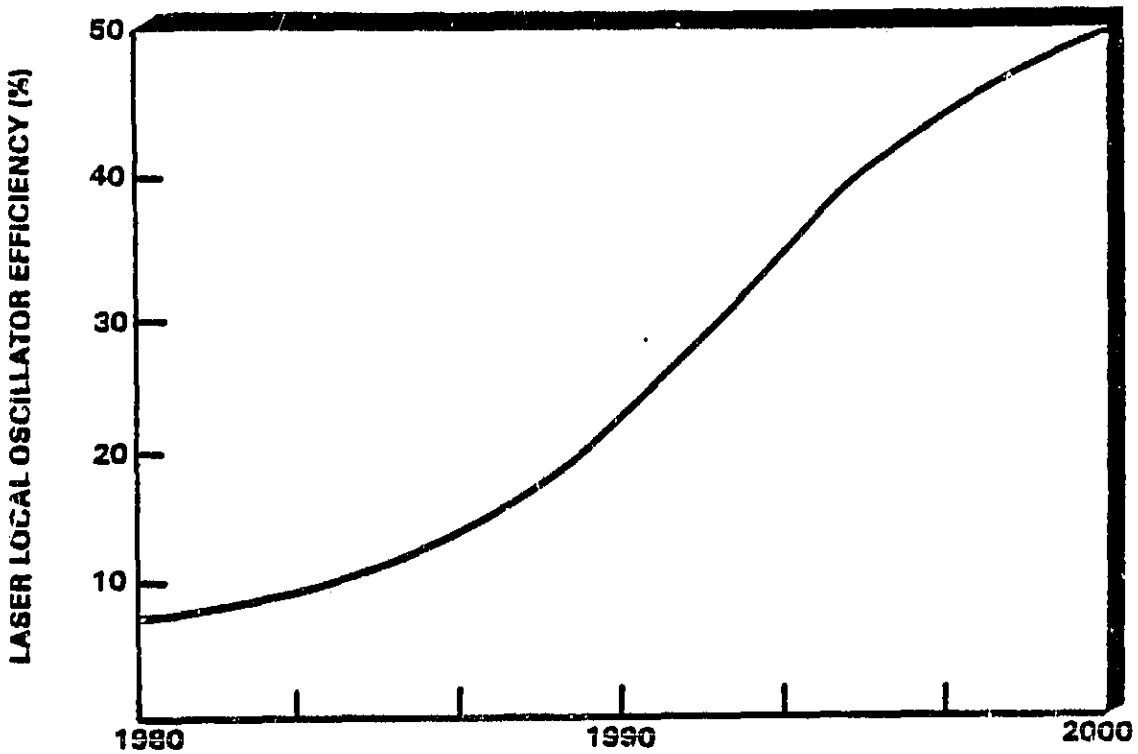

Figure 42. Projected LO Efficiency

TABLE 17

SUBMILLIMETER LASER HETERODYNE SPECTROMETER
PARAMETER FORECAST

Parameter	SOA Value	2000 Value	Theoretical Limit
System Temperature @ 690 GHz	6000 K	500 K	About 100 K
Laser Power	10 mW	100 mW	
LO Power Required	5 mW	0.1 mW	10 nW
Frequency Limit Lasers	3000 GHz	10,000 GHz	
IF Amplifier Temperature	100 K	10 K	
Diplexer Efficiency	75%	90%	
System Weight	200 kg	50 kg	
System Size	3 m^3	1 m^3	

Critical research supporting the development of this system involves the development of LOs that can cover the entire submillimeter band with a few mW output power. So far only the laser is useful above 1000 GHz. Improvements in mixers and LOs to reduce the noise temperature and the LO power requirement are also needed. One method is to cool the Schottky mixer, another is to develop the SIS mixer. Development of low noise GaAs FET amplifiers with wider bandwidth (~10 GHz) would also improve system performance.

Driving scientific programs and projects for high resolution submillimeter heterodyne spectroscopy include detection of molecules in our galaxy from aircraft, balloon, and space telescopes. The LDR is the major program in the 1990s. In preparation for that, aircraft and shuttle experiments are planned. In addition, ESA plans to launch a telescope (FIRST) for submillimeter astronomy. This instrument could also be used for stratospheric research. However, it is unlikely that submillimeter experiments can be ready in time to meet the probable schedules of future telescope programs with current funding levels.

3.4 Prominant Institutions and Individuals

3.4.1 Broadband Radiometers—Planetary Surfaces

NASA/Langley Research Center
H. C. Blume
R. F. Harrington

University of Massachusetts
C. Swift

Jet Propulsion Laboratory
P. N. Swanson
W. J. Wilson
E. G. Njoku

NASA/Goddard Space Flight Center
T. Wilheit

Naval Research Laboratory
J. Hollinger

University of Kansas
R. Moore

Georgia Institute of Technology
S. Newton

3.4.2 Broadband Radiometers—Astronomy

Differential Microwave Radiometer

NASA/Goddard Space Flight Center
J. Mather
D. T. Nace
R. Weber, Engrs. for COBE DMR

University of California, Berkeley
G. F. Smoot

Princeton University
D. T. Wilkinson

Jet Propulsion Laboratory
S. Gulkis
M. Janssen

Far IR Spectrophotometer

NASA/Goddard Space Flight Center
J.C. Mather, P.I. for FIRAS

University of California, Berkeley
P. L. Richards

Massachusetts Institute of Tech.
R. G. Weiss

University of California, Los Angeles
E. L. Wright

Queen Mary College, London
J. Beckman

3.4.3 Millimeter and Submillimeter Heterodyne Radiometers

Mixers--GaAs Schottky

NASA/Goddard Institute for Space Studies
A. R. Kerr

National Radio Astronomy Observatory
S. Weinreb

NASA/Goddard Space Flight Center
T. Walton

Mixers--Superconductor-Insulator-Superconductor

NASA/Goddard Institute for Space Studies
A. R. Kerr

University of California, Berkeley
P. L. Richards

California Institute of Technology
T. Phillips

Chalmers Institute of Technology, Sweden
E. Kolberg

Accousto-Optic Spectrometer

NASA/Goddard Space Flight Center
G. Chin

ITEK, Applied Technology
W. Oakley

Hughes Aircraft Company, Fullerton, CA
D. Isaacs

Westinghouse
R. Mergerian

Naval Research Laboratory
A. Spezio
A. Giaberento

Millimeterwave Radiometers

Jet Propulsion Laboratory
W. J. Wilson
J. Waters
H. Pickett
P. Zimmermann

NASA/Goddard Institute for Space Studies
A. T. Kerr

UCLA
H. Fetterman

National Radio Astronomy Observatory
S. Weinreb

California Institute of Technology
T. Phillips

MIT/Lincoln Laboratory
B. Clifton

University of Massachusetts
N. Erickson

Submillimeter Radiometers

NASA/Goddard Space Flight Center
D. Buhl
G. Chin
S. Petuchowski
J. Bufton

University of California, Berkeley
A. Betz
R. Genzil

Jet Propulsion Laboratory
(Non-Laser Systems)
H. M. Pickett
J. M. Waters
W. J. Wilson
P. Zimmermann

4 PASSIVE INFRARED SENSORS

Infrared sensors can be of three generic types:

- Photometers - broadband instruments capable of measuring thermal continuum radiation thereby permitting the study of the energy balance and surface composition of planets and the infrared brightness of astrophysical sources.
- Spectrometers - such as Fourier Transform Spectrometers (FTS), grating instruments, Fabry-Perot instruments or gas correlation spectrometers permit the measurement of molecular band and pressure broadened line profiles and thus the study of source composition and its pressure and temperature structure.
- Imagers - these consist of linear or area arrays of detectors capable of spatial coverage through scanning or pushbroom techniques (linear arrays) or by staring techniques (area arrays) to map a region of interest.

Sensors used for Earth sensing, atmospheric studies by solar or planetary surface radiance absorption spectroscopy and planetary surface studies are generally limited by the thermal background of the source. Thermal background from the instrument is of less concern. The

important system parameter is the ability to measure small temperature (radiance) differences ($\leq$1 K).

For atmospheric molecular self-emission measurements (limb sounding) and astrophysical observation of relatively cool regions, thermal background and thermal emission from the instrument must be minimized. This is accomplished by narrowband filtering and cooling the instrument and optics (telescope). For most IR systems the desired performance cannot be achieved without cooling.

All passive infrared sensor systems are dependent on sensitive IR detectors and detector arrays. Cryogenically cooled detectors can achieve high sensitivities and can operate background noise limited in Earth sensing systems and zodiacal light limited in astrophysical observations. Detector technology development is therefore, of prime importance for all IR systems and forecasts of system performance is coupled to the development of detectors and detector arrays. Additional areas of importance are the development of advanced optics and improvements in on-board data processing and data transmission.

Conceptual designs of most future space sensor systems include multiple functions for the proposed instruments. Some degree of simultaneous spectroscopic, photometric and spatial information retrieval capability is attempted. The following classes of proposed infrared instruments illustrate this point. Discussion of individual sensor systems will be followed by a section devoted to the development of infrared detectors and detector arrays.

4.1 Fourier Transform Spectrometer (2-1000 μm)

The fourier transform spectrometer (FTS) offers the best combination of throughput, resolution, bandwidth, and imaging of any spectrometer for application in the IR portion of the spectrum. The fourier transform spectrometer in the infrared has a proven performance record in space applications. FTS instruments have successfully flown on spacecraft (Nimbus, Mariner, Voyager), aircraft (C141), and balloons, and have been operated at ground-based observatories. By the year 1990,

cryogenic instruments will be available for space applications with 2 to 1000 m spectral coverage with 0.01 cm^{-1} spectral resolution. Applications include studies of planetary and astrophysical composition and dynamics, as well as terrestrial atmospheric studies.

This type of instrument can achieve a spatial resolution on the order of a few arc seconds, and is limited in spectral resolution by the maximum practical distance traversed by the retroreflectors. This, in part, also determines the system size. Its sensitivity is limited by detector noise when the spectrum is band-pass limited.

In order to realize the full potential of the FTS for future space use (particularly for astronomy), the instrument must be cryogenic and must operate on a cryogenic telescope such as SIRTF. This will allow optimum use of infrared detectors which now have NEPs around 10^{-16} $WHz^{-1/2}$ and may approach 10^{-18} $WHz^{-1/2}$ by the year 2000. For high-flux sources such as the Earth and planets, a further improvement is gained by placing a cryogenic postdisperser and linear detector array at the FTS output.

A measure of sensitivity is given in terms of Minimum Detectable Flux (MDF). An illustration of system performance is provided in Fig. 43 where the flux from various sources is plotted versus frequency. The MDF is indicated for various FTS resolutions and integration times (τ). It is seen that with the addition of the postdisperser the system sensitivity is greatly improved.

A proposed postdisperser detector system, is composed of a liquid-helium-cooled, grating monochromator used in conjunction with FTS instruments. The monochromator disperses the radiation and images the dispersed spectrum at an infrared detector array. This narrows the instantaneous spectral bandwidth on the detector and since all components are also cooled, background radiation is reduced and system sensitivity is improved. The system can also be designed to be used as a conventional broadband FTS with a single element detector. If a two-dimensional detector array is operated in the FTS focal plane, the

utilized in source mapping. The post disperser system can also be used separately as a low resolution grating photometer.

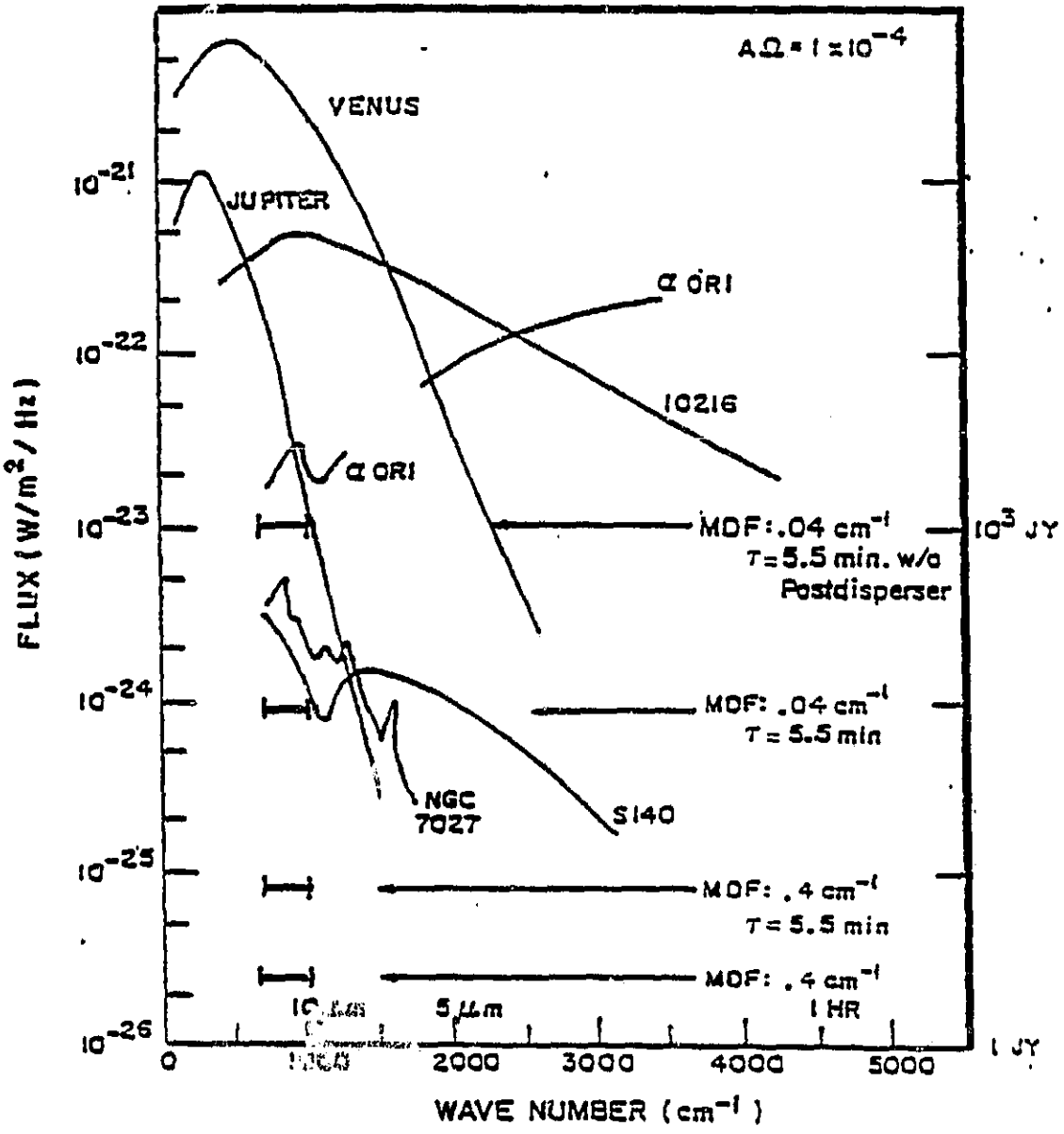

Figure 43. Post-Dispersion Sensitivities Compared with Various Sources

The system performance parameters are forecast in Table . 18 and the critical system components are listed in Table ". 19.

TABLE ..18

CRITICAL SYSTEM PARAMETERS FOR FTS

Parameter	SOA Value	2000 Value
Resolution	0.1 cm^{-1}	0.01 cm^{-1}
MDF	10^{-22} W m^{-2} Hz^{-1}	10^{-26} W m^{-2} Hz^{-1}
Size		30 x 30 x 100 cm^3
Weight		<10 kg - determined by cryogenics
Power Input		<10 W
Cooling		<10 K
Data rate		10^4 bits/sec

TABLE .. .19

CRITICAL SUBSYSTEM PROJECTIONS FOR FTS

Critical Component and Characteristic	SOA Value	2000 Value
Cryogenic Mechanism For Moving Retro-Reflector	5 cm travel	25 cm travel
Cryogenics FTS, Telescopes Diameter	0.85 m (SIRTF)	3 m
Postdisperser	64 element	1000 element
Detector NEP	10^{-16} W $Hz^{-1/2}$	10^{-18} W $Hz^{-1/2}$

FTS Instruments for Solar Absorption Spectroscopy (2-16 μm). An FTS flight instrument for the study of the Earth's atmosphere using absorption spectroscopy is proposed in the Atmospheric Trace Molecule Spectroscopy (ATMOS) program. It is a multiflight shuttle instrument designed to determine compositional structure and variability of the upper atmosphere using IR spectroscopy. The instrument consists of an uncooled Fourier transform spectrometer in a double pass Michelson configuration and a single element HgCdTe photoconducting detector. It could be used in the 2 to 16 μm spectral region with a spectral resolution on the order of 0.01 cm^{-1} and a spatial resolution of 2 kilometers vertical height. The instrument is source and background shot noise limited and the performance limit is described by the detectivity D^* ($D^* = 5 \times 10^{10}$ cm $Hz^{1/2}/W$ at 14 μm). The system D^* is determined by that of the HgCdTe detector and the forecast to the year 2000 is given in Fig. 44. Table 20 below quantifies this projection.

Since this instrument is meant to make measurements in solar absorption, detector sensitivity is of less concern. The HgCdTe detector D^* is at least 1 order of magnitude lower than that of the best available IR detectors. The best detectors (e.g., extrinsically doped silicon) however, operate near liquid helium temperatures. HgCdTe detectors operate at liquid nitrogen temperatures or above. In order to obtain higher detector temperature operation and broader spectral coverage, advances in materials science are of significant importance for this system.

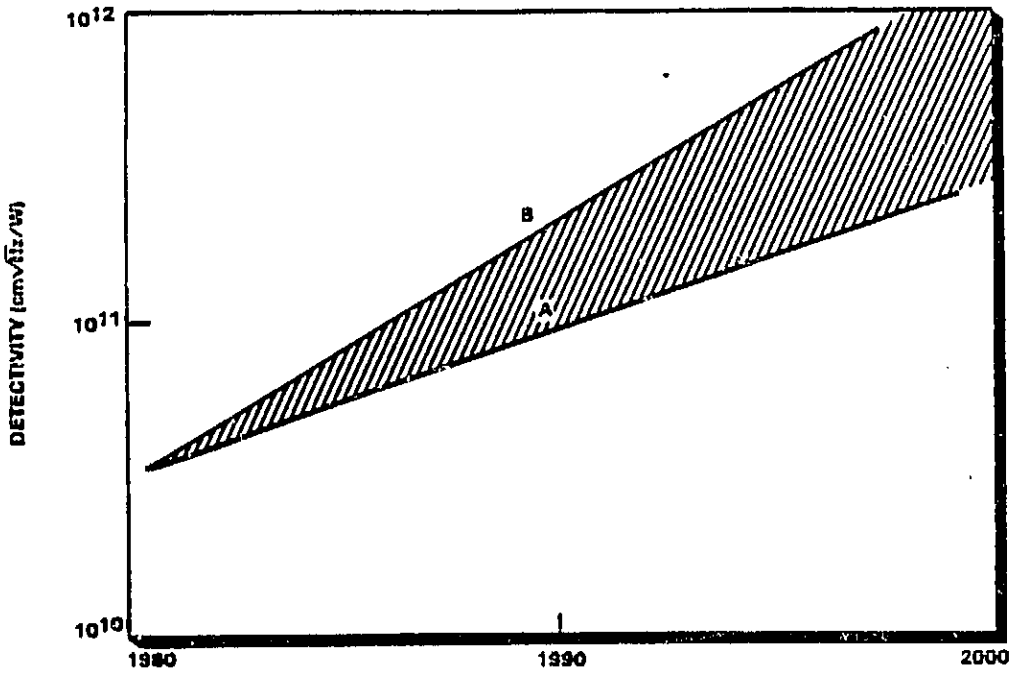

Figure 44 Sensor Detectivity

TABLE 20

DETECTIVITY PROJECTION FOR ATMOS

Parameter	SOA Value	2000 Value
D^*	$5x10^{10}$ cm $Hz^{1/2}/W$	10^{12} cm $Hz^{1/2}/W$

4.2 Grating Spectrometers - Mappers

Spectral mapping is the simultaneous acquisition of spatially and spectrally resolved data. The radiation from the scene is imaged upon

the spectrometer slit. The spectrometer section of the instrument preserves the spatial image quality in one direction and the grating disperses the spectrum in an orthogonal direction allowing an image of the object line to be formed at each of a number of wavelengths in the focal plane. The spectral and spatial information is collected and read out simultaneously. This process is repeated as the field of view sweeps over the target body, either from relative spacecraft-planet motion (pushbroom imaging) or from a scanning motion of the instrument platform.

..4.2.1 Astronomy Applications

The forecast for this class of mapping spectrometer is developed on two instruments. The first instrument is the Galileo near-infrared mapping spectrometer (NIMS). Its development is sufficiently mature so that its performance can be described with confidence. The real forecast is provided by the advanced mapping spectrometer (AMS)--an instrument concept developed for outer planet missions in the 1990s.

The Near Infrared Mapping Spectrometer (NIMS) (0.6-5.2 μm). This instrument is scheduled to fly on Galileo to map geologic features on the Jupiter satellites and to determine Jovian atmospheric structure and composition. The NIMS has a focal plane consisting of 3 silicon and 14 InSb photodiodes, each with a filter defining the spectral band. The optical system has a Ritchey-Chretien telescope and Cassegrain grating spectrometer. The spectral region covered is 0.6 to 5.25 μm. It has a resolution of 0.15 μm in the 0.6 to 1.05 μm region and 0.30 μm above 1.05 μm. Its instantaneous field of view IFOV is 0.50 milliradians and its performance is measured by the noise equivalent power (NEP). The system NEP is expected to improve from a value of 10^{-15} W $Hz^{-1/2}$ to 10^{-16} W $Hz^{-1/2}$ as illustrated in Fig. 45. The most critical components are the detectors. Inherent detector noise needs improvement to meet the projected system capability. State of the art systems detect noise at the 1000 electron level (Fig. ..46). It is projected that continued improvement in detectors can reduce this to 100 electrons thus providing on order of magnitude enhancement. Basic detector materials research will be required to achieve this goal.

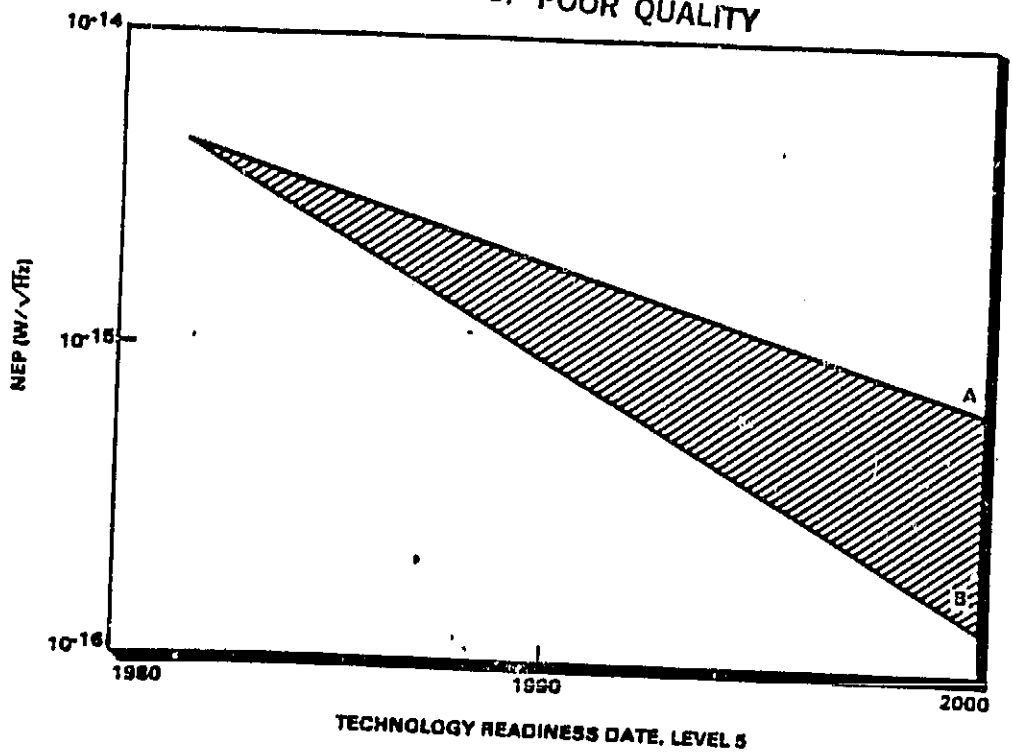

Figure 45. NIMS Sensor Performance

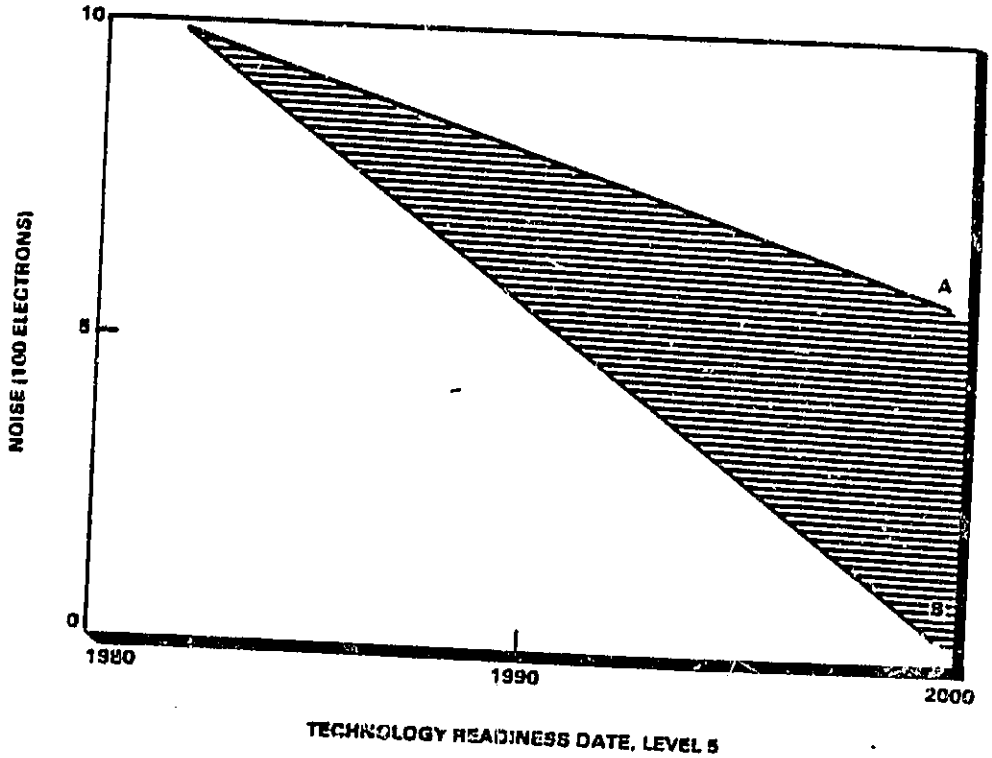

Figure 46. NIMS Detector Noise

Advanced Mapping Spectrometer (AMS). This instrument is an advanced version of this class of sensors. Rough calculations indicate that filling the focal plane by means of detector arrays would provide a more efficient instrument; that is, virtually all of the energy reaching the focal plane would be collected, resulting in an improvement in signal-to-noise ratio which scales with the square root of the number of detector elements. For the focal plane arrays, the relevant figure of merit is the product of the average detector D^* (detectivity in $cm\text{-}Hz^{1/2}/W$) and the square root of the number of detector elements on the focal plane $D^*_{eff}=N^{1/2}D^*$.

The Galileo NIMS instrument is cooled radiatively to 160 K, and a two-stage radiator cools the focal plane to 80 K. Improved radiative coolers may be possible. However, with the severe weight constraints it does not seem reasonable to expect an improvement of more than 10 K, resulting in focal plane temperatures of 70 K. It is implicitly assumed that the focal plane power dissipation is small compared to parasitic sources. An increase in the aperture for the AMS is projected based on the development and utilization of lightweight optics, resulting in an instrument aperture of about 33 cm (1 m focal length f/3 optical system).

Two trends in the data rate from planetary spacecraft have been observed. First, the total data rate (normalized to a common spacecraft-Earth range) have been increasing with time. This growth can be expected to continue based on technological developments both in spacecraft transmitting equipment and in receiving equipment, especially larger antennas. Second, the fraction of the telemetry stream occupied by visual imaging has been declining. With the demonstrated utility of infrared mapping instruments, it is reasonable to assume that an advanced mapping spectrometer would occupy a significant share of the total telemetry bandwidth. Furthermore, the use of data compression and advanced coding of data is assumed, resulting in a raw data rate allocation for the instrument in the neighborhood of 10^5 bits/sec.

With the rationale described above, the instrument parameters for the two benchmark instruments and a projection for the year 2000 are given in Table 21. The Detector D^* values are given at 5 μm. A curve showing the required D^* for the entire spectral range representing a constant signal-to-noise performance for the AMS instrument is given in Fig. 47. The forecast for detector performance (Fig. 48), temperature (Fig. 49), optics parameters (Fig. 50), and data rate (Fig. 51) are reasonable assumptions and should be compared to forecasts from other discipline areas with constraints to planetary missions taken into account. Important application of infrared mapping spectrometers are in future planetary missions and for use in Space Telescope, SIRTF or Space Station platforms.

TABLE 21

DEFINITION OF BENCHMARK INSTRUMENTS.
PLANETARY INFRARED REMOTE SENSING

Parameter	NIMS (1980)	AMS	Extrapolation (2000)
Detector D^* at 5 μm ($cm \cdot Hz^{1/2} \cdot W^{-1}$)	2×10^{13}	2×10^{13}	1×10^{14}
Number of Elements	17	128 x 128	128 x 128
Detector Product $N^{1/2} \cdot D^*$	8.2×10^{13}	2.8×10^{15}	1.3×10^{16}
Detector Temperature (K)	80	70	60
Instrument Temperature (K)	160	150	150
Optics Focal Length (m)	0.4	1.0	1.0
Optics Diameter (cm)	23	33	50
Data Rate (bits/sec)	11×10^3	10^5	10^6

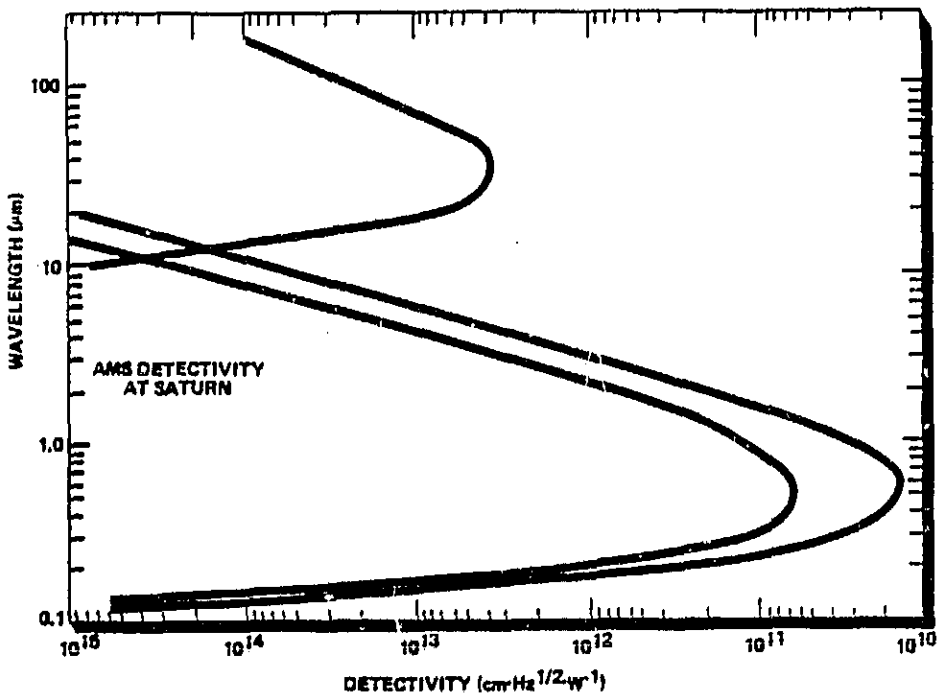

Figure 47. Infrared Remote Sensing Required Detectivity for Various Wavelengths (AMS 1985 Requirements)

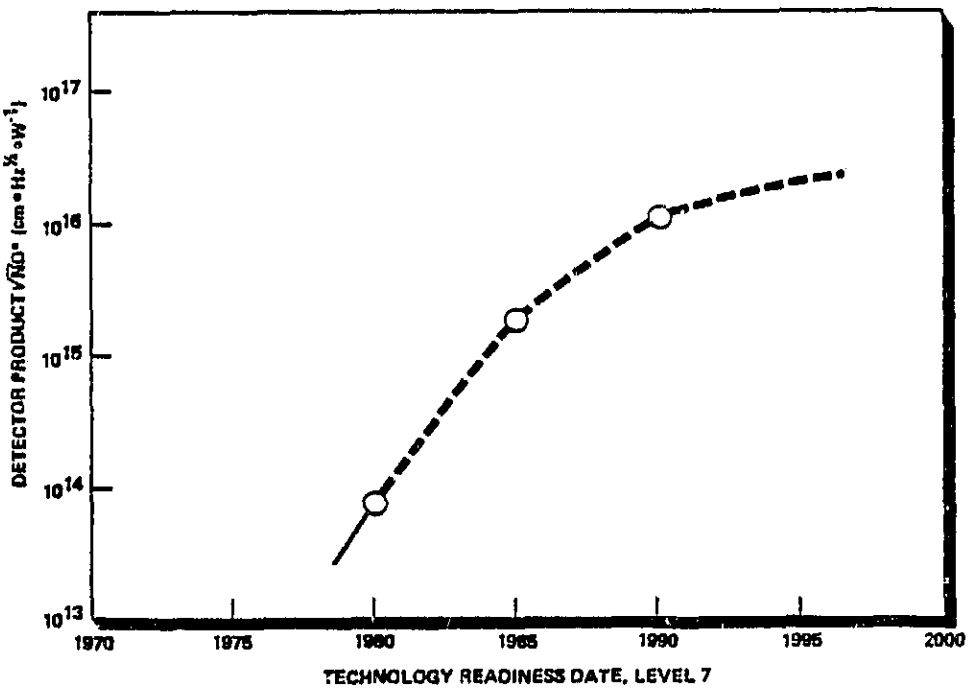

Figure 48. Infrared Detector Array Performance

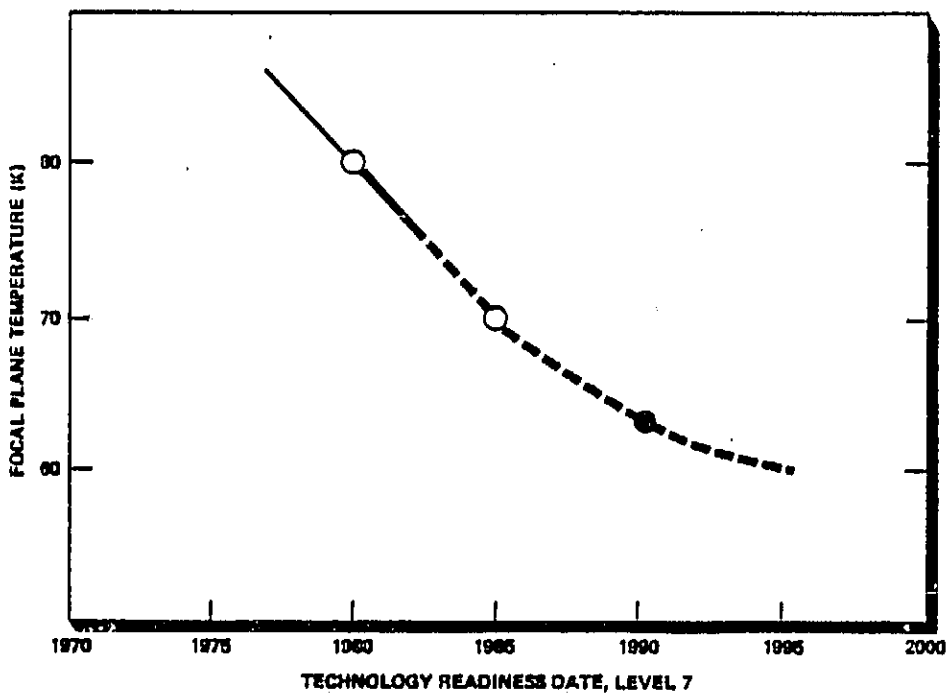

Figure 49. Performance of Radiative Cooler

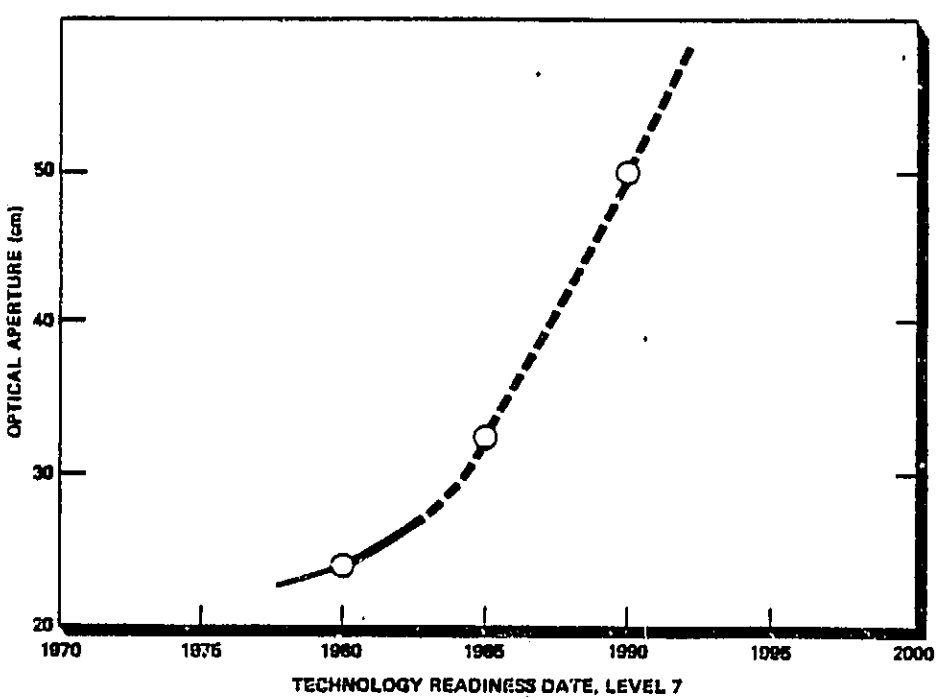

Figure 50. Development of Lightweight Optics

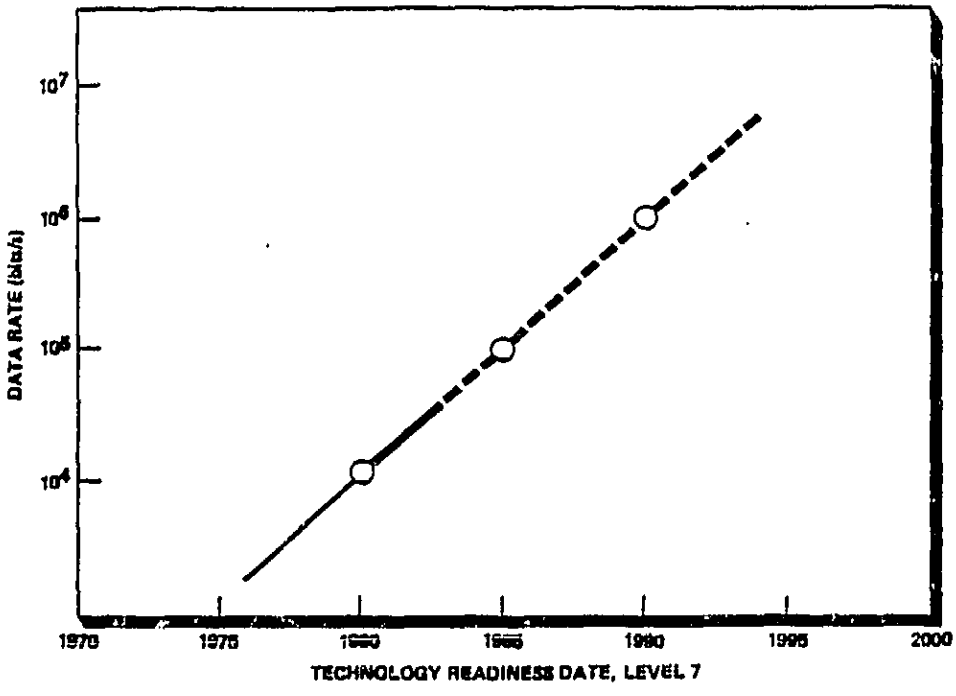

Figure 51. Instrument Data Rate for Planetary Spacecraft

4.2.2 Earth Sensing Applications

Atmospheric Moisture and Temperature Sounder (AMTS)(3.7-16.5 μm). This proposed atmospheric sounder (AMTS) is a conceptual design for a second generation temperature sounder. The data acquired with this instrument will be used in numerical global weather prediction models. Data on water vapor, clouds and ozone are also measured. The instrument is a multichannel grating spectrometer. Twenty-eight spectral channels simultaneously view sixteen footprints on the ground. The 16 footprints are in a linear array and stepped-scanned across track. The free flyer instrument will have 100% global coverage each 24 hours. A shuttle instrument of essentially the same design can also be used to retrieve significant scientific data.

The spectral region covered by this system varies from 3.7 to 16.5 μm. The system spatial resolution in the free flyer mode of operation is 10 x 10 km^2, and the performance is limited by detector temperature, spectral resolution, and noise in the detector-preamplifier combination. The system is best described in terms of detectivity and the random

radiometric noise equivalent change in temperature (NEΔT). These parameters are illustrated in Figs. 52 and 53. Data for projections illustrated in these figures are presented in Table 22.

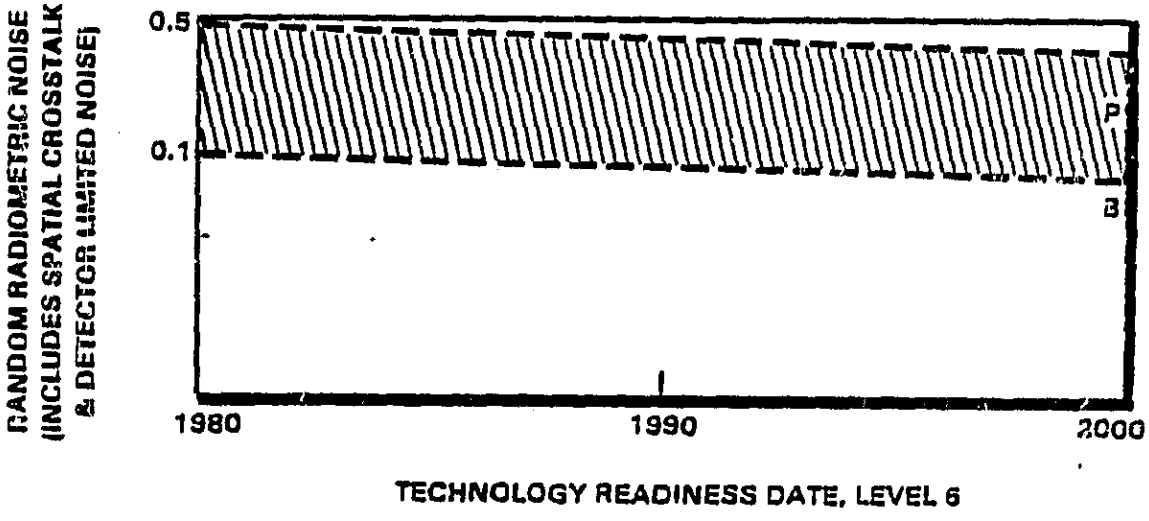

Figure 52. AMTS Random Radiometric Noise (NEΔT)

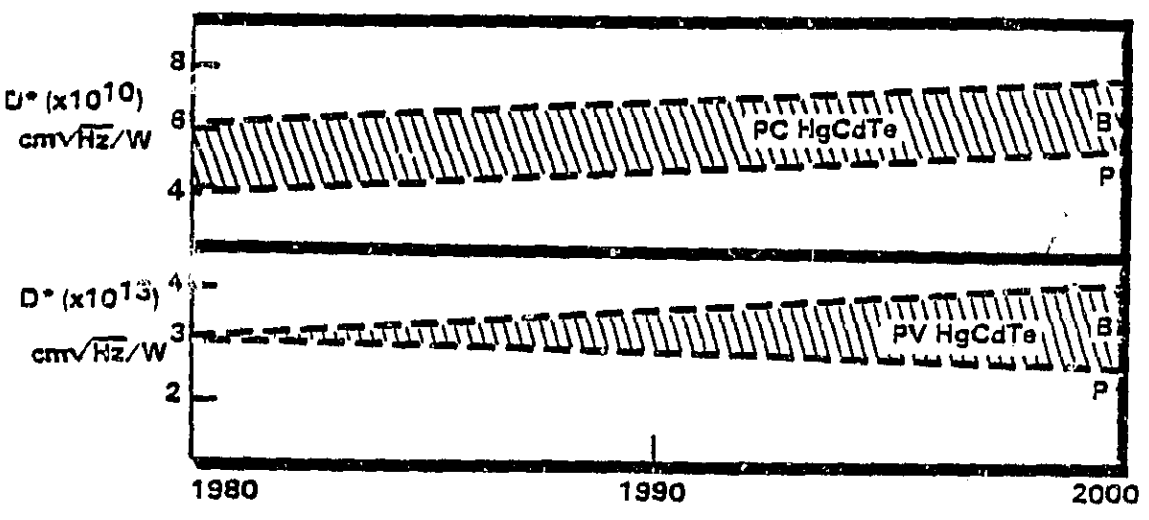

Figure 53. D* for 16 μm Photoconductive (PC) and 3.7 μm Photovoltaic (PV) HgCdTe through 2000 Under AMTS Conditions

TABLE . - 22

AMTS PARAMETER FORECAST

Parameter	SOA Value	2000 Value
Detector Temperature (Radiative Coolers)		
Geosynchronous Orbit	75 K	40 K
Low Earth Orbit	90 K	80 K
D^* ($cmHz^{1/2}W^{-1}$):		
PC HgCdTe at 16 μm	4×10^{10}	6×10^{10}
PV HgCdTe at 3.7 μm	4×10^{13}	6×10^{13}
Lens Diameter	30 cm	63 cm

Immersion: Various detector manufacturers feel that PC HgCdTe immersion could be possible without performance degradation. However, insufficient data exists to permit a forecast of performance.

Critical components for this system include large, super smooth transparent lenses, immersion lenses for PC HgCdTe detectors, good quality detectors including PC HgCdTe, PV HgCdTe, and PV InSb. These detectors must be cooled. The lens and detector cooling requirements are projected as presented in Table _ 22. The degree of technological dificulty is presented in graphical form in Fig. . . ,54.

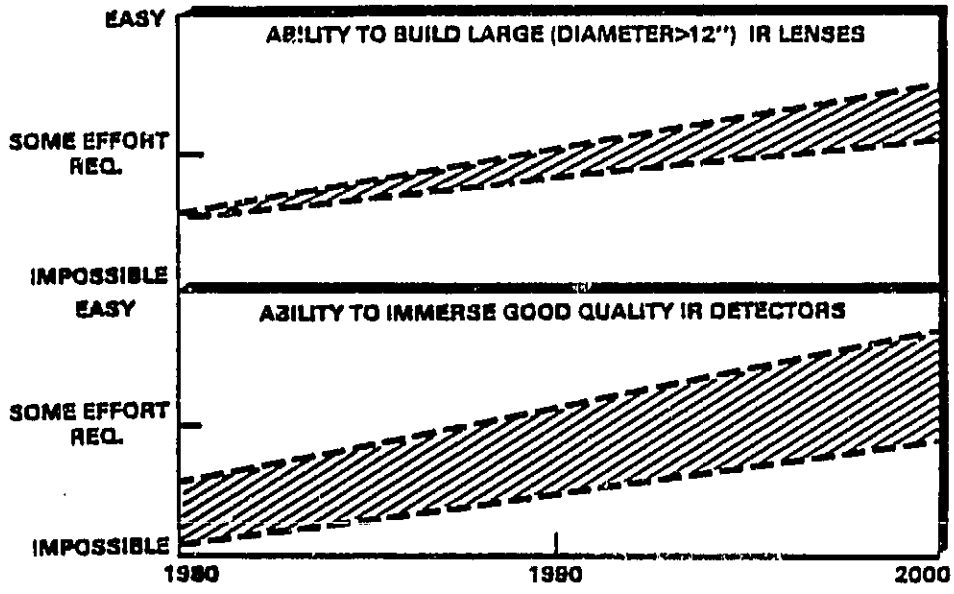

Figure 54. Subjective Forecast of AMTS Component Development

4.3 Infrared Imagers - Mappers

These sensor systems rely on detector array technology and on staring or "pushbroom" spatial coverage techniques. For earth sensing applications system sensitivity is generally limited by background or source noise and the relevant measure of sensitivity is noise equivalent change in reflectivity (NEΔR) for short wavelengths and noise equivalent change in temperature (NEΔT) in the thermal IR region. For astronomical observations, noise equivalent power is the relevant parameter and the sensors are detector or space background noise limited.

4.3.1 Earth Resources Imagers

Earth imaging systems such as those used in the Landsat program have obtained data in the infrared and visible spectral regions on such things as: flood damage assessment, oil spills, forestry, earth crust minerals (coal, iron oxide, etc.), snow pack for water runoff predictions, beach erosion, air pollution, crop assessment, surface feature

mapping, and sea state mapping. Over eighty applications of these types of measurements have evolved as the user community has grown. New sensor systems promise to increase the applicability of this type of data in the future. High resolution multispectal imagers may be flown on shuttle missions or in free-flyer spacecraft developed for future Landsat missions.

High-Resolution Multispectral Earth Imaging Sensor: Multispectral Linear Array (MLA) (0.4-12.5 μm). Potential sensors for future earth observation missions include existing Landsat instruments such as the Multispectral Scanning System (MSS) and the Thematic Mapper (TM), and the proposed "pushbroom" Multispectral Linear Array (MLA) instruments which will provide improved performance to the science and applications user communities. The spectral bands covered will be determined by optical filters and the total spectral region covered will be 0.4-12.5 μm. The proposed NEΔR is ~0.5% and the NEΔT ~0.5 K.

These new instruments exploit large scale integrated circuit technology which allows many thousands of solid-state devices to be put on a single integrated circuit and makes feasible long arrays of detectors and the associated signal processing on a single chip. The advantage of using these detector arrays in an earth observation sensor is that they allow elimination of the object plane scan mirror which is a very difficult item to produce (especially if high spatial resolution is desired). The arrays also potentially allow improving the signal-to-noise ratio (SNR) of the sensor or reducing the spatial or spectral bandwidth of the various channels at the same SNR. The major disadvantages associated with using arrays of detectors are that the more complex and larger optics are required to image the wider optical field-of-view on the detectors and that many thousands of detectors in each spectral band must be accurately calibrated in order to achieve the required system SNR. If a spatial resolution of significantly less than 30 meters on the Earth's surface (e.g., 15 or 20 m) is required from orbit, use of this technology is necessary because of the difficulties in mechanizing the scan mirror and in achieving reasonable signal-to-noise performance.

Decrease of the instantaneous field of view (IFOV) is desirable from the point of view that this produces more detail in the images and allows a better classification of scene content. However, as the IFOV is decreased the total quantity of data that must be processed to cover a fixed area on the ground increases proportionally. This presents quantifiable challenges for future ground systems. For example, using the nominal 80 m IFOV and the standard image size, each MSS band contains over 10^6 pixels. The full four band scene contains over 32 million pixels. The TM uses a nominal 30 m pixel, requires over 39 million pixels for each band, and more than 300 million pixels for the full seven band scene. The MLA will use a nominal 10 m pixel, 300 million pixels per band, and over $2x10^9$ pixels for a seven band scene. This progression of image data volume is illustrated in Fig. 55. A quick assessment of the volume of data generated by present and future systems illustrates that some unique ground processing will be necessary in the future. One prospect for solving this data management problem lies in pre-processing the data in real time, as it is acquired, using the satellite's on-board computer and downlinking data after this first step of standard processing. Current research in optical signal and image processing may rectify this problem.

Currently four MLA designs are under active study for future applications. Any final design will be driven by the state of the art for detector arrays and the desired application for the data. This is illustrated further in Table 23 and 24. Table 23 contains reference to the four new proposed sensor types with a brief description of their application. Table 24 then illustrates the projected IFOV, the spectral resolution, the number of bands available, the data transmission rates, the pointing capability of the system and an assessment of the relative complexity of the system. These should be compared directly with the data presented for TM in the same tables. This TM data is representative of the state of the art for Earth remote sensing systems and is an integral part of the Landsat 4/5 program. Figures 56 and 57 contain plots for the expected evolution of spatial and spectral resolution capabilities.

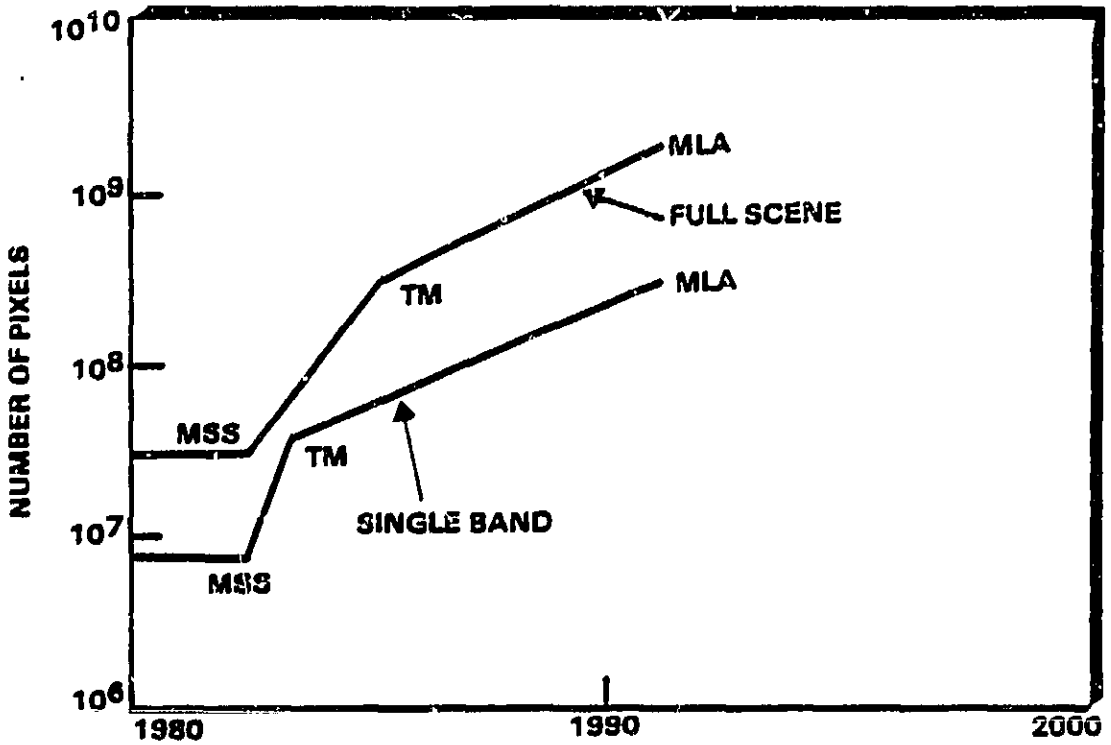

Figure 55. Projection of Single Band and Full Scene Data Processing Requirement for the Future (Landsat)

TABLE 23

MULTISPECTRAL LINEAR ARRAY - POTENTIAL SENSORS

Pointable High Resolution Imaging Radiometer (PHRIR)
Supports Experiments Requiring the Highest Spatial Resolution, Off Nadir Viewing, Modest Field-of-View, and High Spectral Resolution with Bands Defined Prior to Flight

Pointable Imaging Spectrometer (PIS)
Supports Experiments Requiring In-Orbit Selection from Many High Resolution Spectral Bands, Moderate Spatial Resolution, Small Field-of-View

Moderate Field-of-View Imaging Radiometer (MFIR)
Supports Experiments Requiring 3-5 Day Coverage of Large Areas with Modest Spatial Resolution and a Limited Number of Spectral Bands

Wide Field-of-View Imaging Radiometer (WFIR)
Supports Experiments Requiring 1 to 2 Day Coverage on Large Areas with Low Spatial and Spectral Resolution

Thematic Mapper (TM)
This Sensor Has Flown on Landsat 4 and is Shown for Reference Purposes

TABLE 24

MULTISPECTRAL LINEAR ARRAY - POTENTIAL SENSORS - PERFORMANCE

	*PHRIR	PIS	MFIR	WFIR	TM
Field-of-View (km)	60-180	10-30	200-800	1000-2000	185
Instantaneous Field-of-View (m)					
VIS/NIR (0.4-1 μm)	5-20	30-60	50-200	300-600	30
SWIR (1-2.5 μm)	10-40	30-60	100-400	300-600	30
MIR (3.4-4.2 μm)	20-80	60-120	200-800	300-600	—
TIR (8.5-12.5 μm)	40-160	60-120	400-1200	300-600	120
Spectral Resolution (nm)					
VIS/NIR	20	10-20	100	200	80
SWIR	20	10-20	100	200	200
MIR	100	50-100	200	400	—
TIR	100	50-100	500	1000	1200
Number of Bands Available					
VIS/NIR	8	30-60	3	3	4
SWIR	8	100-200	2	2	2
MIR	4	8-16	2	2	—
TIR	4	40-80	2	2	1
Number of Bands Transmitted	TBD	TBD	All	All	All
Data Rate (Mb/s)	300	TBD	<30	<10	85
Pointing Capability	Yes	Yes	No	No	No
Complexity	High	Very High	Moderate	Low	High

*See Table 23 for definition of sensor acronyms.

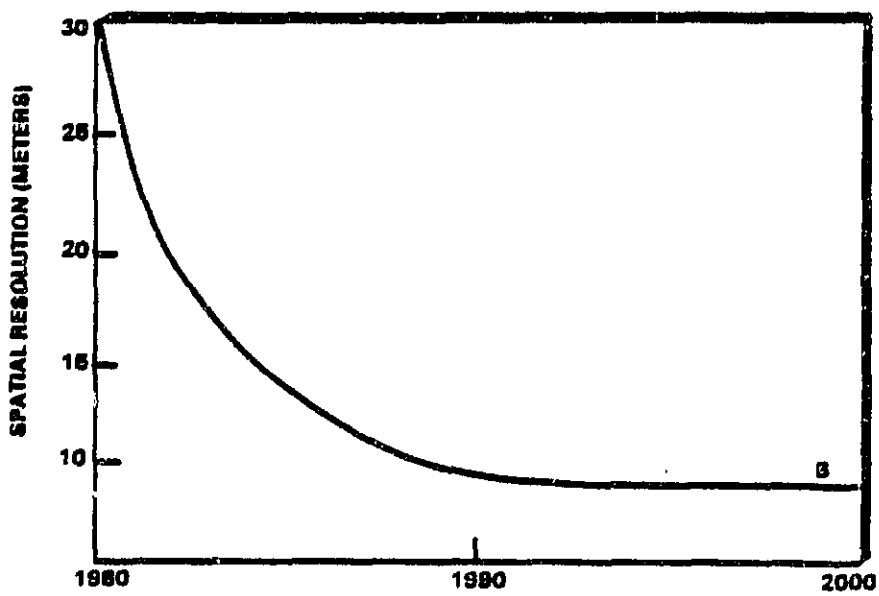

Figure 56. Spatial Resolution Capability Projection

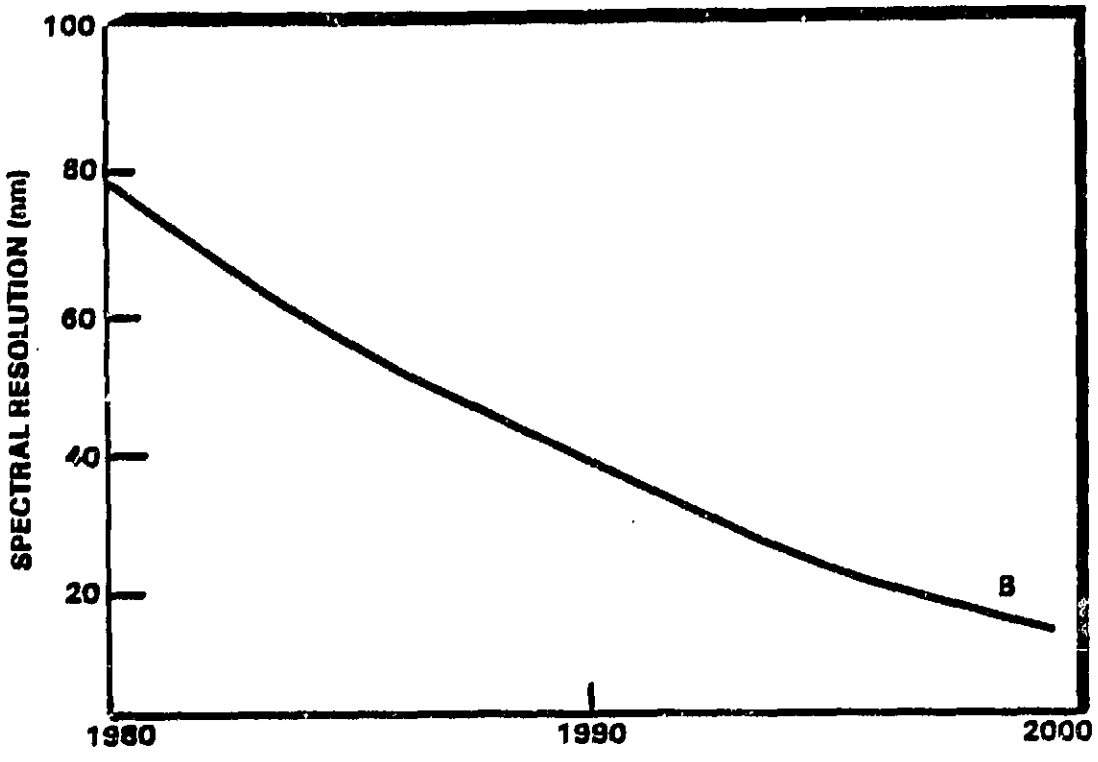

Figure .57. Spectral Resolution Capability Projection

Table 25 contains a summary of parameter projections for a possible MLA system.

TABLE 25

PERFORMANCE PROJECTIONS OF MLA

Parameter*	SOA Value	2000 Value
IFOV	20-30 meters	<5 meters
$\Delta\lambda$	60 nm	<20 nm
SNR	100-300	1000
Data Rate	100 Mbs	500 Mbs

*The parameters listed are interrelated and trade-offs can often be made between them. For example, SNR can be improved by increasing the spectral bandwidth ($\Delta\lambda$) or increasing the size of the IFOV.

Critical system and subsystem components required for future high performance multispectral linear array sensors include: (1) short wave infrared (SWIR) detectors; (2) thermal infrared (TIR) detectors; (3) wide-field, broadband optics; and (4) cryogenic coolers.

Linear Detector Arrays for Earth Imaging. Additional development of detector arrays is required primarily in the 1 to 3 μm and 10 to 13 μm spectral regions for use in earth resource applications. Two approaches are being pursued for the 1-3 μm detector arrays: (1) Schottky barrier IRCCD arrays and (2) HgCdTe/CCD arrays in which the ternary detector material is compositionally tuned to provide high sensitivity in the preferred spectral region.

The advantages of the Schottky barrier devices arise from the fact that the structure is fabricated in monolithic silicon which is a very well understood material. The primary disadvantage is in the quantum efficiency (QE) of the device which is relatively low, on the order of 2 to 5% for palladium silicide detectors at the cutoff wavelength (λ_c) of 2.3 μm. Table 26 provides a forecast of performance parameters for these detectors.

TABLE 26

PROJECTED PERFORMANCE PARAMETERS - SCHOTTKY BARRIER IR DETECTOR ARRAYS

Year	No. of Elements Per Chip	λ_c (μm)	QE (%)	Operating Temperature (K)	Detector Type
1982	256	2.3	2	120	Pd_2Si
1985	512	5.0	3-4	80	PtSi
1990	2048	8.0	2-3	70	IrSi
2000	4096	10-13	3-4	50	IrSi

Thermal IR array technology development activities are being funded primarily by DoD. Of particular interest to NASA is the use of photovoltaic (PV) HgCdTe coupled to silicon CCD multiplexers. PV devices present minimal thermal loads and thus ease the cryogenic cooler

requirements. However, if long life, low temperature cryogenic coolers become operational in the future, it may be possible to operate the detectors at temperatures substantially below those provided by passive radiative coolers and thus simplify the detector design problem. A forecast is given in Table .. 27.

TABLE . .27

THERMAL IR LINEAR DETECTOR ARRAYS - (PV) HgCdTe/Si CCD

Year	No. of Elements Per Chip	λ_c (μm)	Operating Temperature (K) (1)	Operating Temperature (K) (2)	D^* (cm-Hz$^{1/2}$W^{-1})
1982	64	9.5	100	105	1×10^{10}
1985	128	11.5	95	100	2×10^{10}
1990	512	12.5	90	100	4×10^{10}
2000	1024	15.0	90	105	$>5 \times 10^{10}$

(1) Will be able to operate at this temperature.

(2) With suitable development should be able to operate at this elevated temperature.

Additional areas where development is needed for adv nced high resolution multispectral sensor systems for use in future generations of Earth and planetary multispectral imaging systems are:

- Wide field, high angular resolution, wide spectral range optical systems
- Long life, high capacity cryogenic coolers
- Data compaction techniques
- Very high data rate communications links.

Future development of these components is discussed elsewhere in this volume.

Visible/Infrared Imaging Spectrometer (0.4-2.5 μm). This instrument is an outgrowth of previous Earth remote sensors such as MSS, TM, and MLA and provides greater spectral and spatial resolution allowing identification of vegetation and geologic formations. A specific example, the Shuttle Infrared Spectrometer-A (SIS-A), has already flown on the Space Shuttle.

The sensor contains focal plane arrays sensitive to both visible and longer wavelengths. These HgCdTe detector area arrays are operated in a pushbroom mode acquiring 128 simultaneous spectral images. The optical system consists of a triple Schmidt telescope and dual beam prism spectrometer. It covers the 0.4 to 2.5 μm spectral region. The spectral resolution is 10 nm in the visible and 20 nm in the infrared. At shuttle orbit altitude, it has a spatial resolution of 30 m. Shot noise dominates in the visible and detector noise is most important in the infrared. The system figure of merit is the noise equivalent change in reflectance or NEΔR. This parameter varies from 0.1% to 0.5% in the visible and from 0.5% to 1% in the infrared.

The infrared sensor performance is projected to improve by an order of magnitude during the next two decades as illustrated in Fig. 58. The most critical components for this system are the detectors. All aspects of detector performance including noise, dark current, uniformity, linearity of response, stability, and element yield are important. It is projected that these requirements can be achieved through continued study of narrowband semiconductors in general and HgCdTe in particular. Projections for noise, responsivity, and yield are presented in Figs. 59, 60, and 61, respectively. The year 2000 projections are itemized in Table 28.

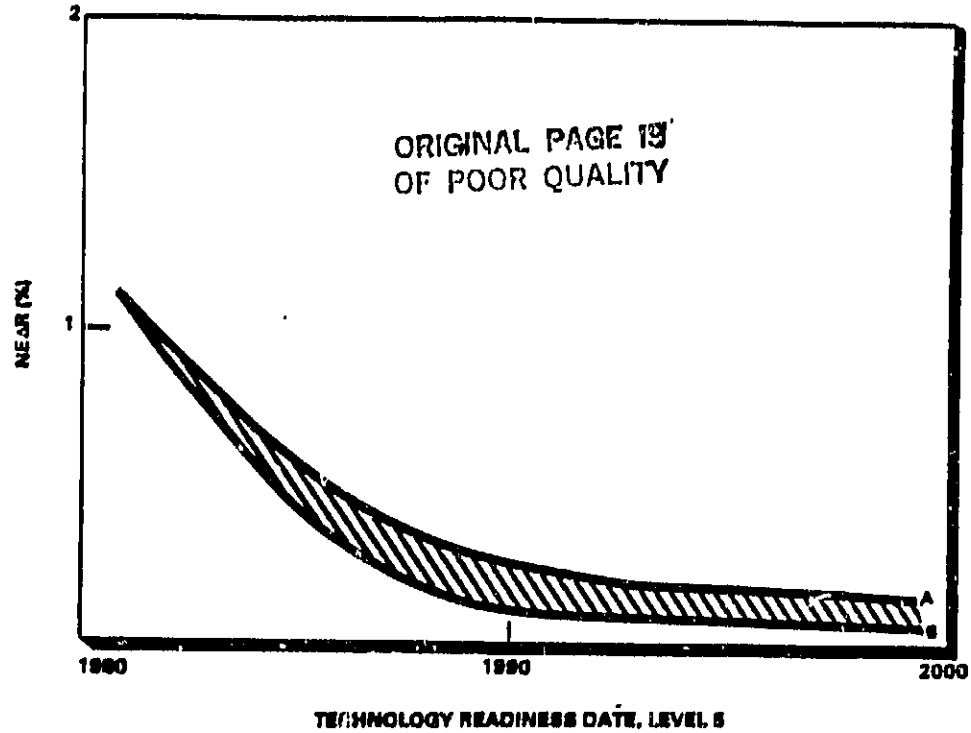

Figure 58. Infrared Sensor Performance Projection

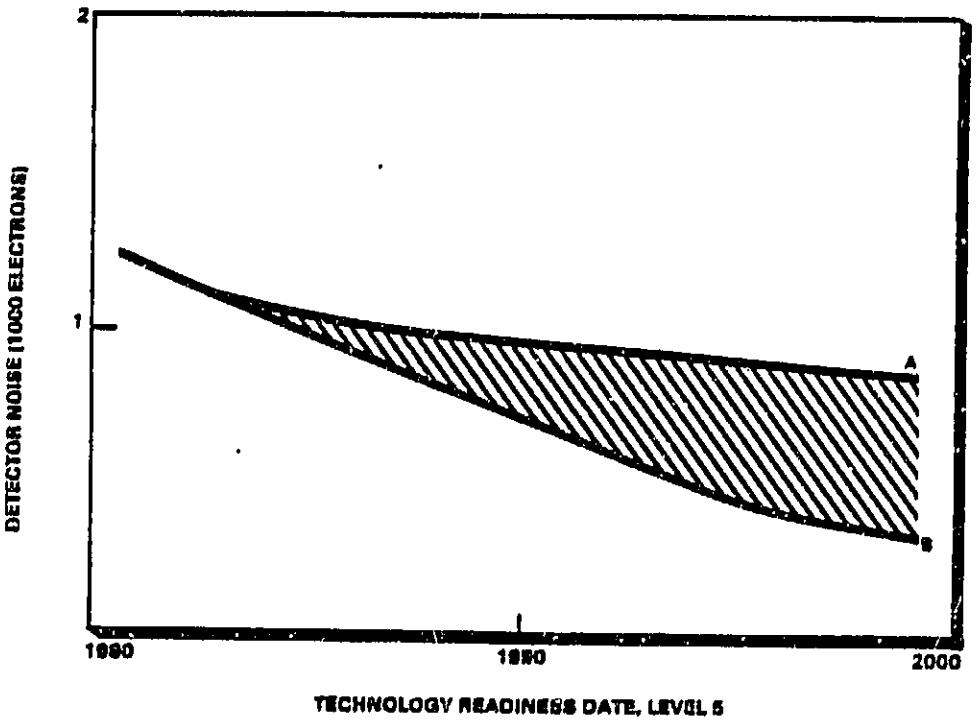

Figure 59. Noise Performance of 2.5 μm HgCdTe PV Detector Area Arrays (120 K)

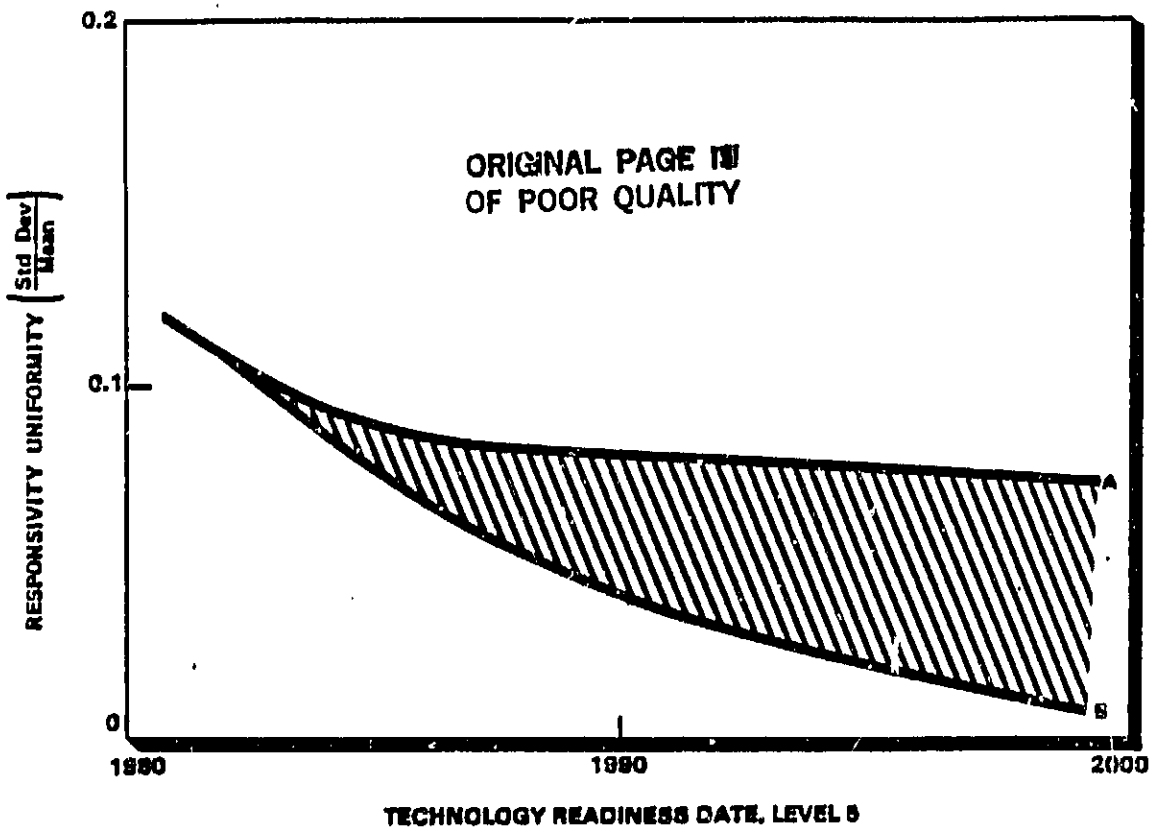

Figure 60. Responsivity Uniformity of 2.5 µm HgCdTe PV Detector Area Arrays (120 K)

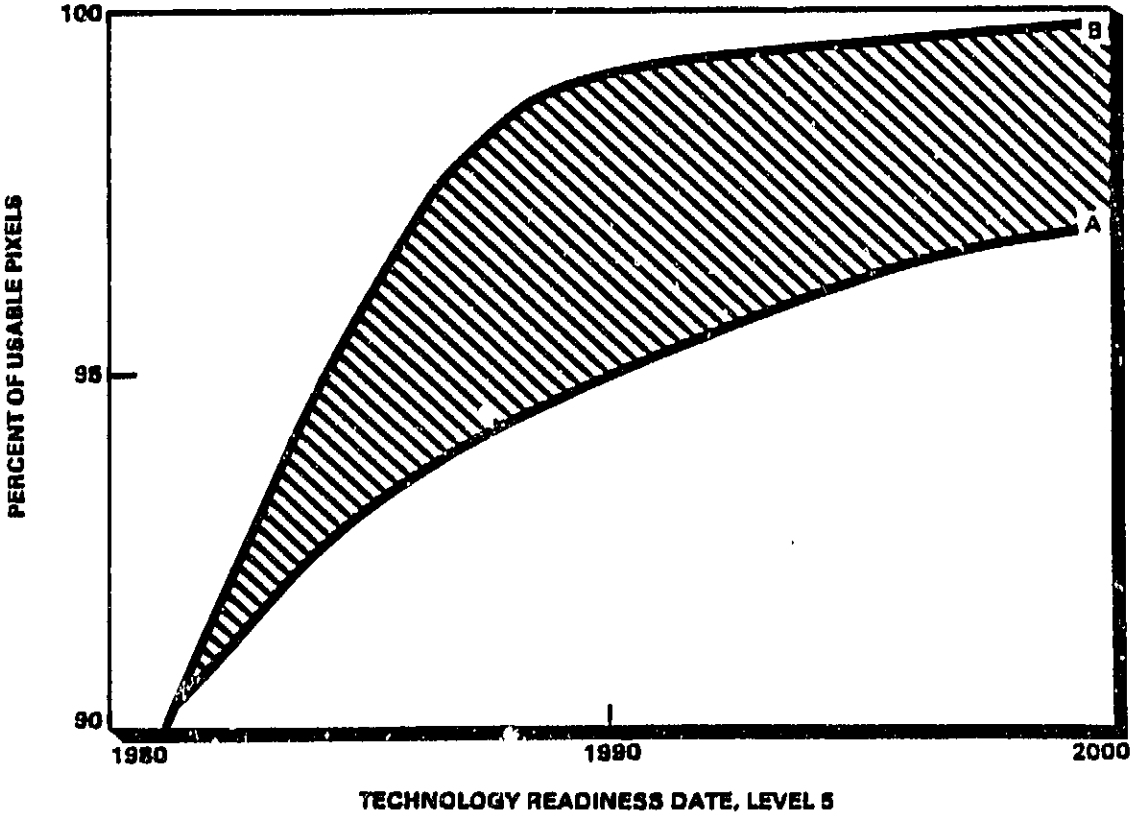

Figure 61. 2.5 µm HgCdTe PV Detector Area Array Element Yield

TABLE 28

PV HgCdTe DETECTOR PARAMETER FORECAST

Critical Component and Characteristic	SOA Value	2000 Value
PV HgCdTe Detectors:		
Noise	1000 e	500 e
Dark Current	1 pA	0.1 pA
Uniformity*	10%	5%
Linearity**	15%	1%
Stability	10%	1%
Yield	90%	98%

*Ratio (Std. Dev./Mean detector response).

**Residual non-linearity after Ax+B corrections.

4.3.2 Infrared Cameras for Astronomy

These imaging systems are composed of detector arrays, cryogenic readout electronics, cold IR filters, cryogenic cooling systems, and collecting optics which along with detector (pixel) size determine the spatial resolution. Spectral information is obtained through optical filters which also limit the background noise bandwidth. Highest sensitivity is obtained with cooled optics.

IR array performance can never exceed the background limit, which for a photoconductive detector, is given by

$$NEP_{BLIP} = 2hc(\dot{\phi}^{1/2})/\lambda$$

where h is Planck's constant, c is the speed of light, λ is the wavelength, and $\dot{\phi}$ is the arrival rate of incident photons. In low background applications, such as SIRTF, and especially in instruments

with high spectral resolution, ϕ becomes quite small, and background noise is negligible. Performance limits are then set only by the particular detector/electronics configuration [including preamplifier (FET) noise] of the array. The ultimate theoretical limit would be reached when an IR array is sufficiently sensitive to count single photons.

A number of IR astronomical instruments could use high-sensitivity arrays. IR cameras will require two-dimensional formats. Dispersive spectrometers, such as the FTS, can utilize one-dimensional arrays, or two-dimensional arrays for simultaneous spatial and spectral information. Spatial maps of polarization could also be obtained with a polarizing, array-based IR camera. Infrared cameras for ground-based observations based on 16 x 16 Si:Si arrays operating in the 4-17 μm spectral range exist today. Size and weight of an infrared camera for spaceflight use will be determined by the needed cryogenic systems. The instrument alone should weight <10 kg. Power requirements per array are low, <10 mW. Required data rates are less than 10^4 bits/sec.

Integrated Detector Arrays (2-30 μm). In this spectral region, the most promising detectors are the extrinsically doped Si CCD and CID arrays. Integrated extrinsic silicon IR arrays combine large numbers of IR detector elements with readout multiplexing electronics. Photolithographic techniques are also used to produce arrays with detection and readout processes on a single substrate (monolithic) or on separate substrates which are "bump bonded" together (hybrid). The multiplexing capability dramatically simplifies the wiring requirements to the cold focal plane assembly; n-element IR arrays would allow a map to be generated in 1/n the time required with a single detector; and on-chip integration of charge affords increased sensitivity.

This technology draws on previous development of discrete extrinsic silicon IR detectors (excellent detector material is required for both discretes and arrays), and recent advances in semiconductor microcircuit processing.

IR arrays require both dc and clocked voltages, and typically, correlated double sampling of the on-chip FET amplifier output. They also require cooling to a sufficiently low temperature (typically 8-40 K) so that thermal generation of carriers in the detector is suppressed.

IR cameras based on these arrays have square pixels equal to 100 μm on a side. 64 x 64 element arrays are possible today. IR array technology is a rapidly moving field. Dramatic progress has been made since the first rudimentary Si:X CCD array was produced in 1974. We can project performance levels into the future with modest level of confidence, but it is very unlikely that this performance will be achieved with current CCD or CID technology. New configurations for low-noise readout, such as the switched sample and source-follower-per-detector schemes, are already under development as alternatives to the CCDs.

Figure 62 contains a projection for the system NEP at 15 μm and 1 sec integration time.

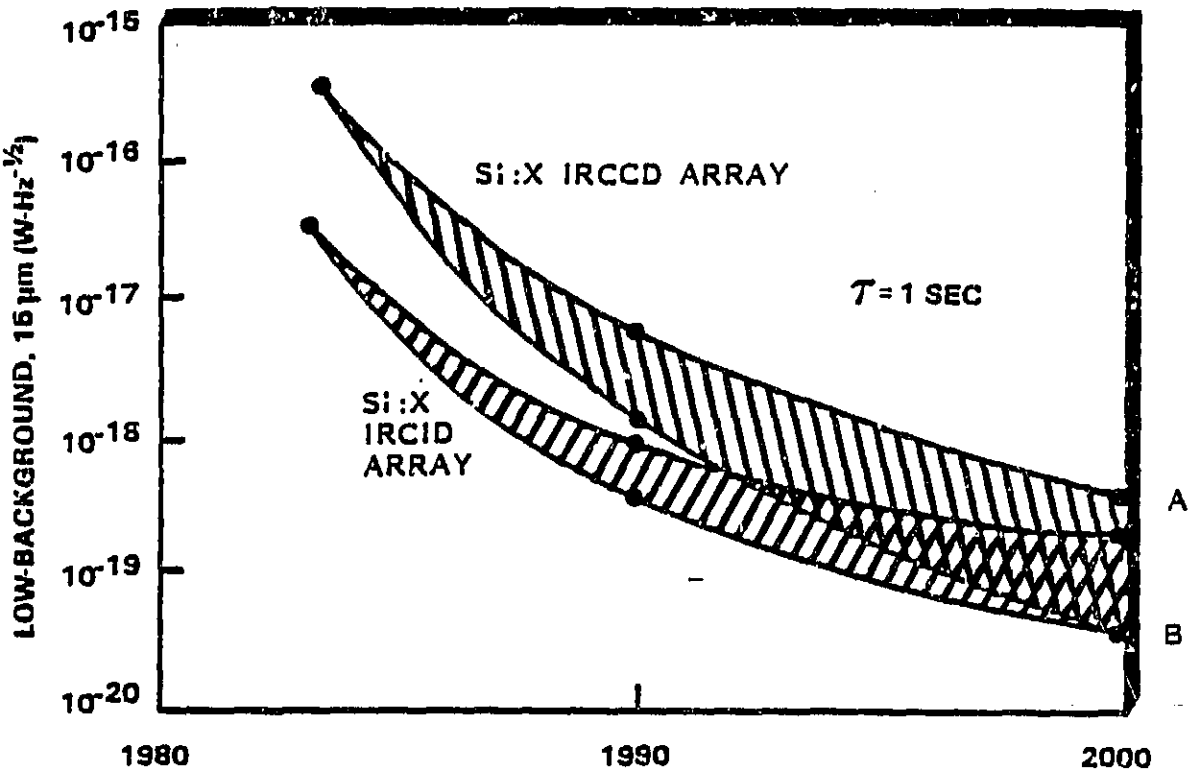

Figure 62. Si:X Array NEP Projection (<30 μm)

It is expected that additional NASA funding would be required to accelerate development progress from curve "A" to curve "B". This assumes a continued high level of DoD support for this technology, to serve as a starting point for optimizations by NASA of array technology specific to astronomical applications.

Table 29 contains the projections for parameters of interest.

TABLE 29

ARRAY TECHNOLOGY PROJECTION (λ<30 μm)

Parameter	SOA Value	2000 Value
NEP ($W/Hz^{1/2}$) at 15 μm, τ = 1 sec	7×10^{-16}	5×10^{-19}
NEP ($W/Hz^{1/2}$) at 30 μm, τ = 1 sec	**	1×10^{-18}
Array Size (15 μm)	64 x 64	500 x 500
Read Noise (Electrons)		
CCD	800	10
CID	150	10
Cooling		
4 μm	40 K	
30 μm	8 K	

**Longest available IRCCD wavelength is 24 μm.

In many cases, arrays and, hence, astronomical instruments are (or will be) limited by noise in the cold FET preamplifier. Continued development is clearly needed. Chances are that entirely new techniques (GaAs?, superconducting?) will be used in 2000 AD. It is, however, possible to at least guess future performance levels. A forecast of preamplifier noise is given in Table 30.

TABLE 30

PREAMPLIFIER NOISE IMPROVEMENT PROJECTION

Critical Component and Characteristic	SOA Value	2000 Value
Preamplifier (FET) Noise, at 1 Hz, 4 K ($V/Hz^{1/2}$)		
Ge JFET	1×10^{-7}	1×10^{-9}
Si MOSFET	5×10^{-7}	1×10^{-9}

Parallel research activities for high performance astronomical instrumentation for low background astronomy includes:

- Cryogenic electronics (FETs and other components, including load resistors, capacitors, operational amplifiers, and eventually A/D converters for operation at $\leq$4 K).
- Improved cold IR filters, especially for $\lambda > 20$ μm.

Integrated Long Wavelength IR Detector Arrays (>30 μm). Integrated arrays of detectors sensitive to wavelengths >30 μm do not presently exist. Steps toward building and evaluating small prototype arrays have been initiated. An array concept for Ge:Ga photoconductive detectors multiplexed with switched sample FET readout has been established. Ge:Ga arrays will differ from Si:X arrays in that (a) the detectors will be physically larger, since diffraction-limited detector dimensions grow with increasing wavelength; (b) integrated cavities or similar schemes must be incorporated to compensate for the low inherent absorption in extrinsic germanium; and (c) bias levels will be on the order of a few 100 mV rather than a few volts.

Long wavelength arrays will clearly evolve from discrete Ge:X detector technology, which is not presently in a state of maturity. The clocking requirements will be similar to those of a Si:X CCD. Cooling to lower temperatures will be required.

Projected low background NEPs at 100 μm for discrete and integrated Ge:Ga detectors are presented in Fig. 63. Negligible DoD interest in >30 μm IR detectors exists, so this development must be carried solely by NASA. It is expected that additional funding would be required to move from curve "A" to curve "B". Array size data and NEP projections are presented in Table 31.

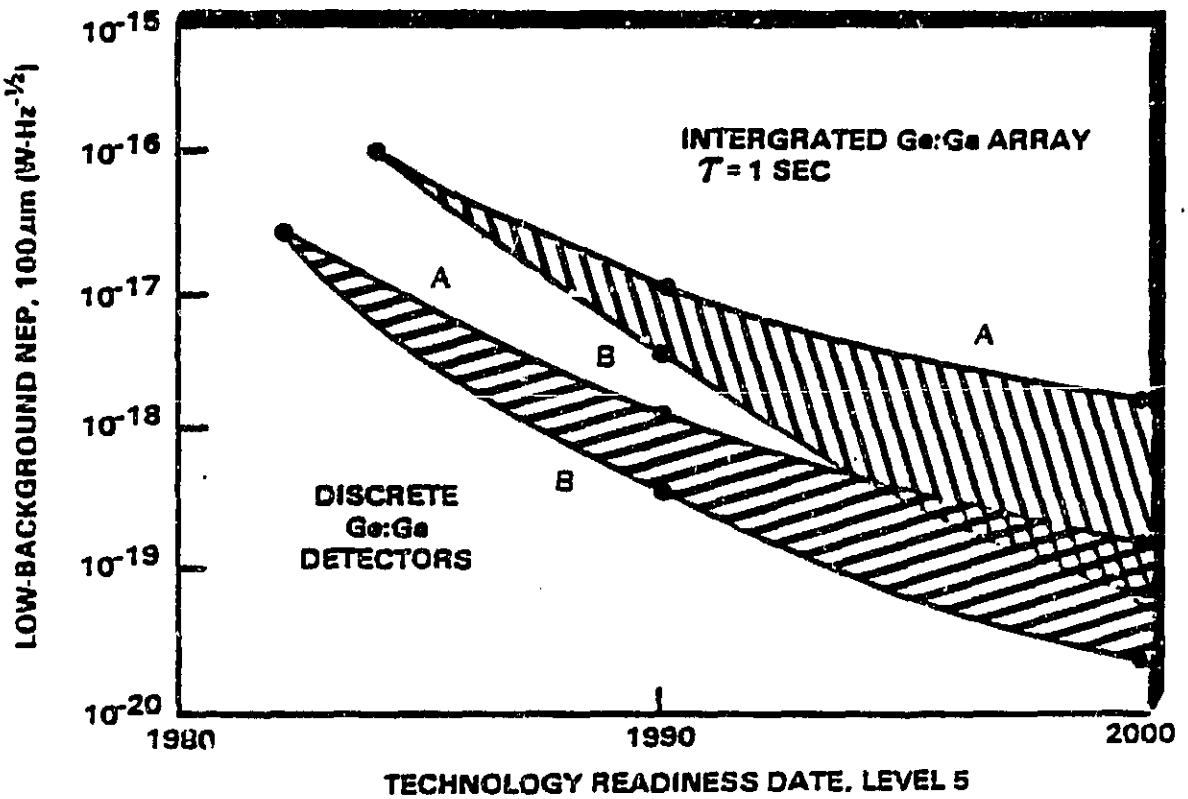

Figure 63. Projected NEP for Ge:Ga Detector Arrays

TABLE 31

100 μm ARRAY TECHNOLOGY PROJECTION

Parameter	SOA Value	2000 Value
NEP (W/Hz$^{1/2}$) at 100 μm		
Discrete Detector	3×10^{-17}	1×10^{-19}
Array with τ = 1 sec	—	4×10^{-19}
Array Size	—	64 x 64
Read Noise, e	—	30

Overall, the same set of subsystems critical to the 2 to 30 μm arrays are important for this 30 to 219 μm system.

4.4 Infrared Detector and Array Technology

Detector technology is the critical area for all infrared sensors. Description and forecasts for specific detectors have been provided in connection with the various sensor systems forecast. This section attempts to treat some general aspects of infrared detector and detector array technology.

Sensitivity is the characteristic which makes infrared detectors most useful in low background astronomical applications. The best InSb photoconductors and the detectors which are used in the four IRAS focal plane instruments provide a state of the art example of the optimum single element detector performance from 1-100 μm (Table 32).

TABLE 32

IRAS FOCAL PLANE AND InSb DETECTORS

Wavelength			NEP	
Center (μm)	Bandwidth (μm)	Material	($WHz^{-1/2}$)	
12	6	Si:As	7×10^{-16}	in flight
25	11	Si:Sb	2×10^{-16}	in flight
60	40	Ge:Ga	2×10^{-16}	in flight
100	37	Ge:Ga	1.5×10^{-16}	in flight
2.2	1-5	InSb	1.2×10^{-16}	Lab

Below 50 μm, the lowest NEP values reported are for the extrinsic silicon photoconductive detectors with NEP $\sim 3 \times 10^{-17}$ $WHz^{-1/2}$. These devices are amplifier noise limited. The quantum efficiencies of these extrinsic detectors are generally somewhat lower than the quantum efficiencies of intrinsic detectors (InSb, HgCdTe, etc.), but the sensitivity, which is a function of noise and quantum efficiency, is an order

of magnitude better in doped silicon. The chief disadvantage of doped silicon detectors is that they must be operated near liquid He temperature, which places more of a burden on the cryogenic system than an intrinsic detector does with its liquid N_2 system. A major obstacle to the effective use of Si:X detectors at low backgrounds is the presence of the well known but poorly understood "anomalies."

Figure 64 shows the trend in noise equivalent power (NEP), for 100 μm Ge:Ga photoconductive detectors. These devices are currently the most sensitive for broadband detection at wavelengths above 30 microns. Performance of discrete Ge:Ga detectors is shown for the past 20 years. The experience gained in the Infrared Astronomy Satellite (IRAS) project has helped push the sensitivity of these discrete detectors to near astrophysical (zodiacal background) limits. The long wavelength cut-off can be extended to 210 μm with an NEP ~ 6×10^{-17} $WHz^{-1/2}$ by applying uniaxial stress along the [100] crystallographic direction. These devices also operate at liquid helium temperatures (~2 K).

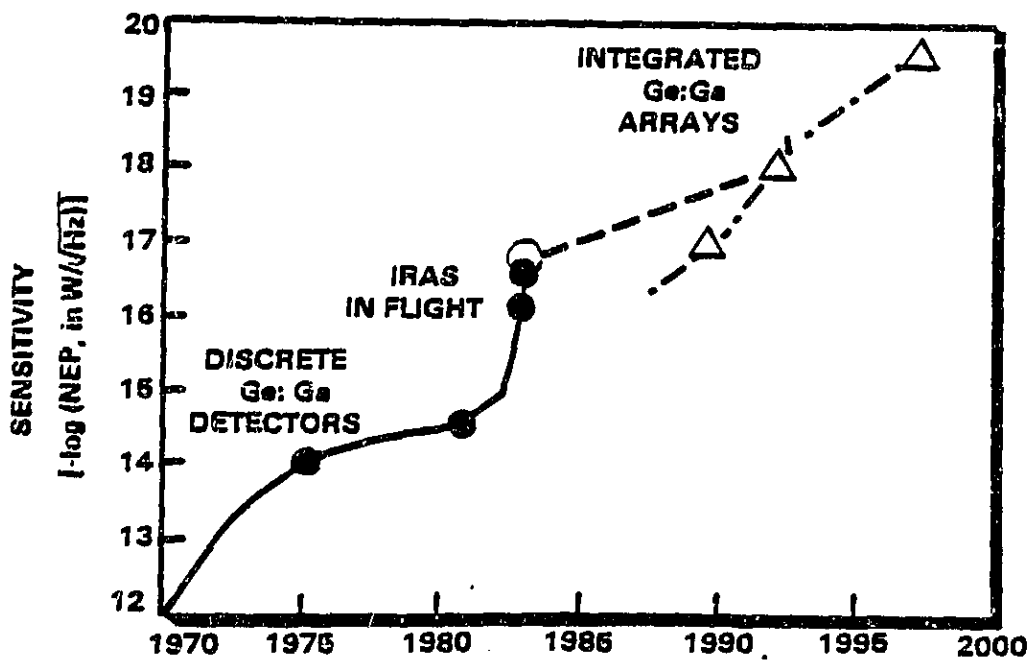

Figure 64. Infrared Detection Sensitivity at 100 μm

In low background operation, all these photoconductors are amplifier noise limited and they are susceptible to radiation present in space environments. Continuing work on these devices is needed to improve their production yield, fundamental understanding of their performance characteristics, and their resistance to high energy radiation effects. Blocked impurity band photoconductors show promise of less radiation effects and more linear response.

Improvements in sensitivity can be achieved through on-chip-time integration. Time delay and integration (TDI) is one method of reducing effects of amplifier noise. The prospect of significantly improved sensitivity comes through the integrated array concept. High-density, multielement arrays of Ge:Ga detectors can be coupled to cryogenic silicon charge-coupled-device (CCD) multiplexers to allow time integration and multiplexing of signals on the focal plane. Sensitivity improvements are expected through the low-noise readout which becomes possible, and the parallel sampling of the scene (in this case, NEP improves as τN, where N is the number of detectors). Projections of sensitivity were made using the relationship

$$NEP \approx \frac{en}{R} \quad (2/N\tau)^{1/2} \qquad WHz^{-1/2}$$

where e is the electronic charge, n is the number of RMS equivalent noise carriers per readout, R is the detector responsivity, and τ is the integration time. It is expected in a "realistic" sense that the array parameters shown in Table 33 will be available in the given time frame.

TABLE 33

Ge:Ga ARRAY PARAMETERS

Year	Number of Array Elements	Responsivity (A/W)	RMS Noise Carriers (electrons)	Maximum Integration Time (s)	NEP ($WHz^{-1/2}$)
1983	50	8	800	0.1	10^{-17}
1990	50	15	500	1	10^{-18}
2000	500	15	250	10	5×10^{-20}

Figure 65 shows the long wavelength cutoff λ_c of various intrinsic and extrinsic photon detectors. Horizontal lines are used in cases where a range of values of λ_c can be obtained by alloying or by the application of a uniaxial stress. An arrow indicates that further extension of the range is possible.

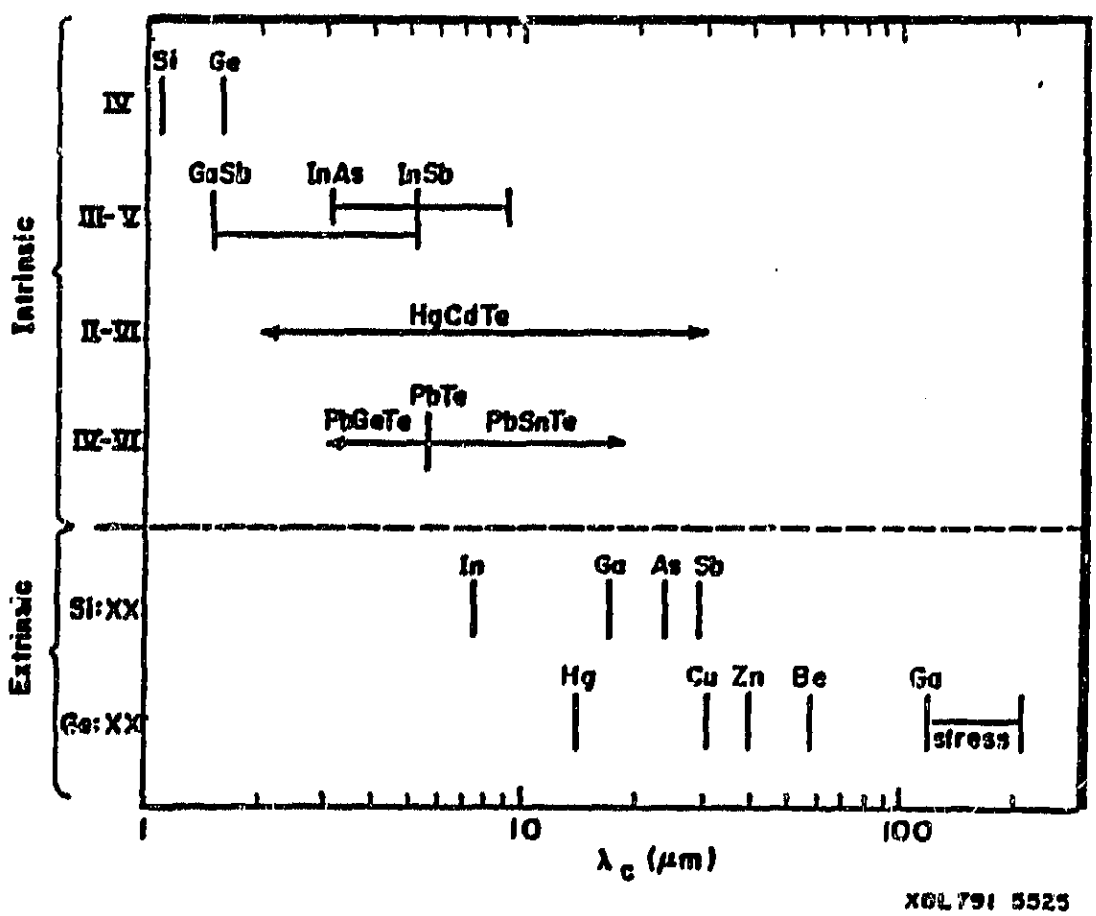

Figure 65. Cutoff Wavelength of Various Infrared Detectors

4.4.1 Array Technology

The feasibility of multiplexing large numbers of detectors on a focal plane has clearly been demonstrated in the past decade; large focal planes are likely in the future. The major thrust of the next decade's activity will be towards "smart" focal planes with substantial signal processing capability.

IR Focal-Plane Size—Linear Arrays. Figures 66 and 67 estimate the growth in the detector count for focal planes using long wave (LWIR, $\lesssim$30 μm) and short wave (SWIR, $\lesssim$5 μm) linear arrays. The number of detectors per cm curve for LWIR detectors is for detectors photolithographically defined on a single piece of detector material. Diffraction limits the smallest size detectors that are useful in the arrays. IRAS uses discrete detectors that are much larger, ~10 to 20 per cm.

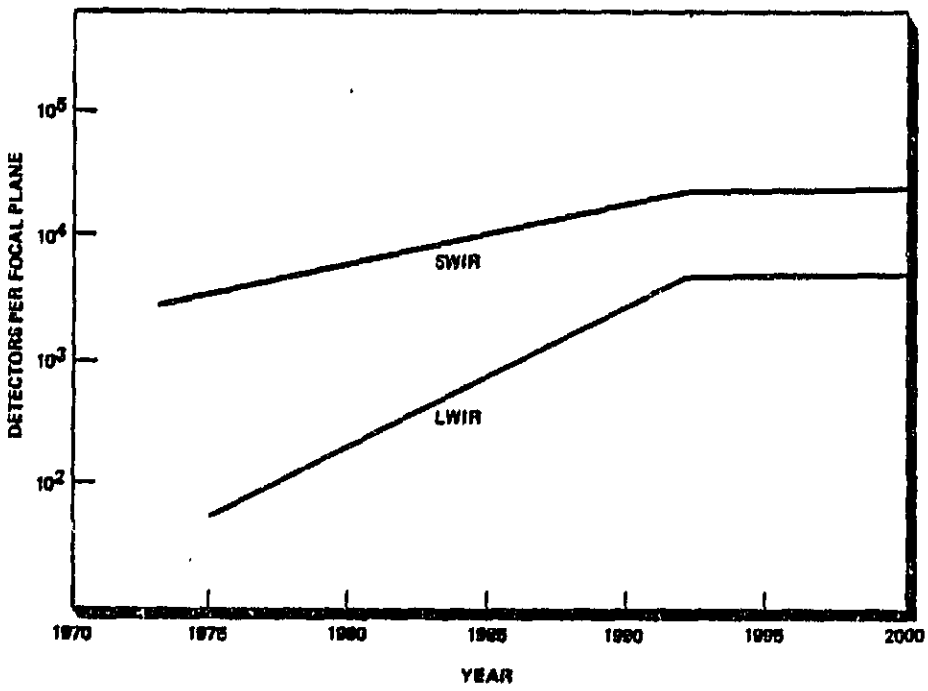

Figure 66. IR Focal Plane Size—Linear Arrays: Number of Detectors per Focal Plane Forecast

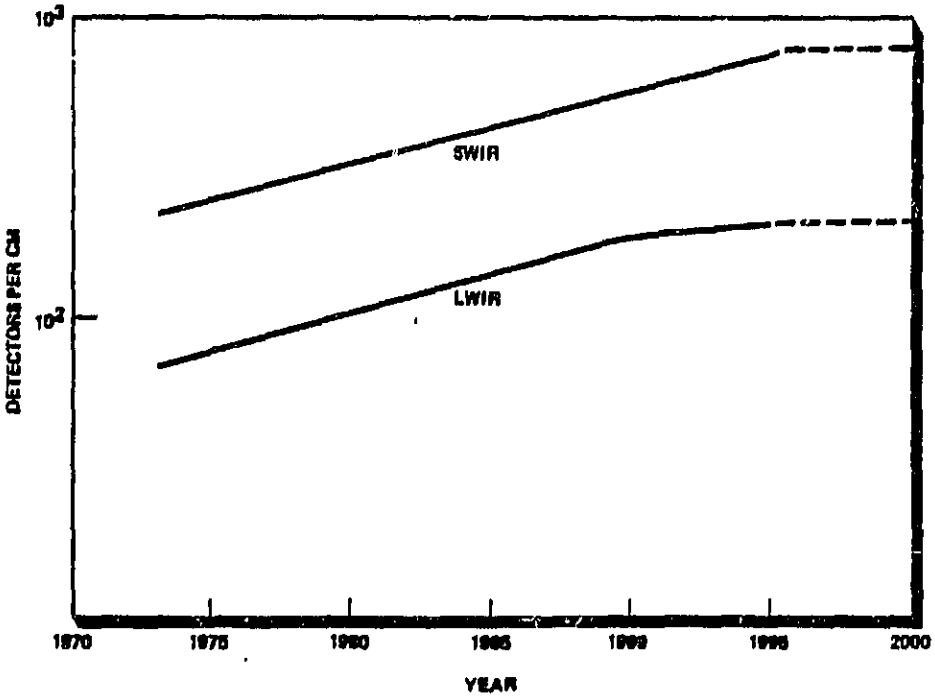

Figure 67. IR Focal Plane Size—Linear Arrays: Detector Density Forecast

Monolithic Linear Arrays. Monolithic infrared charge coupled devices (IRCCD) consist of devices in which the photodetection, charge generation, and charge transfer are achieved in a one material structure.

Charge coupled infrared imaging devices technology has been aimed mainly at development of monolithic InSb and HgCdTe (for 1-30 μm spectral coverage) linear arrays for operation in the pushbroom mode for planetary, atmospheric, astronomical, earth resource, oceanographic, and pollution measurements. Basically, spectral detectivity (in comparison to discrete detectors) is only limited to the noise produced in the CCD transfer device. Resolution capability is limited to the optics technology and detector size which can be tailored to a specific application. The major obstacles lie in achieving wider spectral range (a

materials technology and device fabrication problem), the achievement of fabrication techniques for long (100s to 1000s) arrays, and the associated integrated circuit technology for achieving the device and reasonable charge transfer efficiency. Linear array technology is directly transferrable to area arrays. The technology now being developed consists of a 100-element linear array and a 20 x 16 time delay and integration (TDI) area array. For area array considerations, the 20 x 16 TDI array can be operated as two 10 x 16 area arrays with 50% coverage.

The major advantages of the monolithic IRCCD development program is that the devices developed will require less power, space, and cooling while providing increased resolution and signal-to-noise ratio than other infrared devices. In addition, improved data handling capability is achieved along with improvements in signal-to-noise ratio and overall detector uniformity of response by going to the TDI mode of operation. TDI provides detector SNR improvements of $\sqrt{N}$, where N is the number of detectors normal to the linear array detectors (such as the 16 in a 20 x 16 TDI array). Also, preprocessing techniques, using on-chip FETs for amplifiers, multiplexing, and signal manipulation, are being evaluated and developed.

Infrared Imaging InSb and HgCdTe IRCCD Monolithic Linear Arrays (Fig. ~ 68). This figure illustrates the various stages of the evolution of the technology in this category. Basically the projection is that, with current infrared materials, wafer-sized 100-element linear arrays will be available in the early 1980s, with the larger arrays achievable through mosaics formed from the 100-element arrays. Improvements in SNR and detector uniformity will also be achievable in this time frame through the use of TDI arrays. The only constraint is the adaptation of the technology to specific mission detector array configuration requirements. If larger element arrays are required without the use of mosaics, then a materials technology program will have to be funded to provide larger infrared material wafers.

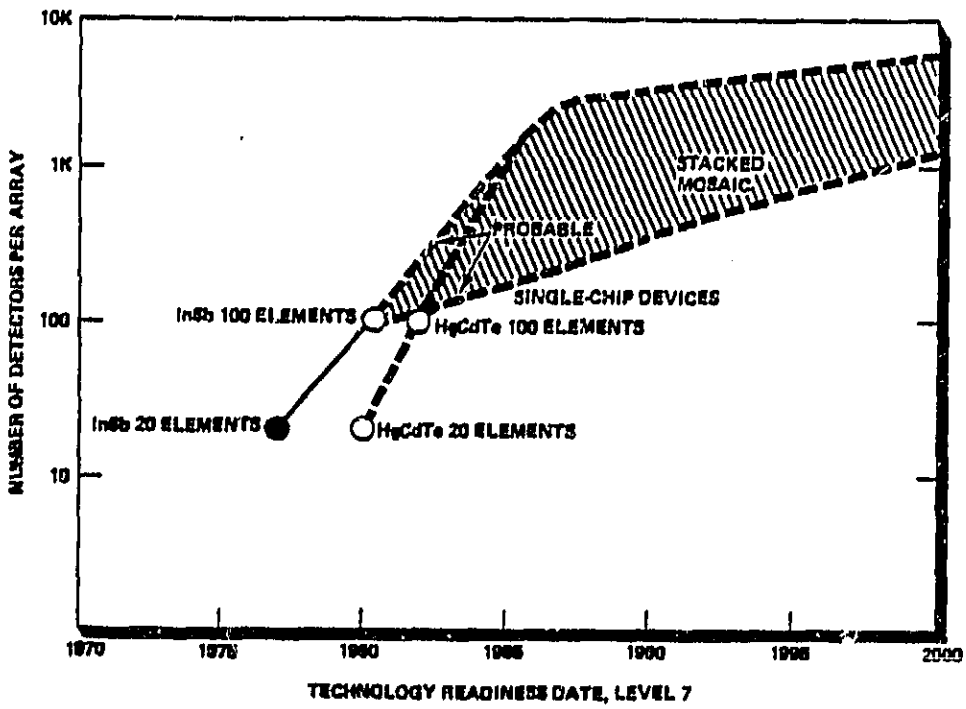

Figure 68. Monolithic InSb and HgCdTe Linear Arrays

Monolithic InSb and HgCdTe Array Sensitivity (Fig. 69). This figure shows some expected improvements in array sensitivity through improvements in the reduction of noise of the on-chip CCD devices and associated electronics readout. These data are for 77 K operation of the arrays and would change with operation at other temperatures. These data are also with a field of view (FOV) of 180° and could be improved by just decreasing the FOV. Increased sensitivities in other spectral regions (beyond 12 μm) will be dependent on materials improvements and improved device structures.

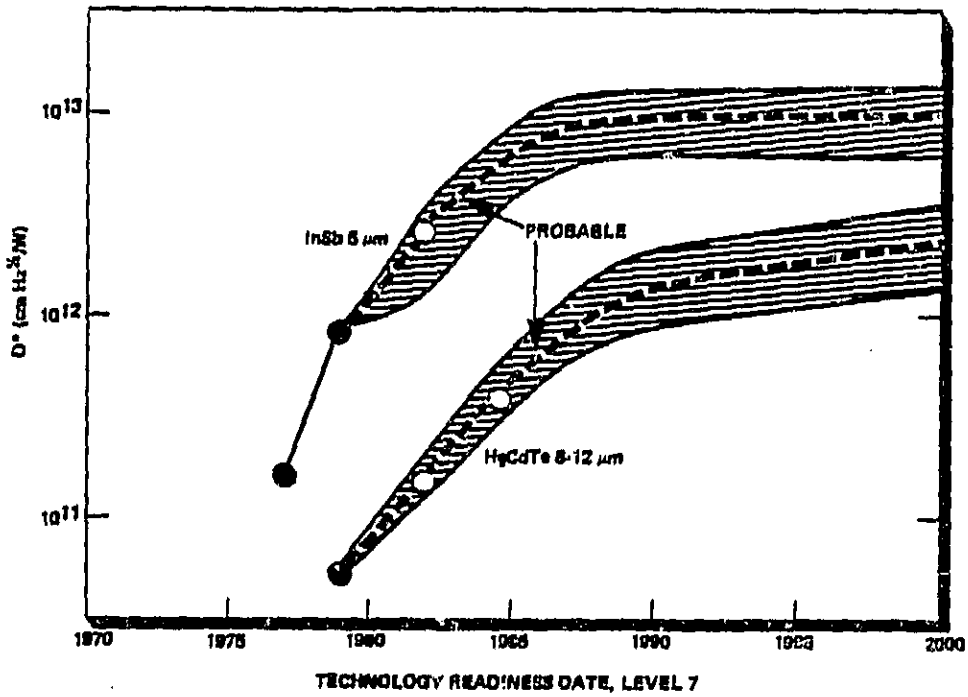

Figure 69. Monolithic InSb and HgCdTe Linear Array Sensitivity

Hybrid Thermal IR/CCD Arrays. Of the several technical approaches to the development of high-density focal plane detector arrays for the thermal IR region (8-14 μm), the hybrid focal plane array represents a pragmatic approach that combines a mature detector technology with a well-developed silicon CCD multiplexer technology. This is the most versatile of the approaches that are available. Its versatility arises from the ability to select and optimize independently the photodetector array and the readout multiplexer.

The separation of the sensing and readout media allows the benefits of CCD readout to be realized in a number of intrinsic detector materials whose MIS properties preclude viable CCD operation. Further, the benefits of intrinsic detectors, i.e., relatively high operating temperatures, high quantum efficiency, and low crosstalk can be realized.

Progress on HgCdTe infrared photodiode arrays hybridized with SiCCD multiplexers has been very good. The hybrid approach, however, does introduce a number of critical issues.

Performance (Fig. 70). To indicate the kind of performance growth that may be expected in the future, it is necessary to first establish some form of quantitative relationship or figure of merit which indicates the interrelationship of the IR imaging sensor parameters. One such figure of merit that can be used is given by:

$$\text{Performance} \sim \left[\frac{(\text{Sensitivity})(\text{Swath Width})^{1/2}}{(\text{Spectral Width})(\text{Linear Resolution})^2}\right]$$

Although other figures of merit could be derived, this form has the desirable attribute that includes most of the major system parameters and the value of the function increases as any of the parameters are made more stringent.

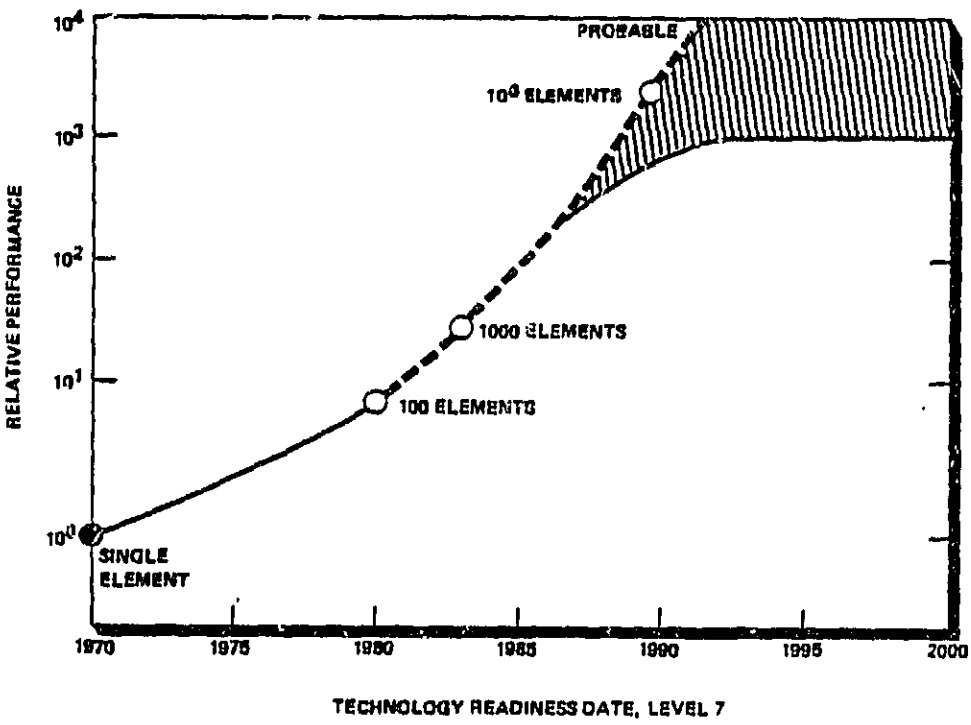

Figure 70. Performance Growth

Normalizing the figure to the year 1970, the curve indicates the improvement in relative performance as a function of the number of resolution elements in the detector array. It can be seen that the relative improvement increase is proportional to the square root of the number of elements in the array. Beyond array sizes of roughly 10,000 elements, one of the performance factors, namely, sensitivity, is shown approaching a limit for typical earth-viewing applications. This occurs for integration times in the millisecond region. Other performance factors such as resolution or swath width are not subject to this limitation.

Cooling Requirements (Fig. 71). As shown in the figure, photovoltaic arrays have an enormous advantage over photoconductor arrays with respect to cooling requirements in the thermal IR region. For long-term missions (years), the current method of cooling is through radiation to space. In earth-orbiting missions, realizable cooling of IR detectors to about 100 K is limited to thermal loads of a few hundred milliwatts.

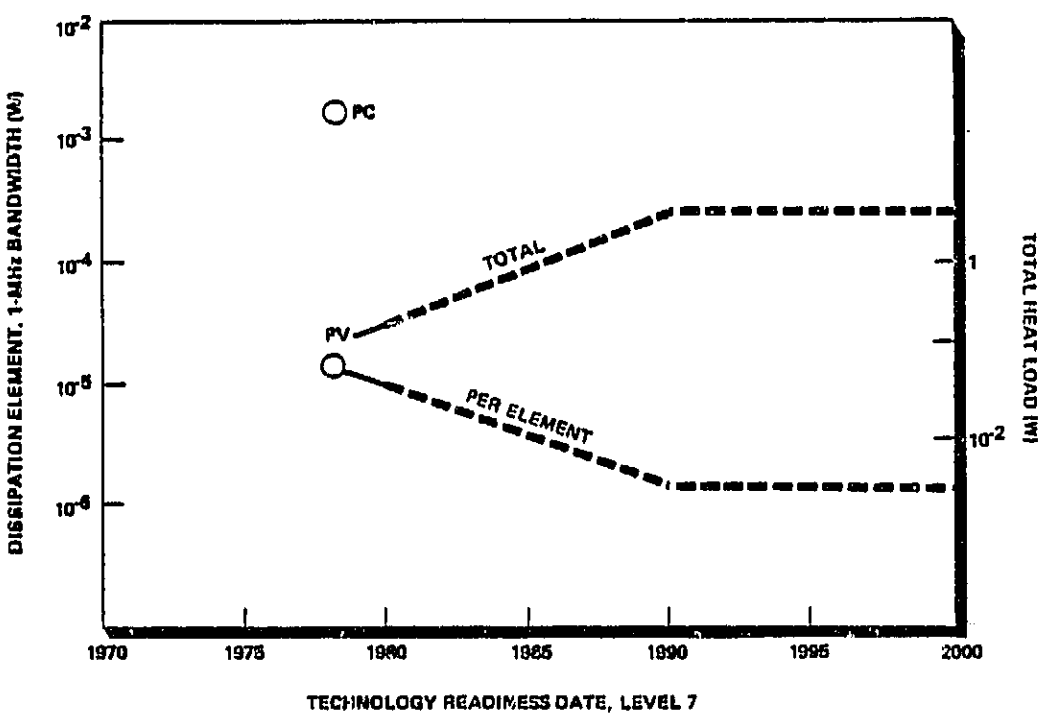

Figure 71. Cooling Requirements

Some improvement (reduction) in heat dissipation per element is anticipated due to smaller detector element sizes and technological improvements in the CCD circuitry.

The total heat load is projected to show a slow increase to 1990 as the number of detectors increases to the neighborhood of 1 million. The power level at this point is projected to be greater than 1 W for 100 K and, space radiators will undoubtedly require an assist from electromechanical coolers.

Reliability (Fig. ,72). As electronic equipment becomes more complex, and uses more components, reliability becomes a most important consideration. The development of solid-state electronics, especially its embodiment in integrated electronics, has removed the barriers of reliability (and unit cost). From 1970, the development of large scale integration (LSI) and the projection to very large scale integration (VLSI) shows a reduced failure rate per element of circuit through ~1995. The solid-state self-scanned array will share, in general, this increasing reliability. However, depending upon the type of interconnect that is finally evolved between the detectors and the charge transfer device, thermal hybrid IR arrays may possess significantly less reliability than the projection for 1995. Such arrays, however, will be many orders of magnitude more reliable than the handwired, mechanically commutated arrays of the 1970s.

4.4.2 Bolometers

Bolometers are broadband detectors, generally operated in the infrared, that work by measuring the heat generated by the absorption of incident radiation. The best bolometers are good absorbers and accurate thermometers. The dominate bolometer noise in a low background environment comes from the statistical thermal fluctuations in the device itself. This noise increases with temperature as T^n $(3/2 < n < 5/2)$.

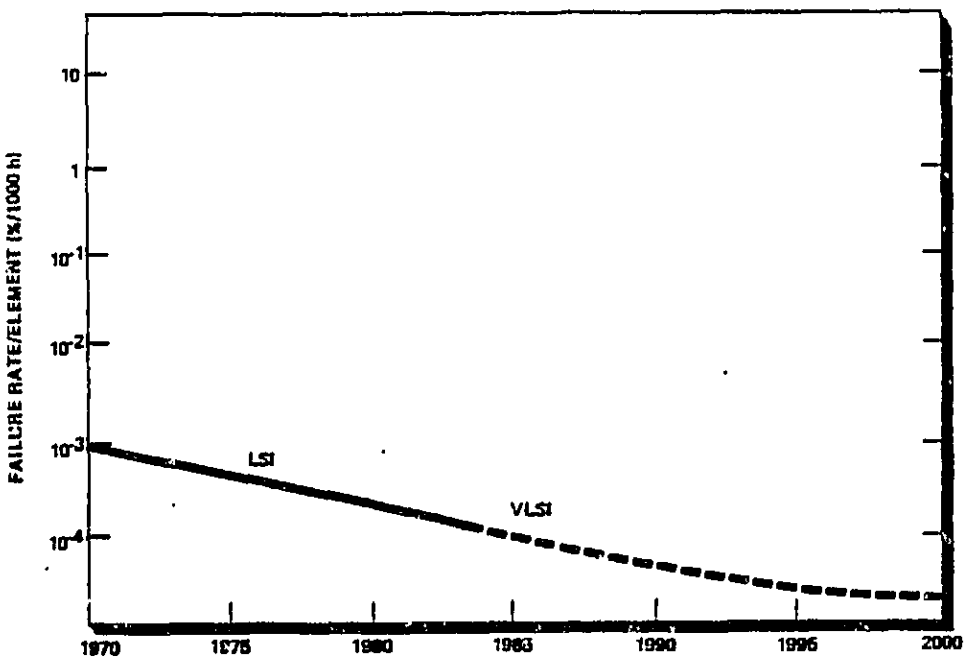

Figure _.72. Reliability

Bolometers can operate over a very wide spectral range, but due to other competing technologies, they are generally used between 100 μm. to 1000 μm.

The forecast of bolometer NEP has been plotted in Fig. _.73. Presently, the SOA for noise equivalent power is 5×10^{-16} $WHz^{-1/2}$. It is projected that by the year 2000, this value can be improved to 10^{-18} for ground applications and 10^{-17} for space applications. The theoretical limit is set by the system operating temperature.

In earth-based operation, temperatures of 0.3 K are routinely used. Devices that operate at 0.1 K or below are being developed. Space-based coolers at these temperatures have not been demonstrated but are under development. Predicted cooler performance is illustrated in Fig. 74.

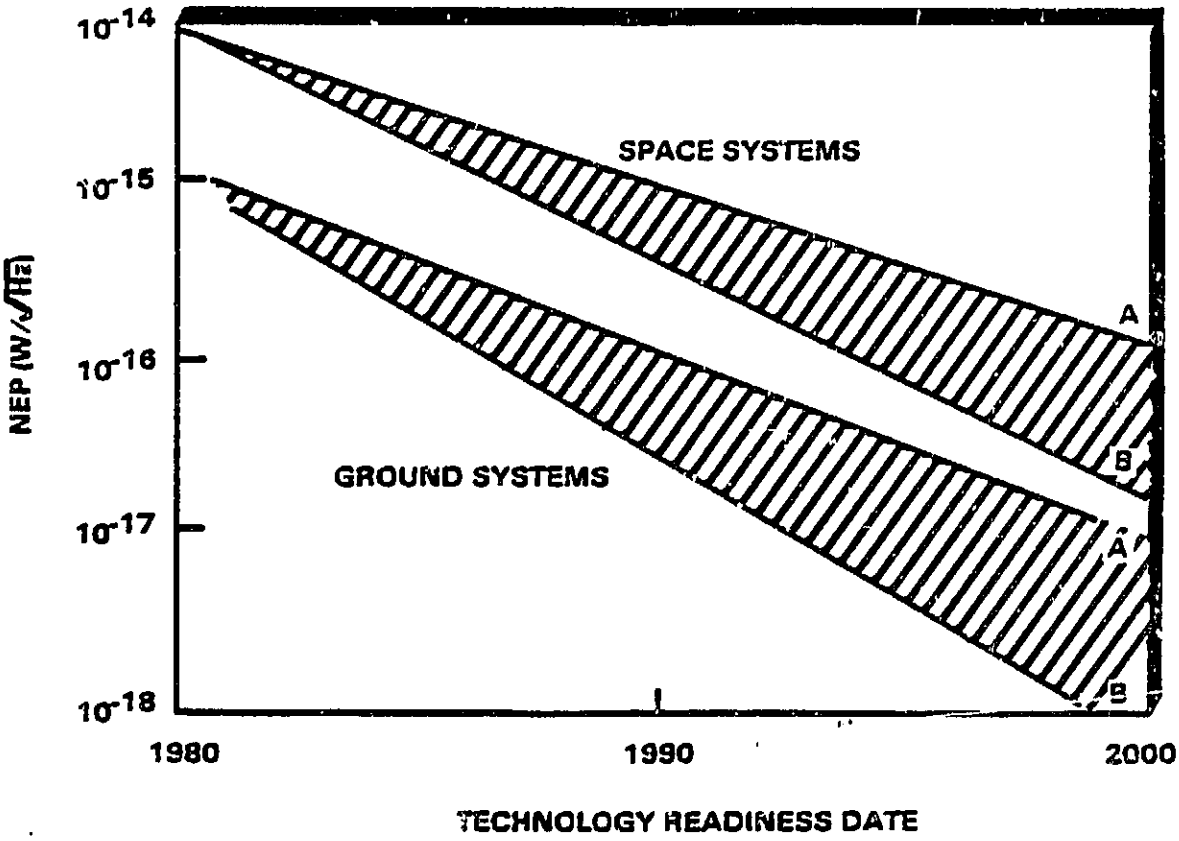

Figure 73. Bolometer NEP Improvement Due to Improved Coolers

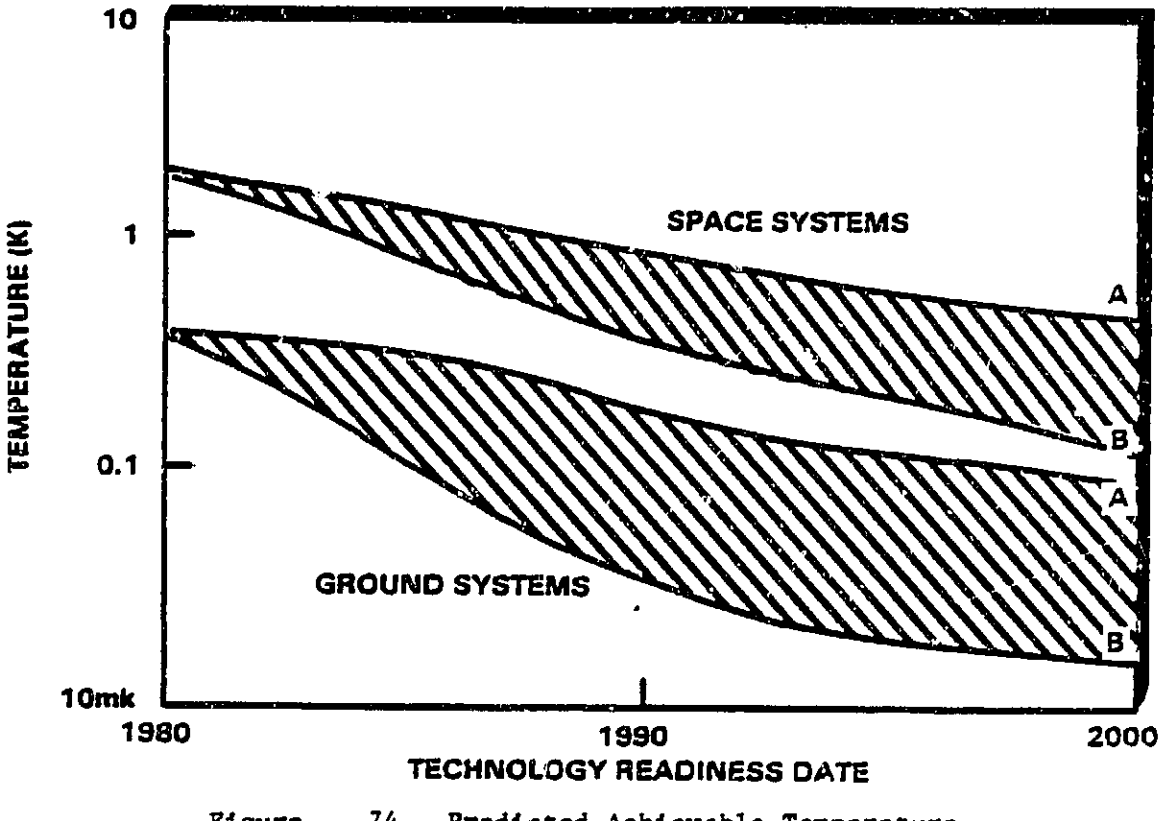

Figure 74. Predicted Achievable Temperature

The values of achievable temperatures are quantified in Table 34.

TABLE - - 34

PROJECTED VALUES OF TEMPERATURE (K) ATTAINABLE

Critical Component and Characteristic	SOA Value	2000 Value	Theoretical Limit	Notes
Coolers for Bolometers				
Ground-Based				
-^{3}He	0.27	0.27	0.27	Vapor pressure limited
-Adiabatic demag	0.1	0.01	0.005	Assuming single-stage device
Space-Based				
-Stored ^{4}He	1.6	1.4	1.1	Vapor pressure limited
-^{3}He	Not Currently Available	0.3	0.27	Vapor pressure limited
-Adiabatic demag	Not Currently Available	0.05	0.005	Assuming single-stage device
-Dilution	Not Currently Available	0.05	0.005	Development effort not yet started

Several points are important relative to the coolers listed in Table 34:

- ^{3}He coolers ($T \gtrsim 0.3$ K) are principally single-shot devices though some continuous devices are available. Coolers of this type for use in the space environment are under development. There has not yet been a flight demonstration of these systems.
- Adiabatic demagnetization coolers produce temperatures on the order of $T \gtrsim 0.005$ K. Laboratory units have been tested

routinely and units suitable for ground-based telescopes are under development. (However, units for space applications are not being developed even though the technology is available.)

- $^3He/^2He$ dilution units are continuous systems capable of $T \geq 0.005$ K. Though lab units are available, these have not yet been used for either ground-based astronomy or space-based systems.

4.5 Prominant Institutions and Individuals

4.5.1 Fourier Transform Spectrometers

NASA/Goddard Space Flight Center
R. Hanel
V. Kunde
J. Mather

Jet Propulsion Laboratory
C. B. Farmer
F. O'Callaghan
N. Evans

University of Arizona
H. Larson

Kitt Peak National Observatory
S. Ridgeway
D. Hall

University of Denver
D. Murcray

4.5.2 Grating Spectrometers

AMTS
Jet Propulsion Laboratory
M. Chahine
N. Evans
H. Aumann
R. Haskins

NIMS
Jet Propulsion Laboratory
R. Carlson
I. Aptaker
G. Bailey

4.5.3 Infrared Imagers-Mappers

High Resolution Earth Imaging Sensor (Multispectral Linear Array)
NASA/Goddard Space Flight Center
H. Ostrow

Rockwell
D. Cheung

Honeywell
A. Sood

RCA
W. Kosonocky

Santa Barbara Research Center
P. Bratt

Visible/Infrared Imaging Spectrometer (Shuttle Imaging Spectrometer-A)
Jet Propulsion Laboratory
J. Wellman
M. Herring
A. Goetz

4.5.4 Infrared Detector and Array Technology

Integrated IR Detector Arrays for Astronomical Applications Extrinsic Silicon Arrays (CCD and CID)

NASA/Ames Research Center
C. McCreight
J. Goebel

NASA/Goddard Space Flight Center
G. Lamb
D. Gezari

University of Rochester
W. Forrest

University of Hawaii
R. Capps

University of California
J. Arens

Naval Ocean Systems Center
W. Eisenman

Hughes Aircraft Company

Aerojet Electrosystem Company

Rockwell International

Integrated Long Wavelength IR Detector Arrays (Ge:Ga)

NASA/Ames Research Center
C. McCreight
J. Goebel

Lawrence Berkeley Laboratory
E. Haller

University of California
P. Richards

University of Arizona
F. Low

Cornell
J. Houck

Naval Research Laboratory
W. J. Moore

Aerospace
R. Russell

Bolometers

NASA/Ames Research Center
P. Kittel
T. Roellig

NASA/Goddard Space Flight Center
H. Moseley

University of California, Berkeley
P. Richards

REFERENCE

General Reference on Infrared Sensors: Infrared Receivers for Low Background Astronomy: Incoherent Detectors and Coherent Devices from One Micrometer to One Millimeter, Final Report, NASA Technical Memorandum 78598, June 1979.

5 PASSIVE LASER SENSORS

5.1 Infrared Heterodyne Spectrometers

These systems are analogous to millimeter wave hetrodyne radiometers. Infrared radiation from a source is combined with the output of a laser local oscillator on a mixer. The generated difference frequency (IF) is in the radio region. The spectral and intensity information contained in the infrared source radiation is thus shifted into the radio region where it can be detected and analyzed using RF or AOS spectral line receivers. The back end electronics (spectral line receivers) are very similar and in some cases identical to those used in the millimeter and submillimeter region. Since infrared radiation is of concern, optical quality telescopes are required to collect the source radiation.

Infrared heterodyne spectroscopy has been shown to be a powerful technique for the study of molecular constituents and local physics and chemistry of the Earth's stratosphere, atmospheres of planets and of stellar sources from ground based observatories and balloon-borne experiments. Heterodyne techniques offer very high spectral resolution ($\lambda/\Delta\lambda \sim 10^7$) which permits the accurate measurements of Doppler broadened molecular line profiles. Analysis of these lines can permit retrieval of information on molecular abundances, temperature structure, gas velocities (winds) and non-thermal effects (e.g., lasers) in the source observed.

The system offers high spatial resolution since, being a coherent technique, the field of view is determined by the diffraction limit of the collecting optics. The FWHM angular FOV $\sim 1.22\ \lambda/D$. For 10 μm this yields a FOV ~ 1 arc sec with a 3 m diameter (D) telescope.

If the absolute frequency of the local oscillator is known to a high accuracy heterodyne detection can provide highly specific and accurate frequency measurements (e.g., absolute frequency determination $\sim 1:10^8$ for a CO_2 laser local oscillator). This facilitates species identification and permits gas velocity measurement to a few meters per second.

The gross spectral coverage is determined by the laser local oscillator. Gas lasers permit limited tuneability about discrete laser lines. Tuneable semiconductor diode lasers can be composition tuned to cover 3-30 μm and can be semicontinuously tuned over ~100 cm^{-1}. The instantaneous total spectral bandwidth is determined by the photomixer and preamplifier frequency response and is presently $\lesssim$2 GHz.

5.2.1 Sensitivity

The optimum operating condition for infrared heterodyne receivers is when the system noise is determined by shot noise generated by the laser local oscillator. In this shot-noise-limit the noise equivalent flux, NEF (photons/sec Hz), is given by

$$NEF = \frac{\Delta}{\sqrt{B\tau}} \text{ photons sec}^{-1} \text{ Hz}^{-1}$$

and the heterodyne signal-to-noise ratio on a blackbody of temperature T is

$$SNR = \frac{2\sqrt{B\tau}}{\Delta(e^{h\nu/kT}-1)}$$

where B is the spectral bandwidth and τ the integration time. The Δ factor is a degradation from ideal and includes losses due to polarization (2), chopping of signal (2), photomixer quantum efficiency (2) and optical losses. Further modification of this expression is necessary when observing hot sources (e.g., the Sun).

The spectral intensity F from a blackbody source is plotted in Fig. 5.75 as a function of wavelength for various blackbody temperatures. The NEF for an optimized CO_2 laser system with Δ=7, B=25 MHz and an integration time of 1 hr is given by the dashed line. The range of temperatures observable on various sources is indicated by the bracketed lines. The corresponding signal-to-noise ratio for a given source spectral intensity can be directly determined and is shown on the right vertical axis. For example, at 10.3 μm, measurement of Mars' equatorial

continuum (~250 K) would yield a SNR ~ 300. Measurements at 12 μm on Jupiter (~150 K) would yield a SNR ~ 30.

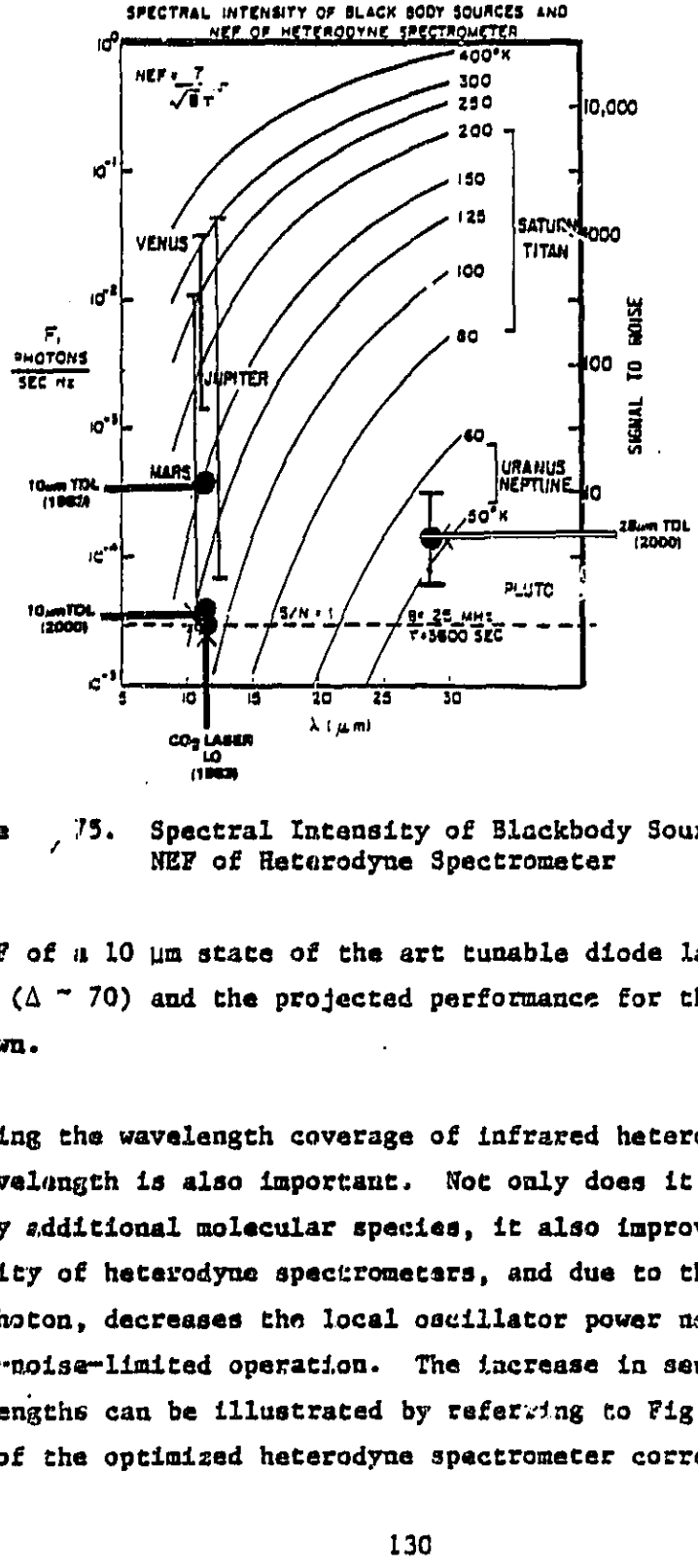

Figure 75. Spectral Intensity of Blackbody Sources and NEF of Heterodyne Spectrometer

The NEF of a 10 μm state of the art tunable diode laser heterodyne spectrometer (Δ ~ 70) and the projected performance for the year 2000 (Δ ~ 8) are shown.

Extending the wavelength coverage of infrared heterodyne receivers to longer wavelength is also important. Not only does it permit the study of many additional molecular species, it also improves the inherent sensitivity of heterodyne spectrometers, and due to the decrease in energy per photon, decreases the local oscillator power needed to achieve shot-noise-limited operation. The increase in sensitivity at longer wavelengths can be illustrated by referring to Fig. 75. At 10 μm, the NEF of the optimized heterodyne spectrometer corresponds to

detection of a ~130 K source with a SNR=1. A system with similar parameters at 30 μm could detect sources well below 50 K and could detect the 130 K source with an SNR > 1000. The projected NEF of a 28 μm diode laser spectrometer in the year 2000 for the same B and τ is also illustrated.

5.1.2 Principal System Components

The principal components for infrared heterodyne spectrometers are laser local oscillators, photomixers, low noise cooled IF preamplifiers matched to the photomixers, beam combining and focusing optics, and a spectral line receiver. To achieve maximum spatial resolution and maximum sensitivity on point sources (stars) a large aperture diffraction limited infrared telescope (>3 m) is also needed.

Components are most highly developed in the 8-13 μm region. However, with the exception of high voltage discharge gas laser local oscillators (e.g., CO_2) in the 9-12 μm region, local oscillators are still inadequate for optimum heterodyne operation in this spectral region. From 13-30 μm, all components are in the early stage of development.

Laser Local Oscillators

- CO_2 Gas Lasers (9-12 μm): Conventional discharge excited CO_2 laser tubes provide adequate power spectral purity and mode structure to obtain optimum heterodyne performance. Using various isotopes of CO_2, the 9-12 μm spectral region can be covered in discrete lines. Total spectral coverage is about 15% of that region using ~2 GHz bandwidth photomixers-preamplifiers. Such tubes have been life tested and achieved half-power lifetimes of >40,000 hours (4.5 years).

  Greater tuneability can be achieved using waveguide lasers. In these lasers, cavity radiation is confined to a narrow diameter stable optical axis which can be conductively cooled, higher gas pressures can permit tuning >1000 MHz, and this design can be made more compact for spaceflight use. Waveguide lasers have been developed for use in a proposed CO_2 laser communication system and RF excited waveguide lasers ~10 cm long and requiring ≤10 W power for excitation are being developed for a proposed CO_2 laser heterodyne spectrometer for planetary observations.

- Semiconductor Diode Lasers: Lead salt diode lasers can be selected to emit from 3-30 μm by adjusting the crystal composition. A given device can be tuned semicontinuously from mode to mode by adjusting the operating temperature and injection current. Continuous tuning in one mode can be achieved over ~1 cm^{-1}. Diode lasers are best developed in the 8-13 μm range. About 10 mW of single mode laser power output is needed for sensitive wide-bandwidth (>500 MHz) heterodyne detection at these wavelengths. Less power is required for narrowband operation and for observation of hot sources (e.g., Sun). The output power must be in a single spectral and spatial mode. These lasers operate at cryogenic temperatures. This fact dictates the size, weight, and power requirements (if mechanical coolers are used) for space applications.

  Current lead salt lasers that operate in this spectral region are available with single-mode powers in the 300 to 400 microwatt range at operating temperatures from 15 K to 50 K. Devices operating from 25-30 μm have been made to emit 80 microwatt per mode near 20 K. Stripe geometry designs have shown promise of better mode output and higher temperature operation ~80 K. A forecast of diode laser parameters is given below.

  Figure 3-76 illustrates the expected improvements in the single-mode power of lead salt lasers. The current and future output power in the 3 to 15 μm range is significantly higher than for the longer wavelength regions. In general, lasers in the 1985 to 1990 time period are expected to exhibit multiple longitudinal modes over portions of their tuning range. Single-mode lasers are expected in the 1990 timeframe. Single-mode power in the 0.7 to 1 mW range is required for narrow bandwidth laser tuned spectrometers (e.g., for solar occultation missions). Power required for future missions requiring high sensitivity, with wide-bandwidth photomixers or arrays, is also shown. These estimates are for the 10 μm spectral range.

  Figure 3-77 illustrates the operating temperature for various spectral regions. In general, lower operating temperatures are required for the longer wavelengths. However, for wavelengths less than 10 to 12 μm, operating temperatures compatible with free flyer requirements are approached.

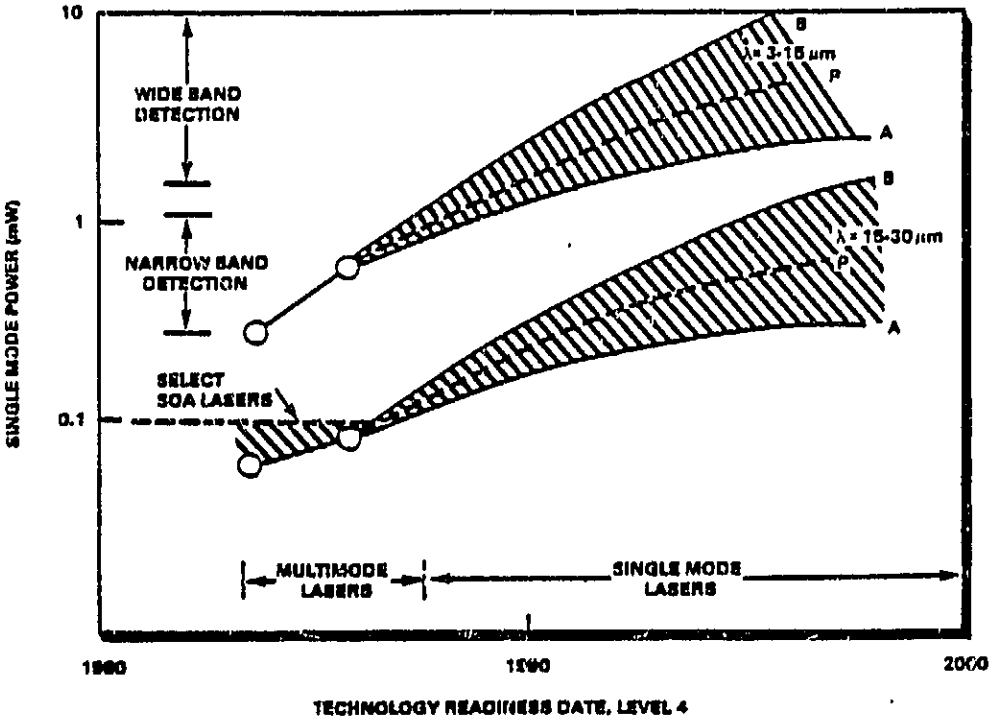

Figure 76. Single Mode Power of Lead Salt Lasers

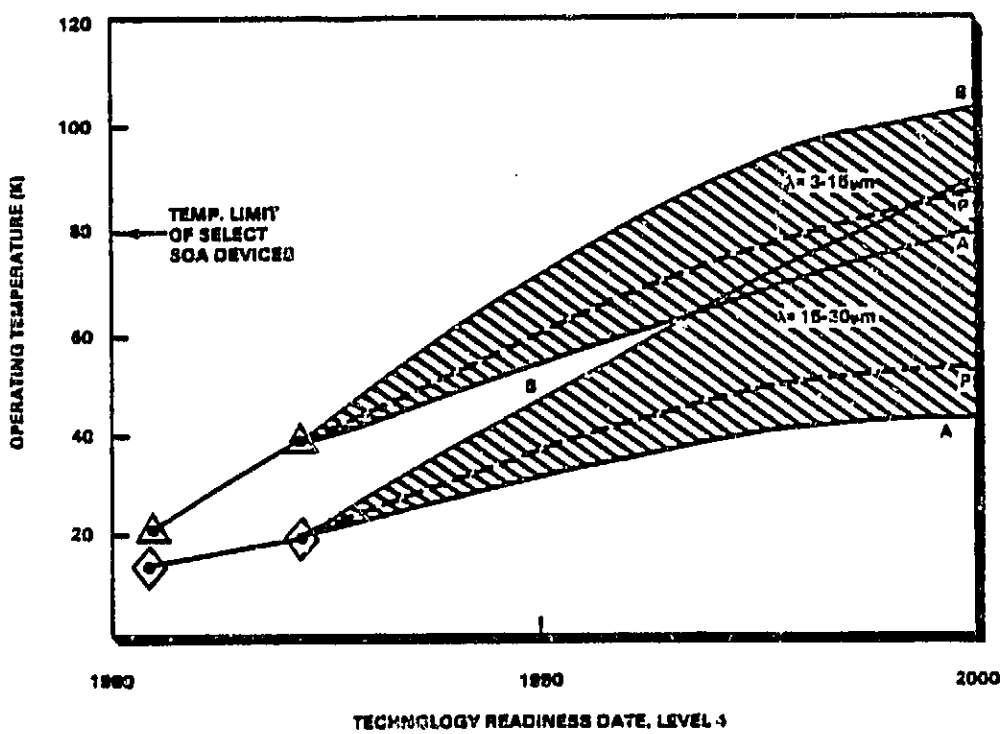

Figure 77. Operating Temperature of Lead Salt Lasers

Other Local Oscillators: Greater tuneability and spectral coverage can be obtained through microwave-laser mixing in wideband electro-optic modulators (e.g., GaAs). In this way

the coverage of the CO_2 9-12 μm region can be 50%. High-pressure CW electron-beam-excited CO_2 lasers and various laser mixing schemes in nonlinear materials can generate power in other wavelengths. All these methods, however, require huge power input and are heavy and large. This at the present time makes them less attractive for proposed use in space platforms.

IR Photomixer-Preamplifier. Although photoconductors or photodiodes can be used as photomixers, in general photodiodes are preferred for sensitive heterodyne detection. Photodiodes require less local oscillator power to reach shot noise limit and permit 2 times higher sensitivity due to absence of recombination noise. Photoconductors, however, are bulk devices and can be more easily made stable and durable. For applications where local oscillator power is deficient and the shot noise limit cannot be reached (e.g., 28 μm), certain proposed photoconductor designs such as small interdigital-electrode HgCdTe photoconductors can be useful.

HgCdTe photodiodes are the best available devices for sensitive wide bandwidth heterodyne application and improved versions of them are expected to be the photomixers in future space instrumentation. Critical parameters are the heterodyne quantum efficiency (η) and the IF bandwidth. η determines to a great degree the overall heterodyne system sensitivity. The sensitivity is also dependent on the efficiency of coupling the IF signal out of the photomixer and the internal noise level of the photomixer and the preamplifier circuit used. The photomixer-preamplifier frequency response affects overall quantum efficiency and bandwidth. HgCdTe photomixers operating from 8-13 μm with bandwidths (3 dB point) $\geq$1.5 GHz exist. Bandwidths of 5 GHz should be possible. Presently the overall bandwidths are limited by the preamplifier. Bipolar devices with reasonable noise figure (<3 dB) are limited to bandwidths of ~1.5 GHz. Cooled GaAs FET preamplifiers can eventually extend the bandwidths to 5 GHz with noise figures $\lesssim$1 dB.

Eight to thirteen micron HgCdTe photomixers with heterodyne quantum efficiencies at the 3 dB bandwidth point of 30-40% exist.

Improvement to >60% is projected. These parameters are for 77 K operation. For space application, operation at radiative cooler temperatures of ~110 K is desired. By composition tuning, it is possible to obtain comparable performance at elevated temperatures. The expected improvements in bandwidth (B) and heterodyne quantum efficiency at 77 K, for 8-13 μm HgCdTe photodiode mixers are presented in Fig. 78.

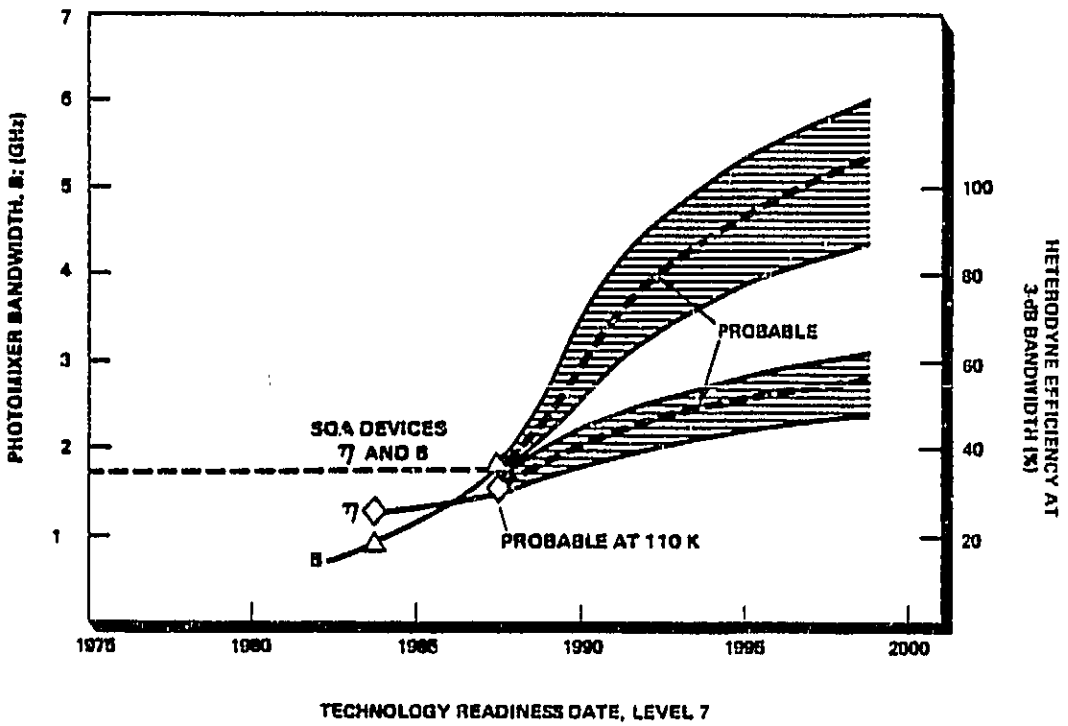

Figure 78. Bandwidth and Heterodyne Quantum Efficiency of 8 to 13 μm HgCdTe Photomixer

HgCdTe diode mixers can be made to operate at longer wavelengths by adjusting material parameters and cooling to lower temperatures. Devices operating at ~20 K between 25-30 μm are being developed. Photomixers with bandwidth ~500 MHz in this spectral region have already been fabricated.

Numerical projections for local oscillator and photomixer parameters are presented in Table 35.

TABLE 35

FORECAST OF IR HETERODYNE COMPONENT PARAMETERS

Parameter	SOA Value	2000 Value
LOCAL OSCILLATOR		
Diode Laser		
- Power/Mode		
10 μm	400 μW	10 mW
28 μm	80 μW	500 μW
- Tuning/Mode	1 cm^{-1}	4-5 cm^{-1}
- Operating Temperature		
10 μm	10-70 K	70-100 K
28 μm	10-40 K	40-70 K
CO_2 Waveguide Laser (Space Qualified)		
Power Out		20 mW
Power In		1 W
PHOTOMIXER		
Bandwidth		
10 μm	1.5 GHz	5 GHz
16 μm	1 GHz	4 GHz
28 μm	500 MHz	1 GHz
Efficiency (η)		
10 μm	40%	>60%
16 μm	25%	60%
28 μm	—	50%
Operating Temperature		
10 μm	80 K	110 K
16 μm	60 K	80 K
28 μm	20 K	30 K
PREAMPLIFIER (GaAs FET)		
Bandwidth	0.5-3.0 GHz	0.1-5.0 GHz
Noise Figure	1.5 dB	<1 dB
Operating Temperature	77 K	110 K
Power Input (Including Voltage Regulator)	0.7 W	<0.5 W

5.1.3 Representative Instruments

Laser Heterodyne Spectrometer (LHS) 8-12 μm. This instrument utilizes cryogenically cooled tuneable diode lasers to scan the optical spectrum. It is being developed to demonstrate technology readiness for measurement of trace species using solar occultation techniques from a Shuttle platform. It could also be used on a Space Station platform.

Advanced Infrared Heterodyne Spectrometer for Planetary Atmospheric Studies (9-12 μm). An RF excited CO_2 waveguide laser would be used as a local oscillator. This instrument is small and compact and would be used on a free-flyer satellite on missions such as: Mars-Geoscience Climatology Orbiter, Venus Atmospheric Probe and could also be used on the Space Telescope, from the Shuttle or Space Station.

Long Wavelength Heterodyne Spectrometer (25-30 μm). Tuneable diode lasers would be used as local oscillators. This system would require cryogenic cooling and would be used on the LDR, Space Shuttle and Space Station.

A forecast for physical parameters for infrared heterodyne spectrometers is given in Table 36.

TABLE 36

FORECAST FOR PHYSICAL PARAMETERS OF IR HETERODYNE SPECTROMETERS

Parameter	SOA Value	2000 Value
CO_2 Laser IRHS		
Weight	32 kg	10 kg
Size (Excluding Radiative Cooler)	0.06 m^3	0.05 m^3
Power Input	97 W	10 W
Cooling (Radiative)	—	110 K
Data Rate	10^3 bits/sec	10^3 bits/sec
Diode Laser IRHS		
Weight	These parameters are dependent on the cooling requirements (15-100 K). Otherwise comparable to CO_2 system.	
Size		
Power Input		
Data Rate	10^3-10^4 bits/sec	10^3 bits/sec

5.2 Prominent Institutions and Individuals

NASA/Goddard Space Flight Center
M. J. Mumma
T. Kostiuk
J. Degnan

NASA/Langley Research Center
J. M. Hoell
S. Katzberg
G. Sachse
F. Allario

Jet Propulsion Laboratory
R. Menzies
E. D. Hinkley

University of California, Berkeley
A. Betz
C. Townes

Spectra Physics, Laser Analytics Division (Diode Lasers)
K. Linden

General Motors Research Laboratory (Diode Lasers)
W. Lo

MIT Lincoln Laboratory (Photomixers)
D. Spears

Honeywell (Photomixers)
J. Shanley

6 ACTIVE LASER SYSTEMS

6.1 LIDAR

Laser radars or LIDARs consists of a laser, optics (telescope), a collocated detector, electronics for data conversion, and a data recording mechanism. The laser is operated in the pulsed mode. The emitted laser radiation interacts with the target (usually the upper atmosphere) and creates a backscatter or fluorescence that is collected by the optical system and measured by the detector/electronics combination. The collecting optical system is generally a Ritchey-Chretien type Cassegrain telescope which focuses the return radiation onto a detector or detector array. Data are then recorded. Some systems use multiple lasers, other use multiple detector systems.

Systems developed to date fall into four generic categories:

- Resonance Fluorescence
- DIAL
- Doppler
- Laser Rangers.

Resonance fluorescence and DIAL systems can be used for the study of atmospheric aerosol, and molecular constituents and atmospheric chemistry. Doppler LIDAR can be used to measure wind velocities and add to the study of global species transport and weather. Laser ranging systems can be used for ranging and altimetry measurements, adding to the study of the Earth's gravitational and magnetic fields, tectonic plate motion, and global geodesy. Each system has unique requirements. As a result, several types of lasers, detectors, mixers, and frequency doubler/frequency tripler subsystems have been developed to enhance the signal detection and tailor the system for the desired application.

Several parameters are basic to LIDAR system performance. Laser transmitted power, in part, determines the range that can be probed [Range $\propto$ (Power)$^{1/2}$] since it determines the intensity of the return signal (resonance fluorescence or scatter). This fact also affects the system sensitivity (measured SNR). Most systems use nonlinear mixing to extend the spectral region of operation. The nonlinear conversion efficiency is a strong function of pump laser power (e.g., $\propto$ Power^2). In this case, increasing power improves system performance even more.

The laser pulse repetition rate determines the number of measurement samples per unit time. Averaging these improves the retrieved SNR and thus sensitivity. The repetition rate can also determine the horizontal resolution from moving platforms (spatial coverage per pulse). The pulse width also determines the ultimate range resolution ΔR; (ΔR = c * Pulsewidth/λ). However, averaging of many pulses is usually necessary, and the useful spatial and range resolution is determined by the signal levels measured and the required measurement uncertainty. Digitization rates also limit range resolution.

The instantaneous spatial resolution is determined by the transmitted beam diameter and optics. From low earth orbit, this resolution can be made quite high and an IFOV of <100 m on the surface is possible.

6.1.1 Resonance Fluorescence and Differential Absorption LIDAR Systems

Differential Absorption Lidar or DIAL, first used in 1966 by Schotland, and resonance fluorescence LIDAR are effective techniques for the measurement of atmospheric species. Over 15 gaseous species have been studied using these techniques. These systems use a pulsed laser as the transmitter and a collocated telescope and receiver. Laser pulses are transmitted into the atmosphere where they are backscattered by aerosols and molecules into the collecting optics and receiver. The laser output wavelength λ_1 is selected to assure that it overlaps with the frequency required to create a resonance fluorescence or absorption in the gas molecule of interest. The collected radiation is detected by the LIDAR and species abundance retrieved.

Using the DIAL technique, the second wavelength λ_2 is selected to have a minimum of absorption by the gas being probed. If it is assumed that the sampling volume is the same for the two wavelengths, and $\Delta\lambda = \lambda_1 - \lambda_2$ is small enough so the atmospheric extinction and volume backscatter coefficients are the same at both wavelengths; the interfering gas concentration and absorption cross section are known, and the absorption cross section for the gas of interest is both pressure and temperature independent; then the gas concentration over a known range can be determined. This, of course, requires a laser capable of radiating light at very specific wavelengths.

Driving scientific programs for resonance fluorescence DIAL systems include:

- Atmospheric Chemistry
- Global Weather
- Aerosol and Cloud Measurements
- Atmospheric Boundary Layer Studies
- Future Planetary Atmospheric Missions.

CO_2 Laser DIAL. The system usually consists of twin CO_2 pulsed lasers that operate directly on specific lines in the 9 to 12 μm spectral region. Use of frequency doublers and sum frequency electronics can extend the applicable wavelength range from 3 to 12 μm. This

frequency manipulation employs nonlinear infrared crystals such as $CdGeAs_2$ or $AgGaSe_2$.

The NEP for CO_2 IR DIAL systems is currently of the order of 10^{-12} $WHz^{-1/2}$ using a nominal wavelength of 10 μm. The projected capability is presented in Fig. 79. It is projected that this value of NEP can be reduced to 10^{-16} by the year 2000, though 10^{-17} $WHz^{-1/2}$ is both achievable and cost effective.

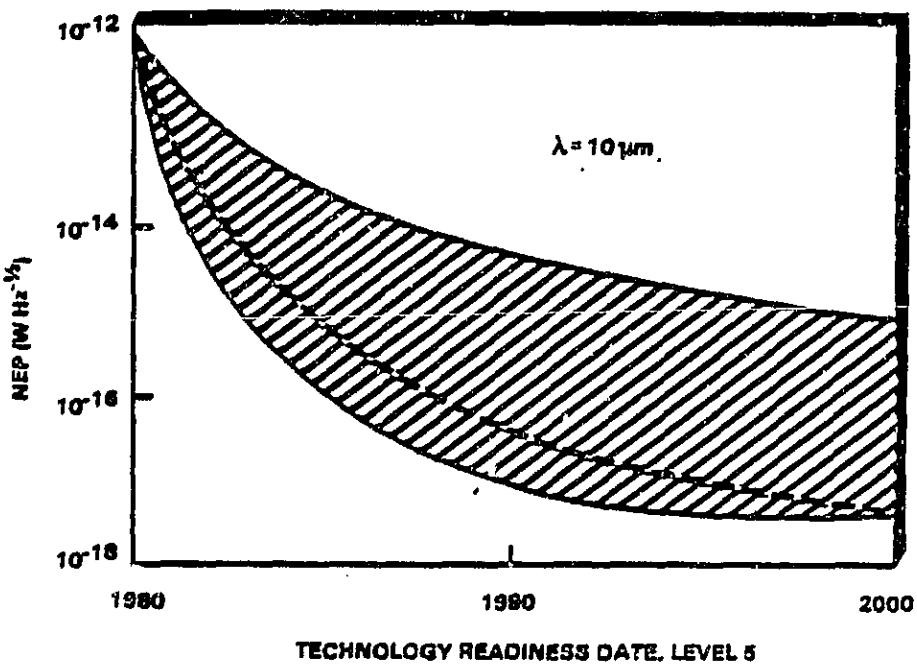

Figure 79. CO_2 DIAL NEP Projection

Future operation of IR DIAL systems in an expanding area of application requires better pulsed CO_2 lasers (1 J/pulse at 10 Hz rate), upgraded direct detection receivers (photon noise limited), nonlinear IR crystals to spread the spectrum for species identification and new high speed data acquisition systems. Detector (e.g., HgCdTe) and laser technology development are closely tied to forecasts given elsewhere. Heterodyne detection techniques can also be used and the forecast in that area is appropriate here. The pulse energy for new lasers is projected to increase by an order of magnitude from current values of 100 mJ to 1 J/pulse by the year 2000. At the same time, it is expected that the nonlinear crystal doubling efficiency will increase from its SOA value of 1% to a value of 50% by the year 2000.

Weight, size, and power requirements are mainly driven by the high power lasers and presently are the limiting parameters for space application.

Transition Metal DIAL. DIAL systems based on transition metal solid state lasers (e.g., Ni or Co:MgF_2) are also being developed in the infrared. An example of such a LIDAR system consists of a solid state Co:MgF_2 laser continuously tunable over the 1.5 μm to 2.3 μm spectral range at output powers on the order of 50 mJ/pulse. With higher output powers (>100 mJ) frequency shifting (Raman) techniques may be used to cover the 3-12 μm region. The system is expected to be of utility for species identification at ranges up to 3 km. The key parameter for this system is peak power. It is projected that by year 2000, pulse power values near 500 mJ will be attainable (Fig. . .80).

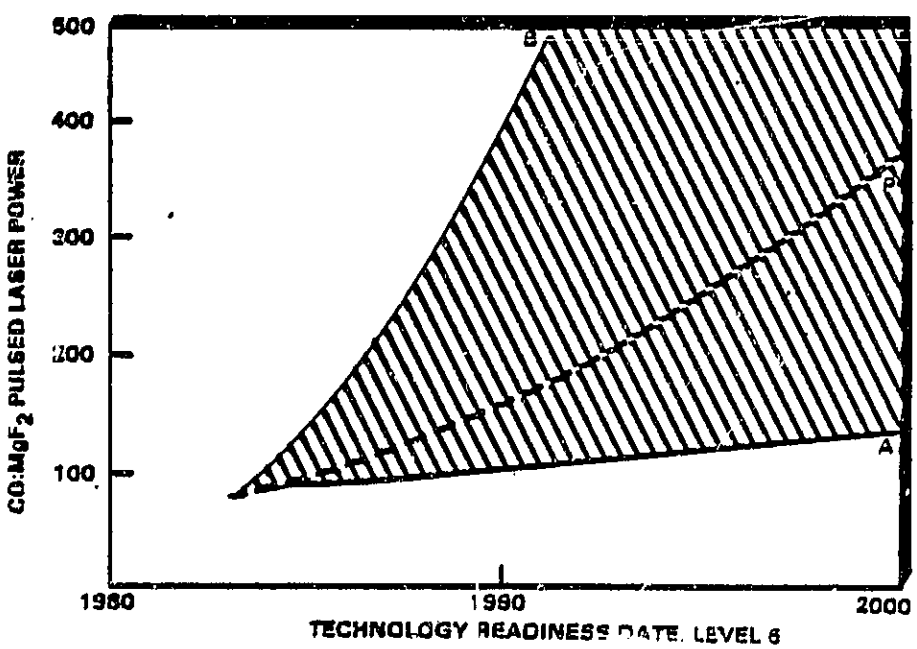

Figure . .80. Transition Metal DIAL: Pulse Power Projection

Dye Laser DIAL. These LIDAR systems use tunable dye laser sources as transmitters with photomultiplier tubes or photodiodes as detectors. Although nitrogen laser pumps can be used, Q-switched Nd:YAG pump lasers can lead to improved dye output energies. Current dye LIDAR system tuneability is determined by the dye laser used. A representative Nd:YAG pumped dye laser DIAL system can be tuned, for example, to

measure the molecular distribution of O_3 at 286 nm, H_2O at 724 nm, and aerosols at 532 nm and 1064 nm.

Critical components include the pump laser, the dye laser, the wavemeter for tuning and wavelength selection ($1:10^7$), the photomultiplier tubes or solid state detectors and data processing systems capable of high data rates (12 bit data at 10 MHz) coupled with the ability to store and transmit large quantities of data. Performance parameters of these components have been projected in Table 37.

TABLE 37

DYE LASER DIAL COMPONENT PARAMETER FORECAST

Critical Component and Characteristics	SOA Value	2000 Value
Pump Laser	Multimode or Quasi Single Mode Flight Hardened	Diffraction Limited Shuttle Flight Qualified
Power	300 mJ/Pulse (Green)	>1 J/Pulse Output in Green
Higher Rep Rate	10 PPS	40 PPS
Dye Laser λ Purity and Tuning	Laboratory Instrument Wavemeter for Pulsed Lasers with Resolution of 1 in 10^7 Just Becoming Available	Wavemeter Resolution Accuracy to Better Than 1 in 10^7 Flight Demonstration (Possibly Replaced by Tuneable Solid State Laser)
Autonomous Laser	One Set λ; Flight Qualified; 1 in 10^7 wavelength accuracy	Programmed or Commandable Wavemeter, Tuneable Over a Range of λ; Flight Hardened Accuracy 1 in 10^7
PMT/Photodiodes		
PMT Quantum Efficiency	1% (1064 nm) 25% (<500 nm)	5% (1064 nm)
Photodiode Quantum Efficiency	50% (1064 nm) - high noise -	80% (1064 nm) - low noise - linearity tested to 0.1%

Areas which need development for future spaceborne DIAL LIDAR are:

1. Flight hardened, diffraction limited beam profile, highly stable pump lasers of high power conversion efficiency. The DIAL application places emphasis on the beam profile quality, and also temporal shape of the pulse, to enable the dye laser to provide the desired spectrally very narrow and pure output; needed for the "on" line emission which then can generate maximum fluorescence of the desired species.

2. A wavemeter with tuning capability, to allow for instance, tuning on more than a single H_2O absorption line and to tune to lines of different strength to obtain improved altitude coverage by the experiment. This wavemeter should be capable of 1 in 10^7 or better accuracy and be flight hardened, and autonomous.

3. Photomultiplier tubes (PMTs) characterized in linearity to better than 0.1% over four or more orders of magnitude dynamic range; or high quantum efficiency solid state (GaAsSb) photodiodes which are now at comparable SNR performance levels at 1064 nm.

The ultimate goal is a DIAL experiment from Shuttle orbit that will achieve wide geographic coverage. This requires development of the above technology for autonomous instrument operation and a system that remains in alignment through launch conditions. It may also be necessary to use a well developed, more durable solid-state tuneable laser to replace the flowing dye laser for space applications. A forecast of the physical parameters of a Shuttle DIAL system are given in Table 38. These values, especially the present power requirements, are quite high. The instrument operates at ambient temperature, but 2-8 kW of laser waste heat must be rejected.

TABLE 38

PHYSICAL PARAMETER FORECAST FOR DYE LASER DIAL

Parameter	SOA (Airplane)	2000 (Shuttle)
Weight	450 kg	1000 kg
Size	1.7 x 1.2 x 1.4 m^3	1.5 m diameter x 3 m
power required	1-8 kW (mostly laser)	

Tuneable Solid-State Laser LIDAR Systems. Until recently dye lasers provided the largest continuous wavelength tuning (200 cm^{-1} per dye) of any known laser system in the visible and near infrared regions of the spectrum. Utilization of laser dyes in space-based sensors has been hampered by their limited lifetime in solution and by their inability to store energy from conventional pump sources such as flashlamps. The latter characteristic results from the few nanosecond lifetime of the upper laser level and makes the achievement of high peak powers, important to all nonlinear frequency shifting mechanisms, more difficult.

New solid-state laser materials, such as chromium-doped alexandrite and emerald, are a factor of 5 to 7 more tuneable (1000 to 1500 cm^{-1}) than individual dyes. In addition, they have long upper level lifetimes on the order of several hundred microseconds and hence, can be Q-switched and/or cavity dumped to achieve high peak powers for efficient nonlinear frequency conversion. The lifetimes of these lasers are limited by the pump source and hence, should be comparable to other flashlamp pumped or pulse-discharge pumped systems.

The spectral output of the alexandrite and emerald lasers (700 to 800 nm) overlaps with oxygen lines which may permit the profiling of pressure and temperature within the atmosphere. In addition, water vapor and carbon dioxide have absorption bands in this region. Through stimulated electronic Raman scattering in a single high pressure atomic vapor, it may be possible to continuously tune through the important 2 to 5 μm band where carbon dioxide, nitrous oxide, carbon monoxide, and many major pollutants and trace species have absorption features. Frequency tripling in nonlinear crystals or gases could produce continuously tuneable radiation in the near ultraviolet from 230 to 280 nm where a number of electronic transitions important to stratospheric chemistry lie. Further Raman shifting would permit further coverage toward the visible. The efficiency of these nonlinear processes depends heavily on the peak power from the source laser. With intensities on the order of a Gigawatt/cm^2, conversion efficiencies up to 80% may be

achievable. Peak power is, therefore, a relevant parameter for such systems. Figure -81 contains the projected value of peak power through the next two decades.

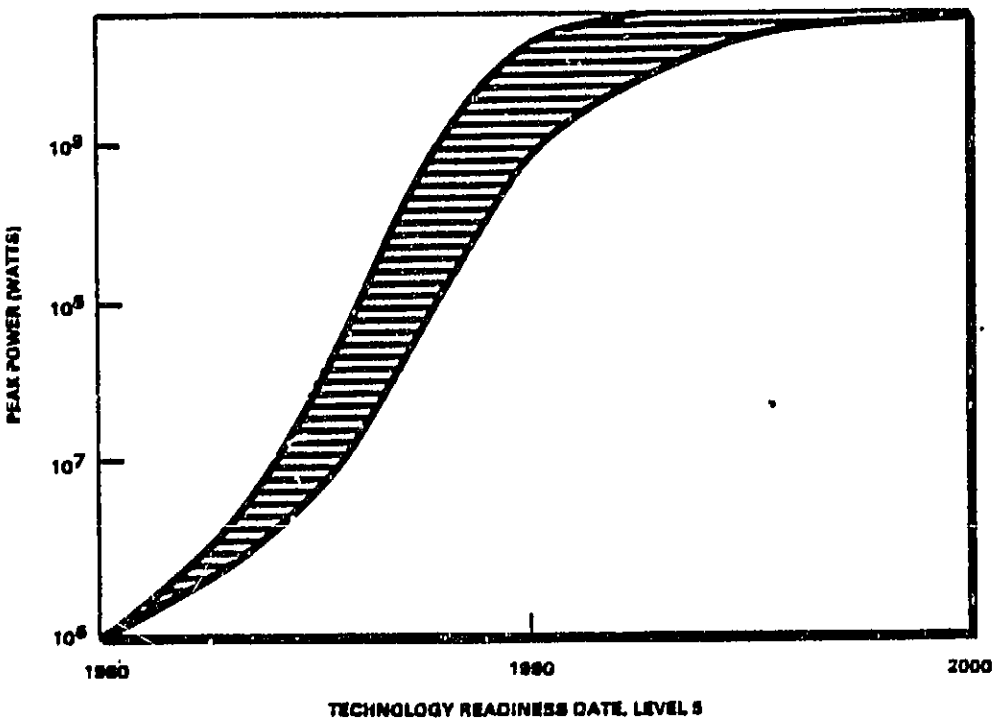

Figure -81. Peak Power Projection for Alexandrite Lasers

Estimated physical parameters of an alexandrite laser DIAL system are:

Mass:	311 kg
Size:	0.32 m^3
Power Requirement:	<3 kW

Size, power, mass, and a 2 kW power dissipation requirement are dictated primarily by inefficient pumping of the alexandrite laser. Major reductions are possible with further research.

Key components for this proposed system include:

- A cavity dumped alexandrite laser with high peak power
- A compact absolute wavelength monitor for pulsed lasers
- A tuneable narrowband receiver with range gating

- A third harmonic generation module that allows tuning from 230-280 nm
- A stimulated electronic Raman scattering module with tuning range from 2.0 to 5.0 μm.

Current parameters versus year 2000 values for these components are presented in Table 39. Development in all areas listed is needed.

TABLE .39

ALEXANDRITE DIAL COMPONENT PARAMETER FORECAST

	SOA Value	2000 Value
Peak Power	3×10^6 W	$>10^9$ W
Absolute Monitor:		
Resolution	0.01 nm	0.01 nm
Size	0.2 m^3	0.03 m^3
Tuneable Receiver with Range Gating:		
Resolution	Does Not Exist	0.05 nm
3rd Harmonic Generation Module	Does Not Exist	230-280 nm
Tuning Range	Does Not Exist	2-5 m
SERS Module:		
Tuning Range	Does Not Exist	2-5 m

Excimer Laser Systems. These are LIDAR systems consisting of a tuneable oscillator-injection locked excimer (rare gas halide, e.g., XeCl) laser system with one or more passive wavelength shifting devices (e.g., crystals-optical parametric oscillators or gas filled Raman cells), and electro-optical devices to measure laser energy/pulse, wavelength, and spectral bandwidth. The excimer laser is a pulsed laser with greater than 1% electrical efficiency at 10-100 Hz operation. Output power from the laser in the UV is in the range of 1 to 100 W. An optical telescope is collocated with the laser source to transmit the laser beam and to collect the return signal. A filter-photomultiplier tube detector combination is used followed by digitization circuits and computer storage.

The excimer laser LIDAR applications are: (1) gas species concentration measurements using laser absorption-DIAL for species such as O_3, SO_2; and (2) laser fluorescence scattering for measurements of gas species (e.g., NO and OH), phytoplankton concentrations, mineral identification, and aerosol profiles.

Key parameters describing system performance are narrowband laser pulse energy, laser efficiency, tuneability, and lifetime. Figure ..82 illustrates the expected pulse energy output from narrowband UV lasers. Excimer lasers have been built with output <1 J (points on graph) and the technology exists for building 2-3 J/pulse systems. Figure 83 forecasts the improvement in laser efficiency. The efficiency is the ratio of laser output energy per pulse over the electrical "wall plug" energy input. Efficiencies of 2% are possible today. Figure 12.84 forecasts UV laser tuneability. Excimer lasers today cover piecewise the 200-400 nm spectral region. Nearly 100% coverage of this spectral region is expected in the year 2000. UV laser lifetime is also of concern for long term space applications. Table .40 summarizes values projected in the figures.

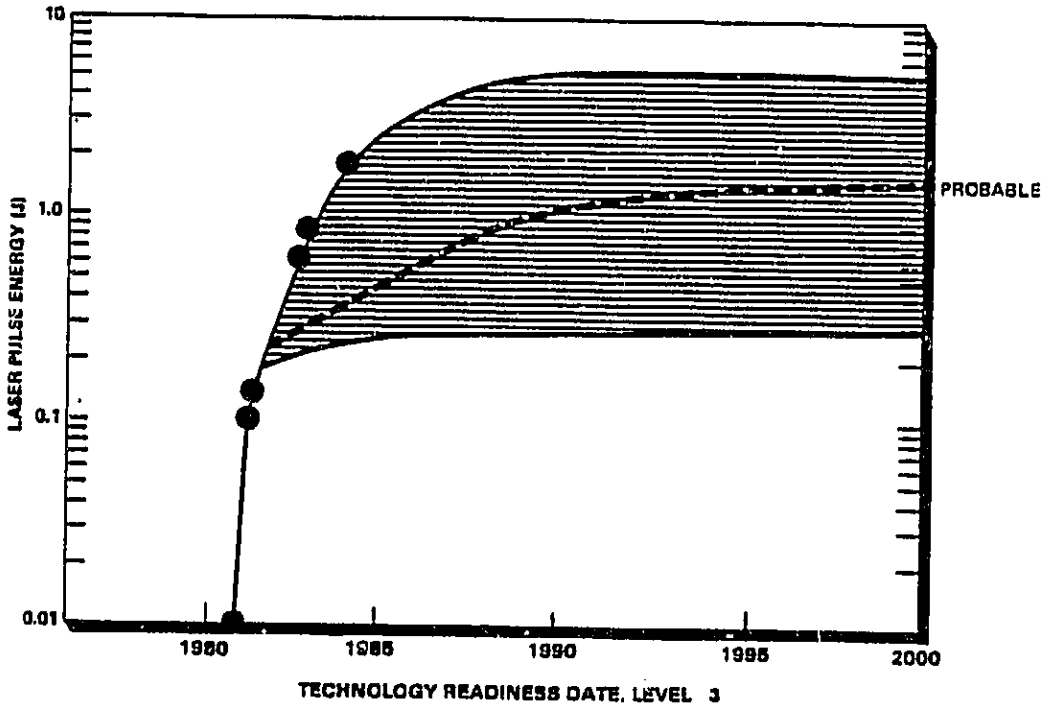

Figure 82. Narrowband UV Laser Pulse Energy

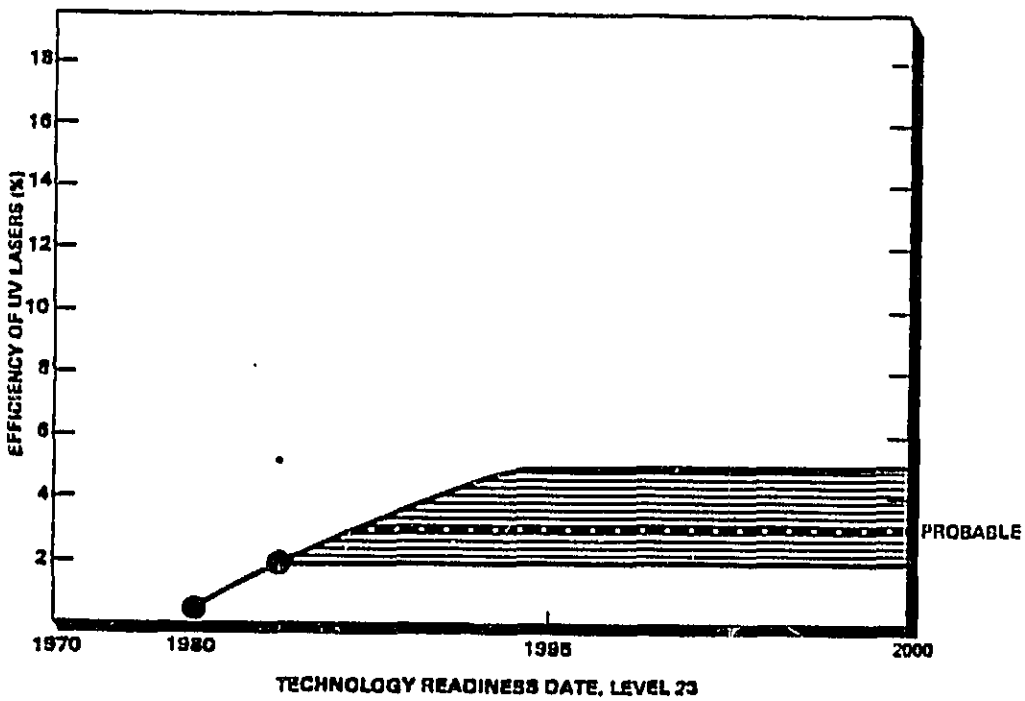

Figure 83. Electric Efficiency of UV Gas Lasers

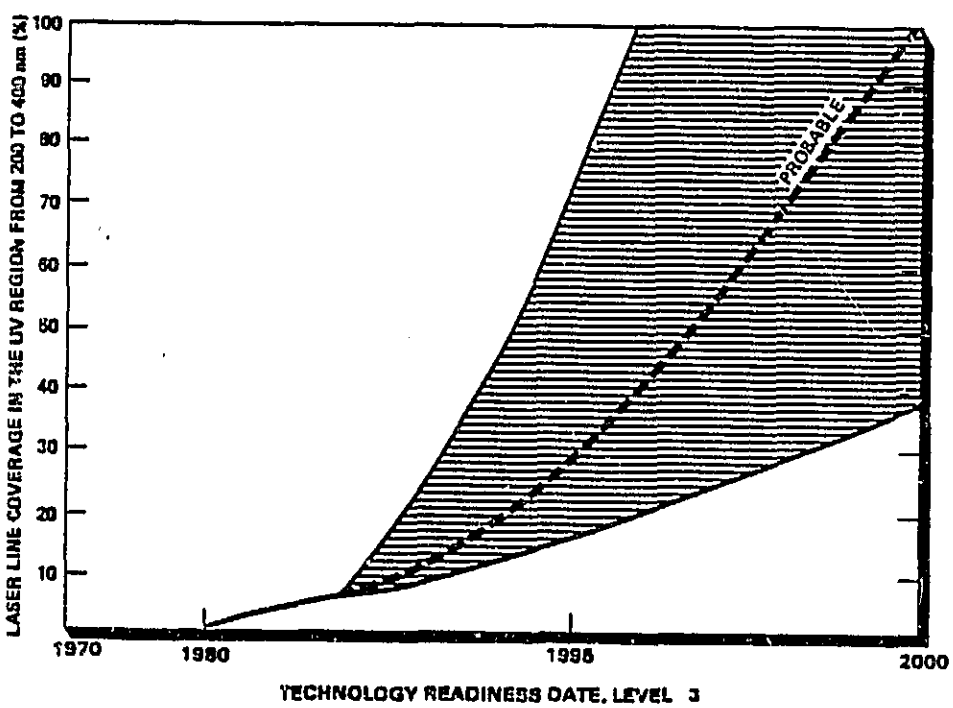

Figure 84. Wavelength Coverage of UV Lasers

TABLE 40

PROJECTED VALUES OF EXCIMER LASER LIDAR PARAMETERS

	SOA Value	2000 Value
Pulse Energy	2 J/Pulse	25 J/Pulse
Wavelength Coverage	10% of 200-400 nm	100% of 200-400 nm
UV Laser Efficiency	2%	>4%
Gas Lifetime	10^7 Shots for XeCl	$>10^8$ Shots for XeCl, KrCl, KrF

Critical components for excimer LIDAR systems include high voltage switches, high contrast narrowband UV visible filters (Fabry-Perot interferometers), electro-optical stabilizers for the pulsed lasers, and preionizers necessary to enable discharge and excitation. These are summarized in Table 41. In addition, more efficient detectors and enhanced software are required to make the year 2000 performance goal.

6.1.2 Doppler LIDAR

Infrared LIDAR systems are used in a Doppler mode to detect such things as tropospheric winds by measuring the Doppler shift of the backscattered laser signals (from aerosols). These systems normally utilize a CO_2 LIDAR system in the 9-11 μm spectral range and are capable of detection of wind speeds down to a 1 m/sec limit. They have an accuracy driven by the purity of the laser frequency emitted. Dominant noise sources are atmospheric turbulence and speckle effects. These systems are capable of a 2 km vertical spatial resolution and 10 km horizontal resolution from space platforms. The LIDAR system contains heterodyne electronics for frequency change detection. As in the case of DIAL systems considerations of wavelength optimization, atmospheric backscattering, laser frequency stability, laser lifetime, and laser pulse repetition frequency (PRF) are of concern. In addition, the heterodyne detector array is important.

TABLE . 41

COMPONENT FORECAST

Critical Component and Characteristic	SOA Value	2000 Value
1. HV Magnetic Switches	In Development	10^{10} Shots With <10% Loss
2. High Contrast Narrow-band UV/VIS Filters		
Bandwidth	0.01 Å	<0.005 Å
Contrast	10^{10}	$>10^{14}$
3. Electro-Optic Wave-meter Stabilization of UV/VIS Pulsed Lasers		
Stability	5 Parts in 10^7 (VISIBLE)	1 Part in 10^7 (UV and VISIBLE)
4. X-Ray Preionizers	100 Hz for 10^4 Shots	1 kHz $>10^8$ Shots
5. Narrowband High Throughput Detectors in UV/VIS		
Bandwidth	0.01 Å	<0.005 Å
Throughput	20%	20%
Contrast	10^{10}	$>10^{14}$

COMMENTS

1. Magnetic switches can solve the critical lifetime factor for space-based pulsed laser systems. JPL has patented and is developing this concept for UV excimer lasers.
2. Such filters are presently available on a custom basis, but need to be adapted to specific LIDAR experiments.
3. Commercial wavemeters for visible pulsed lasers have just been developed but extension into the UV plus feedback to control the wavelength of pulsed lasers is necessary.
4. Several commerical preionizers are available, but more compact, lower power, longer-lived versions are needed.
5. These subsystems include the UV/visible filters in item 2.

The advantages of high pulse repetition frequencies was discussed earlier. A large number of pulses per second may permit not only improved SNR measurement but also the removal of interfering coherent phenomena such as speckle effects. A forecast of CO_2 laser PRF is given

in Fig. 85. From the figure, it may be seen that the SOA value of PRF is 1 Hz. This value is projected to be 100 Hz by 2000. In addition, the laser lifetime and the IR heterodyne detector array are important for the total system. Present and projected values are presented in Table 42.

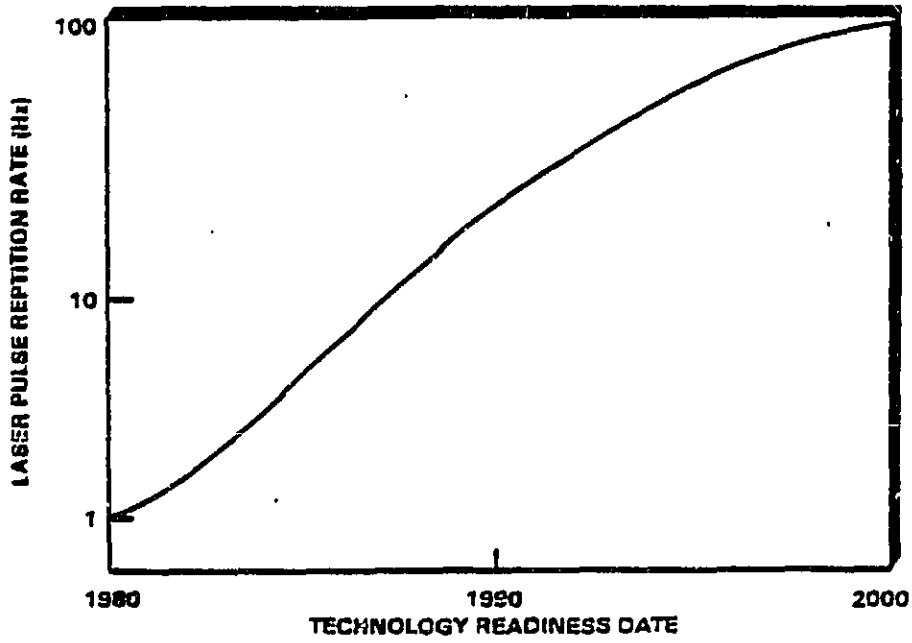

Figure 85. Pulse Laser PRF for CO_2 Doppler LIDAR

TABLE 42

CO_2 DOPPLER LIDAR PARAMETER FORECAST

Parameter	SOA Value	2000 Value
Laser PRF	1 Hz	100 Hz
Laser Lifetime	10^6 Shots	10^9 Shots
IR Heterodyne Detector Array	2 x 2 Array	4 x 4 Array

Present estimates of system physical parameters are:

Mass:	3000 kg
Size:	1m x 1m x 2m
Power Requirement:	3 kW
Cooling:	77-110 K for detectors

Enhancements for the future will require fundamental laser research directed towards frequency stabilization and laser lifetime enhancement. Accuracy of the system will be increased as the variability in both space and time of the atmospheric backscatter coefficients for 9-11 μm radiation becomes better known.

6.2 Laser Ranging

One of the oldest applications of spaceborne lasers has been ranging and altimetry. Pulsed lasers were first used to range to artificial satellites in 1964. The precision of these early systems was approximately 3 m which represented a factor of 20 improvement over the best contemporary microwave radars.

By 1982, an advanced prototype field instrument was measuring the pulse time of flight with 100 picosecond precision while laboratory instruments were approximately a factor of two more precise. Ground-based satellite laser ranging systems have been used for precise orbit determination, measurements of the Earth's gravitational and magnetic fields, for Earth dynamics studies such as polar wobble, tectonic plate motion, and rotation rate, and for global geodesy. These scientific endeavors will require millimeter accuracies in the next decade.

To determine the actual geometric range to the satellite from time-of-flight measurements, one must be able to account adequately for the effect of the atmosphere on the pulse group velocity and on the paths of the light rays. Current uncertainties in the atmospheric models are believed to result in centimeter uncertainties in the absolute range. The parametric inputs to these models are surface measurements of pressure, temperature, and humidity at the station. These often neglect horizontal gradient effects. The most promising technique for making the atmospheric correction is to generate ultrashort pulses at two frequencies and to measure the time delay introduced between the pulses by the dispersive atmosphere during their round trip to and from the target. To deduce the atmospheric correction to the mm level will require a timing resolution between 200 and 800 femtoseconds depending on the wavelengths chosen. Current receivers have resolution

on the order of 40 to 50 picoseconds. Frequency-doubled, mode-locked Nd:YAG lasers are used in current state of the art field systems.

The 1 mm absolute accuracy goal requires the development of high power frequency-doubled laser transmitters with pulsewidths on the order of a few picoseconds and a 200 femtosecond resolution optical time interval unit which takes advantage of developing streak tube technology. Such a system would provide an absolute range accuracy of 30 μm in vacuum and 500 μm for ground to satellite paths in air.

When placed on airborne or spaceborne platforms, the sensor can perform ultraprecise geodetic surveys and monitor global tectonic plate motion.

The same instrument can measure surface pressure over the oceans with 0.1 mbar accuracy. This is achieved by transmitting two pulses with different wavelengths in the nadir direction, recording the waveshapes reflected off the ocean surface into the receiver at the two wavelengths, and measuring the time delay between sharp features in the profiles resulting from specular glints off the crests and troughs of the waves. The time interval between crest and trough spikes yields the amplitude of the wave. The frequency and direction of the wave can be ascertained by taking readings off nadir. The accuracies of all these measurements are determined solely by the timing precision of the instrumentation. A forecast of timing precision is given in Fig. . 86. A summary of this projection as well as a forecast of other system performance parameters is given in Table . 43.

6.2.1 Alexandrite Laser Ranging System

When one considers factors such as adequate dispersion between wavelengths, good atmospheric transmission and good detector sensitivity, one finds that wavelengths of 400 to 800 nm are optimum for this application. Frequency-doubled alexandrite and emerald lasers operate in this region of the spectrum, are capable of high output energies, and their bandwidths can support subpicosecond pulsewidths when mode-locked. A forecast of laser parameters is given in Table .44.

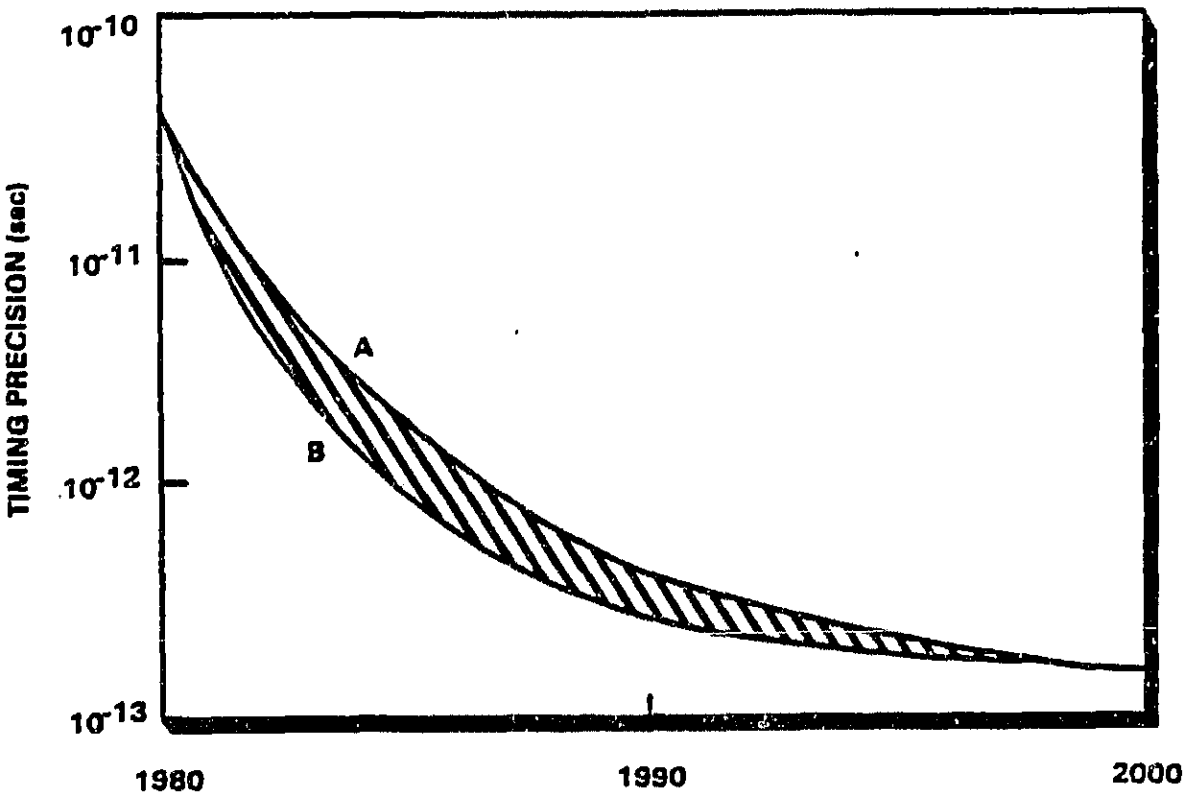

Figure 86. Projected Timing Precision

TABLE 43

CRITICAL SYSTEMS PARAMETERS FOR LASER RANGING

Parameter	SOA Value	2000 Value
Time of Flight Precision	5×10^{-11} sec	2×10^{-13} sec
Absolute Range Accuracy	10 mm	0.5 mm
Surface Pressure Accuracy	10 mbar	0.1 mbar

TABLE . 44

COMPONENT PARAMETER FORECAST FOR ALEXANDRITE LASER RANGERS

Component and Parameter	SOA Value	2000 Value
Solid State Laser:		
Pulse Width		
- High Energy	10^{-7} sec	10^{-11} sec
- Low Energy	10^{-11} sec	10^{-13} sec
Energy	200 mJ	250 mJ
Range Receiver:		
(Optical Time Interval Unit) Resolution	10^{-10} sec	2×10^{-12} sec
Short Term Stability	10^{-9}	10^{-11}

As technology progresses from Q switching to cavity dumping to mode-locking, the pulsewidth will decrease from its current value of 10^{-7} to the desired value of 10^{-11}. The expected progression of activities in illustrated in Fig. 87.

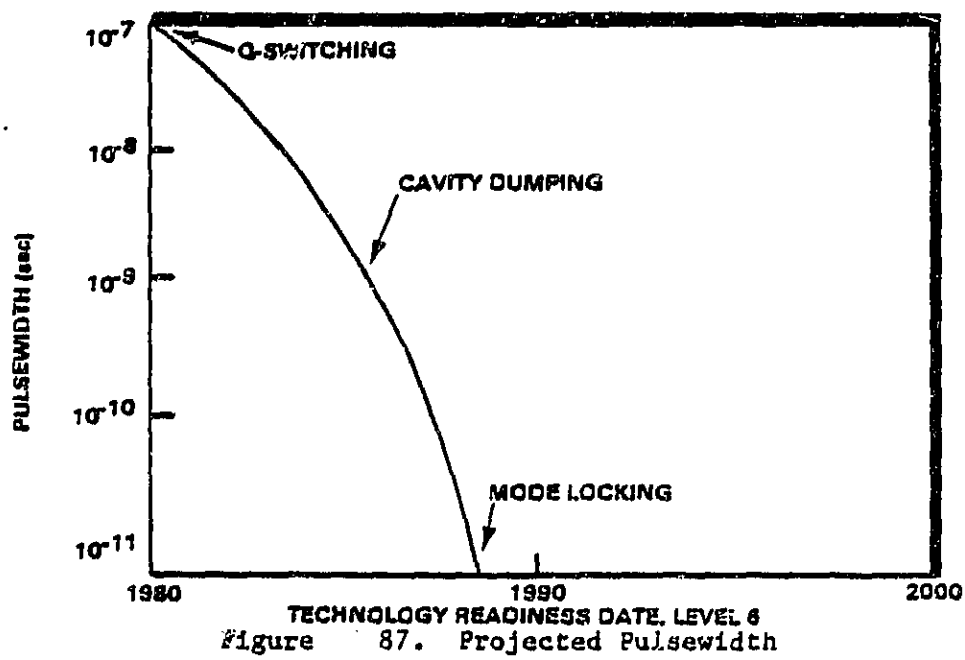

Figure 87. Projected Pulsewidth

Since timing is the critical factor for this system, a significant supporting research activity includes the development of an optical time interval unit consisting of:

- Diode based optical clock (<5 picosecond pulsewidth)
- Synchronous 200 femtosecond resolution streak camera.

Resolution and short term stability are forecast in Table .-44. With these developments, additional and more precise measurements can be made for the crustal dynamics program area including global geodesy, tectonic plate motion, Earth geopotential and Earth and lunar dynamics. In addition, when used for the measurement of pressure and sea state, this system can provide useful data in the development of new mathematical models for weather forecasting.

6.2.2 Other Laser Ranger Systems

In addition to the alexandrite system discussed in the previous section, a visible (500-600 nm) copper vapor laser system is in development. The system has a 3 m spatial resolution vertically and a 30 m resolution horizontally due to its high PRF (20 kHz). The height accuracy is currently 100 m and is projected to reach 10 m by the year 2000 as illustrated in Fig. 88. The critical system parameter is the laser efficiency which has a current value of 0.1% and a projected value of 1% in the year 2000. Currently laser lifetime of only 100 hr is possible.

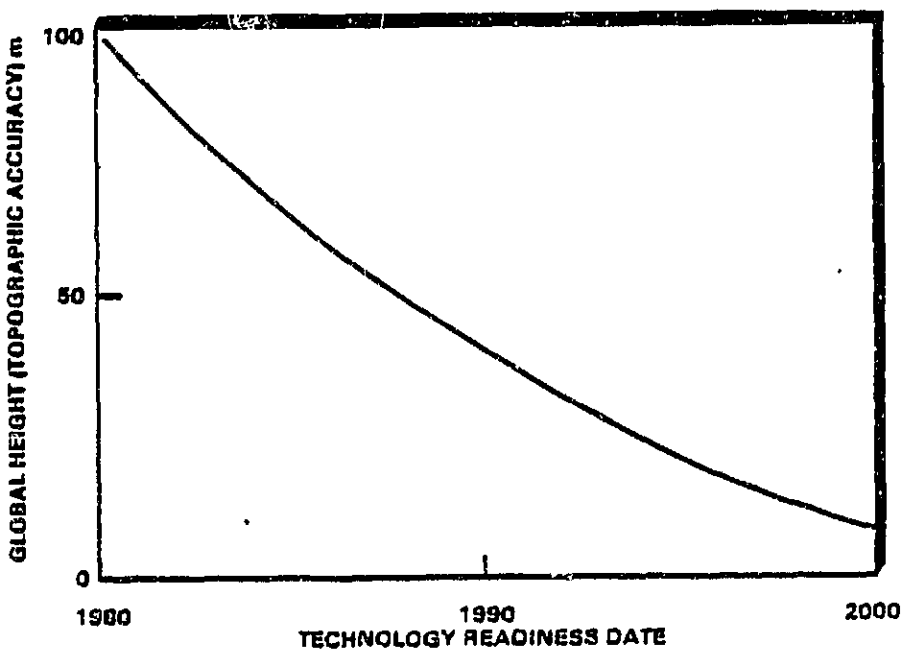

Figure 88. Copper Vapor Laser Ranger Height Accuracy Forecast

Since current systems have outgassing problems there is a requirement to spend some future research time and money on optical and material technology that will limit this effect and prolong the laser lifetime. It is projected that a value of 2×10^8 hr lifetime can be achieved by the year 2000.

Narrowband solar blind detectors used in the receiver have current efficiencies of ~0.10%. It is projected that future (year 2000) values of 10% can be achieved.

6.3 Prominent Institutions and Individuals

6.3.1 LIDAR

NASA/Goddard Space Flight Center
J. Bufton
J. Degnan
B. Heaps

NASA/Langley Research Center
R. Hess
P. Brockman
C. Bair
E. Browell
W. Hall
A. Jalink
F. Allario

NASA/Marshall Space Flight Center
J. Bilbro

NASA/Ames Research Center
P. Russell

University of Arizona at Tucson
R. Schotland

University of Maryland
T. Wilkerson
T. McIlrath

University College, London, England
D. Rees

Jet Propulsion Laboratory
R. Menzies
M. Shumate
B. Grant
J. Laudenslager
S. McDermid
T. Pacala
D. Hinkley

NOAA
F. Hall
M. Hardesty

Los Alamos National Laboratory
J. Figuera
N. Kurnit

MIT Lincoln Laboratory
D. Killinger
N. Menyuk

Georgia Institute of Technology
D. Davis
M. Rogers

University of Hull, Hull, England
B. Rye

6.3.2 Laser Ranging

NASA/Goddard Space Flight Center
J. Degnan
J. Abshire
T. Zagwodski
R. Coates

Jet Propulsion Laboratory
N. Narheim
T. Pivirotto
N. Marzwell
C. Elachi

University of Maryland
C. Alley

University of Texas at Austin
P. Shelus

Smithsonian Astrophysical Observatory
M. Pearlman

Geodetic Institute, University of Bonn, W. Germany
P. Wilson

7 PASSIVE VISIBLE SENSORS

Passive visible systems are presently well developed. Needed advances lie mainly in larger lightweight collecting optics (telescopes) and large detector arrays. Large telescopes would permit greater light gathering capability and allow measurement of fainter and more distant astrophysical sources. In the absence of seeing effects above the Earth's atmosphere, astrophysical objects could be observed at greater spatial resolution (limited by the diffraction of the telescope aperture). In Earth sensing applications, the visible region has great promise. Measurement of reflected solar radiation and luminescence can permit the mapping of geological and geographical features as well as the distribution of Earth resources.

7.1 Charge-Coupled Devices

Future visible sensors (mappers or cameras) will most likely be based on some sort of solid-state detector array. Charge-coupled devices (CCDs), more than any other solid-state camera sensors, offer the capability of high resolution, high sensitivity, low cost, high reliability cameras of minimal size, weight, and power consumption. They are expected to replace vidicon and other devices for planetary camera sensors almost entirely. The size, weight, cost, and monolithic nature of the sensor will make possible universal modular camera designs compatible with a variety of planetary and Earth-orbital imaging applications.

The primary parameters forecast are those of resolution (sensor format) and sensitivity. Absolute threshold exposures are not well known at this time, but a reasonable value for a current photon-in CCD using a precharge preamp and exposed to a 2800 K source is about 3 microjoules per square meter. In addition, significant improvements are expected in intrinsic noise reduction and broader spectral bandwidth capability. Present silicon CCDs have a bandwidth covering 0.4 to 1 μm. As other materials are adopted, the limits will be extended below 0.2 μm and (not the same device) out to about 10 μm. An alternative that is under development is based on internal photo emission from metal/semiconductor Schottky-barrier arrays on a silicon or germanium substrate. These arrays can employ either vidicon readout or CCD readout and signal processing.

The performance forecast shown in Figs. 7.89 and 7.90 was made on the basis of trend extrapolation of current CCD technology and anticipated improvements in fabrication techniques which should overcome current definition limits. Because of its applicability to several classes of devices, CCD technology is being advanced rapidly at present, benefitting both from large military and commercial funding support and from advances in the related technology of large scale integrated circuit fabrication. NASA or other government funding for CCD imaging system technology will be required to use applicable technology advances and to develop, in parallel, specific sensors for flight systems.

7.2 Representative Instruments

7.2.1 Visible and Near Infrared Imager (0.4-1.1 μm)

This camera system has been designed to act as a wide field of view planetary camera for use by the Space Telescope. Similar cameras can be used on the Solar Optical Telescope (SOT) and on various future planetary missions (e.g., Mars Geoscience Climatology Orbiter, Comet Sample Return, Lunar Orbiter, Saturn and Titan Probes). It has a selectable, highly variable tuneability and is limited in its performance by detector shot noise and the data readout speed.

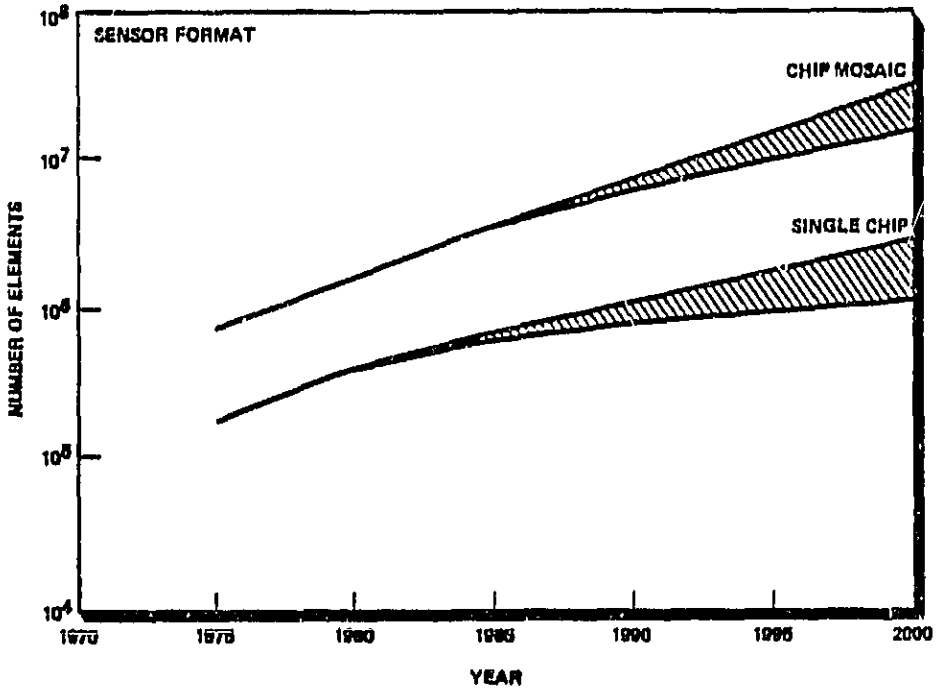

Figure 89. Solid-State Cameras (Sensor Format)

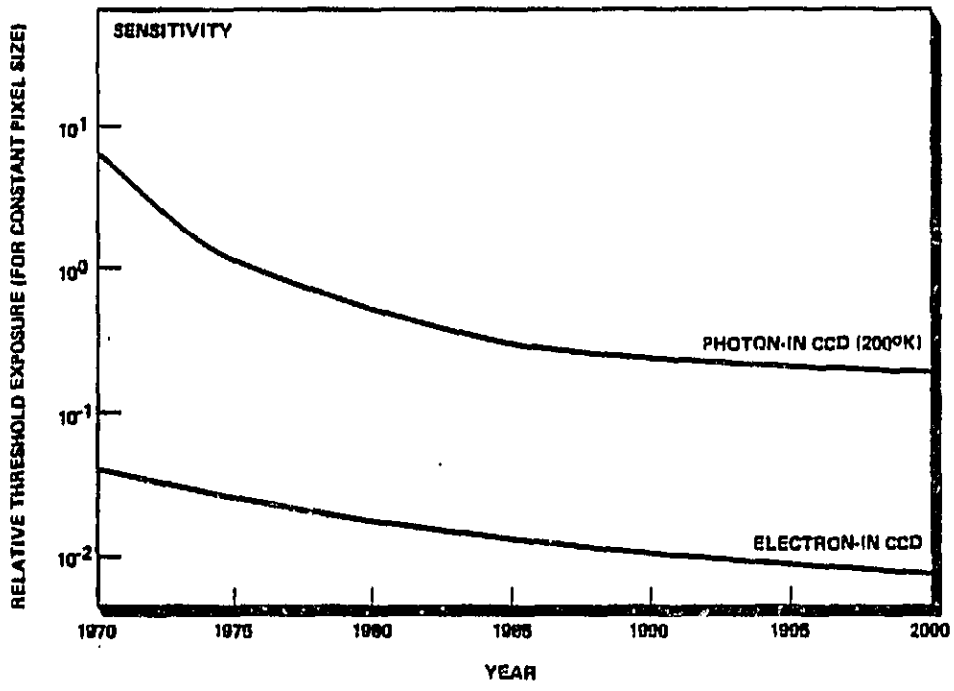

Figure 90. Solid-State Cameras (Sensitivity)

The instrument consists of an objective lens, focal plane detector and electronic signal chain. Operating mechanisms include both a focal plane shutter and filter wheel. The detector consists of a CCD array. It has a "silicon" response which extends from 0.4 to 1.1 μm. The optics for this spectral range may be all reflecting, catadioptric, or all refractors.

Critical performance parameters include noise sensitivity, array size, dynamic range, radiation resistance, and operating stability. The thrust of current efforts involves programs to reduce noise both for individual detectors and for arrays. When applied to astrophysical targets, the dynamic range will be of major concern. Furthermore, the array resistance to surface damage by varying types of radiation is not yet known.

Figure 91 contains a plot of projected noise levels and CCD array sizes. The complete set of significant system parameters is presented in Table 45.

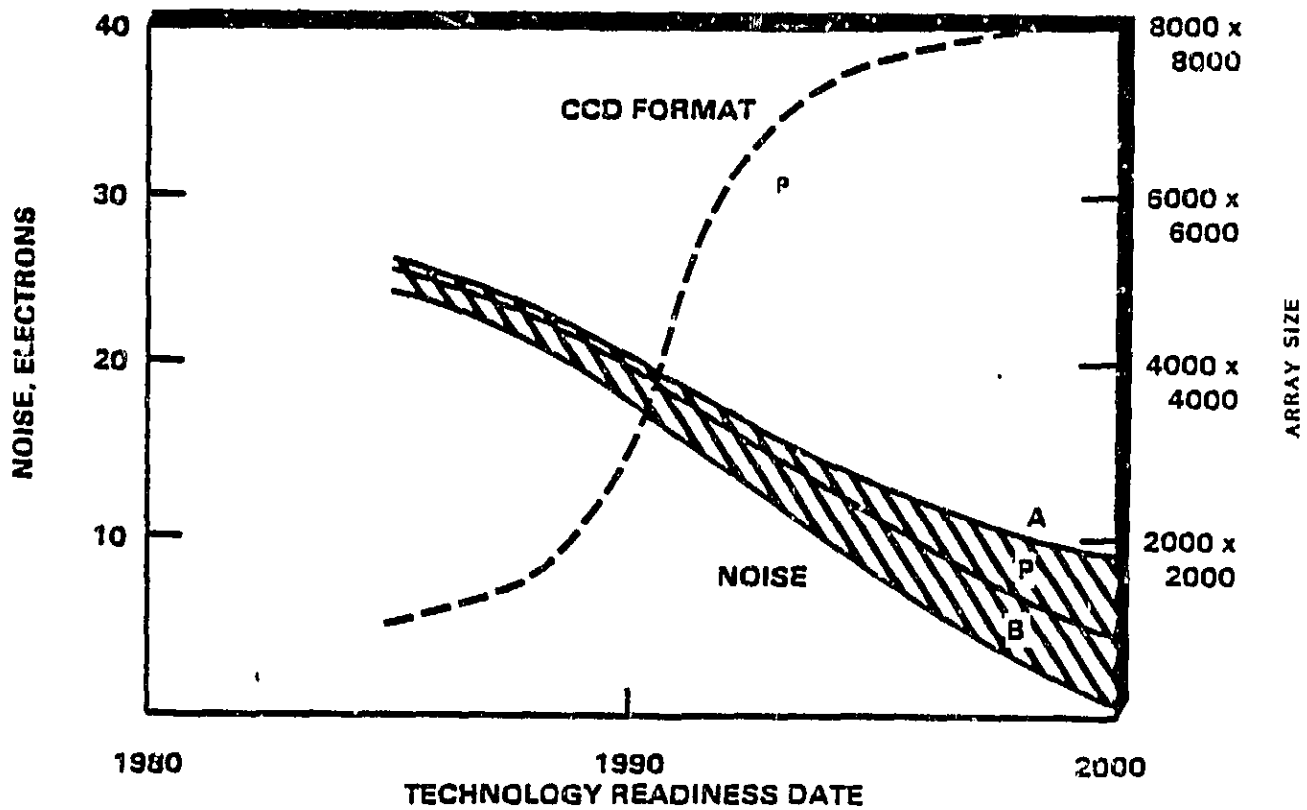

Figure 91. Noise Level and Array Size Forecast

TABLE 45

SYSTEM PARAMETER PROJECTIONS

Parameter	SOA Value	2000 Value
Noise	15 e^-	2 e^-
Detector Size	800 x 800	4096 x 4096
Dynamic Range	10^4	5×10^6
Quantum Efficiency	10% @ 0.6 μm 5% @ 1.0 μm	60% @ 0.4 μm 20% @ 1.0 μm
Readout Rate	10^6 pixels/sec	10^9 pixels/sec

Critical subsystems for this system include:

- CCD Detectors
- On-Chip Amplifier Development
- Lightweight Optical Systems
- Better Shutter Mechanisms
- Filters (limited by UV cutoff)
- A-D Convertors
- Cryogenics
- Optics.

It is projected that on-chip amplifiers currently in use can be improved by a factor of 3 by the year 2000 (the theoretical limit to improvement is a factor of 15). Data rates are also important. Current A-D converters operate at 1 Mbit/sec on words 16 bits long. It is projected that future rates can reach 50 Mbits/sec.

7.2.2 Fraunhofer Line Discriminator (0.4-0.9 μm)

A Fraunhofer line discriminator (FLD) measures solar-stimulated luminescence to locate mineral outcrops, liquid pollutants and tracer dyes and changes in vegetation. FLD techniques were originally applied to measurements of lunar luminescence in the 1950s and 1960s. Airborne

FLDs have been built and successfully used to measure luminescent Earth features since the late 1960s.

An FLD system calculates a fractional coefficient of broadband luminescence from two pairs of intensity measurements, one pair of the incident solar radiation at wavelengths in the center of a Fraunhofer absorption line and in the adjacent continuum and a second pair of the reflected radiation at the center of the line and in the adjacent continuum. If no luminescence is present, the line depth as a fraction of the incident continuum will be unchanged on reflection. If luminescence is present, the line depth will be a different fraction and a coefficient of luminescence may be calculated.

FLD sensors, compared to other orbital sensors, require (1) high spectral resolution (0.1 nm) over small bandwidths, and (2) very high sensitivity to measure small intensity changes against the high reflected solar background. High spectral resolution is achieved with Fabry-Perot etalons. High sensitivity requires high throughput [ground instantaneous field of view (IFOV) area times solid angle subtended by the sensor aperture] or long integration times. Large aperture sensor optics with large Fabry-Perot etalons will satisfy both requirements. Such etalons can be physically large or can be designed as field-widened etalons within the optical system. Staring mode systems will reduce the aperture size requirement somewhat by allowing longer integration times than pushbroom mode systems.

The sensitivity of an orbital FLD sensor may be specified as the ratio of the coefficient of luminescence, L, over the standard deviation of L. The luminescence, L, is a combination of the four intensity measurements mentioned above. In orbit, the two incident intensities will be constant. The reflected intensities will cause noise in L, probably through the intrinsic shot noise of photon detection. The noise can be reduced by increasing the throughput-integration time product to increase the absolute intensities measured. The physical parameters of this product, the linear IFOV, the solid angle subtended by the instrument aperture, and the integration time, limit the

performance of orbit[illegible] FLD systems. The system to be discussed covers the 0.4 to 0.9 μm portion of the optical spectrum; it is tuneable across selected Fraunhofer absorption lines, and it has a spatial resolution in the range of 10 to 100 m IFOV.

Figure [illegible]92 presents the signal-to-noise ratio of the luminescence measurement as a function of four horizontal scales. Assuming shot-noise-limited behavior, the signal-to-noise ratio L/σ_L is of the form:

$$L/\sigma_L \simeq t^{1/2} * IFOV * DIAM$$

where t is the integration time and DIAM is the diameter of the clear aperture.

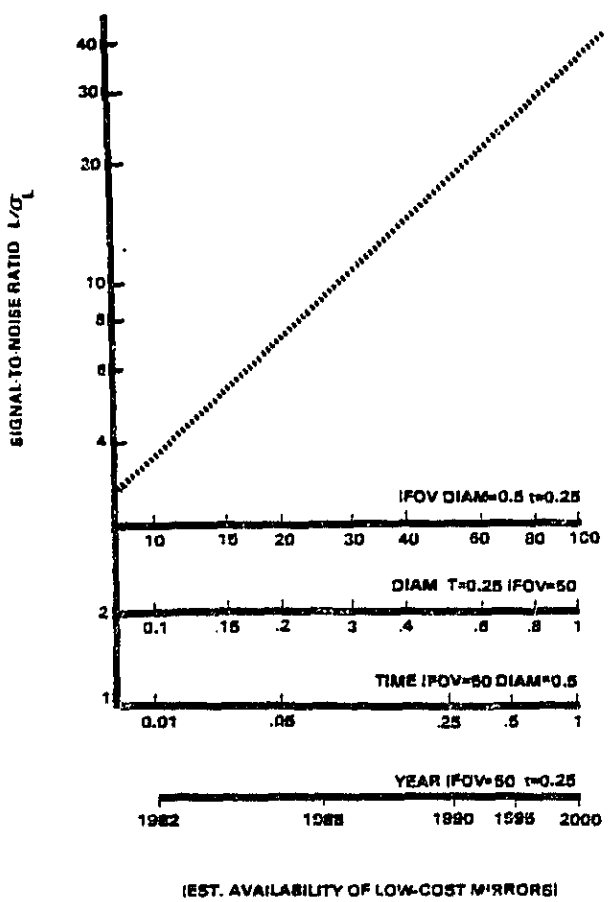

Figure [illegible].92. Signal-to-Noise Ratio and Critical Parameter Projection for FLD

The signal-to-noise ratio calculations assume the following parameters:

Solar model:	5700 K blackbody
Fraunhofer line:	0.6563 μm, H_α line
depth:	0.16 of continuum
Ground reflectance:	0.1
Ground luminescence:	0.001
Irradiation angle:	45^o
View angle:	nadir
Altitude:	250 km
Optics transmission:	0.05
Optics bandwidth:	0.1 nm

For each horizontal scale, two values are fixed and the third is varied. The parameter values for each scale are:

SCALE	VALUES		
	IFOV (m)	DIAM (m)	TIME (sec)
IFOV	10-100	0.5	0.25
DIAM	50	0.1-1.0	0.25
TIME	50	0.5	0.007-1.0

At the far left end of the time scale, the integration time is marked for pushbroom mode operation with one pixel smear, rather than the staring mode operation assumed elsewhere.

The fourth horizontal scale has the estimated year when low-cost mirror substrates will be available. For this scale, signal-to-noise ratio is plotted for fixed integration time and IFOV and increasing optics diameter.

Desired performance for this system requires an appropriate detector array, a low-cost nominal sized collector mirror and more effective Fabry-Perot etalons. These are itemized in Table 46. A forecast of mirror development is given in Fig. 93.

TABLE 4.46

CRITICAL SYSTEM PARAMETER PROJECTION
FOR FRAUNHOFER LINE DISCRIMINATION

Parameter	SOA Value	2000 Value
Low Cost Collection Mirror Diameter[1]	0.4 m	1.0 m
Effective Fabry-Perot Etalon Size[2]	0.1 m	1.0 m

1. Large enough mirrors could be built today, but at excessive cost.

2. Flat Fabry-Perot etalons might be used to 0.25 m diameter; certain other designs may be suitable for the maximum aperture size presented.

Note: Orbital FLD sensors will have both parameters at the same size.

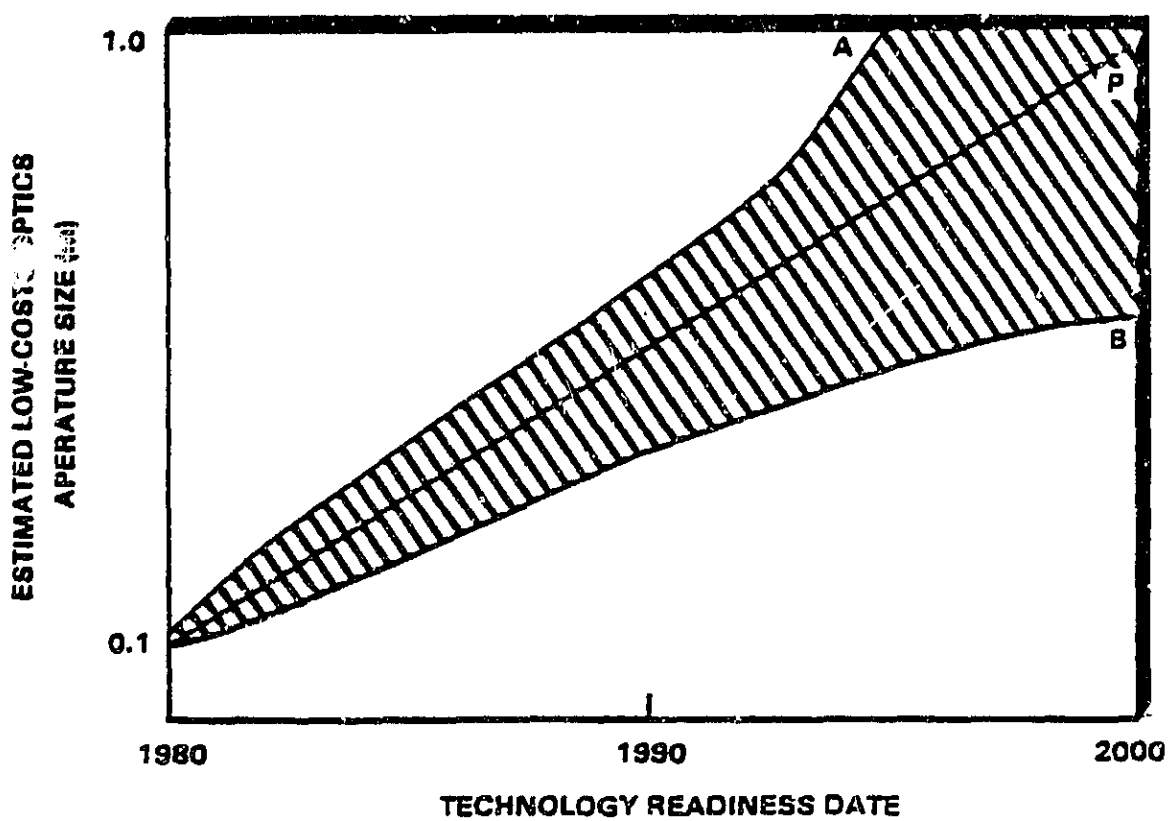

Figure 93. Estimated Low Cost Optics Aperture Size Development

7.3 Prominent Institutions and Individuals

7.3.1 Visible and Near Infrared Imager

Jet Propulsion Laboratory
F. Vescelus

California Institute of Technology
J. Westphal

University of Arizona
B. Smith

Kitt Peak National Observatory
M. Belton

Princeton
J. Gunn

University of Hawaii
C. Pilcher

7.3.2 Fraunhofer Line Discriminator

Jet Propulsion Laboratory
J. B. Breckenridge
J. E. Stacy

University of Arizona
P. N. Slater

Perkin Elmer Corp.

8 PASSIVE ULTRAVIOLET SENSORS

Ultraviolet remote sensing of the universe began shortly after World War II using experiments carried aboard sounding rockets. Since then there has been a steady evolution towards observations from spaceborne platforms. Except for all sky mapping surveys, such as the EUV-Explorer or the Space Schmidt missions, the emphasis has been and will continue to be directed to medium to high resolution absolute spectrophotometric observations. Spectral resolution capability has progressed steadily from the first major UV satellite, OAO-2, through the Copernicus Observatory to the present operational system - the International Ultraviolet Explorer (IUE). Instrumentation on-board the Space Telescope (ST) scheduled for launch in 1986 will push the resolving power of UV sensors into the 10^5 range. Other NASA missions in various stages of development which will drive advances in the extreme and far ultraviolet (EFUV) sensor technology include the Far Ultraviolet Spectroscopic Explorer (FUSE), ST follow-on instrumentation, and STARLAB.

The EFUV spectral region between 10 and 200 nm contains most of the important resonance transitions of cosmically abundant atoms and ions. For this reason, the EFUV region constitutes a critical area for ongoing development in sensor technology.

Because EFUV observations must be carried out above the strongly absorbing atmosphere of the earth, they are ideally suited to be performed on spaceborne platforms and can generally be divided into downlooking (Earth sensing) or uplooking (astronomical) categories. For the case of the former, EFUV observations of the thermosphere offer the possibility of remote optical monitoring of atmospheric constituent abundances and transport phenomena. Observations of the terrestrial aurora provides an important link in our understanding of the coupling of solar wind energy into the atmosphere. The thermosphere is also an invaluable laboratory for testing the validity of radiative transport theories in the regime of very large optical depths.

Fundamental information is contained in the optical footprint of the universe in the EFUV region regarding cosmic evolution, the inter-galactic medium, and the evolution of the solar system. For the case of astronomical observations, the EFUV spectral region is unusually useful in that conditions and phenomena spanning a very large temperature range (10^3-10^7 K) can be probed.

An EFUV sensor consists of three basic elements: (1) an optical front end (telescope); (2) the basic instrument optics (e.g., gratings, mirrors, etc.); and (3) the detectors used to convert photons incident upon the sensor into a usable electronic signal. A specific example for the case of potential FUSE instrumentation would be a 10^o grazing incidence telescope, a normal incidence Rowland spectrograph and a detector consisting of a windowless CsI coated microchannel plate fiber optically coupled to a CCD array. High speed back end electronics are needed for processing the acquired data. Of the subsystems, the most critical areas with respect to enabling advances in the science that can be achieved are detector technology and total sensor throughput (which is largely a function of the collecting area of the optical front end and the reflectivity of the optical surfaces).

Broadly speaking, EFUV sensors can be lumped into two general classifications: (1) broadband imaging cameras which achieve wavelength discrimination by some combination of window, filter, and photocathode materials; and (2) spectrometer systems which use diffraction gratings as dispersive elements.

Figure ·94 schematically illustrates in the form of a "technology tree" the main system components for the case of an EFUV sensor based on dispersive optics. The basic subsystems which comprise the sensor are arranged vertically in the rectangular boxes. Aspects of technology which require development are indicated by the solid lines branching from the subsystem components. A discussion and projection of the major technology elements needing development is given below.

·8.1 Optical Front End (Telescope)

Maximum collection and throughput of photons is of principal concern in the telescope optics. Two approaches are possible: (1) the use of conventional telescopes with improved high reflection coatings and (2) the development of grazing incidence telescopes which improve throughput by the use of higher reflectivities for incident photons nearly parallel to the mirror surface. Greatest gains are expected in grazing incidence design. For observation of point sources, the telescope diameter determines the total number of photons collected and thereby, contributes to overall instrument sensitivity. Table .47 summarizes the forecast of important UV telescope parameters.

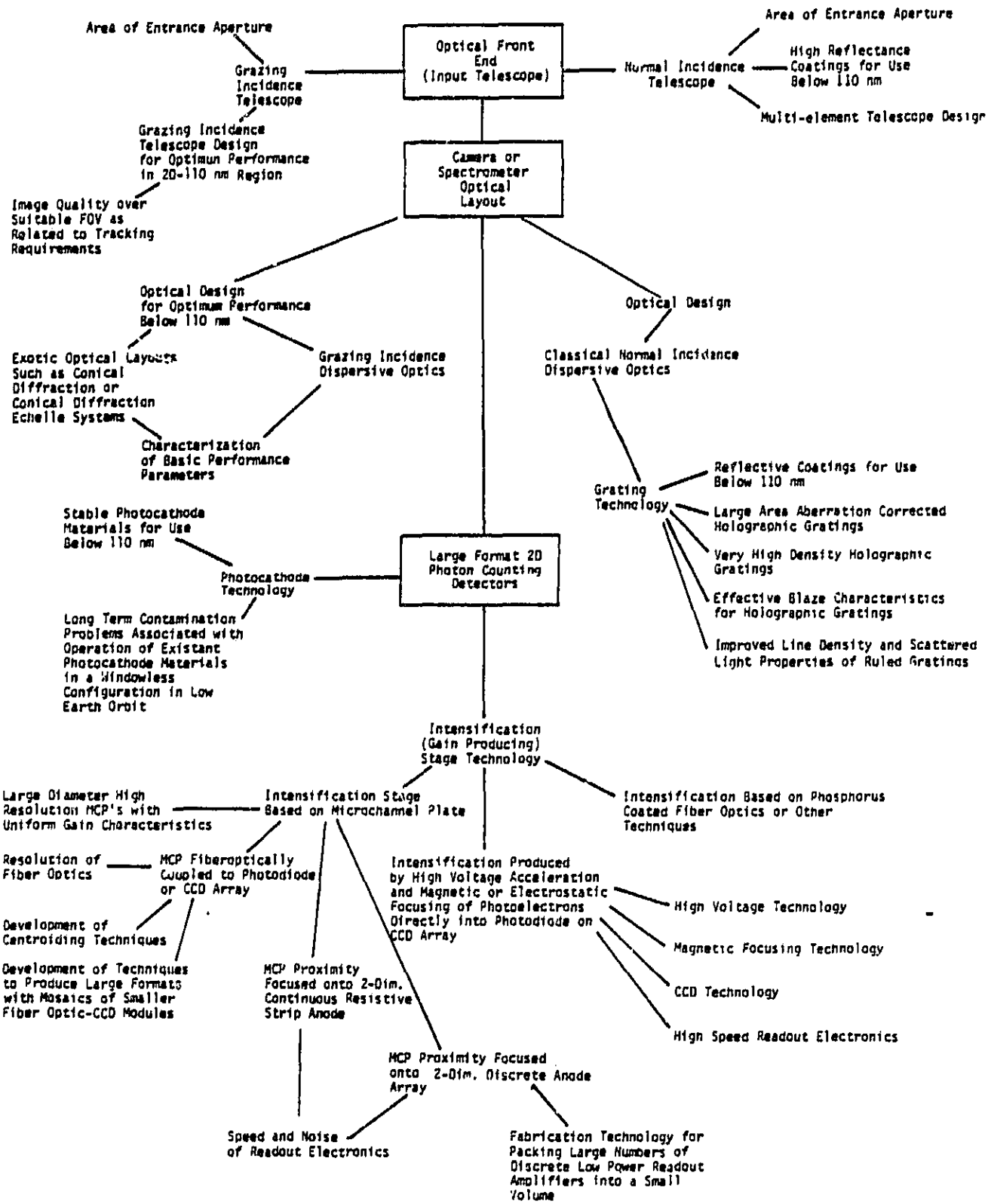

Figure 94. Technology Tree for UV Sensors

TABLE 47

UV SENSOR OPTICS FORECAST

Critical Component and Characteristic	SOA Value	2000 Value
Telescopes:		
Normal Incidence Reflectance (High Reflective Coating)		
>115 nm	85%	90%
<115 nm	25%	50%
Grazing Incidence Reflectance (10^{o} incidence angle)	70%	90%
Total Throughput	50%	80%
Spaceborne Telescope Diameter		
Normal	2.4 m	4 m
Grazing	1 m	2 m
Gratings:		
Relative Efficiency (1st order)		
Classic (ruled)	65%	70%
Holographic	30%	60%
Size		
Classic	0.25 x 0.25 m^2	0.25 x 0.25 m^2
Holographic	1 x 1 m^2	3 x 3 m^2
Ruling Frequency		
Classic	5,000 grooves/mm	7,000 grooves/mm
Holographic	6,000 grooves/mm	18,000 grooves/mm

8.2 Spectrometer Optics

The areas needing development in EFUV spectrometer optics include exotic dispersive optical layouts, such as those based on grazing incidence conical diffraction, and grating technology for normal incidence spectrometer designs. Grazing incidence designs improve absolute grating efficiency and can provide more uniform and efficient blaze properties resulting in a high throughput in the spectrometer along with resolving powers of $\sim 10^4$. The areas in grating technology needing development are listed in Fig. 94.

Efficiently blazed, large area, aberration corrected holographic gratings will receive the most intense development in the future. The use of ion milling technology to control groove shape offers tremendous promise for improving holographic grating efficiency. Efficiency is achieved by a combination of blaze properties and reflective coating. Reflective coating projections are the same as those given for telescope design. Because of better control of blaze characteristics, classically ruled gratings permit higher total throughput at the cost of higher scattered light. However, they are limited to relatively small sizes (0.25×0.25 m^2). Holographic gratings can be made larger, more uniform in efficiency across the surface and can be aberration corrected. The scattered light from holographic gratings is $\geq$1 order of magnitude lower than that for ruled gratings. This fact permits wider dynamic range in some applications. They can also be made with far greater density of lines than is practical with classically ruled gratings. The grating efficiency relative to a perfect mirror (i.e., neglecting the reflective coating) is an important parameter and is forecast along with other UV grating parameters in Table 47.

8.3 Detectors

Detectors are the critical components of UV systems and as can be seen in Fig. 94 present many technological areas which require development. All generic UV detectors contain a photocathode, which converts photons to electric charges, an intensification stage which provides gain, and a readout stage (e.g., anode) which collects the

final signal. State of the art and future detector concepts all attempt to preserve spatial information and thus require a large number of resolution elements. Highly sensitive detectors are characterized by their quantum efficiency and capability to do single photon counting. The limit to EFUV detector sensitivity for space applications is generally determined by thermal noise in the photocathode and the quantum statistics of the signal and cosmic ray background incident on the detector.

8.3.1 Photocathodes

The photocathode quantum efficiency dominates the net quantum efficiency of the detector system. Excluding background noise (e.g., cosmic rays), thermal noise generally sets the minimum achievable noise level. Optimum quantum efficiency is achieved using photocathodes in an opaque configuration. Photocathodes of adequate quantum efficiency presently exist (e.g., CsI, CuI, KI) for the 20 nm to 190 nm region. However, these materials are hydroscopic and are subject to contamination when used in a windowless configuration. Furthermore, below 110 nm, no adequately transmitting window materials exist. Stable photocathode materials need to be developed as well as better UV transmitting window materials. However, progress in these areas is expected to be slow. The photocathode quantum efficiency is forecast in Table ..48.

8.3.2 Intensification Stage - Readout (Anode) Stage

With regard to future detector requirements, several approaches are particularly attractive; the two-dimensional digicon (2D-Digicon) and two detectors based on microchannel plate (MCP) technology.

2D-Digicon. The 2D Digicon is a generalization of a digicon type device to two dimensions. In such a device, electrons from a suitable photocathode are accelerated (through 20-30 keV) and magnetically focused onto a CCD or photodiode array, giving rise to a net gain as the accelerated electrons lose energy to generate electron hole pairs in the device. The diode array provides intermediate storage of the signal prior to electronic readout into the data processing stream. This method has the potential for high spatial resolution limited only by the

CCD or photodiode pixel size. Because the pulse height distribution in this system is very narrow, a minimum of gain noise after the photocathode is introduced into the system and single photon counting can be achieved. The major disadvantage of this device is that it requires cooling (e.g., thermoelectric) to reduce diode leakage currents. A projection of single CCD array element resolution and size is given in Table ..48. Mosaics of CCD arrays can in principle be used to increase the fractional resolution.

TABLE .. 48

DETECTOR COMPONENT PARAMETER FORECASTS

Component/Parameter	SOA Value	2000 Value
Photocathode QE	50%	90%
Detector Technology		
2D Digicon		
CCD Element Size	15 x 15 μm^2	7 x 7 μm^2
Single Array Size	800 x 800	1600 x 1600
MCP		
Pore Size/MCP Diameter	7 μm/25 mm	7 μm/150 mm
Gain Characteristics	$10^6 \pm 6\%$ over 25 mm	$10^7 \pm 3\%$ over 150 mm
MAMA		
Resolution/Length	50 μm/25 mm	25 μm/50 mm
Anode Array Size	500 x 500	2000 x 2000
MOSAIC		
Resolution/Diameter	15 μm/35 mm	7 μm/35 mm
Mosaic Array Size	2300 x 2300	4800 x 4800
CCD Readout Rate	50 kHz	$\geq$50 MHz

MCP Based Detectors. Two of the most promising techniques using intensification based on microchannel plate technology are detector systems using discrete multianode arrays - (multianode microchannel plate arrays (MAMA)); and devices based on fiber optic coupling between the MCP and a single or mosaiced CCD array. In a microchannel plate intensification occurs as photoelectrons are accelerated at ~2 kV through narrowly spaced holes (pores) in a semiconducting glass material. Gains of $\sim 10^6$ in 2-3 mm thicknesses can be achieved. Spatial

resolution is limited by the pore size and is forecast in Table 48 and Fig. 95. A photocathode deposited on the front end determines the wavelength sensitivity.

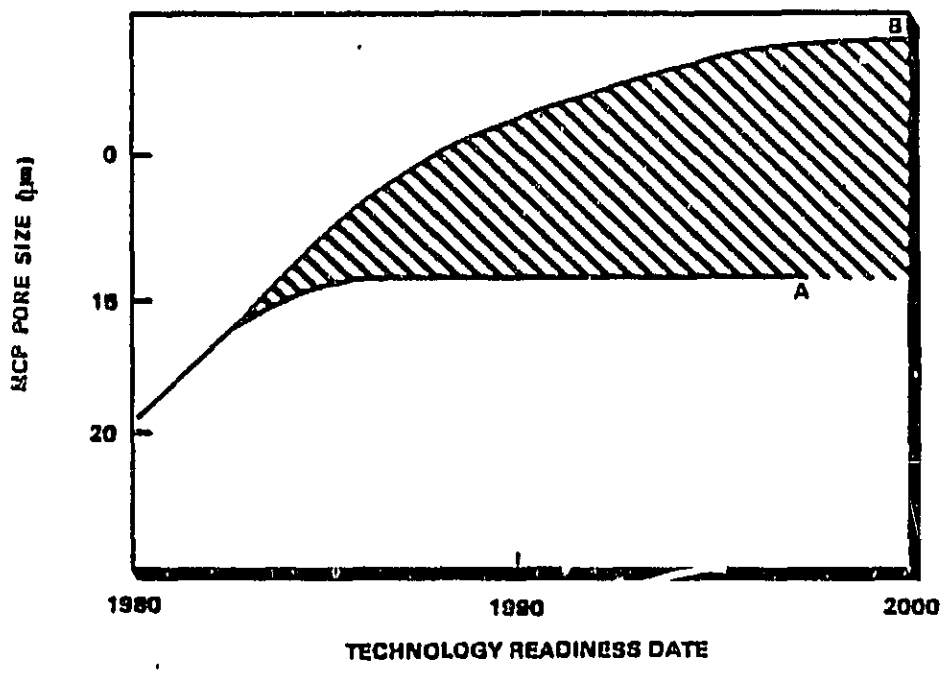

Figure 95. MCP Resolution Element for Large Diameter (150 mm) Plate

MAMA: In the MAMA detector, the charge cloud from the MCP is proximity focused onto a two-dimensional array of wire grids. In this detector, AxB pixels are read out by A+B discrete amplifiers using a coincidence technique. Current technology limits the maximum number of discrete amplifiers to about 10^3, however, advances in packing large numbers of amplifiers into a small volume using large scale integrated circuit technology should increase the fractional resolution capability of this technique by a factor of 4 by the year 2000. A forecast for MAMA detector resolution and size is given in Table 48. The MAMA detectors have many advantages. These include low geometric distortions, high time resolution, and relatively low voltage requirements. Several of these detectors are being built for use in sounding rocket and Shuttle instrument payloads.

MCP-Fiber Optic Coupling in CCD's (MOSAIC): In the fiber optic coupled device, the output of the MCP is proximity focused onto a phosphor coated fiber optic bundle which is coupled to a CCD or photodiode array. Several fiber optic bundles and CCD arrays can be used in a mosaic format thereby increasing the effective array size. In one version of this detector under development (MOSAIC), the fiber optic coupler has nine tapers arranged in a 3 x 3 mosaic, each with a CCD at its output. This detector will be a photon counting device with a large field and high resolution (more than 2300 x 2300 pixels). Perhaps the most exciting aspect of the MOSAIC design is its versatility. Once the feasibility of using fiber optic modules to couple the MCP output to several CCDs has been established, the output format can be customized for particular missions. A linear mosaic of CCDs may be appropriate for some spectroscopic observations while larger fields of view and/or higher resolution can be obtained by increasing the number of CCDs used. The resolution is presently limited by the CCD pixel size and ultimately by the pore size of the MCP. A forecast of several fiber optic coupled device parameters is given in Table 48.

8.3.3 Electronics

Except when used in a Digicon configuration, the readout rate of the CCD is critical to the capability of the device to do single photon counting. A projection of CCD readout rates is given in Table 48 and Fig. 96. Faster electronics are clearly desirable. To obtain the highest possible resolution from a detector, it may be necessary to centroid the output to find the precise location of an event. In photon counting systems, where only the location of individual events is stored in accumulating memories, a centroiding operation must be performed in real time. With the large number of pixels in current and next generation detectors, very high speed electronics are required to accomplish such calculations.

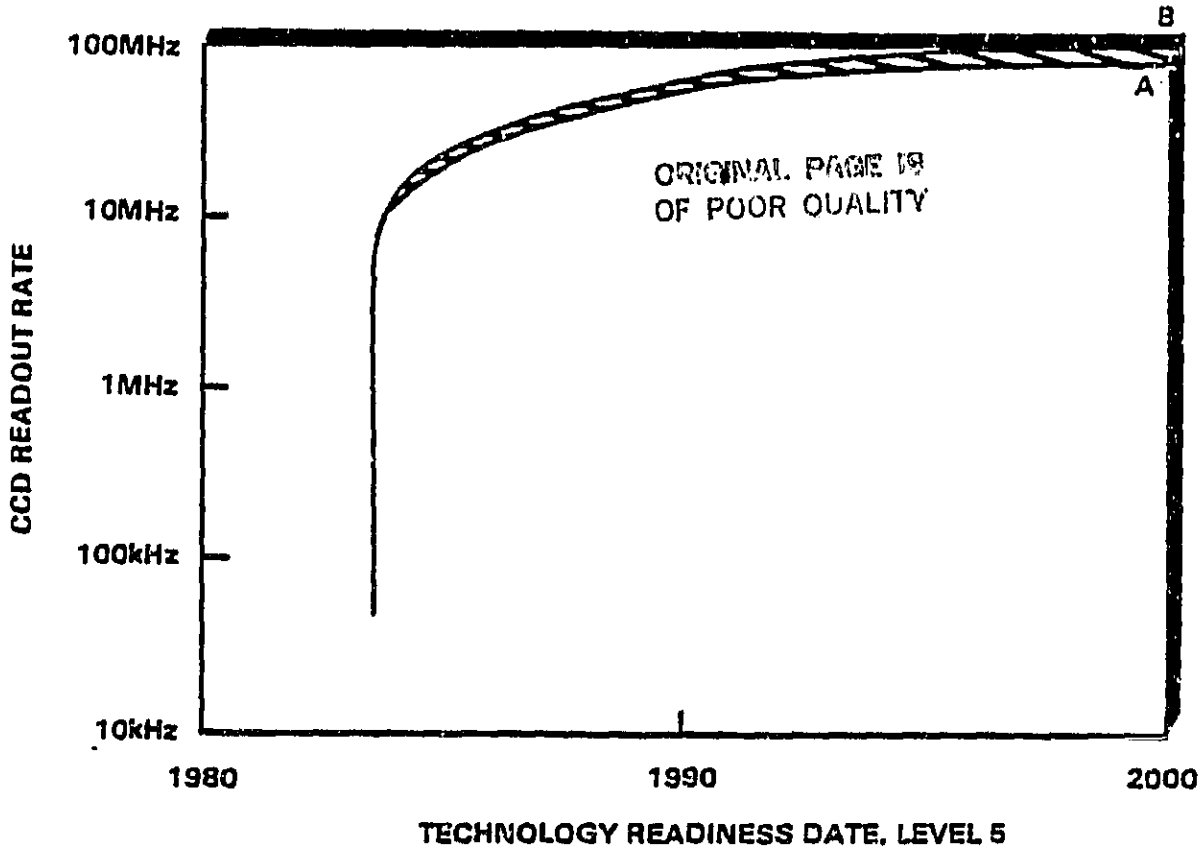

Figure 96. CCD Readout Rate Projection

It is also clear that large high resolution two-dimensional photon detectors will generate enormous data rates and place severe demands on associated data processing and storage technology. For example, 400 Mbits of data are contained in a 16 bit 5000 x 5000 array. Methods must be found to store all these data, yet retrieve them quickly and efficiently. Computers with parallel processing capabilities will be needed for rapid reduction of two-dimensional data. Systems capable of displaying the data from 2500 x 2500, and ultimately 10^4 x 10^4 pixel arrays will be required. For the data analysis, areas of interest will include pattern recognition, extraction of meaningful physical parameters from a series of images, and restoration techniques to recover as much detail as possible. Methods to deal with low intensity images must also be developed.

The weight and volume of the support electronics for a detector can be much larger than for the detector subsystem itself. For example, in the MOSAIC system described above, the support electronics will

comprise about 27 kg of the 28 kg of the entire system, and will occupy 0.09 m^3 of the total volume of the system, 0.11 m^3. To minimize costs, mass and volume must be as small as possible in a space mission, so the need to develop small and light support electronics is compelling.

8.4 Prominent Institutions and Individuals

NASA/Goddard Space Flight Center
A. Boggess
E. P. Gentieu
D. Weistrop
B. Woodgate

Space Telescope Institute
F. Paresce

Night Vision Laboratory
J. T. Cox

Naval Research Laboratory
G. R. Carruthers
G. H. Mount
D. Michels

Air Force Geophysics Laboratory
H. E. Hinteregger
R. Hoffman

California Institute of Technology
J. B. Oke

Utah State University
D. G. Torr

Service d'Aeronomie du C.N.R.S.,
Verrieres le Buisson, France
J. E. Blamont

Jet Propulsion Laboratory
J. Janesick
F. Vescelus

Johns Hopkins University
H. W. Moos
P. D. Feldman
A. F. Davidson

University of Colorado, Boulder
C. Barth
G. Lawrence
G. Timothy

University of California
C. S. Bowyer

USC
A. L. Broadfoot

University of California,
San Diego
E. Beaver

University of Texas, Austin
R. Tull

Princeton University
P. Everett

9 X-RAY SENSORS

The energy region spanned by x-ray instruments ranges from 40 eV to more than 100 keV. This energy range overlaps at low energy with the ultraviolet and at high energy with gamma ray photon energies. Neither end of this spectral energy range is sharply defined. X-ray sources include radiation emitted due to inner shell transitions of electrons, Compton scattering, and Bremstrahlung.

X-ray measurements can be used for elemental analysis and elemental mapping of planetary surfaces, for the study of the internal

structure of solar coronal loops and reconnection regions of solar flares, and the observation and mapping of astrophysical sources. X-ray spectra associated with pulsars, quasars, and black holes have been identified.

X-ray sensor systems currently being prepared for future space applications include spectrometers and imaging spectrometers. These systems utilize grazing incidence telescopes and unique detectors to cover each specific energy range. Optimum sensitivity is achieved with moderate cooling of the detectors.

9.1 X-Ray Detectors

X-ray detectors are normally composed of either high purity germanium, HP(Ge), or silicon [e.g., Lithium doped silicon, Si(Li)]. Recent research on new materials for x-ray detection has illustrated that mercuric iodide (HgI_2) detectors hold promise for future applications.

Present and future x-ray sensors require the use of detector arrays. Thus, detector development is focused on array and CCD technology including detector material improvements as well as the development of new low noise preamplifiers and readout electronics. The development of passive and active cooling systems (>100 K) which are required for detection with optimum sensitivity is also needed.

A forecast of detector parameters is provided in the following system and component descriptions.

9.2 Representative Instruments

9.2.1 X-Ray Imaging Spectrometers (41-410 eV)

This class of spectrometer for low energy x-rays utilizes EFUV technology already discussed. A representative system covering the 3-30 nm spectral region consists of a grazing-incidence soft x-ray optical system coupled to a multianode microchannel array plate. Spectral dispersion is provided by a holographic grating and spatial resolution

is obtained in the perpendicular direction using focusing optics. The spatial resolution is on the order of 5 to 8 arc seconds over a 0.12° field of view. The dark count rate is the dominant detector noise source. System performance is limited by scattering due to optical surface roughness.

The development of CCDs for the soft x-ray region (3-30 nm) is important for the spectrometer. The energy discrimination of the CCDs will allow order sorting, so that a single spectrometer could cover more than 1 octave wavelength range.

The spectral and spatial resolution are forecast in Fig. 97 and Table 49. Curve B in Fig. 97 depends upon a technology improvement in the accuracy of figuring optical surfaces and ensuring low scatter at soft x-ray wavelengths.

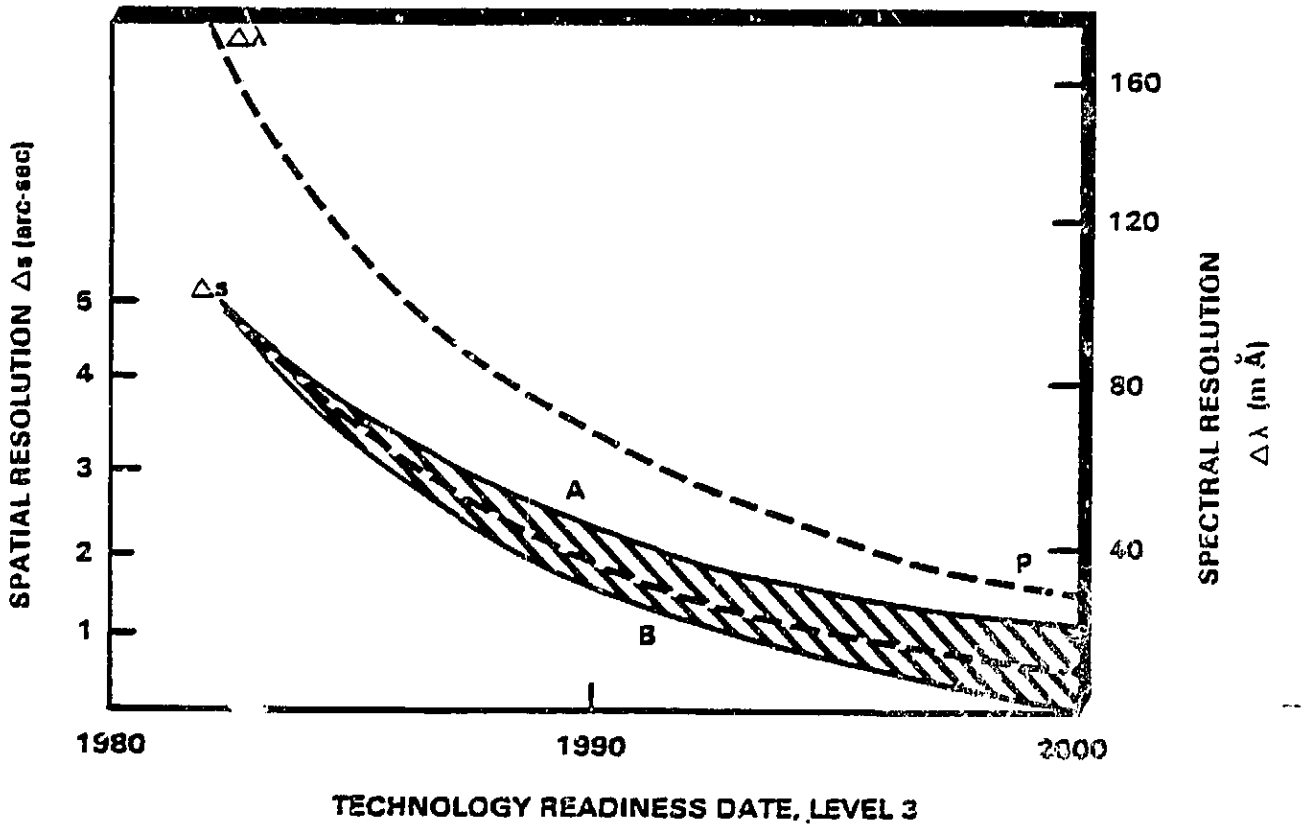

Figure 97. Performance Projection for the X-Ray Imaging Spectrometer

TABLE . 49

PERFORMANCE PROJECTION FOR THE X-RAY IMAGING SPECTROMETER SYSTEM

Parameter	SOA Value	2000 Value
Spatial Resolution	5 arc sec	0.5 arc sec
Spectral Resolution	165 mÅ	30 mÅ

Critical subsystems for this system include holographic toroidal gratings and multianode microchannel 2-way plates with a sensitivity to soft x-rays. The mirror technology and that for the microchannel plate are of most importance for proper operation. Table . . 50 illustrates the current and projected values for these subsystem elements.

TABLE . . 50

CRITICAL SUBSYSTEMS FOR THE X-RAY IMAGING SPECTROMETER

Critical Component and Characteristic	SOA Value	2000 Value
Mirror Technology		
Surface Figure Accuracy for an Aspheric Surface	$\pm$0.5 arc sec	$\pm$0.03 arc sec
Surface Roughness	0.25 nm	0.1 nm
Microchannel Plate		
Pixel Size	25 x 25 μm^2	10 x 10 μm^2

The SOA mirror technology values of Table .50 were obtained from the manufacture of the Einstein x-ray telescope (1978). The year 2000 values are based on a projection of the technology thought possible for the AXAF telescope (1990).

9.2.2 X-Ray Imager (0.1-8.0 keV)

This class of instrument based on silicon CCD array detectors is designed specifically for astrophysical applications. It covers the spectral region from 0.1 to 8.0 keV, has a tuneability of 150 eV, and its spatial resolution on the focal plane is 33 line pairs per millimeter. Its data readout rate is limited to 10 Mb/s. The optics consist of a grazing incidence telescope. The focal plane incorporates one or more Si charge coupled devices (CCD) which have been optimized for x-ray performance. The detector is cooled to ~223 K. A conventional CCD signal chain is utilized. A forecast of system sensitivity, areal coverage, and spectral resolution at 5.9 keV is illustrated in Fig. 98.

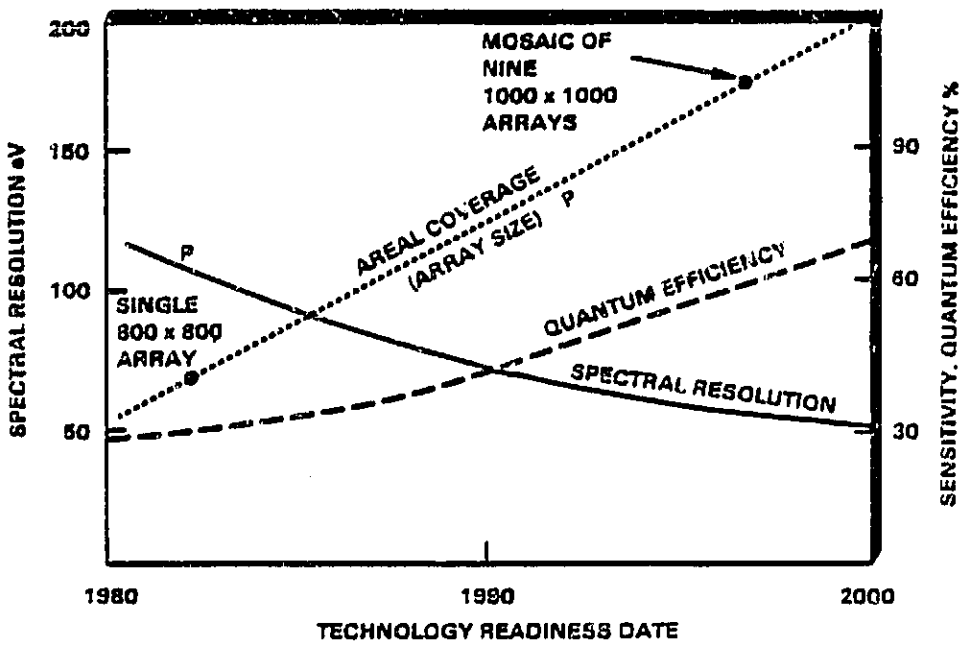

Figure 98. Forecast of X-Ray Imager Parameters at 5.9 keV

Spectral resolution is currently ~100 eV and is projected to reach 50 eV in the year 2000. The quantum efficiency is expected to double by the year 2000, and at the same time, it is expected that the current value for areal coverage (one 800 x 800 CCD array) will be increased to a mosaic of nine 1024 x 1024 arrays. The CCD dynamic range is expected

to increase from its current value of 1000 to a value of 10,000 by the year 2000. This will require further CCD development and new work in the area of x-ray optics.

9.2.3 Solid State (Deep Diode) Si Detector X-Ray Imaging Array (1-30 keV)

The Imaging X-Ray Spectrometer is a solid-state silicon detector using "deep diodes" through the wafer formed by thermomigration of aluminum. Thermomigration is a method in which temperature gradient diffusion is used to drive aluminum posts through a silicon substrate with a lateral spread of a few percent (less than 5%) of the substrate thickness. The first such x-ray detectors were designed, fabricated, and tested at the Goddard Space Flight Center (GSFC). The detector array is unique because it offers both good energy and spatial resolution for the analysis of x-rays in the 1 to 30 keV range. Because the aluminum posts go completely through the detector substrate, the complete thickness of the wafer can be depleted, leading to high quantum efficiencies for x-rays in the 1 to 30 keV range. The quantum efficiency is a function of the silicon thickness. A 400 μm silicon substrate will stop all but 1/e of incident 15 keV x-rays. Thicker silicon substrates can be used for higher energy x-rays. The thickness of the wafers to be used is only limited by the ability to drive posts because depletion voltages are now independent of substrate thickness. To date good posts have been driven through 1300 μm wafers. Spatial resolution is attained by forming a grid structure of individual thermomigrated aluminum posts. In the middle of each pixel is a post which forms the electron collection terminal for the individual pixel. An array of greater than 100 pixels, 1 mm^2 per pixel, is planned for the AXAF mission.

The critical parameter of interest is the noise level of the detector system. This is measured as the full width of the line at half maximum of the peak (FWHM). Recent work has enabled the separation of the detector noise from the overall electronics. The noise levels add in quadrature. Total noise levels have dropped from 2.25 keV measured on the initial successful detectors to about 280 eV measured on a recent

batch. Of this 280 eV, about 200 eV was due to the detector while about 170 eV was due to the electronics. Improvements in on-chip integration electronics and detector arrays should reduce system noise levels.

Figure 99 shows the progress made since 1979 in reduction of system noise as well as a forecast for the future. The research is well into technology level 4, critical function/characteristic demonstration. By the end of FY 86, a level 7 technology, engineering model, ready to be tested in space should be obtained.

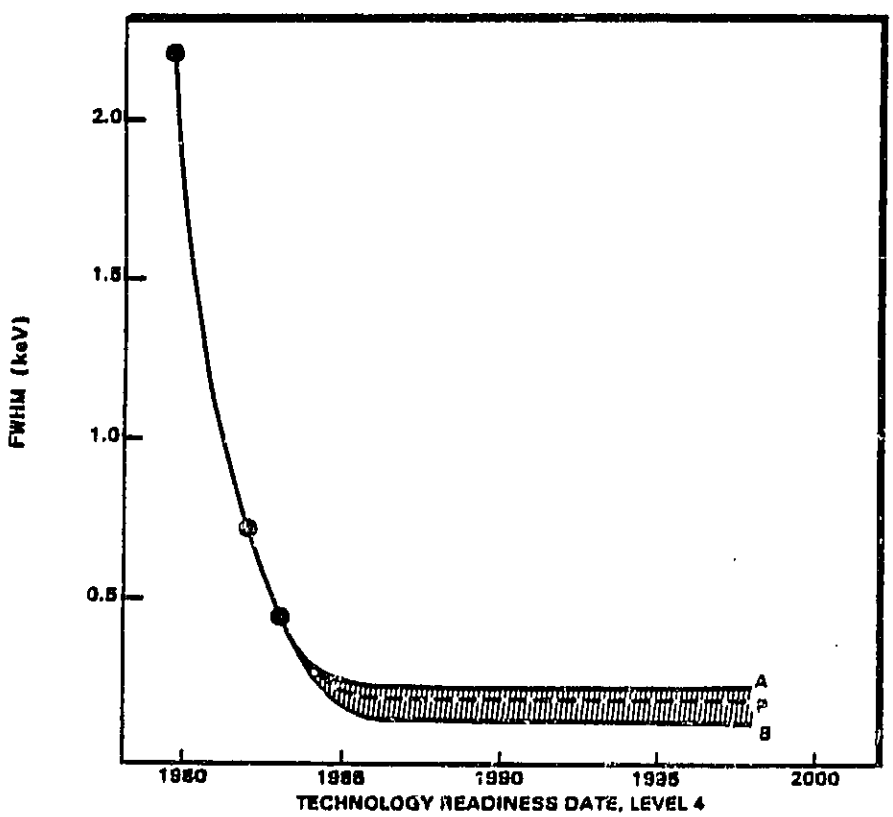

Figure 99. Projection for Imaging X-Ray Spectrometer System FWHM Noise Level

Electronics is now a hybrid system with unique problems. Further noise reduction is obtainable by putting completely redesigned electronics on the chip. Reduction of surface leakages and the use of higher resistivity material reduces capacitance thereby reducing electronic noise of the detector. However, this also leads to higher surface leakage problems which can be solved by extra surface passivation and surface treatments.

Present material used has resistivity of a few hundred ohm-cm. Later development will use material of several thousand ohm-cm. A significant part of x-ray detector fabrication research will be solving the resistivity degradation problem at high processing temperatures (greater than a 1000 C). A forecast of improvements in detector and electronics noise levels is given in Figs. 100 and 101. Table 51 summarizes these forecasts and gives the expected increase in array size.

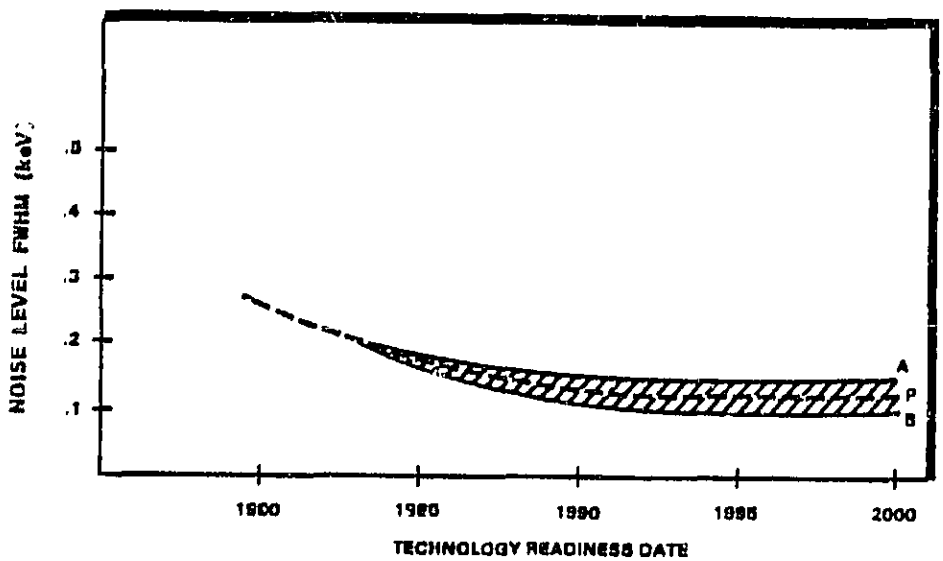

Figure 100. FWHM Noise Level for Imaging X-Ray Detector

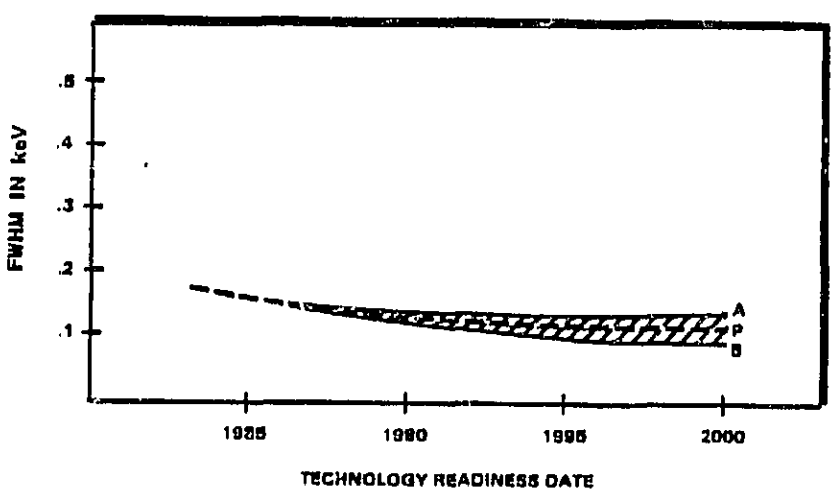

Figure 101. Preamplifier Electronics FWHM Noise Levels

TABLE 4.4.51

PROJECTED X-RAY ARRAY CAPABILITIES

Critical Component and Characteristic	SOA Value	2000 Value	Theoretical Limit
X-Ray Array Noise (Total)	280 eV FWHM	180 eV	Approx. 140 eV
Detector Noise	Approx. 200 eV FWHM	130 eV FWHM	Approx. 100 eV
Electronic Noise	Approx. 170 eV FWHM	120 eV FWHM	Approx. 100 eV
Number of Pixels	9 (number for first array)	>1000	

To achieve these values, a concurrent program in cryogenics must be actively pursued that will provide cooling to ~100 K. A Stirling cycle refrigerator can allow proper cooling with minimum size, power, and weight constraints. The physical parameters of an imaging spectrometer based on this detector concept are:

Weight:	67 kg (including Stirling cooler)
Size:	0.75 x 0.75 x 0.5 m^3
Power Requirement:	150 W
Cooling:	100 K
Data Rate:	64 kbits/s

9.2.4 Solid State HgI_2 Energy Dispersive X-Ray Spectrometer (0.5-150 keV)

This detector system operates as an energy dispersive x-ray spectrometer in the 500 eV to 150 keV energy range. An example of its resolution is provided by its response to 5.9 keV (Fe-55) x-rays. Using this source, the FWHM is 300 eV at room temperature and 200 eV when the input FET of the preamp is cooled. This parameter baseline is used to characterize the system and is projected in Fig. 4.4.102.

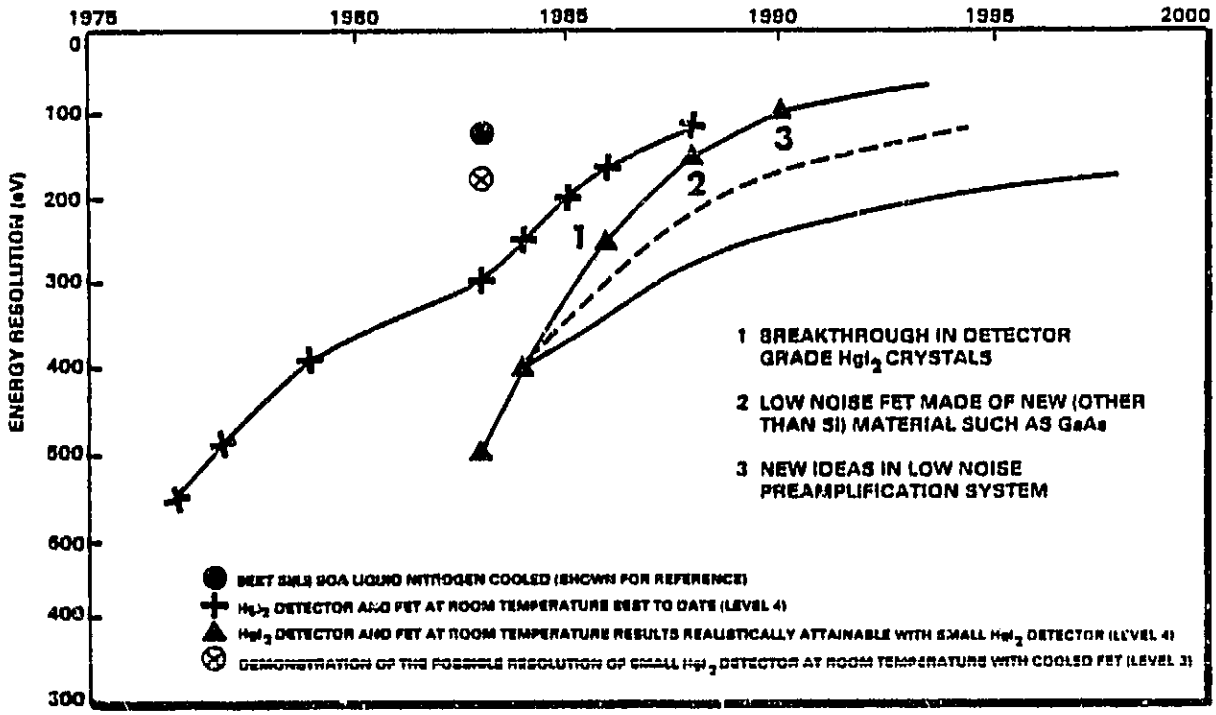

Figure 102. Energy Resolution of HgI_2 X-Ray Spectrometer for 5.9 keV X-Ray

Mercuric iodide (HgI_2) is a solid-state x-ray detector material which because of its large energy band gap can be used to make detectors having leakage current of the order of picoamperes at room temperature. X-ray spectrometry with an HgI_2 detector can thus be accomplished without the need for cryogenic cooling, allowing very substantial savings in space and mass. The energy resolution which can be attained at present makes HgI_2 an attractive alternative to other solid state detectors, and projected improvements in resolution with further research and development will make it closely competitive with Si(Li) and HP(Ge). The state of the art clearly demonstrates the outstanding progress which has been made in energy resolution in the past several years.

A forecast of system parameters is given in Table 52.

TABLE . 52

SYSTEM PARAMETER PROJECTIONS

Parameter	SOA Value	2000 Value
Energy Resolution for 5.9 keV X-Rays	300 eV (FWHM)	100 eV (FWHM)
Mass	Few Ounces	30 gm
Size	Approx. 16 cm^3	<1 cm^3
Power Required	3 W (mostly for Peltier cooler if used)	<100 mW

Critical parameters for this system are itemized as follows:

1. HgI_2 single crystals: the critical parameter is the product of electron mobility and mean trapping time; the yield of high quality crystals is an important consideration.

2. HgI_2 x-ray detectors: these must be stable in their performance with time (i.e., no polarization effects).

3. Preamplifier input FET: the critical parameter is the electronic noise level.

Future research and development will be concentrated in the areas of HgI_2 purification and crystal growth and in reduction of the noise of the field effect transistor used in the first stage of signal amplification.

The FETs must be capable of low noise ambient temperature operation or associated low power miniature cooler development will be necessary. A forecast of these technology areas is given in Table 53.

TABLE 53

PROJECTION FOR HgI_2 CRITICAL COMPONENTS

Critical Component and Characteristic	SOA Value	2000 Value
Yield of High-Quality HgI_2 Crystals	1 to 5%	Up to 100%
Noise of Input FET	225 eV (FWHM) at Room Temperature	Below 50 eV if a New Material Other Than Si is Developed

Applications of these systems are foreseen in the areas of elemental anlaysis by XRF, elemental mapping in SEM, and the study of extraterrestrial x-ray sources in x-ray astronomy.

.9.3 Prominent Institutions and Individuals

NASA/Goddard Space Flight Center
G. Alcorn
S. Holt
P. Serlemitsos

University of Southern California
A. Dabrowski
G. Huth
J. Iwanczyk
J. Kusmiss

University of Chicago
A. Turkevich
T. Economou

Imperial College, London, England
R. J. Speer

Hebrew University of Jerusalem, Israel
M. Schieber

Jet Propulsion Laboratory
M. P. Chrisp
S. A. Collins
G. Riegler
J. Janesick

MIT
G. Ricker
J. Vallerga
G. Clark

Colorado State University
P. Leyden

Pennsylvania State University
G. P. Garmere

Universita di Padova, Italy
G. Tondello

10 GAMMA RAY SENSORS

The importance of gamma ray systems for astrophysical purposes was first noted theoretically in the decade of the 1950s. However, the experimental development of gamma ray astronomy was initially quite slow. Balloon experiments prior to 1960 were not successful. It was not until 1972 that high energy celestial gamma rays were detected with certainty. This was accomplished by upgrading the detector systems and using larger, high altitude balloons. The first gamma ray telescope was launched in late 1972 on the Small Astronomy Satellite (SAS-2). This was followed by the launch of the Cosmic Ray Satellite (COS-B) in 1975 and other satellites carrying gamma ray detectors including the Solar Maximum Mission (SMM). Data acquired from these systems have had applications in the study of:

Primary and Secondary Galactic Cosmic Interactions
Solar Astrophysics
Galactic Matter Distribution
Galactic Cosmic Ray Distribution
Neutron Stars
Pulsars
Supernovae
Black Holes
Extra Galactic Radiation
Cosmology
Diffuse Radiation.

Flight systems normally include electronics, a detector, and a thermal shield. For scintillator systems like those carried on the Apollo missions, the detector subassembly consisted of a right cylindrical NaI(Tl) crystal with an area of 7×7 cm^2. In contrast, the gamma ray spectrometer used for the SMM contained seven high resolution detectors. Each detector was of the order of 7.6×7.6 cm^2, composed of NaI(Tl). The increased area allowed an increase in the sensitivity to low gamma ray flux. Gamma ray detectors and detector arrays can be divided into two general categories based upon the energy of the incident photons; detectors for energies <10 MeV and those for energies >10 MeV.

10.1 Detectors (100 keV to 10 MeV)

Detectors for photons of less than 10 MeV are used for the detection and compilation of the electron-photon interactions due to the photoelectric effect, fluorescence radiation, pair production and annihilation radiation, and Compton scattering. These systems use both crystal scintillators and semiconductors.

10.1.1 Scintillator Systems

Common detector materials include NaI(Tl), CsI(Tl), and CsI(Na). Photomultipliers are used to convert the scintillation to an output voltage or count rate. The resolution of these systems depend on the photomultiplier used and is limited by such things as the collector efficiency of the photocathode, emission by the photocathode, phosphor emission, and statistical fluctuations.

10.1.2 Semiconductor Detector Systems

Semiconductor devices have their resolution defined in terms of the full width at half maximum (FWHM) in pulse height units which can be converted to energy units. Types of semiconductor detectors include Si(Li), Ge(Li), high purity germanium Ge[Ge(HP)], and mercuric iodide. These have improved energy resolution compared to gas proportional counters and scintillators. Germanium is best for energies between 10 keV and 20 MeV. However, these detectors must be cooled to liquid nitrogen operating temperatures <100 K.

Other semiconductor materials have been studied as gamma ray detectors. Most promising of these is at present mercuric iodide which may eventually emerge as an alternative to germanium as a detector offering high density and good resolution without the cooling requirement, if sufficiently large crystals can be grown. Further improvement of gamma ray sensors can be achieved through the development and use of detector arrays for these energies and coded aperture detectors as needed.

Germanium Gamma Ray Detectors. Germanium crystal gamma ray detectors are solid-state ionization devices. Absorption or scattering of gamma rays within the intrinsic region produces electrons which lose their energy by creating electron-hole pairs to act as free-charge carriers. These carriers are collected by introducing a voltage gradient across the intrinsic region and integrating and amplifying the resulting current. The observed charged spectrum consists of a continuum and one or more narrow peaks from which one can infer the energy spectrum of the incident gamma ray flux. The areas under the peaks are a function of the detector size and shape, the position of the source with respect to the detector, and the photon energy. The widths of the peaks and the heights relative to the continuum are determined by the energies of the photons, the intrinsic resolution of the detector, and the noise contributed by the amplifying and measuring system. It is the height of the characteristic gamma ray peaks relative to the continuum which one wishes to optimize by means of high efficiency and high resolution. In order to bring the inherent noise of the Ge detector to a level which allows its operation as a gamma ray detector, the temperature must be maintained below 100 K. Lithium drifted germanium detectors must be maintained at these temperatures at all times to prevent Li redrifting. High purity (intrinsic) detectors may be stored at room temperature when not in use. These detectors are made in two basic configurations, planar for x-ray and low energy gamma ray detection and the larger cylindrical or coaxial for higher energy gamma rays.

The energy resolution of these detectors is directly related to the detector volume. Detector sensitivity is proportional to $(\text{volume})^{1/2}$. Current detector volumes are on the order of 200 cm^3. It is projected that this value can reach >400 cm^3 in the future. A plot of projected Ge detector volume is given in Fig. 103.

Detector efficiency and energy resolution is forecast in Fig. 104. These parameter projections as well as preamplifier noise projection are tabulated in Table 54.

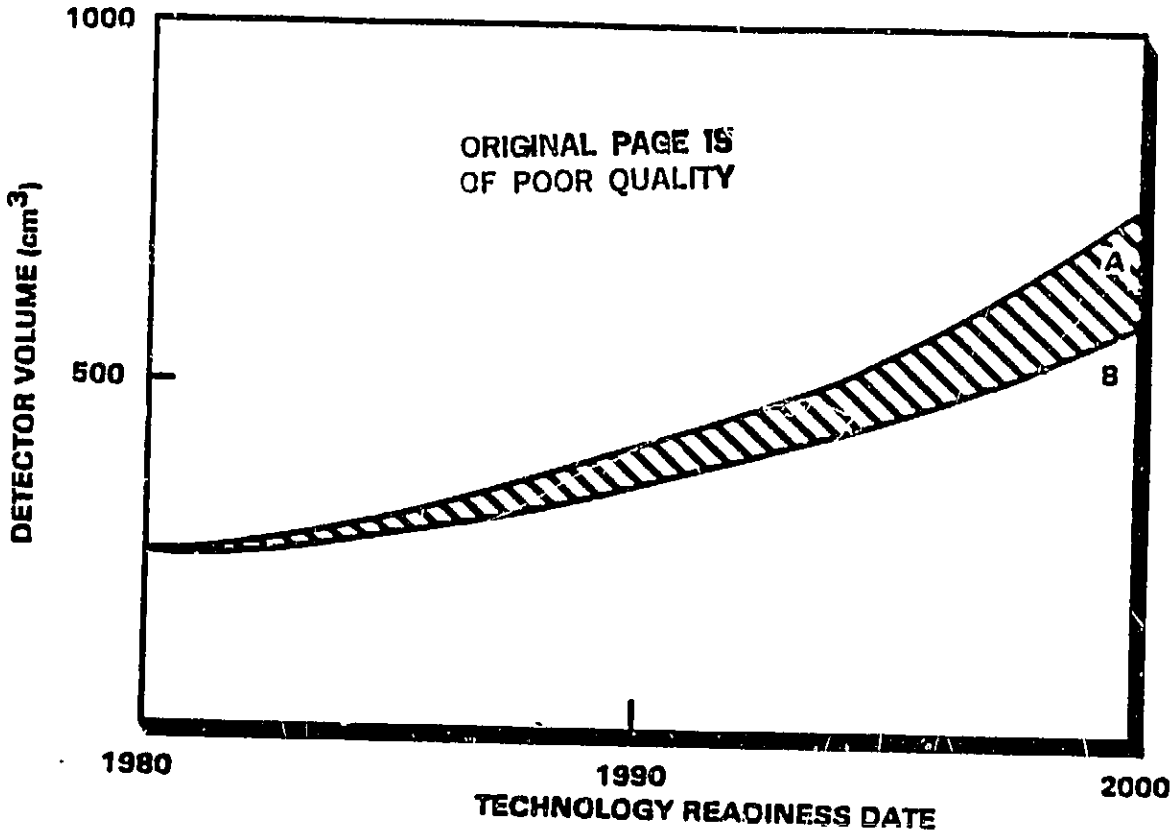

Figure 4.103. Projected Ge Detector Volume

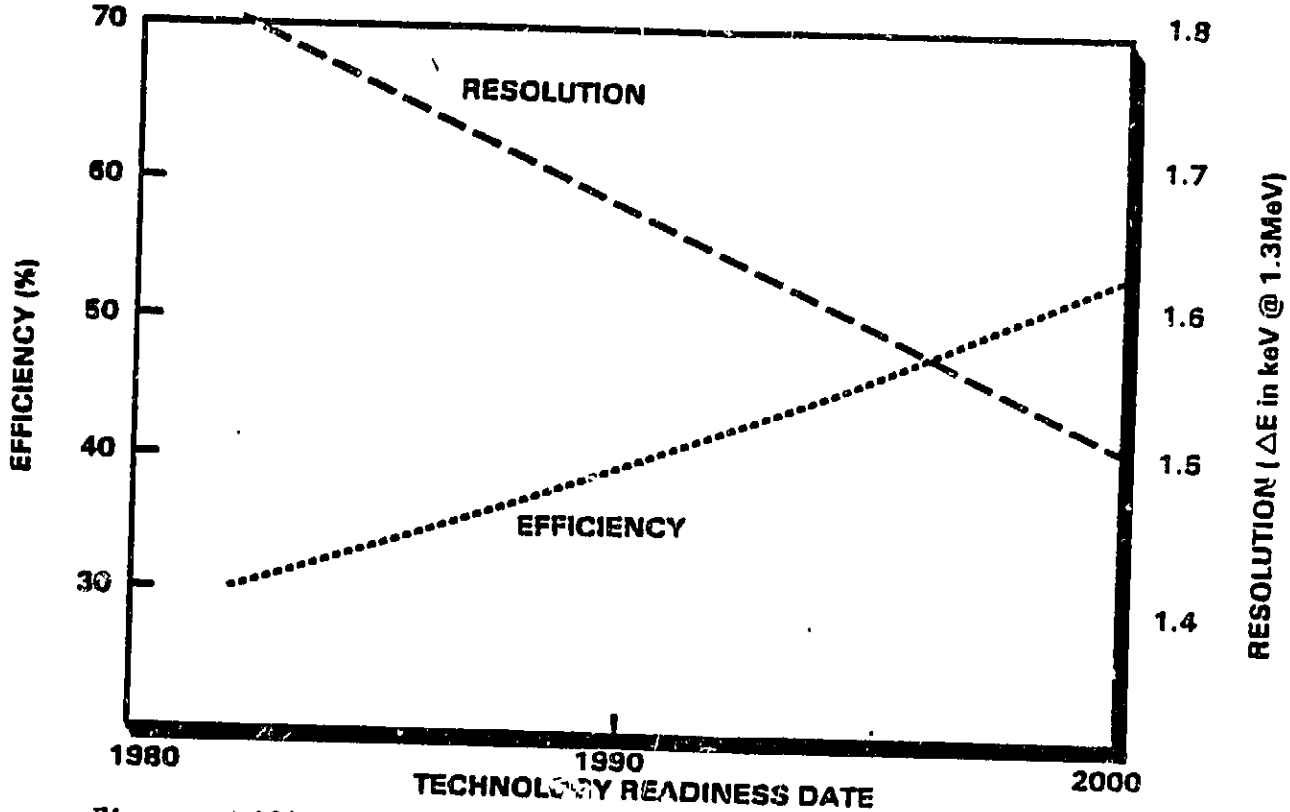

Figure 4.104. Gamma Ray Detector Performance Projection (Germanium)

TABLE 54

PROJECTIONS FOR GE DETECTORS

Parameter	SOA Value*	2000 Value
Efficiency	35%	60%
Resolution	1.8 keV	1.5 keV
Preamplifier Noise	250 eV	125 eV

*Available rather than exceptional.

Improvements for these detectors require increased crystal purity, better preamplifiers for detector systems, and the utilization of both active and passive cooling systems.

Gamma Ray Detection Using HgI_2 (No Scintillator). Mercuric iodide (HgI_2) is a solid-state gamma ray detector material which combines the properties of a wide-bandgap material with high stopping power because of the high atomic numbers of its constituent elements. As a consequence of the large energy bandgap (2.13 eV) of HgI_2, detectors made from it have a very low leakage current at room temperature and have low electronic noise. This allows construction of highly efficient spectrometers which can be operated at room temperature.

The energy resolution and efficiency values recently obtained with thick HgI_2 gamma ray detectors operated in the current-pulse mode will make them competitive with the scintillation-photomultiplier combination now in wide use. HgI_2 already presents distinct advantages over other gamma ray detectors (such as cryogenically cooled Ge detectors) in size, weight, and power consumption. Future developments in HgI_2 purification and crystal growth technology will produce improvements in energy resolution and will allow advantage to be taken of the reduced spread in

charge generation statistics of a solid-state ionization detector compared with scintillation counters. The system operating range for detection is 20 keV to several MeV. Applications can be foreseen in gamma ray detection and spectrometry from space where the combination of compactness, ruggedness, high detection efficiency, and low power consumption is needed.

Critical performance parameters include energy resolution and detection efficiency. Forecasts of parameter values are presented in Table 55. Physical parameters are also provided.

TABLE 55

FORECAST OF PARAMETERS FOR HgI_2 GAMMA-RAY DETECTORS

Parameter	SOA Value	2000 Value
Energy Resolution	10% for Cs-137 Gamma Rays (662 keV)	1/2%
Detection Efficiency for 5-cm Thickness	92%	Close to 100%
Weight	0.45 kg	Primarily Weight of HgI_2 Material
Size	130 cm^3	Primarily Size of HgI_2 Material
Power Requirement	100 mW	50 mW

The theoretical limit is set by the statistical fluctuation in the charge produced in the detector; a measure of this is the Fano factor, of which only an upper limit is known at the present time.

Three critical areas needing development for this gamma ray detector are:

(1) Large volume HgI_2 single crystals: The critical parameter is the product of electron mobility and mean trapping time. The yield of high-quality crystals is an important consideration.

(2) Uniformity of electrical properties throughout the volume of the crystals.

(3) HgI_2 gamma ray detectors: These must be stable in their performance in time (i.e., no polarization effects).

These activities require ongoing research in the growth and purification of large volume, thick, single crystals of HgI_2 and the further development of low noise electronics suitable for application to the current pulse method of spectrometry.

Gamma Ray Detector (With Scintillator). This new gamma ray sensor consists of an HgI_2 photodetector optically coupled to a scintillator crystal. Nearly all incoming gamma rays are stopped in the scintillator crystal and the scintillation light is detected by the HgI_2 photoconductor. The spectral response of HgI_2 is well matched to the light output from many scintillators. The scintillation light is absorbed within a very thin surface layer of the HgI_2 photodetector and generates charge carriers which are collected in much the same way as in an HgI_2 x-ray detector. With the entrance electrode negatively biased, only the electrons give rise to the output signal. Unlike the photomultiplier tube, which has a typical quantum efficiency of about 20%, for a solid-state photodetector, the quantum efficiency can be much higher, even approaching 100%, so that the ultimately attainable energy resolution may be much better than can be obtained with a photomultiplier-scintillator device. The HgI_2 photodetector scintillator gamma ray detector thus combines the advantages of the high stopping power of the scintillator and the high quantum efficiency of a solid-state photodetector.

Future research and development will be concentrated on improving the quantum efficiency of the HgI_2 photodetectors and the low noise amplification electronics. In the area of HgI_2 purification and crystal growth, efforts will be made to obtain a better yield of larger, more uniform single crystals with good electron transport properties.

Applications of these detectors can be foreseen in gamma ray detection and spectrometry when the combination of compactness, ruggedness, high detection efficiency, and low power consumption is needed, as it is in space applications. In addition, HgI_2 photodetectors do not need to be shielded from magnetic fields (as photomultipliers do).

The system covers the 50 keV to several GeV energy region. It is tuneable and has a spatial resolution on the order of 1 mm for low energy gamma rays. Its performance is limited by its energy resolution of 10% at 511 keV; dictated by the use of a HgI_2 detector with a 5 mm thick CsI(Tl) crystal with a 27 mm^2 area. The active area of the HgI_2 photodetector is at present limited to a few cm^2. The system is best described by its energy resolution and detection efficiency. These parameters and the physical size parameters are presented in Table 56.

TABLE 56

GAMMA RAY PHOTODETECTOR PERFORMANCE PROJECTION

Parameter	SOA Value	2000 Value
Energy Resolution	10% for 511 keV with CsI(Tl)	3%
Detection Efficiency	63% for 5 mm Thickness	Close to 100%
Mass	Few Ounces	Primarily Mass of Scintillator
Size	49 cm^3	Primarily Size of Scintillator
Power Requirement	100 mW	50 mW

Note: The theoretical limit depends on the statistical process of scintillation light production.

This technology will be driven by items similar to those described previously:

(1) Large area HgI_2 single crystals: The critical parameter is the product of electron mobility and mean trapping time. The yield of high quality crystals is an important consideration. Uniformity of electrical properties throughout the volume of the crystals will be crucial.

(2) HgI_2 photodetectors: These must be stable in their performance in time (i.e., no polarization effects). Higher quantum efficiency will be sought for the photodetectors.

Gamma Ray Detection for Energies >10 MeV. When energies are in excess of 10^5 MeV, the intensities of celestial gamma rays are too low to be seen with space telescopes. At present the upper limit for satellite experiments is $\sim 10^3$ MeV. Larger available detectors may extend this limit to $\sim 10^4$ MeV. Counter telescopes are the principal sensors in this energy region. The first of the counter telescopes to be flown in space was a scintillator Cerenkov counter detector flown on Explorer 11. Since then, technology evolution has led to the utilization of spark chamber counter systems for this region of the energy spectrum. Five different types of image chambers have been developed to the point of being included in a gamma ray telescope. They are the conventional optical spark chamber, the vidicon, the sonic spark chamber, the proportional counter, and the multiwire magnetic core digitized spark chamber.

10.2 Prominent Institutions and Individuals

Jet Propulsion Laboratory
A. Metzger
A. S. Jacobson

University of California, San Diego
J. Matteson

USC
A. Dabrowski (HgI_2)

NASA/Goddard Space Flight Center
B. J. Teegarden

Lawrence Berkeley Laboratory
R. Pehl (Ge)

Bell Laboratories
M. Leventhal

Reference: Gamma Ray Astrophysics, NASA SP-453, C. E. Fichtel and J. I. Trombka, GSFC (1981).

11 PARTICLE SENSORS

11.1 Charged Particle Detectors

11.1.1 High Energy Particle Detectors (>100 Mev)

Magnetic spectrometers use position-sensitive detectors (e.g., spark chambers or nuclear emulsions) to measure the amount of deflection

of high energy charged particles traversing a magnetic field. In combination with other types of particle detectors, magnetic spectrometers may be used to: (1) distinguish matter from antimatter in the cosmic rays, (2) resolve isotopes of cosmic ray nuclei, and (3) measure the composition and energy spectrum of cosmic-ray particles at high energy.

The magnitude of the deflection of a particle in the field and, hence, the resolution of the spectrometer is proportional to the strength of the field and the length of the particle's path in the field (i.e., the "field integral," $\int B \cdot dl$). This is the primary parameter forecast.

This forecast (Fig. 105) is based on development of existing technology; no "breakthrough" is required. The forecast assumes constant level R&D support for spectrometers and associated experimental equipment. The forecast through 1990 is based on scaled-up versions of existing balloon-borne superconducting spectrometers that use the same commercially available superconductive wire (Nb Ti). Extrapolation beyond this date will require more efficient superconducting material.

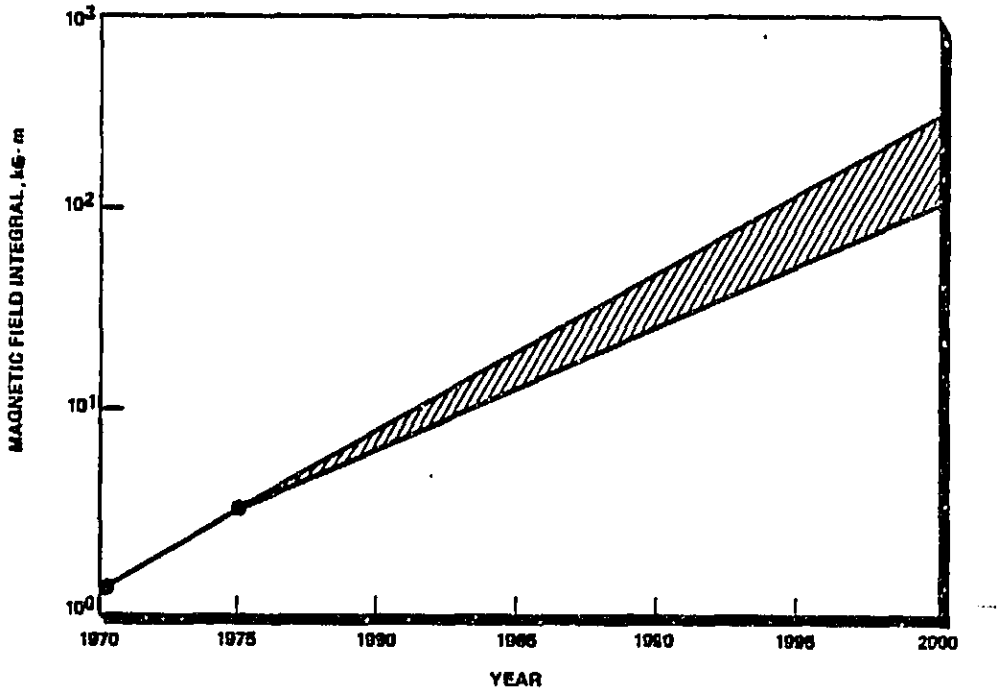

Figure 105. Superconducting Magnetic Spectrometer

11.1.2 Mid-Energy Particle Detectors (>50 keV)

Middle energy particle detectors utilize either solid-state silicon or solid-state germanium. The major advantage of these solid-state detectors is high sensitivity to small amounts of energy and the inherently uniform charge resolution. However, neither sensor sensitivity for the minimum detectable flux nor the energy resolution capability shows a recognizable trend. Energy resolution in particular is not limited by the sensor but by the nature of the plasma being investigated. The minimum detectable flux is related to the energy bandwidth impinging on the detector, the time constant over which the energy is collected, the size of the exposed detector face, and bit rate available. The first two relate to types of particles of interest and their inherent temporal and spectral variability. The size of detector is the main technology limit on sensitivity toward higher energies. The detector trends for existing solid-state silicon or germanium detectors are shown in Fig. 106. A University of California at Berkeley device with area 125 cm^2 appears to represent present technology. Areas in the 100 to 1000 cm^2 regimes appears to be feasible in the 1990s, especially as Shuttle space processing can be implemented for low gravity crystal growing.

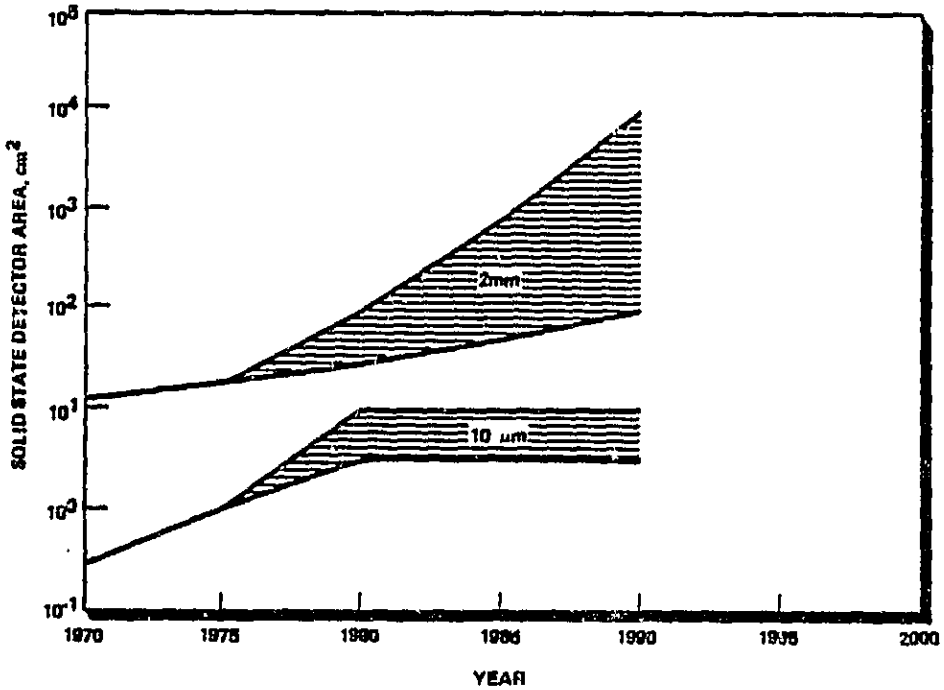

Figure 106. Trends in Solid-State Charged Particle Detector Size

11.1.3 Low Energy Particle Detectors (<50 keV)

Low energy particles are detected using channeltrons or electron multipliers. The detection of particles in space using channeltrons is a mature technology. Missions where particle detectors have been flown include ISEE, Mariner 10, Voyager, SMM, and Solar Polar. Future missions such as OPEN will benefit from this progression of technology.

Channeltrons are small conducting glass tubes that have a potential applied between their ends. Incident particles or photons produce an electron at the negative end of the partially evacuated tube. This initiates an avalanche. Due to this avalanche, a finite charge pulse is detectable at the positive end of the tube.

Each channeltron tube has a small diameter on the order of millimeters. This allows many tubes to be placed side by side in the focal plane of a detector system. In this configuration, the detector is called a channel plate. Detection by an individual channeltron in the channel plate can be traced to a unique spatial location. Incident particle direction can be determined using this location and the fore optics of the system through a simple ray trace methodology. The energy of particles detected in this manner is dependent upon the adjustable ionization potential for each tube. Pulses are fast. The maximum counting rate for these systems is presently limited to 1 MHz. Because of their light weight and low power, these detectors have been used extensively in past space experiments.

Performance of these systems is normally limited by background radiation. Present development activities are underway to improve both speed and positional accuracy. It is projected that the current 1 MHz counting rate can be increased to 100 MHz by the year 2000. Concurrent activities to improve positional accuracy are forecast to decrease spatial uncertainty from ~1 mm to 0.1 μm by the year 2000.

11.2 Neutral Particle Detectors

Neutral particle detectors rely on either field ionization or charge exchange to generate detectable ions from which the incident flux

can be calculated. Their application for interplanetary space would be especially valuable for the detection of hydrogen and helium.

Slow neutral particles are detected using field ionization. The detectors are normally composed of an arrangement of tungsten needles with very fine points (from a few hundred angstroms to microns in diameter). The needle array is kept at a fixed potential. The geometric configuration of the individual needles results in locally very high electric fields which ionize neutral particles in their vicinity. The sensitivity of the system depends on the ionization efficiency.

Fast neutral particles are detected through charge exchange. Normally the incident flux of particles is passed through a carbon grid or mesh kept at a fixed potential. The known ionization efficiency of this grid, coupled with the count of ionized particles, allows the calculation of the incident flux density of neutrals. Both types of detector systems are directional; i.e., they detect only particles that enter a specific solid angle at an entrance port governed by the collimator-detector combination.

Detector sensitivity depends upon configuration. Present detector efficiencies are of the order of 1% yet can be theoretically increased up to 100%. No neutral particle detectors have yet been flown by NASA. However, this technology is both available and suitable for future missions.

11.3 Prominent Institutions and Individuals

NASA/Goddard Space Flight Center
K. Ogilvie

University of Iowa

Bendix

University of Arizona

University of California, Berkeley

Night Vision Laboratory

Phillips (UK)

12 MAGNETOMETER

12.1 Fluxgate Vector Magnetometer

The detection of magnetic fields and particles requires the use of magnetometers as an instrument class. The specific example to be discussed is the Fluxgate Vector Magnetometer. It is used primarily for space applications in the study of space physics, plasma physics, and measurement of planetary fields. The instrument operates in the DC to 300 Hz frequency range and is sensor noise limited. Its performance limits lie between 0.005 nT to 10^7 nT depending on the design configuration.

Systems utilize balanced, tuned, second harmonic generators and saturable cores. The oscillator signal drives the permeable core to saturation. An external magnetic field introduces an unbalance in the differential winding which produces signals occuring at even harmonics of the oscillator frequency. The amplitude of the signal depends on the magnitude of the external field.

Instruments of this type have a 50 year history of application in the fields of anti-submarine warfare, geophysics, prospecting and aeromagnetic surveys. These initial instruments were adapted to space applications in the 1960s where the state of the art was upgraded for specific missions such as IMP, PIONEER, Mariner, Voyager, HEOS, HELIOS and MAGSAT. The state of the art instruments (1983) are satisfactory for all space missions except for surface penetrometers.

The most important system parameter is sensor noise. This parameter has been plotted as a function of frequency in Fig. 107 in terms of the system power spectral density. Projections have been itemized in Table 57.

Booms are critical subsystems which require careful design. Important considerations include their length, required to assure operation on the spacecraft in an environment that is not contaminated by spacecraft electronics, and trade-offs that must be made between boom

and the angular stability of the boom/sensor combination. The best achieved stability to date is illustrated by MAGSAT where system oscillations are less than 5 arc sec RMS. These factors, cleanliness and accuracy are projected in Table 58.

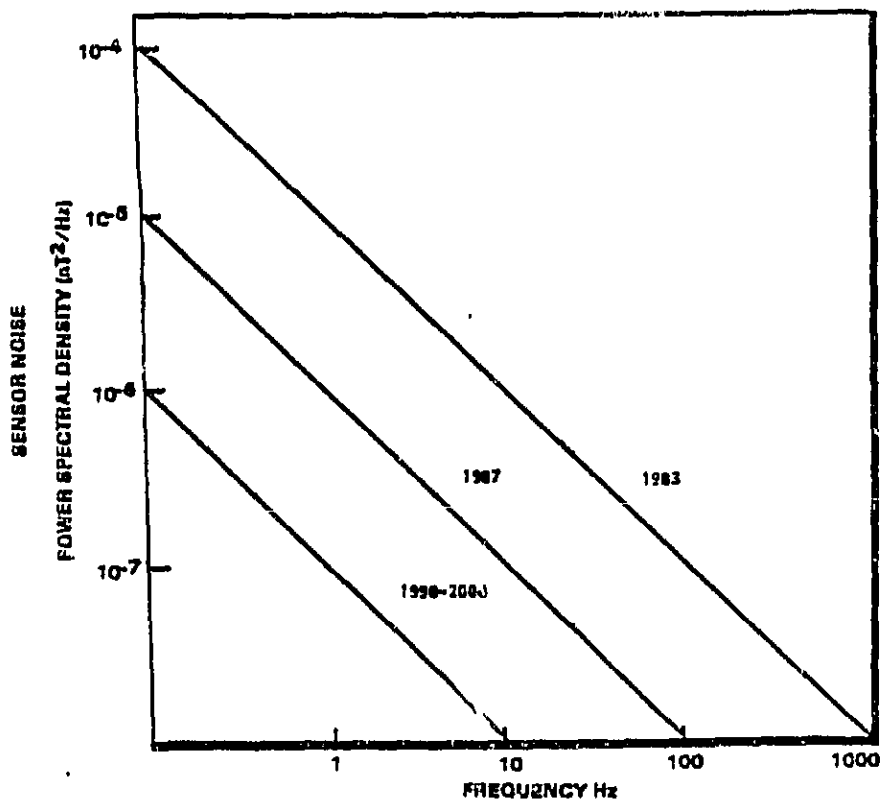

Figure 107. Sensor Noise for Magnetometers

TABLE 57

PROJECTIONS FOR MAGNETOMETERS

Parameter	SOA Value	2000 Value
Noise	0.006 nT (RMS)	0.001 nT (RMS)
Acceleration Survival for Penetrometers (Sensor)	17,000 G's	25,000 G's
(Electronics)	6,000 G's	10,000 G's

TABLE 58

SUBSYSTEM PARAMETERS

Critical Component and Characteristic	SOA Value	2000 Value
S/C Magnetic Cleanliness	0.02 nT	Unknown
Boom/Sensor Angular Accuracy	5 arc sec RMS	1 arc sec RMS

Supporting research activities include:

- Further development of electronics capable of withstanding large accelerations/decelerations (high G electronics).
- Sensor development for the penetrometer class of instrument.
- Analytical techniques to estimate spacecraft fields.
- Fast Fourier Transform/Data compaction of on-board data.
- Autonomous instruments that are self-adaptive to varying ambient conditions such as failures and other data transmission constraints. This will require on-board memory technology including the development of microprocessors.

12.2 Prominent Institutions and Individuals

NASA/Goddard Space Flight Center
M. H. Acuna
N. F. Ness

Jet Propulsion Laboratory
E. J. Smith
J. Slavin

University of Rome (Italy)
F. Mariani
R. Terenzi

UCLA
C. Russell
R. McPherson

University of Braunschweig (FRG)
F. Neubauer
G. Mussman

Imperial College (UK)
R. Hedgecock
A. Baloch

13 CRYOGENICS AND THERMAL CONTROL

13.1 Cryogenic Technology

Projected sensor capabilities presented in this volume rely heavily on parallel research efforts into many different areas. However, one consistent theme mentioned for all systems is that better performance or the projected performance cannot be attained until or unless better cryogenic systems are developed. Table . 59 illustrates this point by presenting a representative sample of required operating temperatures cited for both SOA and year 2000 instrument capabilities.

TABLE [illegible],59

SYSTEM TEMPERATURE REQUIREMENTS

System	SOA	2000
Microwave and Millimeter Wave Radiometers:		
DMR for COBE	295 K (31.4 GHz) 130 K (53 and 90 GHz)	
Far IR Spectrophotometer for COBE	1.5 K	0.1 K
SIS Mixer	<4 K	
Millimeter Wave Spectrometer	20 K	
Infrared Systems:		
Fourier Transform Spectrometer	<10 K	
AMS	70 K	60 K
MLA	50 K (IR)	
Arrays for Astronomy		
Si:X	40 K (4 μm) 8 K (30 μm)	
Ge:Ga	<4 K	
Laser Heterodyne Radiometer	80 K (10 μm) 20 K (28 μm)	110 K 30 K
Visible-UV CCDs	~220 K	
X-Ray Imager (Si CCD)	220 K	
X-Ray Array (Deep Diode Si)	<100 K	
X-Ray Detectors (Si:Li)	<100 K	
Gamma-Ray Detectors (Ge)	<100 K	

Obviously, each system with its unique requirements for active operational lifetime will need a unique cooling scheme, i.e., some instruments can use state of the art coolers while others will require the development of more complex cryogenic systems capable of maintaining the sensor temperature at cryogenic levels over extended periods of time. In either case, the size, weight, and power requirements of passive and active systems must be reduced to make them more compatible with spacecraft limitations. As an illustration of current research in this area, representative systems will be discussed. These include a

Joule-Thomson adsorption cooler for use at 20 K over extended periods of time, and Stirling cycle systems capable of maintaining the temperature at 65 K and 11 K over a 3 to 5 year life cycle.

13.1.1 Joule-Thomson Adsorption Cooler

This passive cryogenic cooler based on the Joule-Thomson effect uses waste heat from the spacecraft, solar energy, or an internal power source to achieve low operating temperatures for extended periods of time. It can provide vibration free cooling for sensitive detectors as well as for the associated telescope systems since it is scalable to high heat loads. The heat load capability of this system is illustrated in Fig. 108.

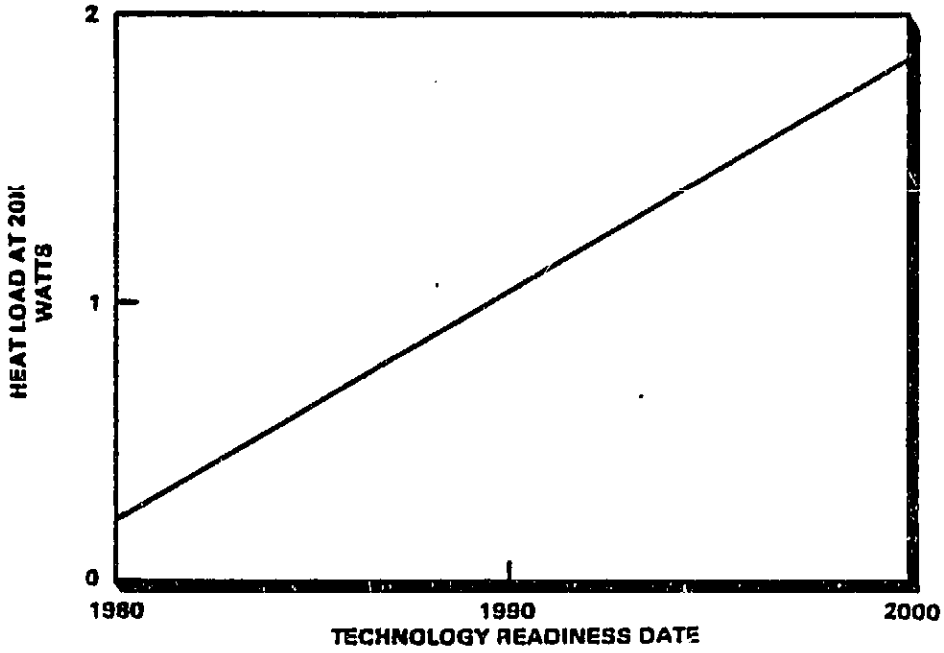

Figure 108. Projected Heat Load Capability

At 20 K, the 1982 value of heat load removable by this type of system is 0.2 W. It is projected that by the year 2000 this value will increase to >1.0 W.

Critical research for this system involves enhancement of the efficiency of the adsorption-desorption process and research into materials that will extend the long lifetime capabilities of these coolers.

13.1.2 Stirling Cycle Coolers

The expected lifetime of performance for the 65 K, 5 W heat load Stirling cycle cooler to support missions with infrared, x-ray, and gamma ray sensors is illustrated in Fig. 109.

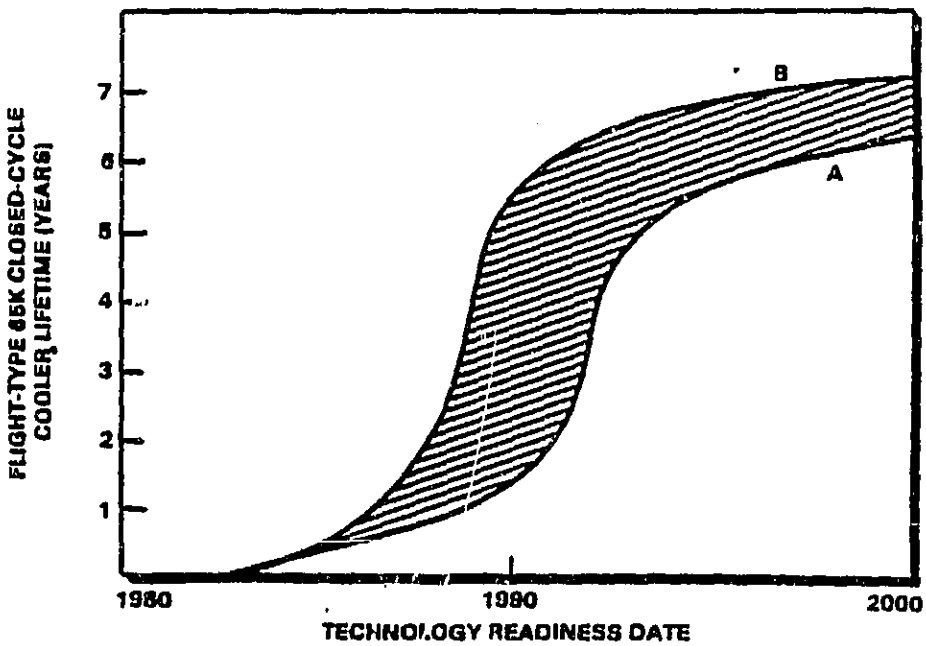

Figure 109. Cooler Performance

Expected lifetime of performance for the 11 K, closed Stirling cycle cooler (e.g., for extrinsic silicon detectors in 30 μm range) is illustrated in Fig. 110.

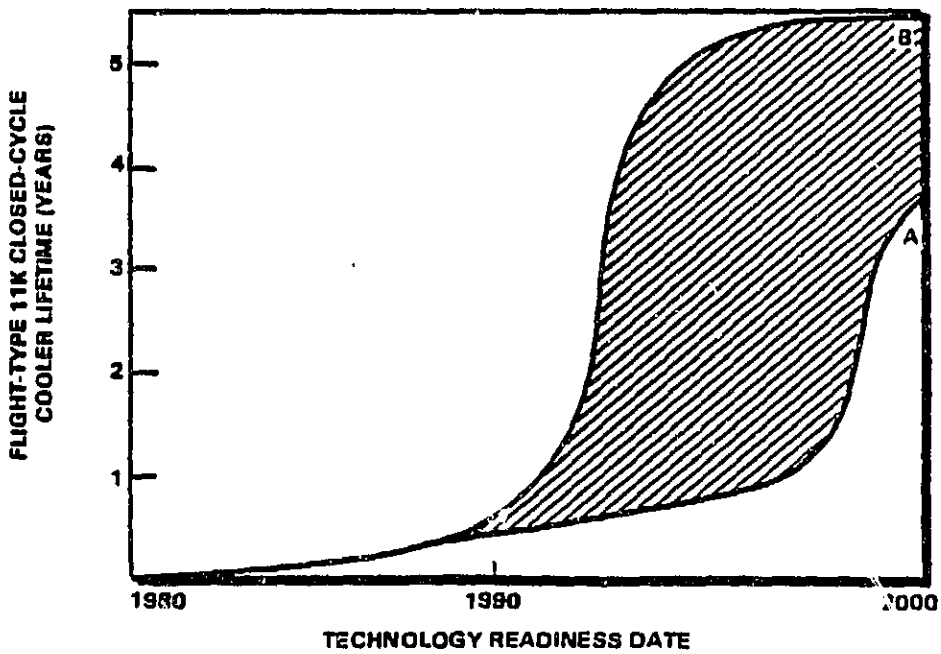

Figure 110. Projection for the 11 K Stirling Cycle Cooler

Such systems require the development of a method by which the working material (solid and liquid helium for 4 K to 100 K cooling) can be retained and used over an extended lifetime. A projection of this improved capability is presented in Fig. 111.

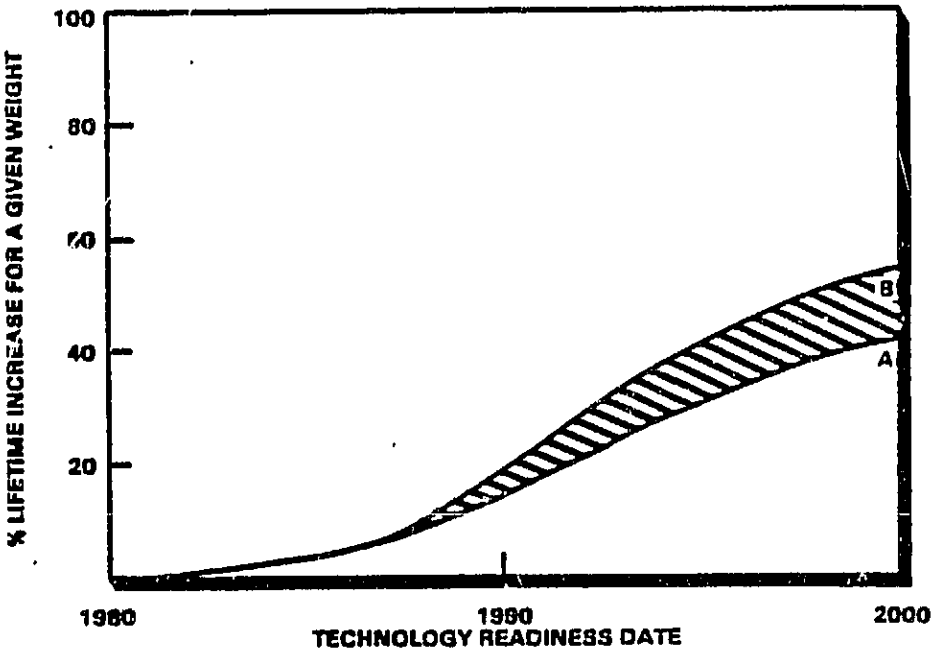

Figure 111. Projected Lifetime Increase for Cooler Working Medium

Different missions require different capabilities. For example, the space shuttle missions require a low cost liquid nitrogen sortie cooler. This system is currently about 60% complete and should be flight-ready by 1990. In contrast, infrared astronomy satellites for the future require a long life, closed cycle, helium liquifier using magnetic bearings in the compressor. This will provide the cooling and stability required. At current funding levels, this latter system will not be totally developed by the year 2000.

13.2 Power Dissipation and Thermal Control

Power dissipation and thermal control in spacecraft environments is also an important consideration. Certain systems such as high power laser systems (e.g., alexandrite, CO_2, dye lasers in LIDAR systems) generate substantial waste heat which must be removed. Other instruments require thermal control at nonambient temperatures in order to maintain alignment and mechanical and electronic operation. Systems

that can perform these functions can be an important part of spaceborne sensors. A forecast of a representative thermal control system is given here.

13.2.1 Two Phase Thermal Utility

This capillary and pump assisted cold plate system is used for thermal control of spacecraft instruments. It has an operating range between 263 K and 313 K. Its performance limits are dictated by its ability to dissipate 10 kW of power via radiation from 3 to 10 W per cm^2 over a 5 to 10 m transport length. Current mechanisms of this type operate using capillary systems augmented with mechanical heat pumps to provide energy transport over the total 50 K temperature range. Present research in this area places these systems at the level 3-4 state of development level.

Heat transport capacity and power density of the system serve as its figure of merit. Heat transport capability is defined as the ability to transport energy (watts) over a long distance (meters). Power density is the energy dissipated into the thermal system per unit area. These parameters have been projected forward to the year 2000 and are illustrated in Fig. 112.

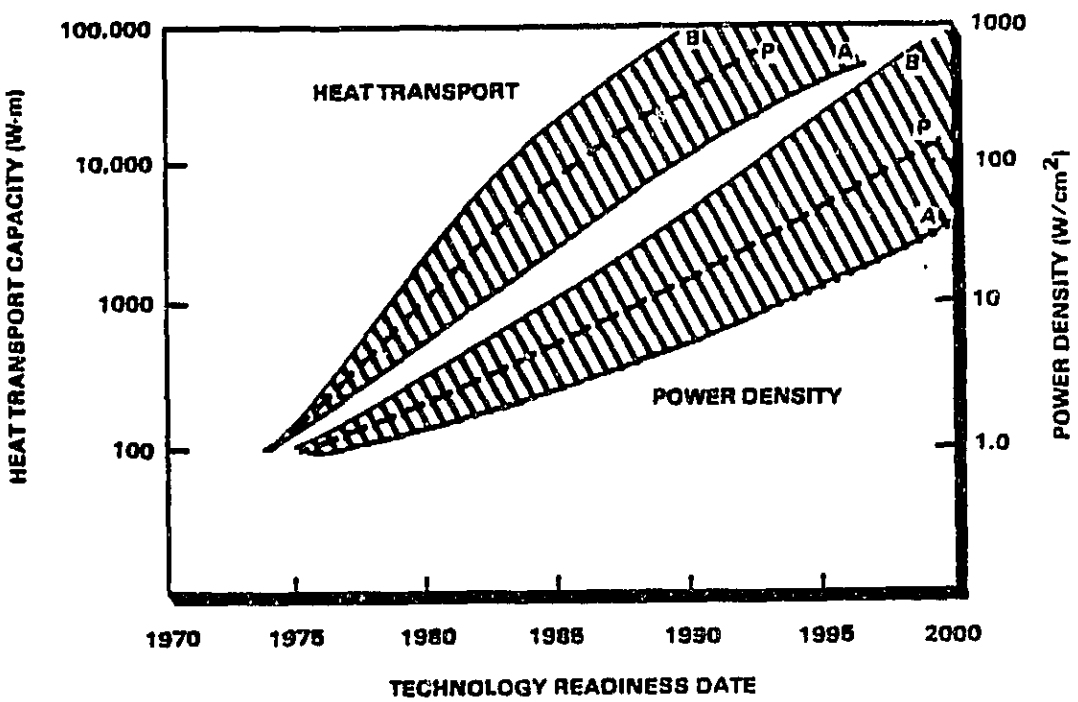

Figure 112. Heat Transport Capability and Power Density of Instrument Thermal Systems

Critical subsystems include cold plate evaporators and condensors which include technologies for the pumping head, fluid management and distribution, and pumps that have proven reliability over extended lifetime. The relationship between the projections for pumping capacity and cold plate power density is forecast in Fig. 113.

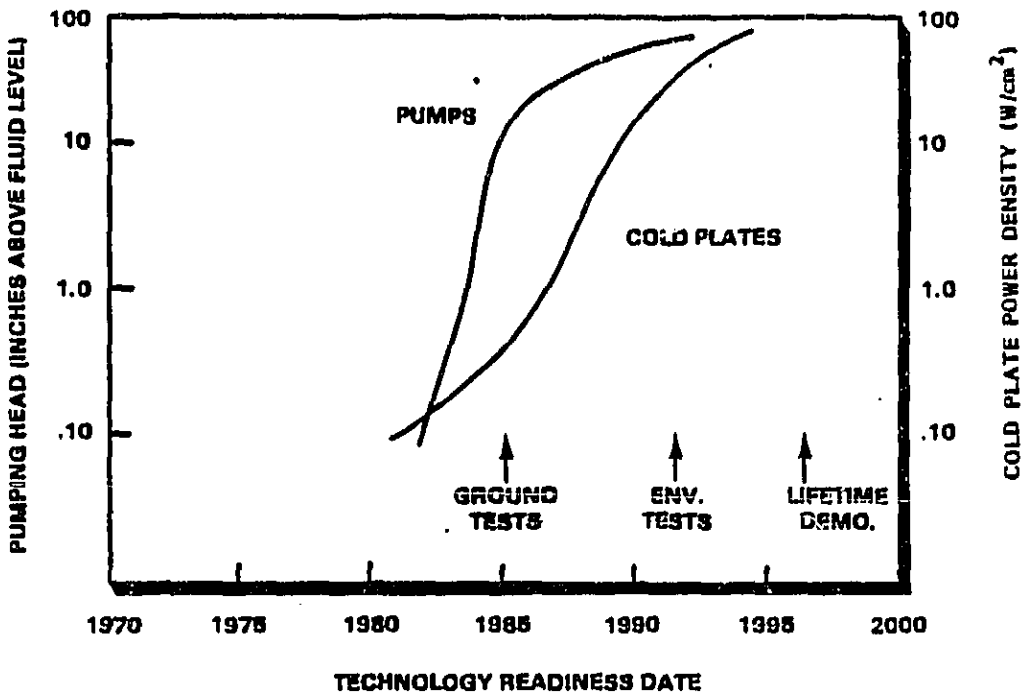

Figure 113. Projections for Pumping Capacity and Power Density

Future supporting research activities include testing and analysis of flow boiling, fluid distribution, fluid separation, further materials research to increase the lifetime of operation of these systems, and further efforts in materials research and thermodynamics to insure material compatibility for all components of the total system. The question of reliability and lifetime are nontrivial and require extensive testing prior to making these systems space ready.

It is projected that driving scientific programs will involve all areas mentioned where instruments requiring temperature control within these limits are needed. It is felt that this utility will be of particular value to large space platforms carrying instruments for multidiscipline users.

13.3 Prominent Institutions and Individuals

13.3.1 Cryogenics

NASA/Goddard Space Flight Center
A. Sherman

NASA/Johnson Space Center
W. Ellis

Jet Propulsion Laboratory
D. Elleman
M. Tward

NASA/Ames Research Center
P. Kittel

13.3.2 Thermal Control

NASA/Goddard Space Flight Center
S. Ollendorf

14 OPTICS

Advanced optical systems usually require large aperture telescopes, often with large fields of view. Virtually all aspects of optical technology and optical system design affect survivability, and a wide ranging effort towards effective protection is important. Above-the-horizon (ATH) viewing systems, looking for space objects require very high levels of out-of-field-of-view rejection (OFVR) for bright sources such as the Earth, Moon, and Sun. High values of OFVR become increasingly difficult as the required field of view (FOV) increases.

For Earth-viewing sensors, avoiding crosstalk from bright sources located within the FOV is another difficult OFVR requirement. OFVR requirements may be different for a scanning sensor and a staring sensor that performs the same mission. Improvements to the mainstays of optics, materials, coatings, and filters are still important, with new requirements imposed by the broad spectrum of sensors discussed.

For astronomical application, large spaceborne telescopes permit observations in spectral regions which are absorbed by the Earth's atmosphere (e.g., 30 μm to 1 mm and UV wavelengths). They also permit higher spatial resolution limited by the diffraction of the optical aperture since atmospheric "seeing effects" are not present. In the absence of atmospheric effects, large telescopes would also permit measurements of more distant astrophysical objects. Opto-mechanical

technology is closely related to the feasibility of the large optical systems, but other issues including optical quality, size, and weight are of concern.

14.1 Lightweight Mirror Technology (Fig. . 114)

The mirror area per unit mass achievable by several large-mirror fabrication technologies is shown. The technology for stiff mirrors made by fusing or frit-bonding a faceplate to a lightweight core structure is predicted to scale with size as shown. The space telescope (ST) primary mirror represents 1980 fused mirror technology and offers a lightening gain of a factor of 4 with respect to a solid mirror. Frit-bonding (ca 1985) may allow a gain of another factor of 5. Other developments may include lighter weight, composite material cores. Mirrors that rely on active control rather than their stiffness to maintain figure accuracy may offer substantial weight reductions for large mirrors if the predicted scaling law (mass per unit area independent of diameter) is obeyed. Existing and planned programs are listed in Table ..60.

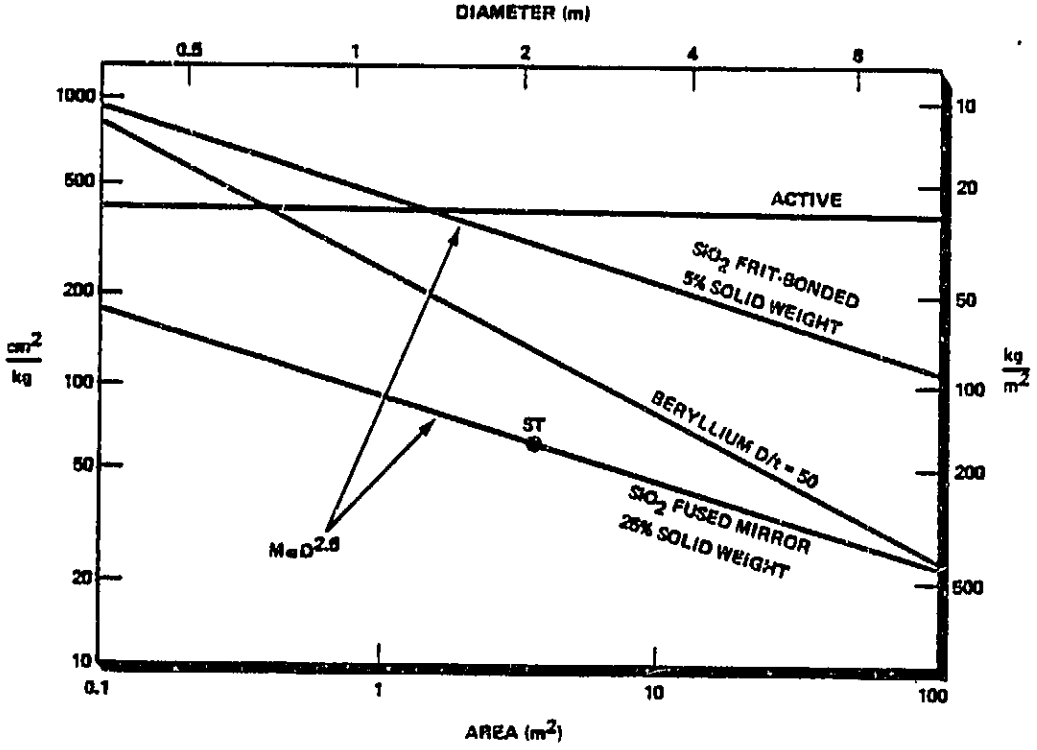

Figure 114. Lightweight Mirror Technology

TABLE 60

SPACEBORNE TELESCOPE PROGRAMS

Agency	Program	Key Goals
NASA	SIRTF	0.85 m diameter, f/24, 0.13° FOV, Ritchey-Chretien beryllium mirrors, 2 to 10 K focal plane
NASA	IRAS	0.6 m diameter, f/6, 1.2° FOV, double-folded Gregorian, 3 to 10 K
NASA	Space Telescope	2.4 m primary, 0.1 sec resolution, ATi/48, 0.007-sec stability

14.2 Adaptive Optics

Large space mirrors are classified into six categories according to continuous versus segmented and passive/semiactive/active characteristics. Adaptive optics include semiactive or active mirrors for which the actuator signals for figure adjustment are generated automatically using real-time image quality measurements.

Figure 115 shows the applicability of various classes of mirror design by diameter showing that the complexity of figure adjustment features increases dramatically with size. Also shown is a forecast curve for mirror mass per unit optical surface area. (This material was provided by the Rome Air Development Center.)

14.3 Large Deployable Reflector (LDR)

This is an example of a future large diameter spaceborne reflector. The National Aeronautics and Space Administration is in the preliminary planning stages for this large submillimeter and far infrared orbiting astronomical telescope facility. The telescope will be between 10 and 30 m in diameter, the upper limit being defined by technology and cost.

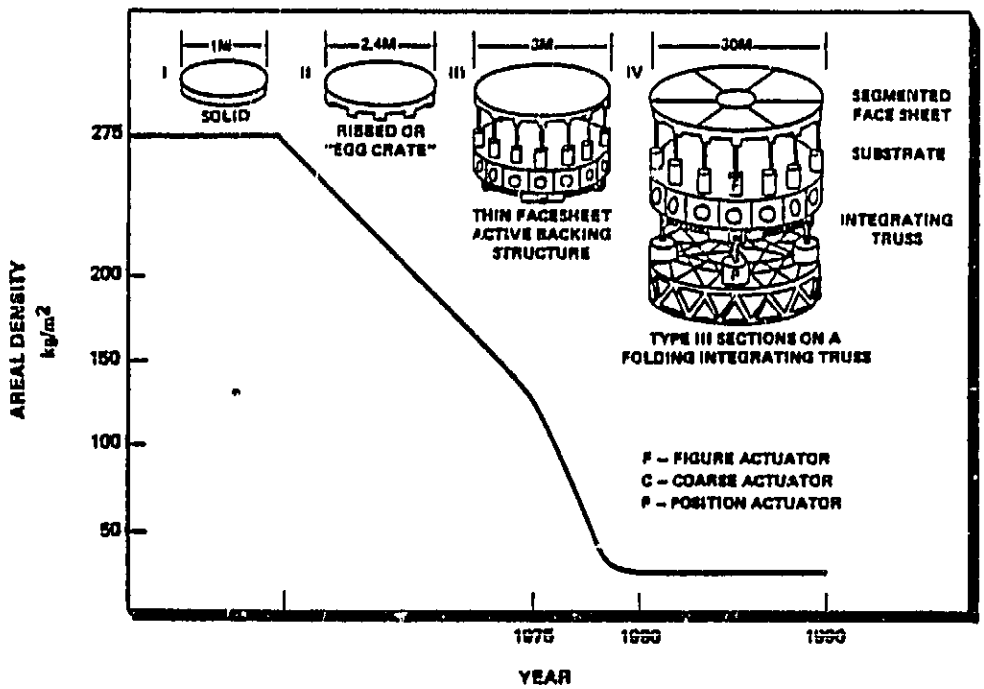

Figure 115. Space Mirror Technology

The operating wavelength will be between 1 mm (1000 μm) and 30 μm. The short wavelength limit is a compromise between the point where smaller cooled telescopes become more sensitive ($\lambda \sim 10$ μm) and practical technology. The short wavelength limit may be increased if the trade-off between cost and scientific return is advantageous. Typical technical requirements for the LDR are presented in Table 61.

The telescope will be a Cassegrain design of approximately f/1. The primary reflector will be made up of a number of close packed panels. Each panel will be actively controlled with three degrees of freedom so that the overall optical figure of the primary reflector can be maintained within a small fraction of the shortest operating wavelength. The panels will be attached to a tetrahedral truss backup structure which will absorb the reaction forces of the panel actuators. Active control and optical surface quality of the individual segments is expected to provide diffraction limited operation to 30 μm wavelengths. The spacecraft and optical reference structure will be behind the vertex

of the primary reflector. The focal plane instruments, surface measurement system, and possibly the central panel will be rigidly mounted to this optical reference.

TABLE 61

LDR TECHNICAL REQUIREMENTS

Wavelength:	$30 < \lambda < 1000$ μm diffraction limited
Light Bucket Blur Circle:	2.0 arc sec
Primary Diameter:	20 m
Mirror Temperature:	150 K, or as cool as possible without active cooling
Stray Light Rejection:	Stray light from Sun, Earth, and Moon is less than telescope emission and zodical light
Telescope Pointing:	0.06 arc sec absolute accuracy, 0.03 arc sec jitter
Retargeting Slew:	20°/min
Launch/Deployment:	Single Shuttle launch to low earth orbit, semiautomatic deployment
Mission:	10-year duration with periodic revisits at 2-year intervals

The heritage of such a system is best illustrated through comparison with other systems either planned for the future or in an active status today. This is illustrated in Fig. 116.

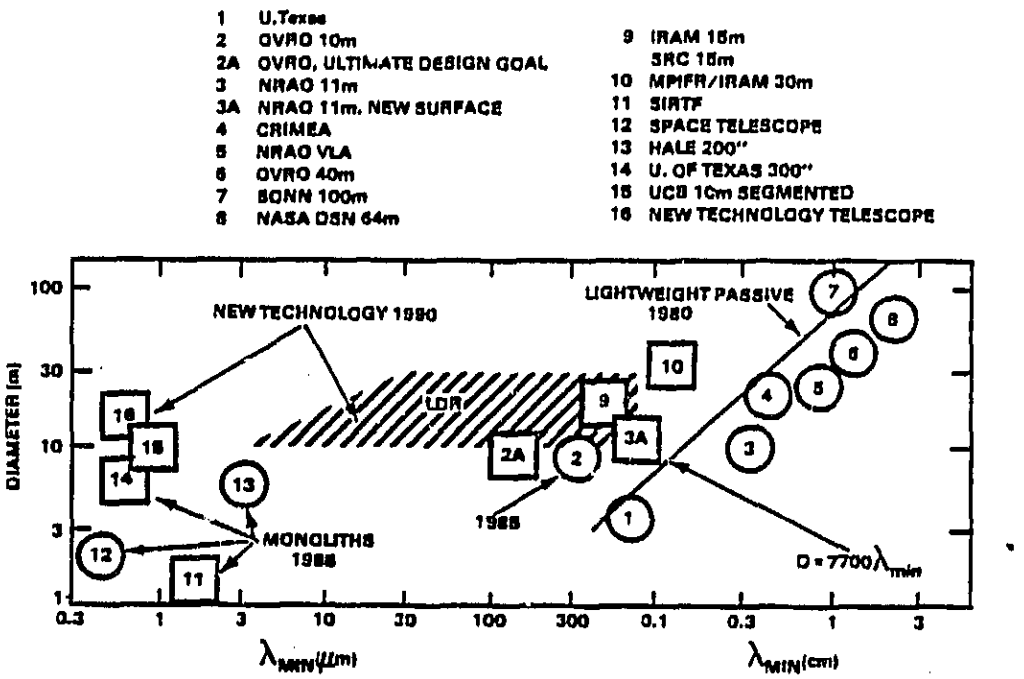

Figure 116. LDR Size and Spectral Region Covered (Shaded) Compared to Other Optical Systems

A forecast of IR/submillimeter reflector diameters for use in space is provided in Fig. 117. A related parameter is the mirror areal density (kg/m^2). Mirror segment areal density will depend upon the type of material selected (glass or composite) and upon the environmental conditions of launch and orbit. The segments must be light but robust enough to survive launch. They must have temporal stability and not be thermally sensitive (prone to distortions when experiencing a thermal gradient). A forecast of areal density is provided in Fig. 118.

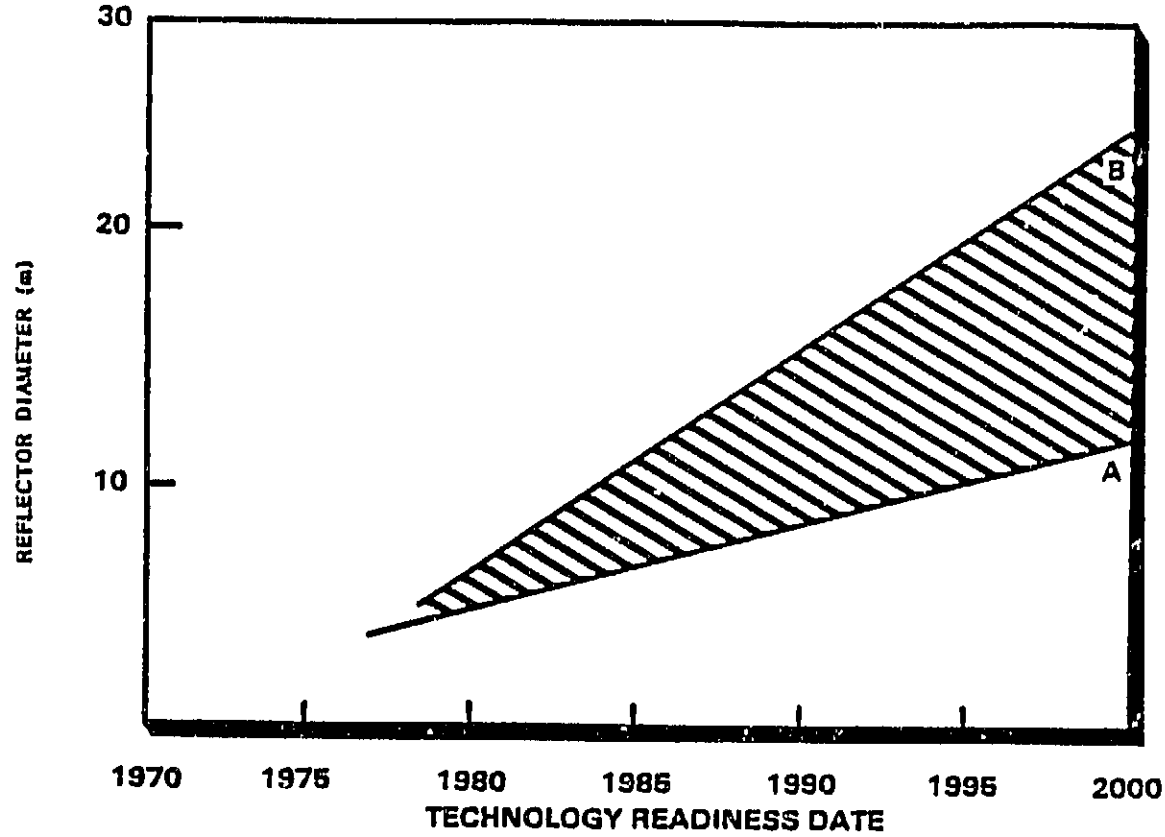

Figure 117. Far IR/Submillimeter Primary Reflector Diameter for Space-Based Observatory

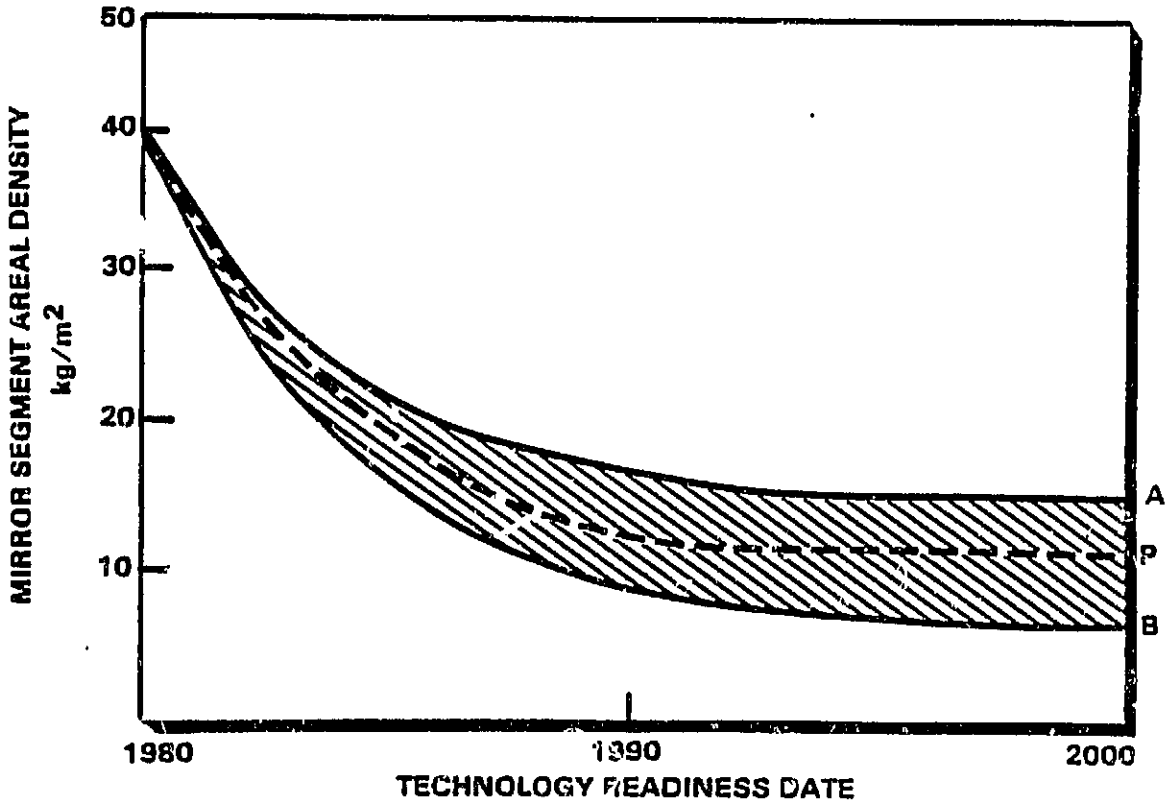

Figure 118. Projection of Areal Density

Performance parameters of the LDR are evolutionary only in the sense that technology has to improve in order to meet the system requirements. Segmented mirror technology is addressed in this forecast. Projection of parameters of large space optics are given in Table 62. These include reflector diameter, measurement and control of structures to within ~1 μm tolerance, and materials research to provide reflector materials with low thermal expansion coefficients and areal density.

TABLE 62

CRITICAL SYSTEM PARAMETERS FOR LDR

Critical Component and Characteristic	SOA Value	2000 Value
Reflector Diameter (@ 30 μm)	~2 m	20 m
Measurement and Control	50 μm	<2 μm
Reflector Materials	Glass	Composite
Reflector Areal Density	50 kg/m^2	10 kg/m^2

Other technology needed for the LDR facility include space quality cryogenics with multiyear lifetimes and millimeter and submillimeter receivers and have been treated elsewhere in this document.

14.4 Advanced Optical Design

In order to obtain maximum information return from a remote measurement great care must be applied to the design and construction of the signal collecting and processing systems. Optical instrument designs often require a compromise of design parameters based on measurement priorities, ease of design and fabrication, and cost. A structured system analysis and computer aided design (CAD) can permit the development of optical systems approaching ideal performance limits at minimum cost. Parameters such as spatial resolution, spectral resolution, sensitivity, instrument size, and number of data channels can all be optimized to produce the maximum information return from any conceptual sensor system. This design capability is especially important for multifunction systems, where various modes of operation may require optimization of different optical parameters for best performance. Computer aided design can generate the best compromise between competing requirements. Such an analysis requires the definition of a system figure of merit and a baseline from which comparisons between systems can be made. A figure of merit describing the overall efficiency of an optical system can be defined in terms of the Relative Information Throughput (RIT),

$$RIT = \frac{(\text{spatial resolution})^2 \times (\text{format size})^2 \times \text{bandwidth} \times \text{No. spectral channels}}{(\text{source intensity})}$$

Most current systems have a value of RIT on the order of 2×10^4. It is projected that future systems such as the ST and LDR will have values on the order of 10^5 with no major change in funding. Increased funding could, however, increase this value to 10^{11}. This is illustrated in Fig. 119.

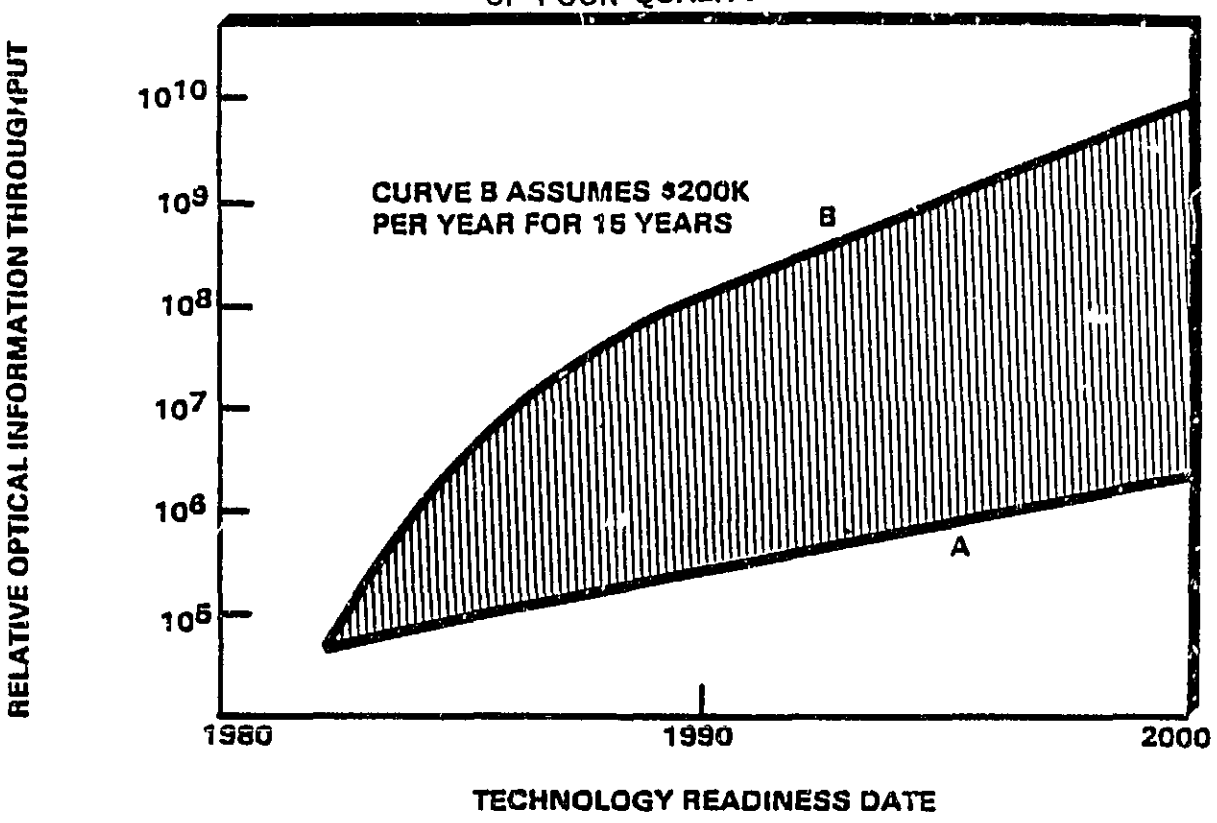

Figure 119. Space Advanced Optical Systems (UV-Vis) Remote Sensing and Measurement Design Approach

As the volume of data (the RIT) increases with new designs, it will be required that new and better methods be developed for data processing. Optical information processing offers one solution to this problem. Construction of an optical electronic hybrid computer for this purpose could lead to an increased information throughput capability up to eight orders of magnitude larger than currently possible. This projection is illustrated in Fig. 120.

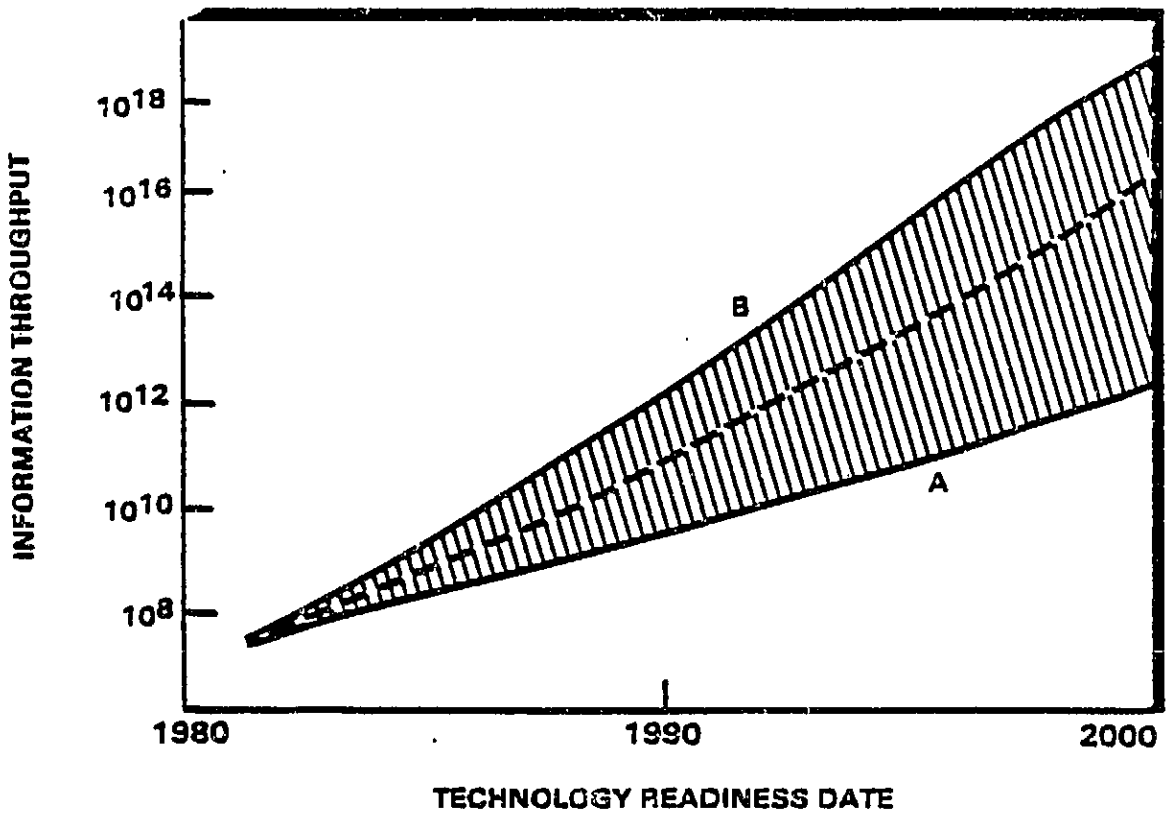

Figure 120. Optical Information Processing Optical Electronic Hybrid Computer

14.5 Prominent Institutions and Individuals

NASA/Ames Research Center
R.K. Melugin
D. J. Ennis
B. Swenson
P. Kittel

Jet Propulsion Laboratory
P. Swanson
J. Breckinridge
K. Ramohalli

California Institute of Technology
R.B. Leighton

Rome Air Development Center
T. Pitts
D. Camill

University of Arizona
R. R. Shannon
J.R.P. Angel
R.E. Parks

Perkin-Elmer Corp.
M.H. Krim

Itek Corp.
E. Galat
L. Soloman

Kodak Corp.
D.A. Crowe

University of Rochester
K. Teegarden
D. Moore

NASA/Goddard Space Flight Center
J. Mangus
J. Osantowski

15 Acronyms

AMS Advanced Mapping Spectrometer
AMTS Atmospheric Moisture and Temperature Sounder
AOS Acousto-Optic Spectrometer
ATMOS Atmospheric Trace Molecule Spectroscopy
ATS Advanced Technology Satellite
A/D Analog to Digital

BMLS Balloon Microwave Limb Sounder

CCD Charge Coupled Device
CID Charge Injected Device

DIAL Differential Absorption Lidar
DMR Differential Microwave Radiometer

EFUV Extreme Far Ultraviolet

FET Field Effect Transistor
FIRAS Far IR Absolute Spectrophotometer
FLD Fraunhofer Line Discriminator
FTS Fourier Transform Spectrometer
FUSE Far Ultraviolet Spectroscopic Explorer
FWHM Full Width Half Maximum

HSRMWR High Spatial Resolution Millimeter Wave Radiometer

IF Intermediate Frequency
IFOV Instantaneous Field of View
IMPATT Impact Avalanche and Transit Time
IRCCD Infrared Charge Coupled Devices
IUE International Ultraviolet Explorer

LAMMR Large Antenna Multifrequency Microwave Radiometer
LDR Large Deployable Reflector
LHS Laser Heterodyne Spectrometer
LO Local Oscillator
LSST Large Space Structures Technology
LWIR Long Wave Infrared

MAMA Multianode Microchannel Plate Array
MCP Microchannel Plate
MFIR Moderate Field-of-View Imaging Radiometer
MLA Multispectral Linear Array
MLS Microwave Limb Sounder
MSS Multispectral Scanning System

NEP Noise Equivalent Power
NIMS Near Infrared Mapping Spectrometer
NOSS National Oceanic Satellite System

OFT Orbiting Flight Test
OFVR Out of Field-of-View Rejection

PBMR Pushbroom Microwave Radiometer
PHRIR Pointable High Resolution Imaging Radiometer
PIS Pointable Imaging Spectrometer
PMT Photo Multipler Tube
PPS Pulses Per Second

RF Radio Frequency
RIT Relative Information Throughput

SAM Simultaneous Astrophysical Mission
SAR Synthetic Aperture Radar
SAW Surface Acoustic Wave
SEM Scanning Electron Microscopy
SFMR Step Frequency Microwave Radiometer
SIR Shuttle Imaging Radar
SIRTF Shuttle IR Telescope Facility
SIS Superconductor-Insulator-Superconductor
SLAR Side Looking Airborne Radar
SMMR Scanning Metrological Microwave Radiometer
SNR Signal-to-Noise Ratio
ST Space Telescope
SWIR Short Wave Infrared

TDI Time Delay and Integration
TDRSS Tracking Data Relay Satellite System
TIR Thermal Infrared
TM Thematic Mapper

UARS Upper Atmosphere Research Satellite

VOIR Venus Orbiting Imaging Radar

WFIR Wide Field-of-View Imaging Radiometer

XRF X-Ray Fluorescence

REFERENCES

1. NASA Space Systems Technology Model: Vol. II, Space Technology Trends and Forecasts, Section 11, Sensors, NASA/OAST (1981).

2. Infrared Receivers for Low Background Astronomy: Incoherent Detectors and Coherent Devices from One Micrometer to One Millimeter: Final Report, NASA Technical Memorandum 78598, (1979).

3. SIRTF, Shuttle Infrared Telescope Facility, Report of the Focal Plane Instruments and Requirements Science Team and the SIRTF Science Working Group (1979).

4. Large Deployable Reflector Science and Technology Workshop, Volume II, Science Rationale and Technology Requirements, Asilomar Conference Center, Pacific Grove, CA, June 21-25, 1982, NASA Conference Publication 2275.

5. The Final Report of the Science Working Group for the Far Ultraviolet Spectroscopic Explorer (FUSE), NASA (1983).

6. C. E. Fichtel and J. J. Trombka, Gamma Ray Astrophysics, NASA SP-453, (1981).

7. J. N. James and R. R. McDonald, Part One: The Forecast Plan, A Forecast of Space Technology in Outlook for Space Working Group V, NASA N79-74757, (1979).

8. Military Space Systems Technology Model (U), Volume IIIA: Technology Trends and Forecasts (U), First Edition, Final Report, SD-TR-82-01, January 1982.

APPENDIX I

TECHNOLOGY READINESS LEVEL DEFINITIONS

LEVEL 1: Basic Principles Observed and Reported

LEVEL 2: Conceptual Design Formulated

LEVEL 3: Conceptual Design Tested Analytically or Experimentally

LEVEL 4: Critical Function/Characteristic Demonstration

LEVEL 5: Component/Breadboard Tested in Relevant Environment

LEVEL 6: Prototype/Engineering Model Tested in Relevant Environment

LEVEL 7: Engineering Model Tested in Space